DAHLGREN DIVISION
NAVAL SURFACE WARFARE CENTER
Dahlgren, Virginia 22448-5100

NSWCDD/TR-97/167

MONOPULSE PROCESSING FOR TRACKING UNRESOLVED TARGETS

BY W. D. BLAIR
SYSTEMS RESEARCH AND TECHNOLOGY DEPARTMENT

M. BRANDT-PEARCE
UNIVERSITY OF VIRGINIA

SEPTEMBER 1997

19971022 040

REPORT DOCUMENTATION PAGE

Public reporting burden for this collection of information is estimated to average 1 hour per response, including the time for reviewing instructions, search existing data sources, gathering and maintaining the data needed, and completing and reviewing the collection of information. Send comments regarding this burden or any other aspect of this collection of information, including suggestions for reducing this burden, to Washington Headquarters Services. Directorate for information Operations and Reports, 1215 Jefferson Davis Highway, Suite 1204, Arlington, VA 22202-4302, and to the Office of Management and Budget, Paperwork Reduction Project (0704-0188), Washington, DC 20503.

1. AGENCY USE ONLY (*Leave blank*)	2. REPORT DATE September 1997	3. REPORT TYPE AND DATES COVERED

4. TITLE AND SUBTITLE
MONOPULSE PROCESSING FOR TRACKING UNRESOLVED TARGETS

5. FUNDING NUMBERS

6. AUTHOR(S)
W. D. Blair   M. Brandt-Pearce

7. PERFORMING ORGANIZATION NAME(S) AND ADDRESS(ES)
Commander
Naval Surface Warfare Center, Dahlgren Division (Code B32)
17320 Dahlgren Road
Dahlgren, VA 22448-5100

8. PERFORMING ORGANIZATION REPORT NUMBER
NSWCDD/TR-97/167

9. SPONSORING/MONITORING AGENCY NAME(S) AND ADDRESS(ES)

10. SPONSORING/MONITORING AGENCY REPORT NUMBER

11. SUPPLEMENTARY NOTES

12a. DISTRIBUTION/AVAILABILITY STATEMENT
Approved for public release; distribution is unlimited.

12b. DISTRIBUTION CODE

13. ABSTRACT (Maximum 200 words)

When target echoes interfere (i.e., the echoes are not resolved in the frequency or time domains) in a monopulse radar system, the Direction-Of-Arrival (DOA) estimate indicated by the in-phase monopulse ratio can wander far beyond the angular separation of the targets. In addition to closely-spaced targets, the problem of unresolved or merged measurements also occurs when targets are observed in the presence of jammer signals or sea-surface induced multipath. The failure to detect the presence of this interference and address it in the DOA estimation can be catastrophic to the performance of the tracking algorithm, since its position and velocity estimates determine the association of any subsequent measurements to the target.

Monopulse processing for tracking unresolved targets is addressed in four parts. The first part involves the development of the Probability Density Function (PDF) and statistics of the measured amplitude of the sum signal for an arbitrary number of unresolved Rician targets. The PDF and statistics are utilized to develop estimators of the target amplitude parameters, which define the Signal-to-Noise Ratio (SNR) of the target and discriminators for models of the target amplitude fluctuations. The second part involves the development of the joint PDF and statistics of the complex monopulse ratio for an arbitrary number of unresolved Rician targets and a fixed-amplitude target in the presence of multipath. The information contained in the sum-channel signal is retained in the PDF of the complex monopulse ratio by conditioning the PDF on the measured amplitude of the sum-signal. The third part involves DOA estimation for single targets and two unresolved targets. DOA estimators are developed for two unresolved Rayleigh targets with known relative Radar Cross Section (RCS) and a Rayleigh target in the presence of a Gaussian jammer. Estimators of the variance of the DOA estimates are also developed so that tracking of the targets can be accomplished with a nonstationary filtering technique, such as the Kalman filter. The fourth part involves the detection of the presence of unresolved targets. A Generalized Likelihood Ratio Test (GLRT) is used to develop a Neyman-Pearson algorithm for the detection of the presence of unresolved Rayleigh targets, and performance predictions of the new algorithm are shown to agree rather well with simulated performance. Cramer Rao Lower Bounds are developed for the various parameter estimators, and the performance of the estimators and detection algorithms are illustrated through the results of Monte Carlo simulations.

14. SUBJECT TERMS
monopulse processing, tracking, unresolved targets, Direction-Of-Arrival (DOA) estimate, Probability Density Function (PDF), Signal-to-Noise Ratio (SNR), Generalized Likelihood Ratio Test (GLRT)

15. NUMBER OF PAGES
220

16. PRICE CODE

17. SECURITY CLASSIFICATION OF REPORT	18. SECURITY CLASSIFICATION OF THIS PAGE	19. SECURITY CLASSIFICATION OF ABSTRACT	20. LIMITATION OF ABSTRACT
UNCLASSIFIED	UNCLASSIFIED	UNCLASSIFIED	SAR

NSN 7540-01-280-5500

FOREWORD

As naval operations address theater warfare, sensor resolution and unresolved targets will become more significant. In theater warfare, the effectiveness of combat identification will hinge on resolving and tracking closely-spaced targets. In Theater Ballistic Missile Defense (TBMD), resolving and tracking closely-spaced targets will be required to separate the debris from the threat. Furthermore, hostile targets may exploit sensor resolution to make the conditions under which they can be engaged successfully more difficult to achieve. In contrast to addressing these challenging problems of sensor resolution through adaptive digital beamforming, this report focuses on the use of a standard monopulse radar with new detection and estimation algorithms to address the problem of sensor resolution and the tracking of unresolved targets.

This report addresses such issues as target amplitude estimation, discrimination between targets with different amplitude distributions, tracking with a monopulse radar, angle-of-arrival estimation for a target in multipath or two unresolved targets, and detection of the presence of unresolved targets. This research has been accomplished in part through funding from the Naval Surface Warfare Center, Dahlgren Division (NSWCDD) In-house Laboratory Independent Research (ILIR) Program sponsored by the Office of Naval Research.

This report has been reviewed by M. A. Bailey, Combat Systems Branch, Dr. C. F. Fennemore, Technical Lead, Target Tracking and Signal Processing; and R. N. Cain, Head, Combat Systems Technology Group.

Approved by:

MARY E. LACEY, Head
Systems Research and Technology Department

iii

DTIC QUALITY INSPECTED

CONTENTS

LIST OF FIGURES

LIST OF TABLES

SYMBOLS

A	Amplitude of the target	2.1
A_o	Rayleigh parameter for the amplitude of the target	2.2
$\tilde{c}$	MM estimate of $\cos\Delta\phi$	3.9
$d(t)$	Difference channel signal	2.1
d	Complex difference channel signal voltage	2.6
d_I	In-phase part of difference signal	2.1
$\bar{d}_I$	Expected value of in-phase part of difference signal	2.4
d_Q	Quadrature part of difference signal	2.1
$\bar{d}_Q$	Expected value of the quadrature part of difference signal	2.4
E_I	Elevation of target's image in multipath	2.5
E_t	Elevation of a low elevation target	2.5
g	Ratio of the sum channel voltages at the target and image angles	2.5
g_o	Parameter characterizing the roughness of the sea surface	2.5
$G_\Sigma(\theta)$	Sum channel voltage gain at the angle θ	2.1
$G_\Delta(\theta)$	Difference channel voltage gain at the angle θ	2.1
h_r	Height of the radar above the sea surface	2.5
h_t	Height of the target above the sea surface	2.5
I_{y_I,y_Q}	Fisher information associated with observations of y_I and y_Q	5.4
J_{y_I,y_Q}	CRLB associated with observations of y_I and y_Q	5.1
J_{y_I}	CRLB associated with observations of y_I only	5.1
J_{y_Q}	CRLB associated with observations of y_Q only	5.1
$I_0(\cdot)$	Zero-order modified Bessel function of the first kind	2.1
$I_1(\cdot)$	First-order modified Bessel function of the first kind	3.2
$I_{1|0}(\cdot)$	$I_1(\cdot)$ divided by $I_0(\cdot)$	3.2
k_m	Monopulse error function	2.1
$N(\mu,\sigma^2)$	Gaussian distribution with mean μ and variance σ^2	2.1
Λ	Measured amplitude of the sum signal	2.1
$n_S(t)$	Receiver noise in the sum channel	2.1
$n_d(t)$	Receiver noise in the difference channel	2.1
n_{dI}	Received errors in the in-phase part of the difference signal	2.1
n_{dQ}	Received errors in the quadrature part of the difference signal	2.1
n_{SI}	Received errors in the in-phase part of the sum signal	2.1
n_{SQ}	Received errors in the quadrature part of the sum signal	2.1
$p(t)$	Envelope of the transmitted pulse	2.1

Δr	Path Length Difference (PDL) from the direct reflection and sea-surface reflection	2.5
$\Delta\phi$	Phase difference between direct and specular reflections	2.5
λ	Wavelength of carrier waveform	2.5
λ_d	Threshold for detection of two unresolved Rayleigh targets	6.0
λ_r	Relative RCS of two Rayleigh targets	5.4
κ	Constant proportional to the transmitted power	2.1
η	DOA parameter	2.1
$\hat{\eta}$	ML Estimate of η	5.2
η_i	DOA parameter for target i	2.4
$\hat{\eta}_i$	Estimate of η_i	5.4
η_I	DOA parameter for the image of a target in multipath	2.5
$\hat{\eta}_{gml}$	"Generalized" ML estimate of η_1	5.1
$\hat{\eta}_{gmm}$	"Generalized" MM estimate of η_1	5.1
$\hat{\eta}_{ml}$	ML estimate of η_1	5.1
$\hat{\eta}_{mm}$	MM estimate of η_1	5.1
η_t	DOA parameter of a target in multipath	2.5
ρ	Correlation coefficient of receiver errors	2.1
ϕ	Phase of the target echo	2.1
ϕ_i	Phase of the fixed-amplitude part of the echo for target i	2.4
φ_i	Phase of the Rayleigh part of the echo for target i	2.4
Φ	Parameter set for phases of M Rician targets	2.4
Φ_F	Parameter set for the phase for fixed-amplitude target	2.1
Φ_D	Parameter set for the phase for dominant-plus-Rayleigh target	3.3
Φ_{Ri}	Parameter set for the phase for Rician target	3.6
Φ_{2F}	Parameter set for the phases for two fixed-amplitude targets	3.8
Φ_{2Ri}	Parameter set for the phases for two Rician targets	3.7
ϕ_{ga}	Grazing angle of sea reflection	2.5
Ψ	Parameter set for monopulse signals of M Rician targets	2.4
Ψ_F	Parameter set for monopulse signals of fixed-amplitude target	4.2
Ψ_{FR}	Parameter set for monopulse signals of fixed-amplitude and Rayleigh targets	4.4
Ψ_{MP}	Parameter set for monopulse signals of fixed-amplitude in multipath	4.7
Ψ_{Ri}	Parameter set for monopulse signals of Rician target	4.5
Ψ_{2F}	Parameter set for monopulse signals of two fixed-amplitude targets	4.6
Ψ_{2R}	Parameter set for monopulse signals of two Rayleigh targets	4.2
ψ	Measured phase of the target echo	2.1
σ	RCS of a target	2.2
σ_{ave}	Average RCS of a target	2.2
σ_d^2	Variance of the received errors in the difference signal	2.1
σ_h	RMS sea-surface elevation above the mean level	2.5
σ_S^2	Variance of the received errors in the sum signal	2.1
$\hat{\sigma}_{y_I}^2$	Estimate of the variance of the in-phase monopulse ratio	2.6
$\hat{\sigma}_{y_Q}^2$	Estimate of the variance of the quadrature monopulse ratio	5.2
$\hat{\sigma}_{\hat{y}_I}^2$	Estimate of the variance of the $\hat{y}_I$	4.1

GLOSSARY

CRLB   Cramer-Rao Lower Bound
DOA   Direction-Of-Arrival
DRFM   Digital Radio Frequency Memory
ECM   Electronic Countermeasure
FIM   Fisher Information Matrix
GLRs   Generalized Likelihood Ratios
GLRT   Generalized Likelihood Ratio Test
GML   Generalized Maximum Likelihood
GMM   Generalized Method of Moments
ILIR   In-House Laboratory Independent Research
IMM   Interacting Multiple Model
LRs   Likelihood Ratios
ML   Maximum Likelihood
MM   Method of Moments
NNPDA   Nearest-Neighbor Probabilistic Data Association
NNPDAMM   Nearest-Neighbor Probabilistic Data Association
            Merged Measurements
NSWCDD   Naval Surface Warfare Center, Dahlgren Division
PDF   Probability Density Function
PLD   Path-Length Difference
RCS   Radar Cross Section
RGPO   Range Gate Pull-Off
RMS   Root-Mean-Square
ROC   Receiver Operating Characteristic
SNR   Signal-to-Noise Ratio
TBMD   Theater Ballistic Missile Defense

Chapter 1

INTRODUCTION

Pulse compression techniques are often employed in radar systems to improve the accuracy of the range measurements, while monopulse techniques are employed to improve the accuracy of angle measurements. Monopulse is a simultaneous lobing technique for determining the angular location of a source of radiation or of a "target" that reflects part of the energy incident upon it [1]. Prior to the development of monopulse, angle measurements were improved with sequential lobing, which required two consecutive measurements to be taken of the target. The first measurement was taken with the boresight of the antenna pointing slightly below (or to the left) of the predicted target position, while the second measurement was taken with the boresight of the antenna pointing slightly above (or to the right) of the prediction position. Then the target was declared to be closer to the angle of the measurement with the larger amplitude, and the predicted angle of the target was corrected. However, sequential lobing is very susceptible to pulse-to-pulse amplitude fluctuations, which are common in radar measurements due to target scintillation. Furthermore, when tracking in azimuth and elevation, sequential lobing requires lobe switching between azimuth and elevation or conical scan, both of which are inefficient with respect to radar time and energy, and easily jammed or deceived by the target.

In an amplitude comparison monopulse radar system, a pulse is transmitted directly at the predicted position of the target, and the target echo is received with two squinted beams as illustrated in Figure 1.1. The Direction-Of-Arrival (DOA) of the target is typically estimated with the in-phase part (*i.e.*, the real part) of the monopulse ratio, which is formed by dividing the difference of the two received signals by their sum. When tracking in azimuth and elevation, four beams are used to receive, and two monopulse ratios are typically formed. Thus, the simultaneous lobing of monopulse allows the transmitted energy to be directed at the predicted position of the target and eliminates the errors due to amplitude fluctuations by forming a

1
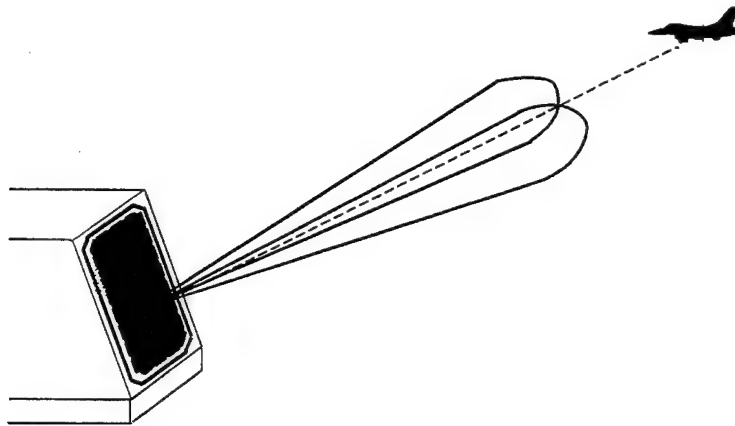
Figure 1.1 Illustration of Amplitude-Comparison Monopulse (ACM)

refinement of the angular accuracy with a single pulse.[1] Thus, since the lobing is simultaneous rather than sequential, monopulse is very efficient with respect to radar time and energy and difficult to jam or deceive, both of which are particularly important to electronically steered radars that are required to maintain simultaneous tracks on many targets as illustrated in Figure 1.2.

At a first glance, monopulse may appear as an array signal processing system as in [2] with two elements. While a phase comparison monopulse system is similar to an array with two elements, in that it receives with two spatially offset beams, monopulse systems tend to be directional, while the sensor array elements tend to be omnidirectional. The directional sensing of monopulse systems gives rise to larger antenna gains for detecting weaker signals and improved spatial resolution. Furthermore, in amplitude comparison monopulse, the sensors are colocated, and the sum and difference signals are often formed in the waveguide prior to frequency conversion and signal detection. Amplitude comparison monopulse is commonly used for many practical reasons. Note also that amplitude comparison monopulse is used in phased array radars, where the two or four squinted receive beams are formed with the array.

---

[1] The term monopulse originated with this idea of a single pulse refinement of the angular accuracy. Some confusion exists concerning monopulse radars because most monopulse radars utilize multiple pulses to form an angular measurement. It is the monopulse ratios that can be formed with each pulse that distinguishes a radar as monopulse.
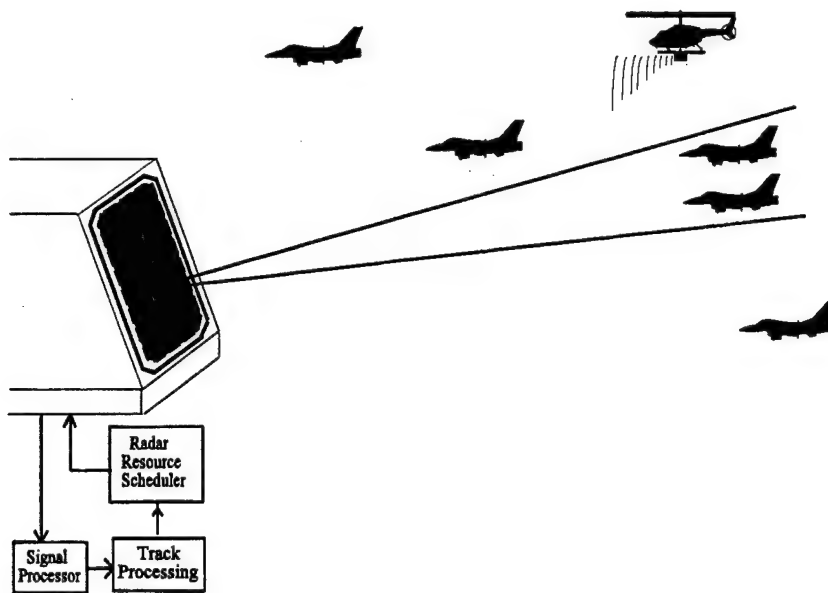
Figure 1.2 Illustration of Tracking Unresolved Targets

1.1 Monopulse Processing and Unresolved Targets

When two or more targets are closely spaced in range and angle with respect to the resolution of the radar as illustrated in Figure 1.2 with the two targets in the beam, and the target echoes interfere (*i.e.*, the echoes are not resolved in the frequency or time domains), the DOA estimate indicated by the in-phase monopulse ratio can wander far beyond the angular separation of the targets [1]. Figure 1.3 shows the trajectories of two point (fixed-amplitude and fixed-phase) targets and the in-phase monopulse measurements with no receiver noise. The measurements in Figure 1.3 were generated by perfectly pointing the radar beam at the true positions of the targets. Since the tracking of the two targets begins when the targets are resolved spatially in angle, two measurement sequences are given as if the presence of the other target was ignored. Figure 1.4 shows the quadrature (*i.e.*, imaginary part) monopulse ratios for one of the two targets shown in Figure 1.3. Note that in Figure 1.3 the targets are considered to be moving right to left, while the quadrature monopulse ratios are plotted versus time (*i.e.*, left to right) in Figure 1.4. Also, note that the trajectories were generated to give a slowly varying relative phase between the two echoes to illustrate the wander of the measurements, while for two typical targets, the relative phase of the two echoes would be random between consecutive measurements. In order to illustrate the effects of random phase and target amplitude fluctuations,

3
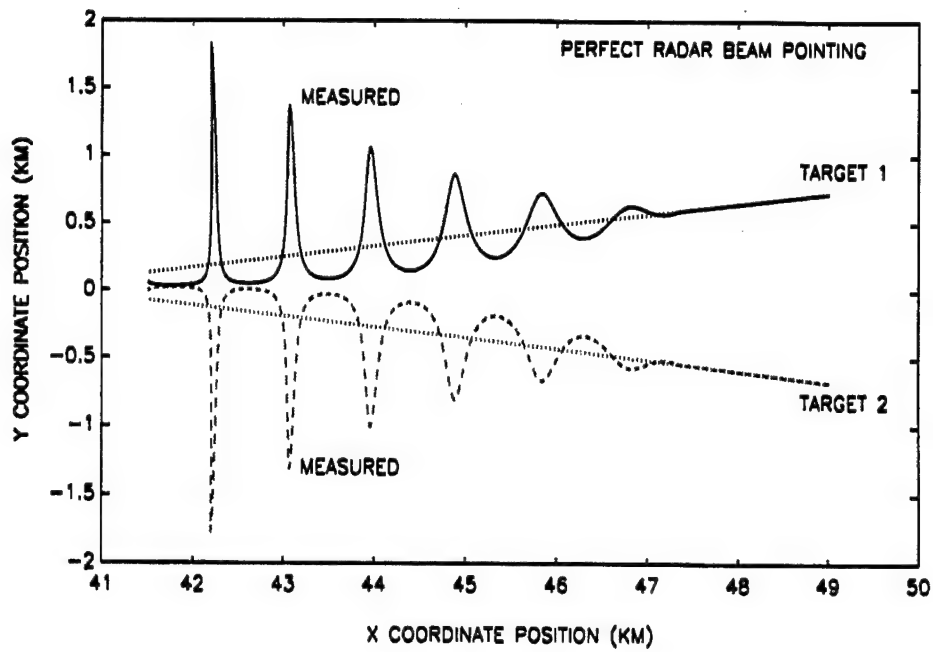
Figure 1.3 In-Phase Monopulse Measurements of Two, Closely-Spaced Point Targets
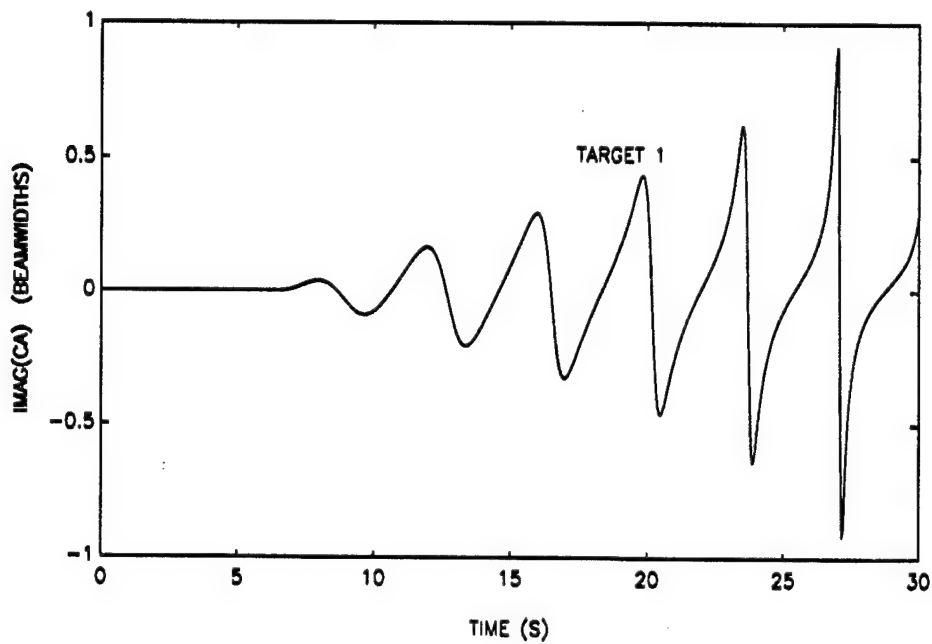
Figure 1.4 Quadrature Monopulse Measurements for One of the Two, Closely-Spaced Point Targets Shown in Figure 1.3

4

two Rayleigh targets were considered. The trajectories of the two targets are shown in Figure 1.5, where the targets are initially separated by 800 m and converge to a separation of about one-half of a beamwidth at $t = 75$ s or $x = 40$ km. An example of the measurement sequences are given in Figure 1.6, where the squares denote measurements taken by pointing at target 1, and the triangles denote measurements taken for target 2. The solid lines show the true bearing angles of the two targets, while the dashed lines denote one beamwidth of antenna pattern with the antenna boresight pointed directly at a bearing of zero. The measurements sequences were generated by perfectly pointing the antenna boresight at each target for its corresponding measurements. When the targets are separated by more than one beamwidth, measurements are easily associated with the correct target, and conventional DOA estimation and tracking works fine. At about one beamwidth separation of the two targets (i.e., $t = 25$ s), the presence of the other target adversely effects the monopulse measurements. Analysis of the time-correlated errors in the DOA measurements of Figure 1.3 and the random errors in Figure 1.6 indicates that the failure to detect the presence of the interference of a second target and address it in the DOA estimation can be catastrophic to the performance of the tracking algorithm, since its position and velocity estimates determine the association of any subsequent measurements to the target.

In addition to closely-spaced targets, the problem of unresolved targets also occurs when the DOA of a target is measured in the presence of a jammer or sea-surface-induced multipath [1,3,4]. A jammer, as denoted by the helicopter in Figure 1.2, transmits unwanted signals toward the radar to corrupt the measurements of targets between it and the radar. Typically, the jammer signals are in the form of wide-band noise or a narrow-band tone. The wide-band noise is usually modeled as a complex Gaussian process, which gives rise to a measured amplitude of the jammer that is Rayleigh distributed. The narrow-band tone is a sinusoidal signal with a fixed-amplitude, which gives rise to a measured amplitude that is Rician distributed. However, unlike the case of two closely-spaced targets, the jammer energy enters into all of the range bins (i.e., outputs of the matched filter) that surround the target. Thus, the range bins that do not include the target can be used to estimate the DOA of the jammer.

Sea-surface-induced multipath occurs when echoes received directly from the target and via the sea surface are measured in the same range bin. Typically, the
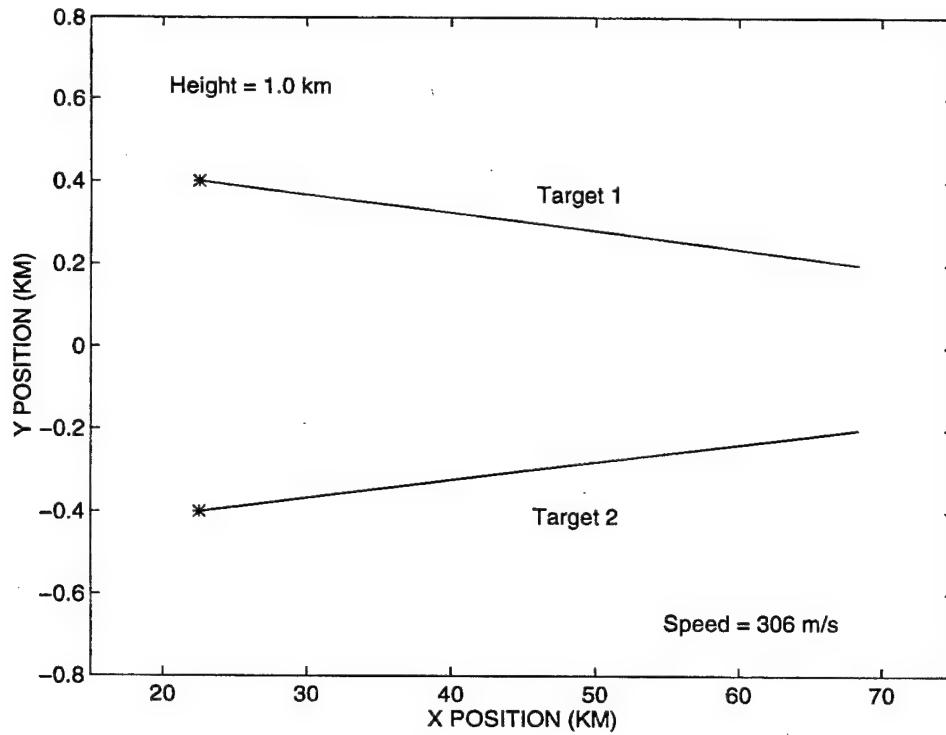
Figure 1.5 Trajectories for Two Rayleigh Targets for Illustration of Measurements
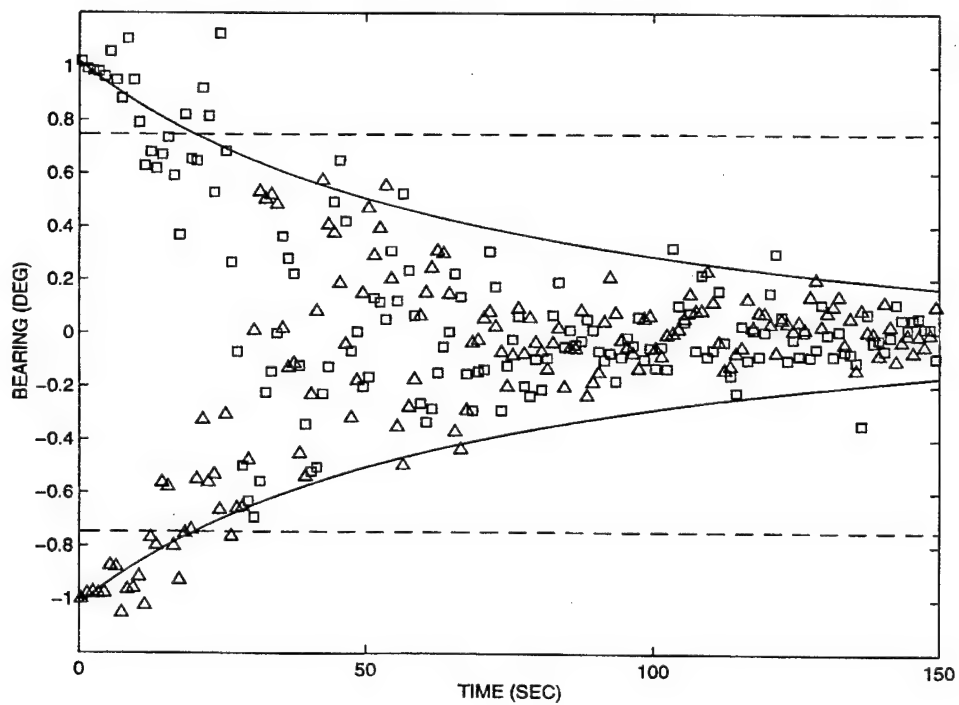
Figure 1.6 Measurement Sequences for Two Rayleigh Targets
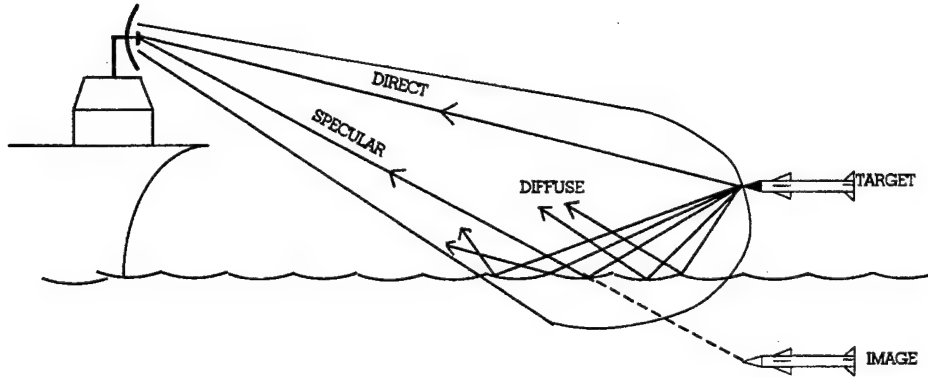
Figure 1.7 Illustration of Sea-Surface-Induced Multipath

multipath is a problem when the target is sufficiently close to the sea surface that the DOAs of the target and its image are in the main lobe of the antenna pattern as illustrated in Figure 1.7. The sea-surface reflection consists of a specular (coherent) component and a diffuse (noncoherent) component [1,5]. The specular reflection is caused by a smooth ("mirror-like") surface, and the diffuse reflection is caused by the surface irregularities. While the specular reflection coefficient is a deterministic number that depends on several unknown parameters, the diffuse reflection has a random nature that is often modeled as a complex Gaussian process. Generally, the sea surface is perturbed by small irregularities, and both reflection components are present. In contrast to the case of two closely-spaced targets, the DOA of the image can be expressed as a function of the DOA and range of the target. Thus, this geometric constraint between the DOAs of the target and image can be used to estimate the DOA of the target.

Comparing Figures 1.3 and 1.4 suggests that the quadrature monopulse ratio contains information concerning the presence of the unresolved targets and the DOAs of both targets. However, the quadrature monopulse ratio was ignored until [4], where the complex monopulse ratio was considered for DOA estimation of unresolved targets. In [4], deterministic expressions for in-phase and quadrature monopulse ratios were used to solve for the DOAs of the two targets. However, the presence of

receiver noise and random target amplitudes and phases due to Radar Cross Section (RCS) fluctuations have severely limited the success of applications of the results in [1,4]. While numerous authors have considered multiple-beam (*i.e.*, more than two beams per angular coordinate) monopulse [6,7] or array signal processing [8] for the DOA estimation of unresolved targets, almost no success has been achieved toward a solution of this problem. The following quote from [9, p. 230] summarizes the success achieved toward this problem.

> "The other multiple-target processes covered in this section and in the references, as well as the Cramer-Rao bounds computed by Sklar and Schweppe and by Pollon, are dependent on (1) *a priori* knowledge of the number of targets present (usually restricted to two), (2) discreteness of each target, (3) high SNR, (4) precise knowledge of antenna patterns, and (5) absence of irregular or diffuse reflections, at least to the level implied by the SNR (often 40 to 50 dB). The inability of the radar designer to ensure compliance with these conditions in the real world should explain the fact that none of the techniques has been designed into practical radar equipment, although several experimental installations have been made."

While this quote is from 1975, it remains very much true in 1997. The lack of success of these previous approaches cited in [9] can be attributed to the fact that each is based on deterministic formulation and analysis of the problem with noise added in simulations. In contrast to the previous approach, a stochastic approach is taken in this dissertation. Detection and estimation algorithms are developed from problem formulations that include the receiver errors and target amplitude fluctuations. Through this alternate approach, the restrictions cited above will be relaxed. The requirement for *a priori* knowledge of the number of targets will be relaxed to one or two targets, where the presence of unresolved targets is detected, not known *a priori*. While the assumptions concerning discreteness of the targets will be continued here to limit the scope of the work, addressing extended targets with the algorithms developed here should be straightforward. The required Signal-to-Noise Ratio (SNR) will be relaxed from 40 dB to near 20 dB, which is achievable with conventional phased array radars. The requirement for precise knowledge of the antenna patterns should be relaxed to approximate knowledge of the antenna patterns, since no gradients of the antenna patterns are required. The required absence of irregular or diffuse reflec-

tions is relaxed through the inclusion of models for the target amplitude fluctuations in the problem formulations. In fact, the diffuse reflections from the sea surface will be included explicitly in the problem formulation.

Some of the limitations of the multiple target estimators as cited in [9] have been relaxed through array processing techniques (a.k.a., superresolution techniques), such as the signal subspace methods [2, p. 64]. However, the superresolution techniques require special instrumentation that is very expensive and not compatible with existing phased array radars. Thus, the focus of this research is on the use of the standard monopulse processing that exists in phased arrays and dish-type radars to track unresolved targets. Since superresolution techniques require significant amounts of radar time and energy, the results of this research can be used in future radar systems to detect the need for superresolution processing and provide initial estimates for the processing [2].

1.2 Objectives and Scope of the Research

The overall objective of this research is the development of detection and estimation algorithms needed to support the tracking (i.e., kinematic state estimation) of unresolved targets. The tracking is typically accomplished with the Kalman filter or Interacting Multiple Model (IMM) algorithm, both of which require a DOA estimate and corresponding error covariance [10, p. 209]. The error covariance, which is typically estimated also, characterizes the DOA estimate as a measurement of target location for the Kalman filter or IMM algorithm. This overall objective gives rise to the following six objectives.

- The first objective involves the estimation of the target amplitude parameters that define the amplitude fluctuations and SNR of a single target or two unresolved targets. These amplitude parameters are utilized in the estimation of the DOAs and the associated variances.

- The second objective involves discrimination of targets according to various amplitude distributions. Since the estimators of the amplitude parameters and the DOAs are dependent on the amplitude distribution, discrimination between amplitude distributions is needed.

- The third objective involves the development of the probability distribution and

statistics of the complex monopulse ratio for various cases of the amplitude distribution for a single target and two unresolved targets. These distributions are needed to develop Cramer-Rao bounds [11, p. 66] and estimators of the DOAs and the associated variances.

- The fourth objective involves estimation of the DOA and the corresponding variance for a single target with various amplitude distributions. For a single target, the in-phase monopulse ratio is typically taken as the DOA estimate, but the monopulse ratio is not, in many cases, superior to the Maximum Likelihood (ML) estimate [11, p. 65] nor the Method of Moments (MM) estimate [11, p. 151] of the DOA.

- The fifth objective involves estimation of the DOAs and the corresponding variances for two unresolved targets with various amplitude distributions.

- The sixth objective involves the detection of the presence of unresolved targets in order to relax the requirement of a *priori* knowledge of the number of targets. The detection of the presence of unresolved targets will be limited to two Rayleigh, since Rayleigh targets represent the worst case.

The focus of this research is the development of detection and estimation algorithms that can be implemented in existing monopulse radars rather than techniques that will require a new radar system. Thus, the following assumptions will be made concerning the radar system.

- The radar waveforms consist of narrow-band pulses that may include subpulses at slightly different frequencies.

- Only two beams per angular coordinate will be used for monopulse processing.

Since the focus of this research is the development of detection and estimation algorithms for unresolved targets and not modeling of target scattering or amplitude fluctuations, the following assumptions are made concerning the target echoes to limit the scope of the work.

- Targets are assumed to be point targets with random phases and either fixed amplitudes or amplitudes that are Rayleigh or Rician distributed.

- The energy received from a target echo is assumed to be completely contained in a single range resolution cell or bin.

- The energy received from two unresolved targets is assumed to be completely contained in a single range bin.

Note that these assumptions concerning the discreteness of the targets will be violated by most measurements of an actual radar system. However, the application of the results to extended targets should be straightforward.

Since the focus of this research is the development of detection and estimation algorithms for unresolved targets and not modeling of the environment, the following assumptions are made concerning the modeling of the environment and noise sources.

- The receiver errors are modeled as white Gaussian processes, with the errors in the in-phase and quadrature parts being independent.

- The specular reflections at the sea surface are deterministic in amplitude and phase.

- The diffuse reflections are a complex Gaussian process that gives rise to reflections with a uniformly distributed phase and a Rayleigh amplitude.

1.3 Organization of the Report

Background material on monopulse radar systems is given in Chapter 2. The sum and difference signals are formulated, and the popular Swerling models for RCS fluctuations are presented along with estimators for the amplitude parameters of Swerling targets. Rician targets are defined, and the sum and difference signals for M unresolved Rician targets are formulated. The geometry and parameters associated with sea-surface-induced multipath are presented, and conventional monopulse processing for DOA estimation is summarized.

In Chapter 3, estimation of the target amplitude parameters, which define the SNR of the target, and discrimination between various models for the target amplitude fluctuations are considered. The PDF of the measured amplitude of the sum signal is developed for M unresolved Rician targets, which are each composed of a fixed-amplitude part and a Rayleigh part. The PDF and associated statistics of the

measured amplitude are used to develop Cramer-Rao bounds, ML estimators and/or MM estimators for the amplitude parameters of Rayleigh, fixed-amplitude, and Rician targets as well as a new dominant-plus-Rayleigh model, which is proposed as an alternative to the Erlang distribution of Swerling 3 and 4 targets. The waveform requirements for reliable discrimination between Rayleigh, fixed-amplitude, and dominant-plus-Rayleigh targets are considered. The PDF of the measured amplitude of two unresolved Rician targets is studied, and an MM estimator is presented for the amplitudes of two unresolved, fixed-amplitude targets. The PDF of the measured amplitude of a fixed-amplitude target in the presence of multipath is presented, and MM estimators of the target amplitude and relative phase of the target and sea-surface echoes are developed. The performances of the estimators are illustrated via Monte Carlo simulations, where the numbers of experiments were chosen to achieve stable results.

In Chapter 4, the amplitude-conditioned joint PDF and the statistics of the in-phase and quadrature monopulse ratios are developed for M unresolved Rician targets. The term "amplitude-conditioned" denotes conditioning the PDF on the measured amplitude of the sum signal, which is known in the receiver. Conditioning the PDF of the monopulse measurements on the measured amplitude of the sum signal gives the in-phase and quadrature monopulse ratios that are approximately Gaussian random variables so that the PDF is approximately specified by the means and variances. Since the SNR of radar targets is typically unknown, the measured amplitude of the sum signal provides no information concerning the DOA of the targets. Thus, the PDF of the monopulse measurements can be conditioned on the measurement amplitude to obtain a Gaussian distribution without any loss of information. The amplitude-conditioned PDF and the statistics are given for various cases of a single target, two unresolved targets, and a fixed-amplitude target in the presence of sea-surface-induced multipath. For a single pulse and a resolved target, the in-phase and quadrature monopulse ratios are shown to be uncorrelated, non-Gaussian random variables for a nonzero DOA, and the marginal PDF of the quadrature ratio is shown to have a mean of zero and be symmetric about zero for all DOAs.

In Chapter 5, DOA estimation is considered for a single target and two unresolved targets. For a single target, the DOA estimation is considered for multiple pulses from a Rayleigh target. Single-pulse DOA estimation is also considered by using the results of Chapter 4 for a fixed-amplitude target. For two unresolved targets, DOA

estimation is considered for a Rayleigh target in the presence of a Gaussian noise jammer and two Rayleigh targets with known relative RCS.

The detection of the presence of two unresolved Rayleigh targets is considered in Chapter 6. A Generalized Likelihood Ratio Test (GLRT) is used to develop a Neyman-Pearson algorithm for the detection of the presence of unresolved Rayleigh targets, and performance predictions of the new algorithm are shown to agree closely with the results from simulation studies. The detection performance of the new algorithm is shown via simulation studies to exceed the predicted performance when the two unresolved targets have fixed amplitudes.

Conclusions are given in Chapter 7 along with suggestions for future research. The incorporation of the results of this research into the tracking of unresolved targets is specifically addressed.

Chapter 2

BACKGROUND ON MONOPULSE RADAR SYSTEMS

In order to facilitate the presentation of the material in the following chapters, some background on monopulse radar systems is given in this chapter. The sum and difference signals of a monopulse radar system are formulated for a single target in Section 2.1, while the Swerling models for RCS fluctuations are presented in Section 2.2. Expressions are developed for the measured amplitude of the sum signal, and estimators for the target amplitude parameters are presented. Rician targets are formulated in Section 2.3, while the sum and difference signals for M unresolved Rician targets are formulated in Section 2.4. The geometry and parameters associated with sea-surface-induced multipath are presented in Section 2.5. Conventional monopulse processing for DOA estimation is summarized in Section 2.6.

2.1 Sum and Difference Channels

In an amplitude comparison monopulse radar system, a pulse is transmitted directly at the predicted position of the target, and the target echo is received with two squinted beams as illustrated in Figure 1.1. Figure 2.1 shows the shapes of the sum and difference voltage patterns for either transverse or elevation of an ACM system. The ratio of the difference pattern voltage to the sum pattern voltage defines a unique off-axis angle within the mainlobe for each ratio of the measured voltages. Note that the ratio can be approximated closely as linear for off-axis angles within one half of a beamwidth of antenna boresight. The slope of the ratio in the linear region is typically called the monopulse error slope and denoted as k_m.

A typical monopulse receiver is shown in Figure 2.2, where the sum and difference signals are inputs that are formed in the waveguide prior to detection and signal processing. The analog-to-digital converters denoted by "A/D" include the match filtering associated with the radar waveforms. The measured amplitude of the sum
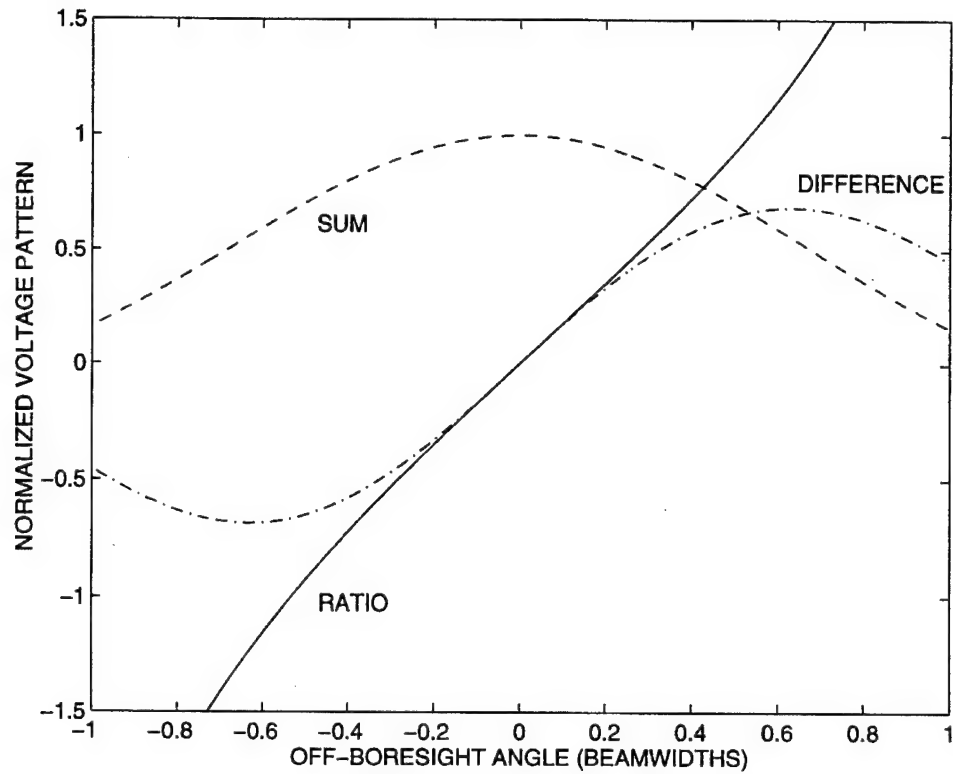
Figure 2.1 Voltage Patterns for ACM System
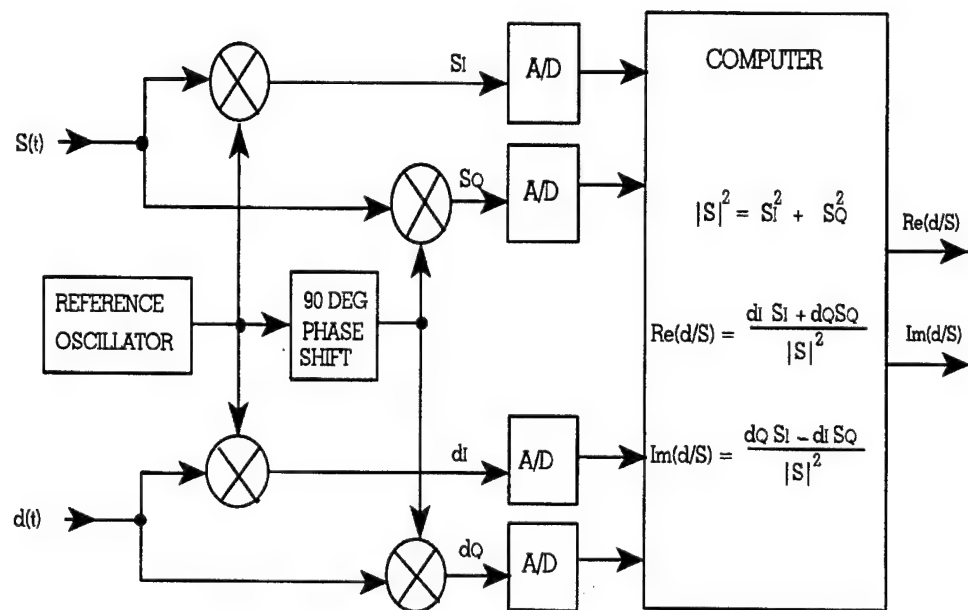
Figure 2.2 Receiver for Monopulse Radar System

16

signal denoted by $|s|^2$ is typically tested for amplitude exceedence of a threshold before the in-phase monopulse ratio denoted by $\text{Re}(d/s)$ or the quadrature monopulse ratio denoted by $\text{Im}(d/s)$ is computed. For a single target the sum and difference signals can be expressed as

$$s(t) = 2\sqrt{\kappa}AG_\Sigma^2(\theta)p(t)\,\cos(\omega_c t - \phi) + n_S(t) \tag{2.1}$$

$$d(t) = 2\sqrt{\kappa}AG_\Sigma(\theta)G_\Delta(\theta)p(t)\cos(\omega_c t - \phi) + n_d(t) \tag{2.2}$$

where

$$
\begin{aligned}
\kappa =&\ \text{constant proportional to the transmitted power} \\
A =&\ \text{voltage amplitude of the target} \\
G_\Sigma(\theta) =&\ \text{sum channel voltage gain at the angle } \theta \\
G_\Delta(\theta) =&\ \text{difference channel voltage gain at the angle } \theta \\
\theta =&\ \text{off-boresight angle of the target} \\
p(t) =&\ \text{envelope of the transmitted pulse} \\
\omega_c =&\ \text{carrier frequency of the transmitted waveform} \\
\phi =&\ \text{phase of the target echo} \\
n_S(t) =&\ \text{receiver noise in the sum channel} \\
n_d(t) =&\ \text{receiver noise in the difference channel}
\end{aligned}
$$

The output of the receiver is match filtered with gain p_0 and sampled at time t_0, and the in-phase and quadrature components of the sum and difference channels are given by

$$s_I = \sqrt{\kappa}AG_\Sigma^2(\theta)p_0\,\cos\phi + n_{SI} \tag{2.3}$$

$$s_Q = \sqrt{\kappa}AG_\Sigma^2(\theta)p_0\,\sin\phi + n_{SQ} \tag{2.4}$$

$$d_I = \sqrt{\kappa}AG_\Sigma(\theta)G_\Delta(\theta)p_0\,\cos\phi + n_{dI} \tag{2.5}$$

$$d_Q = \sqrt{\kappa}AG_\Sigma(\theta)G_\Delta(\theta)p_0\,\sin\phi + n_{dQ} \tag{2.6}$$

where

$$n_{SI} \sim N(0, \sigma_S^2) \tag{2.7}$$

$$n_{SQ} \sim N(0, \sigma_S^2) \tag{2.8}$$

$$n_{dI} \sim N(0, \sigma_d^2) \tag{2.9}$$

$$n_{dQ} \sim N(0, \sigma_d^2) \tag{2.10}$$

with $N(\mu, \sigma^2)$ denoting the Gaussian distribution with mean μ and variance σ^2. The receiver errors in (2.7) through (2.10) are assumed to be independent with the possible exception of real-valued correlation. Let

$$\rho = \frac{E[s_I d_I]}{\sigma_S \sigma_d} = \frac{E[s_Q d_Q]}{\sigma_S \sigma_d} \tag{2.11}$$

where $E[\cdot]$ denotes the expected value. Then (2.3) through (2.6) can be rewritten as

$$s_I = \alpha \cos \phi + n_{SI} \tag{2.12}$$

$$s_Q = \alpha \sin \phi + n_{SQ} \tag{2.13}$$

$$d_I = \alpha\eta \cos \phi + n_{dI} \tag{2.14}$$

$$d_Q = \alpha\eta \sin \phi + n_{dQ} \tag{2.15}$$

where

$$\alpha = \sqrt{\kappa} A G_\Sigma^2(\theta) p_0 \tag{2.16}$$

$$\eta = \frac{G_\Delta(\theta)}{G_\Sigma(\theta)} \tag{2.17}$$

Since the angle-of-arrival θ is determined from η, η is referred to as the DOA. Figures 2.3 and 2.4 give typical voltage gains $G_\Sigma(\theta)$ and $G_\Delta(\theta)$ versus the off-boresight angle for multiple beamwidths, while Figure 2.5 gives η versus the off-boresight angle. The antenna patterns were generated for uniform illumination across the antenna aperture and a squint angle that is 40 percent of the beamwidth. Figure 2.5 shows that η does not uniquely define θ if targets outside the mainlobe of the antenna pattern are considered. Since the gain of the antenna outside the mainlobe is typically less than -10 dB relative to the peak gain of the mainlobe, targets in the sidelobes are often not a problem. However, jammer signals are often strong enough to enter through the sidelobes and interfere with target measurements.

When α and ϕ are given, s_I and s_Q are jointly Gaussian random variables, with PDF given by [12, p. 126]

$$f(s_I, s_Q | \alpha, \phi, \sigma_S) = \frac{1}{2\pi\sigma_S^2} \exp\left[-\frac{1}{2\sigma_S^2}\left((s_I - \alpha \cos \phi)^2 + (s_Q - \alpha \sin \phi)^2 \right) \right] \tag{2.18}$$

Let Λ and ψ denote the measured amplitude and phase of the sum-signal channel, respectively. Then

$$s_I = \Lambda \cos \psi \tag{2.19}$$

$$s_Q = \Lambda \sin \psi \tag{2.20}$$
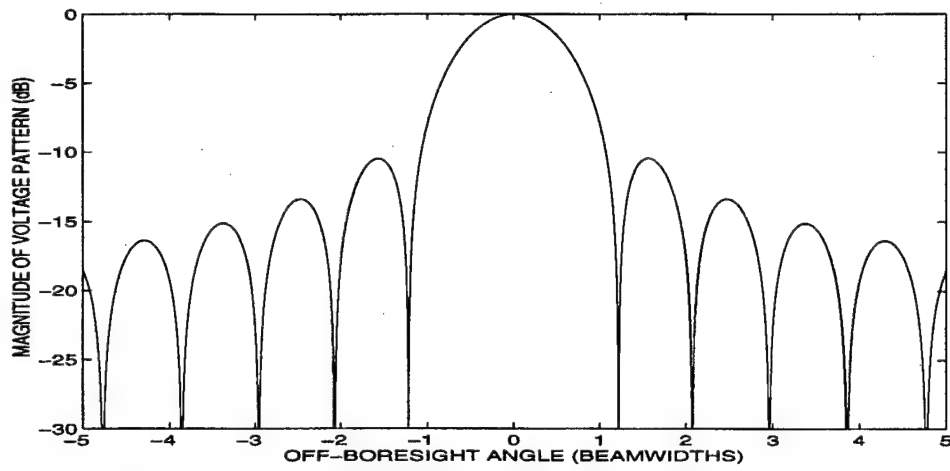
Figure 2.3 Antenna Gain Pattern in the Sum Channel
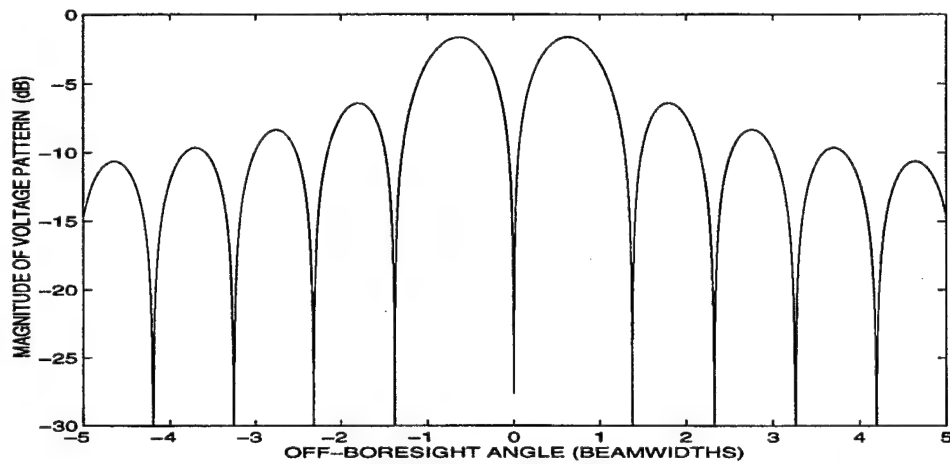
Figure 2.4 Antenna Gain Pattern in the Difference Channel
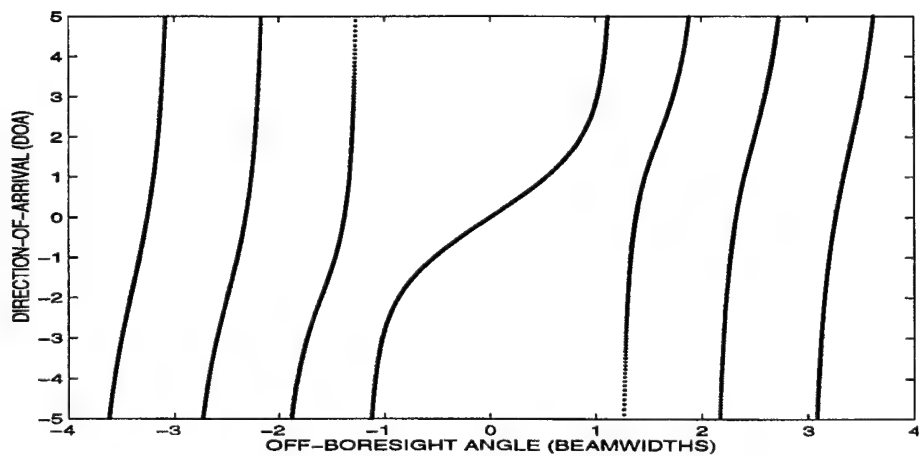
Figure 2.5 DOA Parameter Versus the Off-Boresight Angle

Note that $\Lambda = |s|$ in Figure 2.2. Performing this transformation of random variables [12, p. 143] in the PDF of s_I and s_Q gives

$$f(\Lambda, \psi | \alpha, \phi, \sigma_S) = \frac{\Lambda}{2\pi\sigma_S^2} \exp\left[\frac{\alpha\Lambda}{\sigma_S^2}\cos(\psi - \phi)\right] \exp\left\{ -\frac{\Lambda^2 + \alpha^2}{2\sigma_S^2}\right\} \qquad (2.21)$$

where $\Lambda \geq 0$, and $-\pi < \psi \leq \pi$. The phase is uniformly distributed in the interval $(-\pi, \pi]$. Integrating (2.21) with respect to ψ according to [13, No. 3.937.2] gives

$$f(\Lambda | \alpha, \sigma_S) = \frac{\Lambda}{\sigma_S^2} I_0(\alpha\Lambda\sigma_S^{-2}) \exp\left\{ -\frac{1}{2\sigma_S^2}[\Lambda^2 + \alpha^2]\right\} \qquad (2.22)$$

where $I_0(\cdot)$ is the zero-order modified Bessel function of the first kind.

The "observed SNR" is defined as

$$\Re_o = \frac{\Lambda^2}{2\sigma_S^2} \qquad (2.23)$$

Since $\Re_o$ is actually a signal-plus-noise to noise ratio, the SNR of a target will be defined as

$$\Re = E[\Re_o] - 1 \qquad (2.24)$$

where $E[\cdot]$ denotes expected value. The SNR of a fixed-amplitude target is then given by

$$\Re_F = \frac{\alpha^2}{2\sigma_S^2} \qquad (2.25)$$

Performing the transformation of a random variable [12, p. 90] of (2.23) in (2.22) and using (2.25) gives the PDF of the observed SNR as

$$f(\Re_o | \alpha, \sigma_S) = I_0(2\sqrt{\Re_o\Re_F}) \exp\{ -[\Re_o + \Re_F]\} \qquad (2.26)$$

2.2 Swerling Models for RCS Fluctuations

Since the amplitude fluctuations of the targets will be modeled for amplitude estimation and target discrimination, the popular Swerling models for RCS fluctuations are reviewed in this section. The RCS of a target is the area intercepting that amount of power[2] which, when scattered equally in all directions, produces an echo at the radar equal to that from the target [14, p. 33]. Variations in the echo signal may be

---

[2] RCS corresponds to power gain of the target, while the target amplitude of the previous section corresponds to voltage gain of the target.

caused by meteorological conditions, the lobe structure of the antenna pattern, equipment instabilities, or variations in the RCS. The RCS of typical radar targets is quite sensitive to the aspect angle, and fluctuates from pulse-to-pulse or scan-to-scan. The scan-to-scan fluctuations correspond to RCSs that are independent between scans (a.k.a., sweeps or dwells) of the radar on the target. The pulse-to-pulse fluctuations correspond to RCSs that are independent between pulses within a single scan or dwell of the radar on the target. The pulse-to-pulse fluctuations are often the result of frequency diversity in the radar waveform that is achieved through discrete-frequency coding [15, p. 269]. Each frequency-coded segment of the waveform is often referred to as a subpulse. Thus, pulse-to-pulse fluctuations are often subpulse-to-subpulse fluctuations.

Fixed-amplitude targets are often referred to as Swerling type 0. Both Swerling types 1 and 2 have RCSs that fluctuate according to the exponential distribution, where the Swerling 1 type has RCS fluctuations scan-to-scan, and the Swerling 2 has RCS fluctuations pulse-to-pulse. Note that since RCS is a power-based measure of target amplitude, the fluctuations of the voltage amplitude of the Swerling types 1 and 2 are Rayleigh distributed. Thus, the Swerling types 1 and 2 are also Rayleigh targets as discussed below. Both Swerling types 3 and 4 have RCSs that fluctuate according to the Gamma (Erlang) distribution, where the Swerling 3 type has RCS fluctuations scan-to-scan and the Swerling 4 has RCS fluctuations pulse-to-pulse. The RCS fluctuations of Swerling 3 and 4 targets are also denoted in [14, p. 407] as one-dominant-plus-Rayleigh model. This section summarizes the results of [16], which includes the PDF of the observed SNR and ML estimators of the amplitude parameters for Swerling 2 and 4 types.

Swerling Targets of Types 1 and 2

The PDF of the RCS for Swerling types 1 and 2 is given by

$$f_{Sw2}(\sigma|\sigma_{ave}) = \frac{1}{\sigma_{ave}} \exp\left[-\frac{\sigma}{\sigma_{ave}}\right], \quad \sigma \geq 0 \tag{2.27}$$

where $\sigma_{ave} \doteq E[\sigma]$ is referred to as the average RCS of the target. Figure 2.6 shows the PDF of the RCS for a Swerling 1 or 2 type target with $\sigma_{ave} = 10$. Given that $\sigma = 0.5A^2$, where A is the amplitude of the voltage gain of the target, (2.27) gives rise to pulse amplitudes that are Rayleigh distributed according to

$$f_{Sw2}(A|A_o) = f_R(A|A_o) = \frac{A}{A_o^2} \exp\left[-\frac{A^2}{2A_o^2}\right], \quad A \geq 0 \tag{2.28}$$

where $E[A^2] = 2A_o^2 = 2\sigma_{ave}$.

For Swerling 1 and 2 type targets, the target amplitude A is Rayleigh distributed with parameter A_0 and, thus, α of (2.16) is also Rayleigh distributed, with PDF given by

$$f_R(\alpha|\alpha_0) = \frac{\alpha}{\alpha_0^2}\exp\left(-\frac{\alpha^2}{2\alpha_0^2}\right) \tag{2.29}$$

where $\alpha_0 = \sqrt{\kappa}A_0 G_\Sigma^2(\theta)p_0$. Since α is Rayleigh distributed and the phase ϕ is uniformly distributed on $(-\pi, \pi]$, s_I and s_Q are independent, Gaussian random variables with means of zero and variances given by

$$E[s_I^2|\alpha_0, \sigma_S] = E[s_Q^2|\alpha_0, \sigma_S] = \alpha_0^2 + \sigma_S^2 \tag{2.30}$$

Thus, the PDF of s_I and s_Q for a Rayleigh target is given by

$$f(s_I, s_Q|\alpha_0, \sigma_S) = \frac{1}{2\pi(\alpha_0^2 + \sigma_S^2)}\exp\left[-\frac{s_I^2 + s_Q^2}{2(\alpha_0^2 + \sigma_S^2)}\right] \tag{2.31}$$

Applying the transformation of random variables of (2.19) and (2.20) in (2.31) gives

$$f_{Sw2}(\Lambda|\alpha_0, \sigma_S) = \frac{\Lambda}{\alpha_0^2 + \sigma_S^2}\exp\left[-\frac{\Lambda^2}{2(\alpha_0^2 + \sigma_S^2)}\right] \tag{2.32}$$

Applying the transformation of variable of (2.23) in (2.32) gives

$$f_{Sw2}(\Re_o|\Re_{Sw2}) = \frac{1}{\Re_{Sw2} + 1}\exp\left[-\frac{\Re_o}{\Re_{Sw2} + 1}\right] \tag{2.33}$$

where $\Re_{Sw2}$ is the SNR of a Rayleigh target and given by

$$\Re_{Sw2} = \frac{\alpha_0^2}{\sigma_S^2} \tag{2.34}$$

Thus, the observed SNR of a Rayleigh target (*i.e.*, Swerling 1 or 2 type) is exponentially distributed. The PDF of the observed SNR for a Swerling 1 or 2 type target is shown in Figure 2.7 for $\Re_{Sw2} = 10$.

For N independent pulses (*i.e.*, a Swerling 2 type target), the ML estimate [11, p. 65] of $\Re_{Sw2}$ is given by

$$\widehat{\Re}_{Sw2} = Y_N - 1 \tag{2.35}$$

where

$$Y_N = \frac{1}{N}\sum_{k=1}^{N}\Re_{ok} \tag{2.36}$$

22
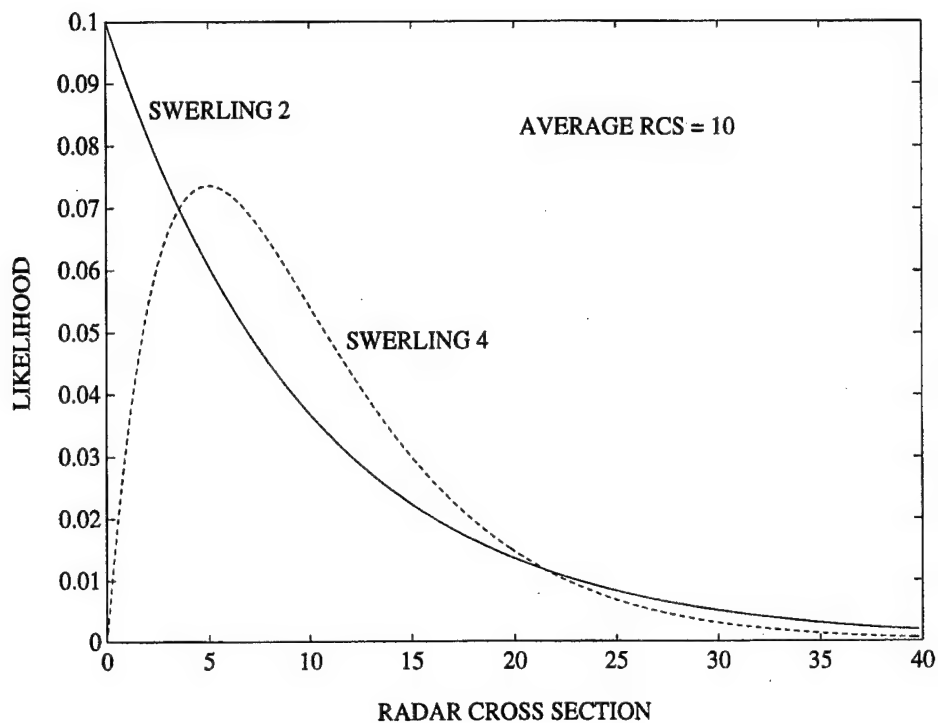
Figure 2.6 PDF of the RCS for Swerling Targets with $\sigma_{ave} = 10$
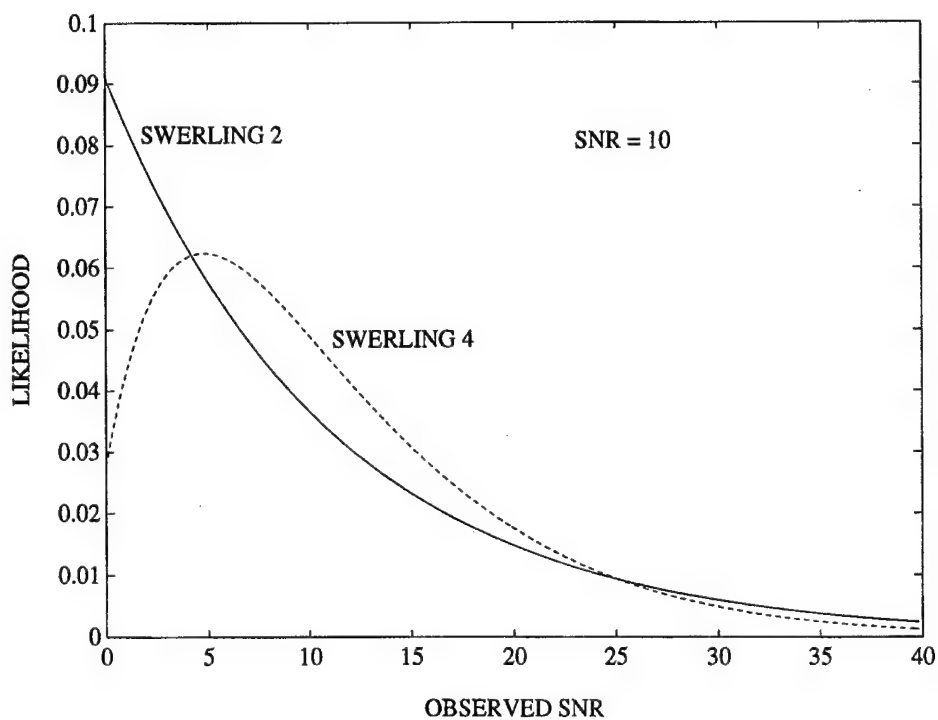
Figure 2.7 PDF of $\Re_o$ for Swerling Targets with $\Re_{Sw2} = \Re_{Sw4} = 10$

23

and $\Re_{ok}$ is the observed SNR of pulse k. The ML estimator is unbiased and efficient in that it achieves the Cramer-Rao Lower Bound [11, p. 66]. The variance of the estimator is given by

$$\text{VAR}[\widehat{\Re}_{Sw2}|\Re_{Sw2}] = \frac{(\Re_{Sw2} + 1)^2}{N} \tag{2.37}$$

Note that Swerling 2 targets are Rayleigh targets, and that Rayleigh will be used to denote these targets throughout the remainder of this report.

Swerling Targets of Types 3 and 4

The PDF of the RCS for Swerling types 3 and 4 is given by

$$f_{Sw4}(\sigma) = \frac{4\sigma}{\sigma_{ave}^2} \exp\left[-\frac{2\sigma}{\sigma_{ave}}\right], \quad \sigma \geq 0 \tag{2.38}$$

where $\sigma_{ave} = E[\sigma]$ is referred to as the average RCS of the target. Figure 2.6 shows the PDF of the RCS for a Swerling 3 or 4 type target with $\sigma_{ave} = 10$. Again, given that $\sigma = 0.5A^2$, where A is the amplitude of the voltage gain of the target, (2.38) gives rise to pulse amplitudes that are distributed according to

$$f_{Sw4}(A|A_o) = \frac{2A^3}{A_o^4} \exp\left[-\frac{A^2}{A_o^2}\right], \quad A \geq 0 \tag{2.39}$$

where $E[A^2] = 2A_o^2 = 2\sigma_{ave}$. Note that (2.39) differs from the corresponding PDF given in [15, p. 407], where $\sigma = 1.5A^2$ for Swerling 3 and 4. The definition of A was altered from that of [15] so that A_o is consistent between (2.28) and (2.39).

If a target amplitude A is distributed according to (2.39) with parameter A_0, the PDF of α in (2.16) is given by

$$f_{Sw4}(\alpha|\alpha_0) = \frac{2\alpha^3}{\alpha_0^4} \exp\left(-\frac{\alpha^2}{\alpha_0^2}\right) \tag{2.40}$$

where $\alpha_0 = \sqrt{\kappa} A_0 G^2(\theta) p_0$. Then using (2.22) and (2.40) gives

$$f_{Sw4}(\Lambda|\alpha_0, \sigma_S) = \int_0^\infty f(\Lambda|\alpha, \sigma_S) f_{Sw4}(\alpha|\alpha_0)\, d\alpha$$

$$= \frac{4\Lambda\sigma_S^2}{(\alpha_0^2 + 2\sigma_S^2)^2} \left[\frac{\alpha_0^2 \Lambda^2}{2\sigma_S^2(\alpha_0^2 + 2\sigma_S^2)} + 1\right] \exp\left[-\frac{\Lambda^2}{(\alpha_0^2 + 2\sigma_S^2)}\right] \tag{2.41}$$

Applying the transformation of variable of (2.23) in (2.41) gives

$$f_{Sw4}(\Re_o|\Re_{Sw4}) = \left[\frac{1}{(\Re_{Sw4} + 2)^2} - \frac{\Re_o}{(\Re_o + 1)} \frac{2}{(\Re_{Sw4} + 2)^3}\right]$$

$$\times 4(\Re_o + 1) \exp\left[-\frac{2\Re_o}{\Re_{Sw4} + 2}\right] \tag{2.42}$$

24

where $\Re_{Sw4}$ denotes the SNR of a Swerling 3 or 4 target. The PDF of the observed SNR for a Swerling 3 or 4 type target is shown in Figure 2.7 for $\Re_{Sw4} = 10$.

For N independent pulses (*i.e.*, Swerling 4 type target), the approximate ML estimate of $\Re_{Sw4}$ is given by

$$\widehat{\Re}_{Sw4} \approx Y_N - 1, \qquad Y_N > 4 \tag{2.43}$$

Thus, for a given $Y_N > 4$, the approximate ML estimate of the SNR of a Swerling 4 target is equal to the ML estimate of the SNR of a Swerling 2 target. The approximate ML estimator is unbiased, with variance given by

$$\mathrm{VAR}[\widehat{\Re}_{Sw4}|\Re_{Sw4}] = \frac{1}{N}(\Re_{Sw4} + 1)^2 - \frac{\Re_{Sw4}}{2N} \tag{2.44}$$

Comparing (2.37) with (2.44) indicates for a given N and $\Re_{Sw2} = \Re_{Sw4}$ that the variance of the SNR estimator for the Swerling 4 target will be slightly less than that for the Swerling 2. However, the stochastic distance between the two distributions of $\Re_o$ is rather small, as suggested by Figure 2.7 and illustrated more specifically in Section 3.3, where an alternative model for the dominant-plus-Rayleigh target is given.

2.3 Rician Targets

Rician targets are composed of a fixed-amplitude part and a Rayleigh part [17]. Thus, the in-phase and quadrature portions for the sum signal of a Rician target can be expressed as

$$s_I = \alpha \cos \phi + \beta \cos \varphi + n_{SI} \tag{2.45}$$

$$s_Q = \alpha \sin \phi + \beta \sin \varphi + n_{SQ} \tag{2.46}$$

where

$\alpha =$ amplitude from the fixed-amplitude part of the target

$\beta =$ amplitude from the Rayleigh part of the target

$\phi =$ phase of the fixed-amplitude part of the target

$\varphi =$ phase of the Rayleigh part of the target

The phase φ is independent of β and is uniformly distributed on $(-\pi, \pi]$. The Rayleigh part of the target is distributed according to

$$f(\beta|\beta_0) = \frac{\beta}{\beta_0^2} \exp\left[-\frac{\beta^2}{2\beta_0^2}\right], \qquad \beta \geq 0 \tag{2.47}$$

Since β is Rayleigh distributed, and φ is uniformly distributed on $(-\pi, \pi]$, s_I and s_Q are jointly Gaussian, independent random variables, when α and ϕ are given. Then

$$E[s_I|\alpha, \phi, \beta_0, \sigma_S] = \alpha \cos \phi \tag{2.48}$$

$$E[s_Q|\alpha, \phi, \beta_0, \sigma_S] = \alpha \sin \phi \tag{2.49}$$

$$\text{VAR}[s_I|\alpha, \phi, \beta_0, \sigma_S] = \text{VAR}[s_Q|\alpha, \phi, \beta_0] = \beta_0^2 + \sigma_S^2 \tag{2.50}$$

The PDF of s_I and s_Q is then given by [12, p. 126]

$$f(s_I, s_Q|\alpha, \phi, \beta_0, \sigma_S) = \frac{1}{2\pi(\beta_0^2 + \sigma_S^2)}$$
$$\times \exp\left[-\frac{1}{2(\beta_0^2 + \sigma_S^2)}\left((s_I - \alpha \cos\phi)^2 + (s_Q - \alpha \sin \phi)^2\right)\right] \tag{2.51}$$

Performing the transformation of random variables [12, p. 143] of (2.19) and (2.20) in the PDF of s_I and s_Q gives

$$f(\Lambda, \psi|\alpha, \phi, \beta_0, \sigma_S) = \frac{\Lambda}{2\pi(\beta_0^2 + \sigma_S^2)} \exp\left[\frac{\alpha\Lambda}{\sigma_S^2}\cos(\psi - \phi)\right] \exp\left\{-\frac{\Lambda^2 + \alpha^2}{2(\beta_0^2 + \sigma_S^2)}\right\} \tag{2.52}$$

where $\Lambda \geq 0$, and $-\pi < \psi \leq \pi$. The phase ψ is uniformly distributed in the interval $(-\pi, \pi]$. Integrating (2.52) with respect to ψ according to [13, No. 3.937.2] gives

$$f(\Lambda|\alpha, \beta_0, \sigma_S) = \frac{\Lambda}{\beta_0^2 + \sigma_S^2}I_0\left(\frac{\alpha\Lambda}{\beta_0^2 + \sigma_S^2}\right) \exp\left\{-\frac{1}{2(\beta_0^2 + \sigma_S^2)}[\Lambda^2 + \alpha^2]\right\} \tag{2.53}$$

Inserting $\sigma_S = 0$ in (2.53) shows that the voltage amplitude of the target is Rician distributed [18] or [19, p. 94]. Performing the transformation of random variable [12, p. 90] of (2.23) in (2.53), and using (2.25) gives the PDF of the observed SNR as

$$f(\Re_o|\Re_F, \Re_R) = \frac{1}{\Re_R + 1}I_0\left(\frac{2}{\Re_R + 1}\sqrt{\Re_o\Re_F}\right) \exp\left\{-\frac{1}{\Re_R + 1}[\Re_o + \Re_F]\right\} \tag{2.54}$$

where

$$\Re_F = \frac{\alpha^2}{2\sigma_S^2} \tag{2.55}$$

$$\Re_R = \frac{\beta_0^2}{\sigma_S^2} \tag{2.56}$$

Then using [13, No. 6.643.2] gives

$$E[\Re_o|\Re_F, \Re_R] = \Re_F + \Re_R + 1 \tag{2.57}$$

Thus, (2.57) and (2.24) give the SNR of a Rician target as

$$\Re = \Re_F + \Re_R \tag{2.58}$$

Thus, $\Re_F$ denotes the SNR associated with the fixed-amplitude part of the target, and $\Re_R$ denotes the SNR associated with the Rayleigh part of the target.

2.4 Unresolved Rician Targets

In a typical monopulse radar system, the outputs of the receivers are match filtered, and the in-phase and quadrature portions of the sum and difference signals for the merged measurements from M Rician targets can be expressed as

$$s_I = \sum_{i=1}^{M} \left(\alpha_i \cos \phi_i + \beta_i \cos \varphi_i \right) + n_{SI} \tag{2.59}$$

$$s_Q = \sum_{i=1}^{M} \left(\alpha_i \sin \phi_i + \beta_i \sin \varphi_i \right) + n_{SQ} \tag{2.60}$$

$$d_I = \sum_{i=1}^{M} \left(\alpha_i \eta_i \cos \phi_i + \beta_i \eta_i \cos \varphi_i \right) + n_{dI} \tag{2.61}$$

$$d_Q = \sum_{i=1}^{M} \left(\alpha_i \eta_i \sin \phi_i + \beta_i \eta_i \sin \varphi_i \right) + n_{dQ} \tag{2.62}$$

where

$$\alpha_i = \text{amplitude from the fixed-amplitude part of target } i$$
$$\beta_i = \text{amplitude from the Rayleigh part of target } i$$
$$\phi_i = \text{phase of the fixed-amplitude part of target } i$$
$$\varphi_i = \text{phase of the Rayleigh part of target } i$$
$$\eta_i = \frac{G\Delta(\theta_i)}{G_\Sigma(\theta_i)} = \text{DOA parameter of target } i$$
$$\theta_i = \text{off-boresight angle of target } i$$

The phases, φ_i, are independent and uniformly distributed on $(-\pi, \pi]$. The Rayleigh parts of the target amplitudes are also independent, and PDF of the Rayleigh part of target i is given by

$$f(\beta_i|\beta_{i0}) = \frac{\beta_i}{\beta_{i0}^2} \exp\left[-\frac{\beta_i^2}{2\beta_{i0}^2} \right], \quad \beta_i \geq 0 \tag{2.63}$$

Since β_i are Rayleigh distributed, and the φ_i are uniformly distributed on $(-\pi, \pi]$; s_I, s_Q, d_I, and d_Q are jointly Gaussian, independent random variables when the α_i and ϕ_i are given. Let

$$\bar{s}_I = E[s_I|\Psi, \Phi] = \sum_{i=1}^{M} \alpha_i \cos \phi_i \tag{2.64}$$

$$\bar{s}_Q = E[s_Q | \Psi, \Phi] = \sum_{i=1}^{M} \alpha_i \sin \phi_i \qquad (2.65)$$

$$\bar{d}_I = E[d_I | \Psi, \Phi] = \sum_{i=1}^{M} \alpha_i \eta_i \cos \phi_i \qquad (2.66)$$

$$\bar{d}_Q = E[d_Q | \Psi, \Phi] = \sum_{i=1}^{M} \alpha_i \eta_i \sin \phi_i \qquad (2.67)$$

where Ψ is the parameter set $\{\alpha_1, \beta_{10}, \eta_1, \ldots, \alpha_M, \beta_{M0}, \eta_M, \sigma_S, \sigma_d\}$, and Φ is the parameter set $\{\phi_1, \ldots, \phi_M, \}$. Also, let

$$p_{11} = \text{VAR}[s_I | \Psi, \Phi] = \text{VAR}[s_Q | \Psi, \Phi] = \sum_{i=1}^{M} \beta_{i0}^2 + \sigma_S^2 \qquad (2.68)$$

$$p_{22} = \text{VAR}[d_I | \Psi, \Phi] = \text{VAR}[d_Q | \Psi, \Phi] = \sum_{i=1}^{M} \eta_i^2 \beta_{i0}^2 + \sigma_d^2 \qquad (2.69)$$

$$p_{12} = \text{COV}[s_I, d_I | \Psi, \Phi] = \text{COV}[s_Q, d_Q | \Psi, \Phi] = \sum_{i=1}^{M} \eta_i \beta_{i0}^2 + \rho \sigma_S \sigma_d \qquad (2.70)$$

where $\text{VAR}[\cdot]$ denotes variance, and $\text{COV}[\cdot, \cdot]$ denotes covariance. Note that

$$\text{COV}[s_I, s_Q | \Psi, \Phi] = \text{COV}[d_I, d_Q | \Psi, \Phi] = 0 \qquad (2.71)$$

and

$$\text{COV}[s_I, d_Q | \Psi, \Phi] = \text{COV}[d_I, s_Q | \Psi, \Phi] = 0 \qquad (2.72)$$

2.5 Sea-Surface-Induced Multipath

The signal received from a low elevation target in the presence of sea-surface-induced multipath includes four components [20, 21] as shown in Figure 1.5. The first part travels directly to the target and returns directly to the radar, while the second part travels to the target via the sea surface and returns directly to the radar. The third part travels directly to the target and returns to the radar via the sea surface, while the fourth part travels to the target via the sea surface and returns to the radar via the sea surface. In the presence of sea-surface-induced multipath, the in-phase and quadrature portions of the sum and difference signals are given by

$$
\begin{aligned}
s_I = \alpha_t \cos\phi &+ 2\alpha_t g\rho_S \cos(\phi + \Delta\phi) + \alpha_t (g\rho_S)^2 \cos(\phi + 2\Delta\phi) \\
&+ 2\alpha_t g\rho_d \cos(\phi + \phi_d + \Delta\phi) + \alpha_t (g\rho_d)^2 \cos(\phi + 2\phi_d + 2\Delta\phi) + n_{SI} \qquad (2.73)
\end{aligned}
$$

$$s_Q = \alpha_t \sin\phi + 2\alpha_t g \rho_S \sin(\phi + \Delta\phi) + \alpha_t (g\rho_S)^2 \sin(\phi + 2\Delta\phi)$$
$$+ 2\alpha_t g \rho_d \sin(\phi + \phi_d + \Delta\phi) + \alpha_t (g\rho_d)^2 \sin(\phi + 2\phi_d + 2\Delta\phi) + n_{SQ} \qquad (2.74)$$

$$d_I = \alpha_t \eta_t \cos\phi + \alpha_t(\eta_t + \eta_I)g\rho_S \cos(\phi + \Delta\phi) + \alpha_t \eta_I (g\rho_S)^2 \cos(\phi + 2\Delta\phi)$$
$$+ \alpha_t(\eta_t + \eta_I)g\rho_d \cos(\phi + \phi_d + \Delta\phi) + \alpha_t \eta_I (g\rho_d)^2 \cos(\phi + 2\phi_d + 2\Delta\phi) + n_{dI} \quad (2.75)$$

$$d_Q = \alpha_t \eta_t \sin\phi + \alpha_t(\eta_t + \eta_I)g\rho_S \sin(\phi + \Delta\phi) + \alpha_t \eta_I (g\rho_S)^2 \sin(\phi + 2\Delta\phi)$$
$$+ \alpha_t(\eta_t + \eta_I)g\rho_d \sin(\phi + \phi_d + \Delta\phi) + \alpha_t \eta_I (g\rho_d)^2 \sin(\phi + 2\phi_d + 2\Delta\phi) + n_{dQ} \quad (2.76)$$

where

$\alpha_t = $ amplitude of the target echo in the absence of multipath

$\phi = $ phase of the directly returned signal echo

$\theta_t = $ off-boresight angle of the target

$\theta_I = $ off-boresight angle of the target's image

$\eta_t = \dfrac{G_\Delta(\theta_t)}{G_\Sigma(\theta_t)} = $ DOA of the target

$\eta_I = \dfrac{G_\Delta(\theta_I)}{G_\Sigma(\theta_I)} = $ DOA of the target's image

$g = \dfrac{G_\Sigma(\theta_I)}{G_\Sigma(\theta_t)}$

$\Delta\phi = $ phase difference between the direct and specular reflections

$\phi_d = $ uniformly distributed phase of the diffuse reflections

$\rho_S = $ specular reflection coefficient

$\rho_d = $ Rayleigh diffuse reflection coefficient with Rayleigh parameter ρ_{d0}

The first term on the right side of (2.73) and (2.74) corresponds to the echo received directly from the target, while the second and third terms correspond to the three echoes that are the result of the specular reflection at the sea surface. The fourth and fifth terms represent three echoes that result from the diffuse reflections at the sea surface. The phase information associated with ϕ in the fourth and fifth terms is lost due to the presence of the random phase, ϕ_d. In the difference signals of (2.75) and (2.76), the second and fourth terms on the right side of (2.73) and (2.74) include echoes from two different DOAs, η_t and η_I. The $\Delta\phi$ includes the phase difference due to both the Path-Length Difference (PLD) and the specular reflection at the sea surface, which is approximately π. Both ρ_S and ρ_{d0} depend on the sea state, properties of the seawater, polarization of the transmitted waveform, grazing angle at the point of the sea-surface reflection, and wavelength λ of the carrier.

Following the development in [21], the PLD is given by

$$\Delta r = r_{t1} + r_{t2} - r_t \tag{2.77}$$

where

$r_{t1} =$ distance from the radar to the sea-surface reflection point

$r_{t2} =$ distance from the target to the sea-surface reflection point

$r_t =$ distance from the radar to the target

In simulations, the r_t is known, and r_{t1} and r_{t2} are found by simultaneously solving

$$r_{t2}(2r_e h_r + h_r^2 - r_{t1}^2) = r_{t1}(2r_e h_t + h_t^2 - r_{t2}^2) \tag{2.78}$$

$$r_e^2[(r_{t1} + r_{t2})^2 - r_t^2] = (2r_e h_r + h_r^2 - r_{t1}^2)(2r_e h_t + h_t^2 - r_{t2}^2) \tag{2.79}$$

where

$r_e =$ radius of the earth

$h_r =$ height of the radar above the sea surface

$h_t =$ height of the target above the sea surface

Then r_{t1} is used to compute the grazing angle as

$$\psi_{ga} = \sin^{-1}\left(\frac{2r_e h_r + h_r^2 - r_{t1}^2}{2r_e r_{t1}}\right) \tag{2.80}$$

The elevation angle of the target's image is given as

$$E_I = E_t - \sin^{-1}\left(\frac{r_{t2}}{r_t} \sin 2\psi_{ga}\right) \tag{2.81}$$

where E_t is the elevation angle of the target from the radar. The off-boresight angles (*i.e.*, angles of arrival) θ_t and θ_I are related to the elevation angles by

$$\theta_t = E_t - E_0 \tag{2.82}$$

$$\theta_I = E_I - E_0 \tag{2.83}$$

where E_0 is the elevation angle of the antenna boresight.

The specular reflection coefficient is computed as

$$\rho_S = \begin{cases} \Gamma \exp(-8\pi^2 g_o^2), & 0 < g_o < 0.1 \\ \Gamma \dfrac{0.81254}{1 + 8\pi^2 g_o^2}, & g_o \geq 0.1 \end{cases} \tag{2.84}$$

Table 2.1 Numerical Values for Multipath Parameters

	10 C	20 C	UNITS
ϵ_S	72.2	69.1	–
τ	1.21×10^{-11}	9.21×10^{-12}	s
σ_i	3.6×10^{10}	4.7×10^{10}	s^{-1}

where

$$g_o = \frac{\sigma_h}{\lambda} \sin \psi_{ga} \tag{2.85}$$

$$\Gamma = \begin{cases} \Gamma_V, & \text{vertical polarization} \\ \Gamma_H, & \text{horizontal polarization} \end{cases} \tag{2.86}$$

$$\Gamma_H = \frac{\sin \psi_{ga} - \sqrt{\epsilon_c - \cos^2 \psi_{ga}}}{\sin \psi_{ga} + \sqrt{\epsilon_c - \cos^2 \psi_{ga}}} \tag{2.87}$$

$$\Gamma_V = \frac{\epsilon_c \sin \psi_{ga} - \sqrt{\epsilon_c - \cos^2 \psi_{ga}}}{\epsilon_c \sin \psi_{ga} + \sqrt{\epsilon_c - \cos^2 \psi_{ga}}} \tag{2.88}$$

$$\epsilon_c = \frac{\epsilon_S - \epsilon_0}{1 + \omega_c^2 \tau^2} - j\left(\frac{(\epsilon_S - \epsilon_0)\omega_c\tau}{1 + \omega_c^2 \tau^2} - 4\pi \frac{\sigma_i}{\omega_c}\right) \tag{2.89}$$

$\sigma_h = $ RMS sea-surface elevation above the mean level

$\epsilon_S = $ static dielectric parameter of the seawater

$\epsilon_0 = $ 4.9 for seawater

$\tau = $ relaxation time of the seawater

$\sigma_i = $ ionic conductivity of the seawater

Table 2.1 gives numerical values for ϵ_S, τ, and σ_i at seawater temperatures of 10 C and 20 C. The Rayleigh parameter for the diffuse reflection coefficient is computed as

$$\rho_{d0} = \begin{cases} \sqrt{2}|\Gamma|3.68g_o, & 0 < g_o < 0.1 \\ \sqrt{2}|\Gamma|(0.454 - 0.858g_o), & 0.1 \leq g_o < 0.5 \\ \sqrt{2}|\Gamma|0.025, & g_o \geq 0.5 \end{cases} \tag{2.90}$$

2.6 Monopulse Processing for DOA Estimation

In this section, conventional monopulse processing for DOA estimation is summarized. In a typical monopulse system, the angle of arrival θ is approximated by

$$\theta \approx \frac{\theta_{BW}}{k_m}\eta \tag{2.91}$$

where $1 < k_m < 2$, and θ_{BW} is the 3-dB beamwidth of the antenna pattern (i.e., the angle between the two one-half power points of the antenna pattern). The linear approximation to the monopulse error function is usually appropriate for $-0.75\theta_{BW} \leq \theta \leq 0.75\theta_{BW}$. Denoting $s = s_I + js_Q$ and $d = d_I + jd_Q$, the in-phase and quadrature parts of the monopulse ratio are given by

$$y_I = \text{Re}(\frac{d}{s}) = \frac{d_I s_I + s_Q d_Q}{s_I^2 + s_Q^2} \tag{2.92}$$

$$y_Q = \text{Im}(\frac{d}{s}) = \frac{d_Q s_I - d_I s_Q}{s_I^2 + s_Q^2} \tag{2.93}$$

Typically, y_I is taken as the estimate of the DOA, which gives the angle-of-arrival estimate as

$$\hat{\theta} = \frac{\theta_{BW}}{k_m}y_I \tag{2.94}$$

The variance of y_I is often reported in the literature [1, p. 309] as

$$\sigma_{y_I}^2 \approx \frac{1}{2\Re}\left[\frac{\sigma_d^2}{\sigma_S^2} + \eta^2 - 2\rho\frac{\sigma_d}{\sigma_S}\right], \quad \Re > 13 \text{ dB} \tag{2.95}$$

where $\Re$ is the SNR of the sum channel. Estimates of the variance of y_I are often computed by setting $\eta = y_I$ in (2.95). An estimate of the variance of the angle of arrival is given by (2.94) and (2.95) as

$$\sigma_{\hat{\theta}}^2 \approx \frac{\theta_{BW}^2}{k_m^2}\sigma_{y_I}^2, \quad \Re > 13 \text{ dB} \tag{2.96}$$

Several authors [1,4-6] have shown that y_I is a notably biased estimate of DOA at moderate and low SNR. The bias is often reported in the literature [1, p. 305] as

$$E[y_I] - \eta = (\rho\frac{\sigma_d}{\sigma_S} - \eta)\exp[-\Re] \tag{2.97}$$

Seifer showed in [4,5] that (2.97) is an optimistic assessment of the bias when the measured amplitude of the sum signal is subjected to a threshold test prior to monopulse processing.

This completes of the background material on monopulse radar systems. Estimation of the target amplitude parameters and discrimination between various amplitude distributions are considered in the next chapter.

Chapter 3

TARGET AMPLITUDE ESTIMATION
AND DISCRIMINATION

The DOA estimation developed in Chapter 5 depends on the amplitude distribution and its parameters. Thus, this chapter addresses the estimation of the target amplitude parameters, which define the SNR, and discrimination between various models for the amplitude fluctuations. The interest in target amplitude or RCS and the distribution of its fluctuations has been motivated by the need to develop Receiver Operating Characteristic (ROC) curves for radar system design [14, p. 46]. In the design process, the amplitude distribution of the targets of interest and the corresponding ROC curves are used to design the radar system, which includes the power of the transmitter, waveforms, detection threshold, etc. The inflexibility of this hardware has limited the dynamic optimization of the system for each target and, thus, real-time or on-line estimation of the target amplitude parameters and discrimination between amplitude distributions have received little attention. However, with the advent of new hardware and digital signal processing, dynamic optimization of the system for each target is now feasible.

The Probability Density Function (PDF) of the measured amplitude of the sum signal is presented for M unresolved Rician targets, which are each composed of a fixed-amplitude part and a Rayleigh part. The PDF and associated statistics of the measured amplitude are used to develop Cramer-Rao Lower Bounds (CRLBs), ML estimators and/or MM estimators for the amplitude parameters of Rayleigh, fixed-amplitude, and Rician targets as well as a new dominant-plus-Rayleigh model, which is proposed as an alternative to the Erlang distribution of Swerling 3 and 4 targets. The waveform requirements for reliable discrimination between Rayleigh, fixed-amplitude, and dominant-plus-Rayleigh targets are considered. The PDF of the measured amplitude of two unresolved Rician targets is studied, and an MM estimator is developed for the amplitudes of two unresolved, fixed-amplitude targets.

The PDF and statistics of the measured amplitude of a fixed-amplitude target in the presence of multipath is also presented, and MM estimators of the target amplitude and relative phase of the target and the sea-surface echoes are developed.

In a typical monopulse radar system, the outputs of the receivers are match filtered, and the in-phase and quadrature components of the sum signal for the merged measurements from M Rician targets can be expressed as

$$s_I = \sum_{i=1}^{M} \left(\alpha_i \cos \phi_i + \beta_i \cos \varphi_i \right) + n_{SI} \tag{3.1}$$

$$s_Q = \sum_{i=1}^{M} \left(\alpha_i \sin \phi_i + \beta_i \sin \varphi_i \right) + n_{SQ} \tag{3.2}$$

where

$$\alpha_i = \text{ amplitude from the fixed-amplitude part of target } i$$

$$\beta_i = \text{ amplitude from the Rayleigh part of target } i$$

$$\phi_i = \text{ phase of the fixed-amplitude part of target } i$$

$$\varphi_i = \text{ phase of the Rayleigh part of target } i$$

$$n_{SI} \sim N(0, \sigma_S^2)$$

$$n_{SQ} \sim N(0, \sigma_S^2)$$

with $N(\bar{x}, \sigma_x^2)$ denoting a Gaussian distribution with mean $\bar{x}$ and variance σ_x^2. Also, with $E[\cdot]$ denoting expected value,

$$E[n_{SI} n_{SQ}] = 0 \tag{3.3}$$

The phases φ_i are independent and uniformly distributed on $(-\pi, \pi]$. The Rayleigh parts of the target amplitudes are also independent, and the PDF of the Rayleigh part of target i is given by

$$f(\beta_i | \beta_{i0}) = \frac{\beta_i}{\beta_{i0}^2} \exp\left[-\frac{\beta_i^2}{2\beta_{i0}^2} \right], \quad \beta_i \geq 0 \tag{3.4}$$

where β_{i0} is the Rayleigh parameter of target i. Since β_i are Rayleigh distributed, and the φ_i are uniformly distributed on $(-\pi, \pi]$, s_I and s_Q are jointly Gaussian, independent random variables when the α_i and ϕ_i are given.

Since s_I and s_Q are jointly Gaussian, independent random variables given the α_i and ϕ_i, the PDF of s_I and s_Q is fully defined the means and variances. Let

$$\bar{s}_I = E[s_I | \Theta, \Phi] = \sum_{i=1}^{M} \alpha_i \cos \phi_i \tag{3.5}$$

$$\bar{s}_Q = E[s_Q|\Theta, \Phi] = \sum_{i=1}^{M} \alpha_i \sin \phi_i \tag{3.6}$$

where Θ denotes the parameter set $\{\alpha_1, \beta_{10}, \ldots, \alpha_M, \beta_{M0}, \sigma_S\}$ and Φ denotes the parameter set $\{\phi_1, \ldots, \phi_M\}$ Also, let

$$p_{11} = \text{VAR}[s_I|\Theta, \Phi] = \text{VAR}[s_Q|\Theta, \Phi] = \sum_{i=1}^{M} \beta_{i0}^2 + \sigma_S^2 \tag{3.7}$$

where $\text{VAR}[\cdot]$ denotes variance. With $\text{COV}[\cdot, \cdot]$ denoting covariance, note that

$$\text{COV}[s_I, s_Q|\Theta, \Phi] = 0 \tag{3.8}$$

Letting Λ and ψ denote the measured amplitude and phase of the sum signal gives

$$s_I = \Lambda \cos \psi \tag{3.9}$$

$$s_Q = \Lambda \sin \psi \tag{3.10}$$

where $-\pi < \psi \leq \pi$. Writing the measured amplitude of the sum signal in the form of SNR gives

$$\Re_o = \frac{\Lambda^2}{2\sigma_S^2} \tag{3.11}$$

where $\Re_o$ is referred to as the observed SNR. From Section 2.4, the SNR of Rician target i is given as

$$\Re_i = \Re_{Fi} + \Re_{Ri} \tag{3.12}$$

where

$$\Re_{Fi} = \frac{\alpha_i^2}{2\sigma_S^2} \tag{3.13}$$

$$\Re_{Ri} = \frac{\beta_{i0}^2}{\sigma_S^2} \tag{3.14}$$

The $\Re_{Fi}$ denotes the SNR associated with the fixed-amplitude part of target i, and $\Re_{Ri}$ denotes the SNR associated with the Rayleigh part of target i. Also, let

$$\Re_F = \sum_{i=1}^{M} \Re_{Fi} \tag{3.15}$$

$$\Re_R = \sum_{i=1}^{M} \Re_{Ri} \tag{3.16}$$

The following theorem gives the PDF, mean, and variance of $\Re_o$, when s_I and s_Q are Gaussian. The development of the PDF of the observed SNR $\Re_o$ utilizes the PDF of the measured amplitude Λ, which is derived by applying the transformation of random variables of (3.9) and (3.10) in the PDF of s_I and s_Q, and integration of the results with respect to ψ.

Theorem 3.1 Let the in-phase and quadrature signals s_I and s_Q be Gaussian signals with

$$\bar{s}_I = E[s_I|\Theta, \Phi] \tag{3.17}$$

$$\bar{s}_Q = E[s_Q|\Theta, \Phi] \tag{3.18}$$

$$p_{11} = E[(s_I - \bar{s}_I)^2|\Theta, \Phi] = E[(s_Q - \bar{s}_Q)^2|\Theta, \Phi] \tag{3.19}$$

and $E[(s_I - \bar{s}_I)(s_Q - \bar{s}_Q)|\Theta] = 0$, where Θ denotes the set of given parameters. Then the PDF of the measured amplitude of the signal is given by

$$f(\Lambda|\Theta, \Phi) = \frac{\Lambda}{p_{11}} I_0\left(\frac{\Lambda}{p_{11}}\sqrt{\bar{s}_I^2 + \bar{s}_Q^2}\right) \exp\left[-\frac{1}{2p_{11}}(\Lambda^2 + \bar{s}_I^2 + \bar{s}_Q^2)\right] \tag{3.20}$$

where $I_0(\cdot)$ is the zero-order modified Bessel function of the first kind. The PDF of the observed SNR of the signal is given by

$$f(\Re_o|\Theta, \Phi) = \frac{1}{\Re_R + 1} I_0\left(\frac{2\sqrt{\Re_o}}{\Re_R + 1}\sqrt{\frac{\bar{s}_I^2}{2\sigma_S^2} + \frac{\bar{s}_Q^2}{2\sigma_S^2}}\right) \exp\left[-\frac{1}{\Re_R + 1}\left(\Re_o + \frac{1}{2\sigma_S^2}(\bar{s}_I^2 + \bar{s}_Q^2)\right)\right] \tag{3.21}$$

and

$$E[\Re_o|\Theta, \Phi] = \frac{1}{2\sigma_S^2}(\bar{s}_I^2 + \bar{s}_Q^2) + p_{11}$$

$$= \frac{1}{2\sigma_S^2}(\bar{s}_I^2 + \bar{s}_Q^2) + \Re_R + 1 \tag{3.22}$$

$$\text{VAR}[\Re_o|\Theta, \Phi] = p_{11}\left(\frac{1}{\sigma_S^2}(\bar{s}_I^2 + \bar{s}_Q^2) + p_{11}\right)$$

$$= \left(\Re_R + 1\right)\left(\frac{1}{\sigma_S^2}(\bar{s}_I^2 + \bar{s}_Q^2) + \Re_R + 1\right) \tag{3.23}$$

Proof: See Theorem A.1 of Appendix A.

The results of Theorem 3.1 are utilized in this chapter to develop the CRLBs, ML, and MM estimators for the amplitude parameters of various amplitude distributions, and discrimination algorithms for various amplitude distributions. In Section 3.1, M unresolved Rayleigh targets are considered. A fixed-amplitude target is considered

in Section 3.2, while the new dominant-plus-Rayleigh target is considered in Section 3.3. The waveform requirements for reliable discrimination between Rayleigh, fixed-amplitude, and dominant-plus-Rayleigh targets are considered in Section 3.4, and an example of discrimination is given in Section 3.5. A single Rician target is considered in Section 3.6, while the PDF of the measured amplitude of two unresolved Rician targets is studied in Section 3.7. An MM estimator for the amplitudes of two unresolved, fixed-amplitude targets is developed in Section 3.8, while the PDF and statistics of the measured amplitude of a fixed-amplitude target in the presence of multipath are presented in Section 3.9.

3.1 Rayleigh Targets

The in-phase and quadrature components of the sum signal for M unresolved Rayleigh targets is given by (3.1) and (3.2) with $\alpha_i = 0$ for all i. Then $\bar{s}_I = 0$, $\bar{s}_Q = 0$ and (3.20) indicates that the measured amplitude of M unresolved Rayleigh targets in the presence of Gaussian receiver noise is also Rayleigh distributed. Setting $\bar{s}_I = \bar{s}_Q = 0$ in (3.21) gives the PDF of the observed SNR for M unresolved Rayleigh targets as

$$f(\Re_o|\Theta_R) = \frac{1}{\Re_R + 1} \exp\left\{ -\frac{\Re_o}{\Re_R + 1}\right\}, \quad \Re_o \geq 0 \tag{3.24}$$

where Θ_R denotes the parameter set $\{\beta_{10}, \beta_{20}, \sigma_S\}$. Setting $\bar{s}_I = \bar{s}_Q = 0$ in (3.22) and (3.23) gives

$$E[\Re_o|\Phi] = \Re_R + 1 \tag{3.25}$$

$$VAR[\Re_o|\Phi] = [\Re_R + 1]^2 \tag{3.26}$$

Since the PDF of $\Re_o$ for M unresolved Rayleigh targets is equivalent to the PDF of a single Rayleigh target, the parameter estimation for a single Rayleigh target is equivalent to that for M Rayleigh targets. Thus, for N independent samples or pulses, the ML estimate of $\Re_R$ is given by

$$\widehat{\Re}_R = arg \max_{\Re_R > 0} \prod_{k=1}^{N} f(\Re_{ok}|\Theta_R) \tag{3.27}$$

where $\Re_{ok}$ denotes the observed SNR for pulse k. Let

$$C_N(\Re_R) = \prod_{i=1}^{N} f(\Re_{ok}|\Phi) = \frac{1}{(\Re_R + 1)^N} \exp\left[-\frac{NY_N}{\Re_R + 1}\right] \tag{3.28}$$

where

$$Y_N = \frac{1}{N} \sum_{k=1}^{N} \Re_{ok} \tag{3.29}$$

Then $\widehat{\Re}_R$ satisfies

$$\frac{d}{d\Re_R} C_N(\Re_R)\Big|_{\Re_R=\widehat{\Re}_R} = 0 \tag{3.30}$$

where

$$\frac{d}{d\Re_R} C_N(\Re_R) = \left[\frac{NY_N}{(\Re_R+1)} - N\right] \left[\frac{1}{(\Re_R+1)^{N+1}}\right] \exp\left[-\frac{NY_N}{\Re_R+1}\right] \tag{3.31}$$

Thus, the ML estimate of $\Re_R$ is given by

$$\widehat{\Re}_R = Y_N - 1 = -1 + \frac{1}{N} \sum_{k=1}^{N} \Re_{ok}, \qquad Y_N \geq 1 \tag{3.32}$$

The estimator is unbiased since

$$E[\widehat{\Re}_R|\Theta_R] = -1 + \frac{1}{N} \sum_{k=1}^{N} E[\Re_{ok}|\Theta_R] = -1 + \frac{1}{N} \sum_{i=1}^{N} (\Re_R+1) = \Re_R \tag{3.33}$$

and the variance of the estimator is given by

$$\begin{aligned}
\mathrm{VAR}[\widehat{\Re}_R|\Theta_R] &= 1 - \Re_R^2 - 2E[\Re_{ok}|\Theta_R] + \frac{(N-1)}{N} E[\Re_{ok}|\Theta_R]^2 + \frac{1}{N} E[(\Re_{ok})^2|\Theta_R] \\
&= -(\Re_R+1)^2 + \frac{(N-1)}{N}(\Re_R+1)^2 + \frac{2}{N}(\Re_R+1)^2 \\
&= \frac{(\Re_R+1)^2}{N}
\end{aligned} \tag{3.34}$$

Since the variance of the estimate in (3.34) is also the CRLB for any unbiased estimate of $\Re_R$, $\widehat{\Re}_R$ is an unbiased, efficient estimator of $\Re_R$.

Since Y_N is the test statistic for the detection of Rayleigh targets with multiple subpulses at distinct frequencies, the PDF of Y_N is useful in characterizing the performance of the detector and selection of the optimal number of subpulses or frequencies for detection. The PDF of Y_N is found by first computing the characteristic function [12, p. 115], which is given by

$$\begin{aligned}
\Phi_{Y_N}(\omega) &= E\left[\exp(j\omega Y_N)\right] \\
&= E\left[\prod_{k=1}^{N} \exp\left(j\frac{\omega}{N}\Re_{ok}\right)\right] \\
&= \frac{1}{(\Re_R+1)^N} \prod_{i=1}^{N} \int_0^{\infty} \exp\left((j\frac{\omega}{N}(\Re_R+1)-1)\frac{\Re_{ok}}{\Re_R+1}\right) dY_N \\
&= \frac{N^N}{\left(1 - j\omega(\Re_R+1)\right)^N}
\end{aligned} \tag{3.35}$$
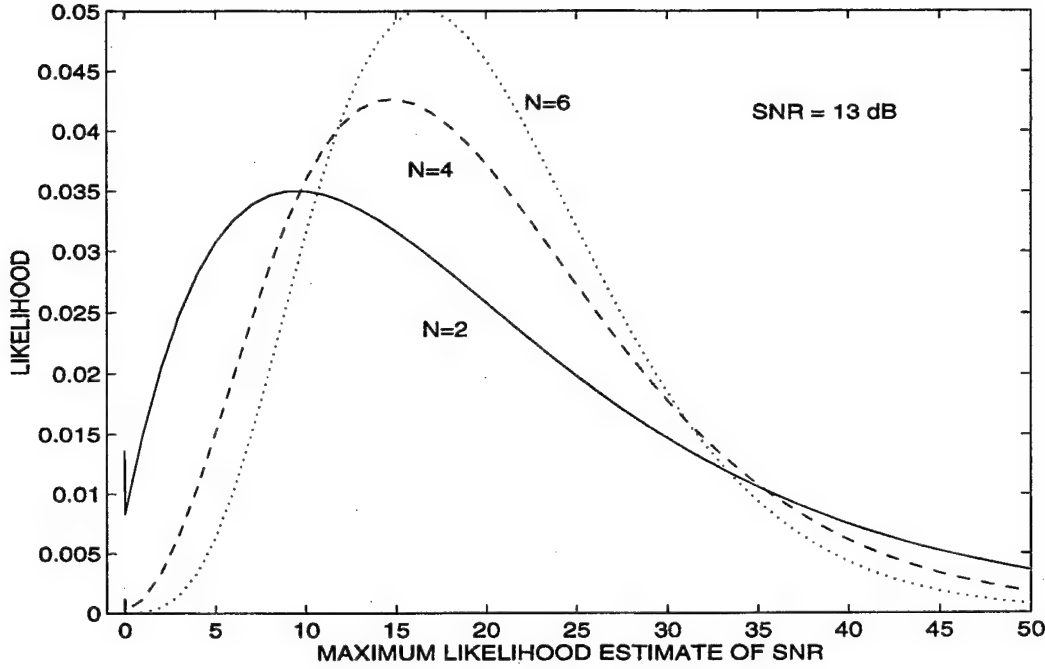
Figure 3.1   PDFs of the ML Estimates of $\Re_R$ for $N = 2$, 4, and 6

Then the PDF of Y_N is given by

$$f(Y_N|\Theta_R) = \int_{-\infty}^{\infty} \Phi_{Y_N}(w) \exp\left(-j\omega Y_N\right) d\omega$$

$$= \frac{N^N}{(\Re_R + 1)^N} \int_{-\infty}^{\infty} \left(\frac{N}{\Re_R + 1} - j\omega\right)^{-N} \exp(-j\omega Y_N) d\omega$$

$$= \frac{N^N}{(N-1)!} \frac{Y_N^{N-1}}{(\Re_R + 1)^N} \exp\left[-\frac{NY_N}{\Re_R + 1}\right], \quad Y_N > 0 \qquad (3.36)$$

which is the Erlang density. The PDF of (3.36) can be shown to be equivalent to the PDF of NY_N given in [15, p. 404].

Assigning $\widehat{\Re}_R = 0$ for $Y_N < 1.0$ gives the PDF of $\widehat{\Re}_R$ as

$$f(\widehat{\Re}_R|\Theta_R) = \delta[\widehat{\Re}_R]\left(1 - \Gamma(N, \frac{N}{\Re_R + 1})\right)$$

$$+ \frac{N^N}{(N-1)!} \frac{(\widehat{\Re}_R + 1)^{N-1}}{(\Re_R + 1)^N} \exp\left[-N\frac{\widehat{\Re}_R + 1}{\Re_R + 1}\right], \quad \widehat{\Re}_R \geq 0 \quad (3.37)$$

where $\Gamma(\cdot, \cdot)$ denotes the Incomplete Gamma function [13, p. 949], and $\delta[\cdot]$ is the Dirac delta function. While assigning $\widehat{\Re}_R = 0$ for $Y_N < 1.0$ gives an ML estimator of $\Re_R$, no claims are made concerning the efficiency of $\widehat{\Re}_R$ when $Y_N < 1.0$.

PDFs of $\widehat{\Re}_R$ are illustrated in Figure 3.1 for $N = 2$, 4, and 6 and $\Re_R = 13$ dB. Note that the PDFs of Y_N and $\widehat{\Re}_R$ given in (3.36) and (3.37) correspond to the case

Table 3.1 $\Re_{th}$ for Various Values of P_{fa} and N

Pulses	Probability of False Alarm (P_{fa})					
N	10^{-3}	10^{-4}	10^{-5}	10^{-6}	10^{-7}	10^{-8}
1	6.91	9.21	11.5	13.8	16.1	18.4
2	4.63	5.89	7.13	8.36	9.57	10.8
3	3.75	4.65	5.53	6.38	7.23	8.07
4	3.27	3.98	4.67	5.34	6.00	6.65
5	2.96	3.56	4.13	4.69	5.24	5.77
6	2.75	3.27	3.76	4.24	4.70	5.17
7	2.58	3.05	3.48	3.90	4.32	4.72
8	2.46	2.86	3.27	3.65	4.02	4.38
9	2.36	2.74	3.10	3.45	3.78	4.10
10	2.27	2.62	2.96	3.27	3.59	3.89

in which no detection threshold test other than the constraint of $\Re_R \geq 0$ has been applied to Y_N (or $\widehat{\Re}_R$), while the tracking requires a threshold test of Y_N in order to prevent the processing of false alarms. For $\Re_R = 13$ dB, $N = 4$, and a detection threshold of $\widehat{\Re}_R$ near 6 dB (or 4.0), Figure 3.1 shows that the PDF of $\widehat{\Re}_R$ will be changed very little by considering the detection threshold test. Letting $\Re_{th}$ be the detection threshold value for Y_N gives the probability of a false alarm as

$$P_{fa} = \int_{\Re_{th}}^{\infty} f(x|\Theta_R, \Re_R = 0) \ dx = \Gamma(N, N\Re_{th}) \tag{3.38}$$

and the probability of detection is given by

$$P_d = \int_{\Re_{th}}^{\infty} f(x|\Theta_R) \ dx = \Gamma(N, \frac{N\Re_{th}}{\Re_R + 1}) \tag{3.39}$$

Then, the PDF of Y_N is given by

$$f(Y_N|\Theta_R, Y_N > \Re_{th}) = \frac{N^N}{(N-1)! \ P_d} \frac{Y_N^{N-1}}{(\Re_R+1)^N} \exp\left[-\frac{NY_N}{\Re_R+1}\right] \tag{3.40}$$

Thus, the corresponding PDF of $\widehat{\Re}_R$ for $\Re_{th} > 1.0$ is given by

$$f(\widehat{\Re}_R|\Theta_R, \widehat{\Re}_R > \Re_{th}+1) = \frac{N^N}{(N-1)! \ P_d} \frac{(\widehat{\Re}_R+1)^{N-1}}{(\Re_R+1)^N} \exp\left[-N\frac{\widehat{\Re}_R+1}{\Re_R+1}\right], \quad \Re_{th} > 1.0 \tag{3.41}$$

For a radar dwell providing total SNR, $\Re_T = N\Re_R$, let N_{opt} denote the number of subpulses (*i.e.*, frequencies) that maximizes the probability of detection, P_d. Thus, the optimization problem can be stated as follows. Given $\Re_T$ and P_{fa}, find

$$N_{opt} = arg \ \max_{N>0} \ \Gamma(N, \frac{N^2\Re_{th}}{\Re_T + N}) \tag{3.42}$$

where $\Re_{th}$ is specified by

$$P_{fa} = \Gamma(N, N\Re_{th}) \tag{3.43}$$

Table 3.1 gives $\Re_{th}$ for various values of P_{fa} and N, while Table 3.2 gives P_d for $P_{fa} = 10^{-3}$ and various values of $\Re_T$ and N. The N_{opt} are denoted in Table 3.2 as bold. For a $P_{fa} = 10^{-3}$, Table 3.2 shows that for $\Re_T = 10$, $N_{opt} = 2$; for $\Re_T = 20$, $N_{opt} = 4$; and for $\Re_T = 30$, $N_{opt} = 7$. Note that for $P_{fa} = 10^{-3}$ and $\Re_R \geq 40$, $N_{opt} > 10$. Tables 3.3 through 3.7 give P_d for $P_{fa} = 10^{-4}$, 10^{-5}, 10^{-6}, 10^{-7}, 10^{-8}, and various values of $\Re_T$ and N. Thus, the results of Tables 3.2 through 3.7 show N_{opt} for $N \leq 10$ and $\Re_R \leq 50$. Note that for $P_{fa} \leq 10^{-4}$ and $\Re_T \leq 10$, $N_{opt} = 1$.

3.2 Fixed-Amplitude Target

The in-phase and quadrature components of the sum signal for a fixed-amplitude target is given by (3.1) and (3.2), with $\alpha_i = 0$ for all $i > 1$ and $\beta_i = 0$ for all i. Then

$$\bar{s}_I = E[s_I|\Theta_F, \phi_1] = \alpha_1 \cos \phi_1 \tag{3.44}$$

$$\bar{s}_Q = E[s_Q|\Theta_F, \phi_1] = \alpha_1 \sin \phi_1 \tag{3.45}$$

$$p_{11} = \text{VAR}[s_I|\Theta_F, \phi_1] = \text{VAR}[s_Q|\Theta, \phi_1] = \sigma_S^2 \tag{3.46}$$

where Θ_F denotes the parameter set $\{\alpha_1, \sigma_S\}$. Using (3.44) through (3.46) for $\bar{s}_I$, $\bar{s}_Q$, and p_{11}, and $\beta_i = 0$ for all i in (3.21) gives the PDF of the observed SNR for fixed-amplitude target as

$$f(\Re_o|\Theta_F) = I_0\left(2\sqrt{\Re_o \Re_{F1}}\right) \exp\left\{-\left(\Re_o + \Re_{F1}\right)\right\}, \quad \Re_o \geq 0 \tag{3.47}$$

which agrees with that given in (2.26). Note that the PDF of the observed SNR is a Rician PDF, where the "Rayleigh part" σ_S is known. Using (3.44) through (3.46) in (3.22) and (3.23) gives

$$E[\Re_o|\Theta_F] = \Re_{F1} + 1 \tag{3.48}$$

$$VAR[\Re_o|\Theta_F] = 2\Re_{F1} + 1 \tag{3.49}$$

For a single, fixed-amplitude target, the CRLB [11, p. 66] of $\Re_F$ for N independent observations of $\Re_o$ is given by

$$J(\Re_{F1}) = E\left[\frac{\partial^2 f(\Re_o|\Theta_F)}{\partial \Re_{F1}^2}\right] = \frac{2\Re_{F1}}{N} g_1(\Re_{F1}) \tag{3.50}$$

Table 3.2 P_d for Rayleigh Targets and $P_{fa} = 10^{-3}$

Pulses	Total SNR ($\Re_T$)		
N	10	20	30
1	0.533	0.719	0.800
2	**0.543**	0.794	0.885
3	0.519	0.817	0.915
4	0.487	**0.823**	0.930
5	0.451	0.821	0.936
6	0.417	0.815	0.939
7	0.385	0.806	**0.941**
8	0.355	0.794	0.940
9	0.327	0.781	0.938
10	0.303	0.768	0.936

Table 3.3 P_d for Rayleigh Targets and $P_{fa} = 10^{-4}$

Pulses	Total SNR ($\Re_T$)		
N	20	30	40
1	0.645	0.743	0.799
2	0.710	0.831	0.891
3	**0.725**	0.864	0.924
4	0.724	0.879	0.941
5	0.714	0.885	0.949
6	0.699	**0.887**	0.954
7	0.681	0.886	0.957
8	0.662	0.882	0.958
9	0.641	0.878	**0.958**
10	0.620	0.872	0.958

Table 3.4 P_d for Rayleigh Targets and $P_{fa} = 10^{-5}$

Pulses	Total SNR ($\Re_T$)		
N	20	30	40
1	0.578	0.690	0.775
2	0.628	0.776	0.851
3	**0.632**	0.807	0.889
4	0.622	0.820	0.907
5	0.603	**0.823**	0.916
6	0.579	0.821	0.922
7	0.555	0.816	0.924
8	0.528	0.808	**0.924**
9	0.503	0.800	0.924
10	0.474	0.788	0.921

Table 3.5 P_d for Rayleigh Targets and $P_{fa} = 10^{-6}$

Pulses	Total SNR ($\Re_T$)		
N	20	30	40
1	0.518	0.640	0.714
2	**0.551**	0.719	0.810
3	0.544	0.746	0.849
4	0.524	**0.755**	0.867
5	0.497	0.754	0.877
6	0.466	0.746	0.881
7	0.437	0.737	**0.882**
8	0.405	0.723	0.880
9	0.376	0.708	0.877
10	0.348	0.692	0.872

Table 3.6 P_d for Rayleigh Targets and $P_{fa} = 10^{-7}$

Pulses	Total SNR ($\Re_T$)			
N	20	30	40	50
1	0.464	0.594	0.675	0.729
2	**0.481**	0.664	0.768	0.832
3	0.463	0.684	0.806	0.874
4	0.434	**0.687**	0.823	0.895
5	0.400	0.680	0.830	0.907
6	0.367	0.668	**0.833**	0.914
7	0.334	0.652	0.831	0.917
8	0.303	0.633	0.827	0.919
9	0.273	0.613	0.820	**0.919**
10	0.247	0.592	0.813	0.918

Table 3.7 P_d for Rayleigh Targets and $P_{fa} = 10^{-8}$

Pulses	Total SNR ($\Re_T$)			
N	20	30	40	50
1	0.416	0.552	0.638	0.697
2	**0.417**	0.610	0.726	0.798
3	0.389	**0.622**	0.760	0.840
4	0.354	0.6187	0.775	0.862
5	0.317	0.605	**0.780**	0.874
6	0.281	0.587	0.778	0.880
7	0.249	0.566	0.774	0.883
8	0.219	0.543	0.766	**0.883**
9	0.194	0.520	0.757	0.883
10	0.169	0.494	0.745	0.879
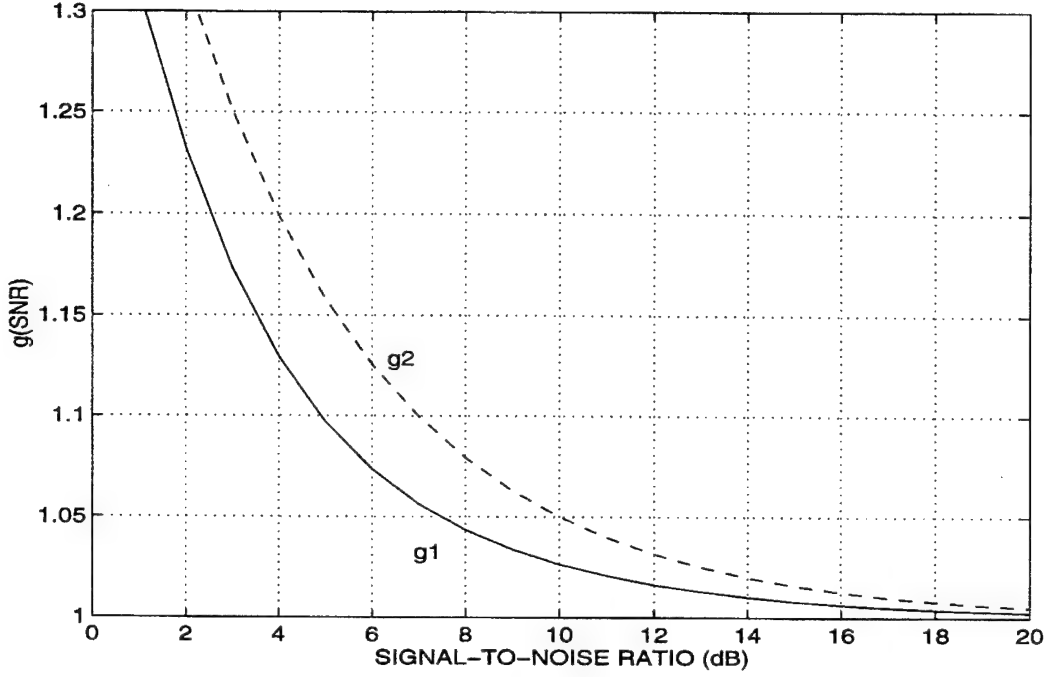
Figure 3.2   Graphical Definition of the CRLB for $\Re_F$ and Efficiency of the MM Estimate $\widetilde{\Re}_F$

where

$$g_1(\Re_{F1}) = \frac{1}{2}\left[-\Re_{F1} + \int_{-\infty}^{\infty} x I_{1|0}^2\left(2\sqrt{x\Re_{F1}}\right)\exp(-x-\Re_{F1})\,dx\right]^{-1} \qquad (3.51)$$

and $I_{1|0}(\cdot)$ is the first-order modified Bessel function $I_1(\cdot)$ divided by $I_0(\cdot)$. Figure 3.2 shows that $g(\Re_{F1})$ varies from 1.3 at $\Re_F = 1$ dB to 1.0 for large values of $\Re_{F1}$. Thus, for $\Re_{F1} > 10$ dB, $J(\Re_{F1}) \approx 2N^{-1}\Re_{F1}$.

Using (3.48) gives the MM estimator of $\Re_{F1}$ as

$$\widetilde{\Re}_{F1} = Y_N - 1 = -1 + \frac{1}{N}\sum_{i=1}^{N}\Re_{ok} \qquad (3.52)$$

Then $\widetilde{\Re}_{F1}$ is an unbiased estimator with variance given by

$$\text{VAR}[\widetilde{\Re}_{F1}|\Re_{F1}] = \frac{2\Re_{F1}+1}{N} = \frac{2\Re_{F1}}{N}g_2(\Re_{F1}) \qquad (3.53)$$

where $g_2(\Re_{F1})$ is shown in Figure 3.2. Comparing $g_2(\Re_{F1})$ with $g_1(\Re_{F1})$ shows that the variance of $\widetilde{\Re}_{F1}$ approaches the CRLB for $\Re_{F1} > 16$ dB.

The ML estimator is considered next for cases where the efficiency of the MM

44

estimator is unacceptable. The ML estimate of $\Re_{F1}$ satisfies [11, p. 65]

$$h(\widehat{\Re}_{F1}) = -\widehat{\Re}_{F1} + \frac{1}{N} \sum_{k=1}^{N} \sqrt{\Re_{ok}\widehat{\Re}_{F1}} I_{1|0}(2\sqrt{\widehat{\Re}_{F1}\Re_{ok}}) = 0 \qquad (3.54)$$

Then $\widehat{\Re}_{F1}$ can be found using Newton's method with the nth iteration given by

$$\widehat{\Re}_{F1}^{(n+1)} = \widehat{\Re}_{F1}^{(n)} - \frac{h(\widehat{\Re}_{F1}^{(n)})}{h'(\widehat{\Re}_{F1}^{(n)})} \qquad (3.55)$$

where

$$h'(\widehat{\Re}_{F1}^{(n)}) = -\widehat{\Re}_{F1}^{(n)} - h(\widehat{\Re}_{F1}^{(n)}) + \frac{1}{N} \sum_{k=1}^{N} \Re_{ok}\left(1 - I_{1|0}^2\left(2(\widehat{\Re}_{F1}^{(n)}\Re_{ok})^{\frac{1}{2}}\right)\right) \qquad (3.56)$$

$$\widehat{\Re}_{F1}^{(0)} = \left[\frac{1}{N} \sum_{k=1}^{N} \sqrt{\Re_{ok}}\right]^2 - \frac{1}{2} \qquad (3.57)$$

The initial value $\widehat{\Re}_{F1}^{(0)}$ is obtained by using the approximation

$$I_{1|0}(x) = 1 - \frac{1}{2x}, \qquad x > 1.0 \qquad (3.58)$$

in (3.54) and the quadratic formula to solve approximately for $\sqrt{\widehat{\Re}_{F1}}$. Also, note that the square-root function of the quadratic formula was approximated by the first two terms of the binomial series expansion in [13, No. 1.114].

Monte Carlo simulations with 20,000 experiments were conducted to study the performances of the ML estimator, $\widehat{\Re}_{F1}$, and the approximate ML estimator, $\widehat{\Re}_{F1}^{(0)}$. In the simulation studies, values of $\Re_{F1}$ from 1 dB to 20 dB and $N = 2$, 4, and 8 were considered. Figure 3.3 shows the sample average of the errors in both estimators, while Figure 3.4 shows the sample standard deviation of the errors normalized with the square root of the CRLB in (3.50). Figure 3.3 shows that the approximate ML estimator is notably more biased than of the ML estimator for $\Re_{F1} < 7$ dB. However, the sample standard deviation of the error of the approximate ML estimator is less than the CRLB for $\Re_{F1} < 7$ dB. Figures 3.3 and 3.4 indicate, as expected [11, p. 71], that the bias in the ML estimator decreases, and the sample variance of the errors of the ML estimator approach the CRLB as N increases. However, for many applications and $\Re_{F1} > 10$ dB, $\widehat{\Re}_{F1}^{(0)}$ provides an acceptable estimate.

45
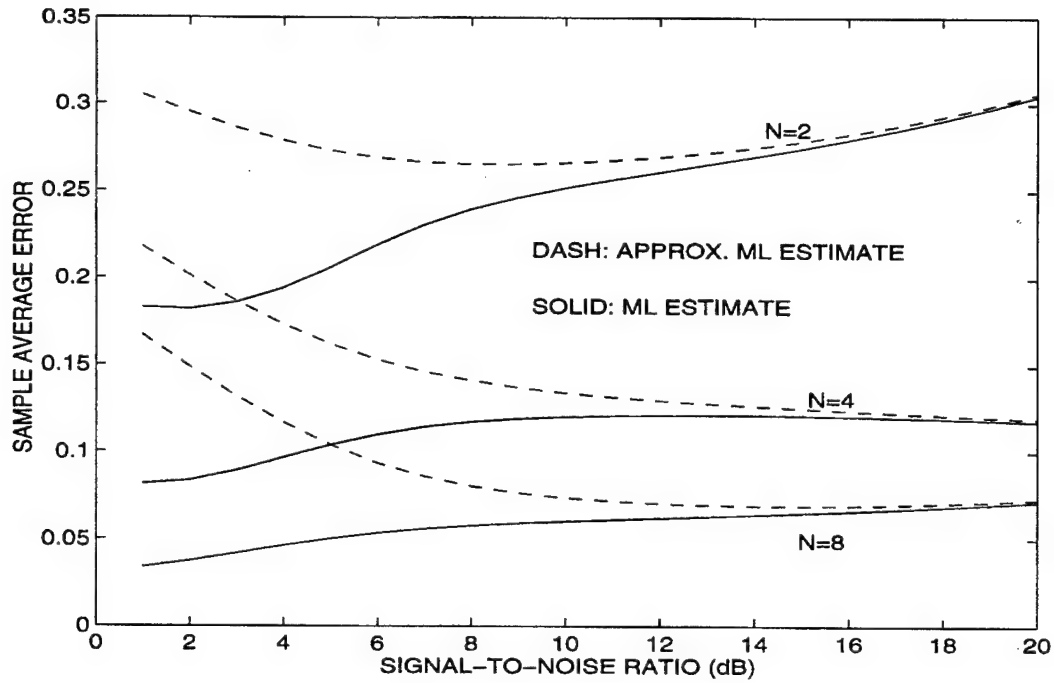
Figure 3.3 Sample Average of the Errors in $\widehat{\Re}_{F1}^{(0)}$ and the ML Estimator $\widehat{\Re}_{F1}$
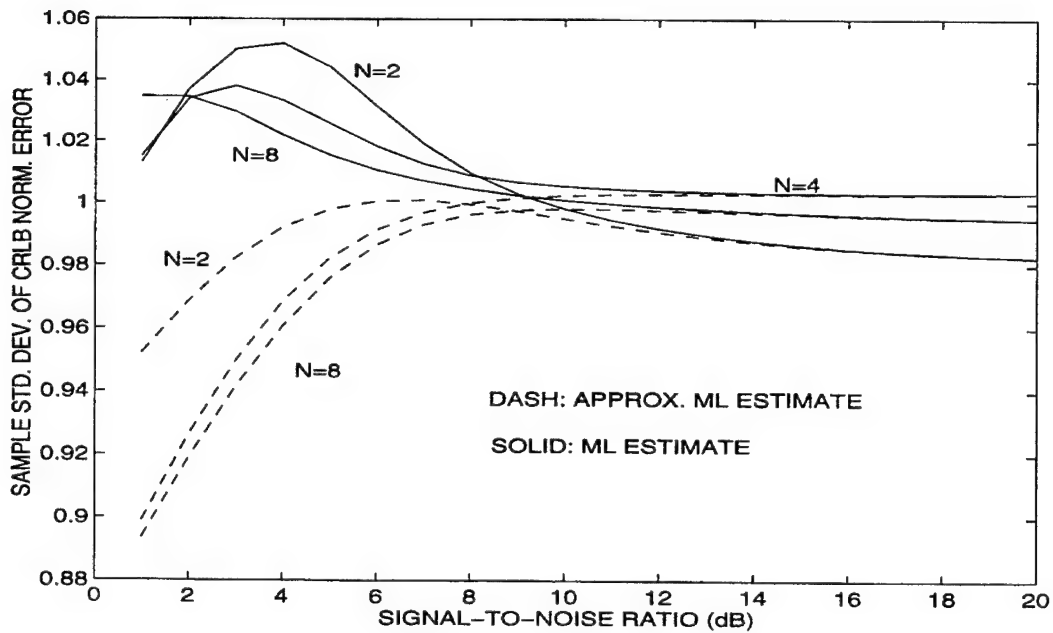
Figure 3.4 Sample Standard Deviation of the CRLB Normalized Errors in $\widehat{\Re}_{F1}^{(0)}$ and the ML Estimator $\widehat{\Re}_{F1}$

3.3 Dominant-Plus-Rayleigh Target

The RCS fluctuations of Swerling 3 and 4 targets are referred to as one-dominant-plus-Rayleigh model in [14, p. 407]. However, discrimination between a Swerling 2 (*i.e.*, Rayleigh) target and a Swerling 4 target using Generalized Maximum Likelihood (GML) detection and 20 subpulses or frequencies is shown via simulation results in [16] to result in error rates of 15 to 20 percent. The stochastic distance between the two distributions for the observed SNR was considered to better understand the poor discrimination. The J-Divergence distance [22, p. 341] between the observed SNR for a Swerling 4 target and the observed SNR of a Rayleigh target is shown in Figure 3.5 for various values of SNR. The J-Divergence distance between the Swerling 4 and Rayleigh targets appears rather small when compared to the J-Divergence distance between the observed SNRs of fixed-amplitude and Rayleigh targets. Furthermore, the J-Divergence distance between the Swerling 4 and Rayleigh targets decreases as the SNR increases. Thus, an alternative to the Erlang distribution of the Swerling 3 and 4 models for RCS fluctuations is proposed in this section.

The new dominant-plus-Rayleigh target is a Rician target with the fixed-amplitude part contributing 90 percent of the SNR, while the Rayleigh part contributes 10 percent of the SNR. The in-phase and quadrature components of the sum signal for the new dominant-plus-Rayleigh target is given by (3.1) and (3.2), with $\alpha_i = 0$ and $\beta_i = 0$ for all $i > 1$ as

$$s_I = \frac{3}{\sqrt{10}}\alpha_1 \cos \phi_1 + \frac{1}{\sqrt{20}}\beta_1 \cos \varphi_1 + n_{SI} \tag{3.59}$$

$$s_Q = \frac{3}{\sqrt{10}}\alpha_1 \sin \phi_1 + \frac{1}{\sqrt{20}}\beta_1 \sin \varphi_1 + n_{SI} \tag{3.60}$$

where $E[\beta_1^2|\Theta_D] = 2\alpha_1^2$. Then

$$\bar{s}_I = E[s_I|\Theta_D, \phi_1] = \frac{3}{\sqrt{10}}\alpha_1 \cos \phi_1 \tag{3.61}$$

$$\bar{s}_Q = E[s_Q|\Theta_D, \phi_1] = \frac{3}{\sqrt{10}}\alpha_1 \sin \phi_1 \tag{3.62}$$

$$p_{11} = \text{VAR}[s_I|\Theta_D, \phi_1] = \text{VAR}[s_Q|\Theta_D, \phi_1] = \frac{1}{20}\alpha_1^2 + \sigma_S^2 \tag{3.63}$$

where Θ_D denotes the parameter set $\{\alpha_1, \sigma_S\}$. Using (3.61) through (3.63) for $\bar{s}_I$, $\bar{s}_Q$, and p_{11}, and $\beta_i = 0$ for all $i > 1$ in (3.21) gives the PDF of the observed SNR for the new dominant-plus-Rayleigh target as

$$f(\Re_o|\Theta_D) = \frac{10}{\Re_D + 10}I_0\left(\frac{6\sqrt{10\Re_o\Re_D}}{\Re_D + 10}\right) \exp\left\{-\frac{10\Re_o + 9\Re_D}{\Re_D + 10}\right\}, \quad \Re_o \geq 0 \tag{3.64}$$
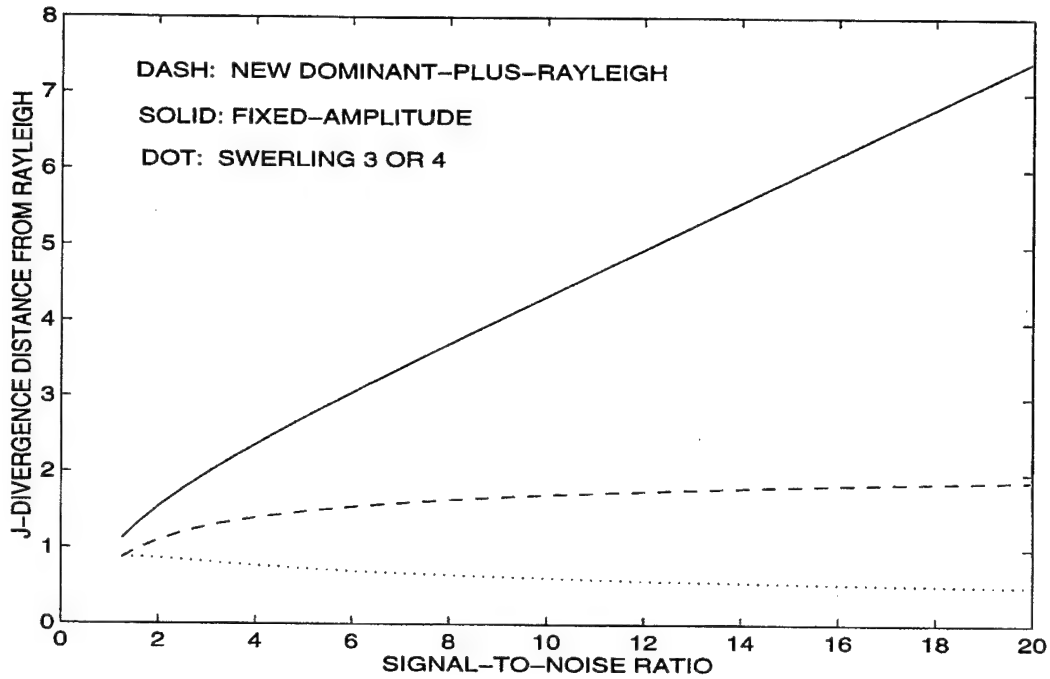
Figure 3.5   J-Divergence of the Observed SNR for Fixed-Amplitude, Swerling 3 or 4, and New Dominant-Plus-Rayleigh Targets from the Observed SNR for a Rayleigh Target

where $\Re_D$ is the SNR of the dominant-plus-Rayleigh target and given by

$$\Re_D = \frac{\alpha_1^2}{2\sigma_S^2} \tag{3.65}$$

Note that the PDF of the observed SNR is a Rician PDF, where a constraint has been imposed on the relationship between fixed-amplitude parameter and the Rayleigh parameter. The J-Divergence distance between the observed SNR of the new dominant-plus-Rayleigh target and a Rayleigh target is shown in Figure 3.5 for various values of SNR. At an SNR of 7 dB (*i.e.*, 5), the J-Divergence distance between the dominant-plus-Rayleigh and Rayleigh targets is about one-half the distance between the fixed-amplitude and Rayleigh targets. Using (3.61) through (3.63) in (3.22) and (3.23) gives

$$E[\Re_o|\Theta_D] = \Re_D + 1 \tag{3.66}$$

$$VAR[\Re_o|\Theta_D] = \left(0.1\Re_D + 1\right)\left[1.9\Re_D + 1\right] \tag{3.67}$$

Using (3.66) gives the MM estimator of $\Re_D$ as

$$\widetilde{\Re}_D = Y_N - 1 = -1 + \frac{1}{N}\sum_{i=1}^{N}\Re_{ok} \tag{3.68}$$

48

Then $\widetilde{\Re}_D$ is an unbiased estimator with variance given by

$$\text{VAR}[\widetilde{\Re}_D|\Re_D] = \frac{(0.1\Re_D + 1)(1.9\Re_D + 1)}{N} \tag{3.69}$$

The CRLB for any unbiased estimator of $\Re_D$ and the ML estimator of $\Re_D$ can be developed in a manner that is similar to that for the fixed-amplitude target in Section 3.2. However, due the complexity of the ML estimator and the CRLB, neither are developed here.

3.4 Discrimination Between Fixed-Amplitude, Rayleigh, and Dominant-Plus-Rayleigh Targets

Since the estimators of the amplitude parameters developed in this chapter and the DOA estimators developed in Chapter 5 are dependent on the amplitude distribution, discrimination of targets according to the amplitude distributions is needed. Furthermore, the radar waveform for optimal detection and parameter estimation varies with the target amplitude distribution. For example, the optimal waveform for detection of a fixed-amplitude target includes one frequency, while the optimal waveform for a Rayleigh target may include one or multiple frequencies as illustrated in Section 3.1. Thus, the waveform requirements for reliable discrimination between Rayleigh, fixed-amplitude, and dominant-plus-Rayleigh targets are considered in this section.

Let the hypotheses for the discrimination be defined as

$$H_0 = \text{ Rayleigh target with SNR } \Re_{R1}$$
$$H_1 = \text{ fixed-amplitude target with SNR } \Re_{F1}$$
$$H_2 = \text{ dominant-plus-Rayleigh target with SNR } \Re_D$$

Since discrimination or detection involves three hypotheses, two Likelihood Ratios (LRs) are required for ML discrimination [11, p. 46]. Furthermore, since the target amplitude parameters $\Re_{R1}, \Re_{F1}$, and $\Re_D$ are assumed unknown, two Generalized Likelihood Ratios (GLRs) are required for GML discrimination. For N subpulses, the two GLRs are given by

$$T_1(\{\Re_{ok}\}_{k=1}^N) = \prod_{k=1}^N \frac{f(\Re_{ok}|H_1, \Re_{F1} = \widehat{\Re}_{F1})}{f(\Re_{ok}|H_0, \Re_{R1} = \widehat{\Re}_{R1})} \tag{3.70}$$

$$T_2(\{\Re_{ok}\}_{k=1}^N) = \prod_{k=1}^N \frac{f(\Re_{ok}|H_2, \Re_D = \widetilde{\Re}_D)}{f(\Re_{ok}|H_0, \Re_{R1} = \widehat{\Re}_{R1})} \tag{3.71}$$

Note that the conditioning on the measured amplitude of the signal associated with target detection has been omitted from (3.70) and (3.71). Thus, the presence of a target is assumed here. Also, note that the MM estimate of $\Re_D$ is used for the ML estimate, because $\widetilde{\Re}_D$ is much simpler and closely approximates the ML estimate. Using (3.24), (3.32), and (3.47) in (3.70) and taking the natural logarithm gives

$$\overline{T}_1(\{\Re_{ok}\}_{k=1}^N) = N\ln(Y_N) - N(Y_N + 1) - N\widehat{\Re}_F + \sum_{k=1}^N \ln I_0\left(2\sqrt{\Re_{ok}\widehat{\Re}_F}\right) \quad (3.72)$$

where $\widehat{\Re}_F$ is given by (3.54) or (3.57). Using (3.24), (3.32), and (3.64) in (3.71), and taking the natural logarithm gives

$$\overline{T}_2(\{\Re_{ok}\}_{k=1}^N) = N\ln\left(\frac{10}{\widetilde{\Re}_D + 10}\right) + N\ln(Y_N) - 9N\frac{\widetilde{\Re}_D}{\widetilde{\Re}_D + 10}$$

$$+ \left[\frac{1}{\widehat{\Re}_R + 1} - \frac{1}{\widetilde{\Re}_D + 10}\right]NY_N + \sum_{k=1}^N \ln I_0\left(\frac{6\sqrt{\Re_{ok}\widetilde{\Re}_D}}{\widetilde{\Re}_D + 10}\right) \quad (3.73)$$

where $\widetilde{\Re}_D$ is given by (3.68). Then the GML decision rule is given by

$$\delta(\{\Re_{ok}\}_{k=1}^N) = \begin{cases} H_1; & \overline{T}_1(\{\Re_{ok}\}_{k=1}^N) > 0, \quad \overline{T}_1(\{\Re_{ok}\}_{k=1}^N) \geq \overline{T}_2(\{\Re_{ok}\}_{k=1}^N) \\ H_2; & \overline{T}_2(\{\Re_{ok}\}_{k=1}^N) > 0, \quad \overline{T}_2(\{\Re_{ok}\}_{k=1}^N) > \overline{T}_1(\{\Re_{ok}\}_{k=1}^N) \\ H_0; & \text{otherwise} \end{cases} \quad (3.74)$$

Note that the prior probabilities for the three hypotheses have been assumed to be equal in the development of the decision rule.

Monte Carlo simulations were conducted to study the probabilities of error in the discrimination for various values of N and SNR. Let the probabilities of error be defined as

$$P_{e1} = P\{H_1|H_0\} \qquad \text{Type I Errors} \qquad (3.75)$$

$$P_{e2} = P\{H_0|H_1\} \qquad \text{Type II Errors} \qquad (3.76)$$

$$P_{e3} = P\{H_2|H_0\} \qquad \text{Type III Errors} \qquad (3.77)$$

$$P_{e4} = P\{H_0|H_2\} \qquad \text{Type IV Errors} \qquad (3.78)$$

$$P_{e5} = P\{H_2|H_1\} \qquad \text{Type V Errors} \qquad (3.79)$$

$$P_{e6} = P\{H_1|H_2\} \qquad \text{Type VI Errors} \qquad (3.80)$$

where $P\{H_i|H_j\}$ denotes the probability of event H_i, given that event H_j is true. The results of the Monte Carlo simulations with 25,000 experiments are summarized in Figures 3.6 through 3.8. The solid lines of Figure 3.6 give the percents of Type I
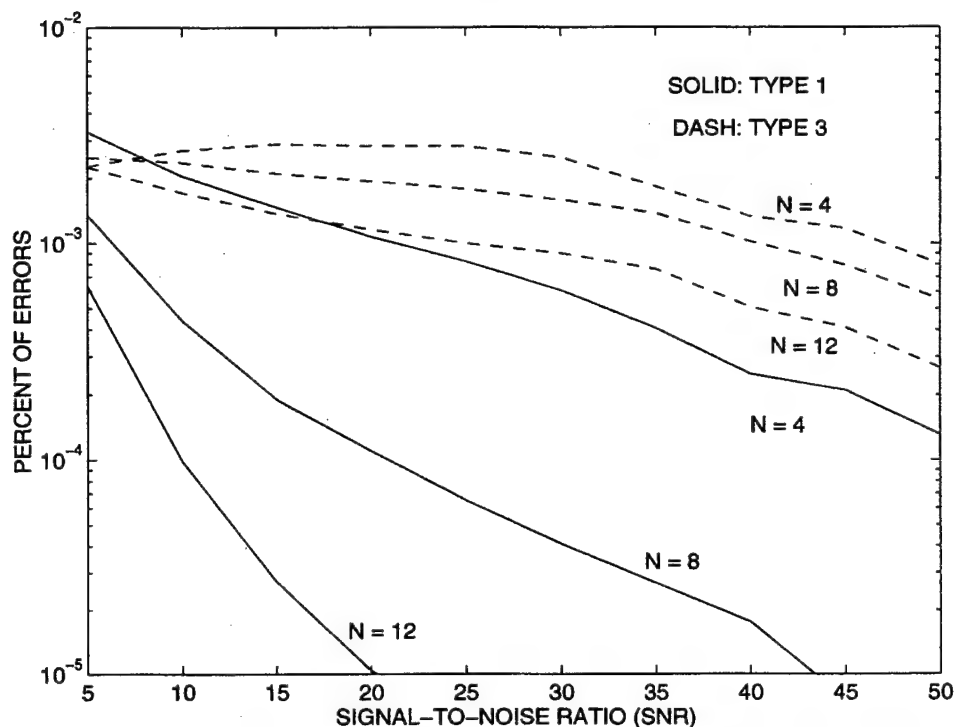
Figure 3.6 Percents of Types I and III Errors for Rayleigh Target

errors for $N = 4$, 8, and 12, while the dash lines give the percents of Type III errors. The solid lines of Figure 3.7 give the percents of Type II errors, while the dash lines give the percents of Type V errors. The solid lines of Figure 3.8 give the percents of Type IV errors, while the dash lines give the percents of Type VI errors. Figures 3.6 and 3.7 show that discrimination between Rayleigh and fixed-amplitude targets can be achieved rather reliably with eight or more subpulses. Figures 3.6 and 3.7 show that discrimination between the Rayleigh and dominant-plus-Rayleigh targets can be achieved reasonably well with 12 or more subpulses, while Figures 3.7 and 3.8 show that discrimination between the fixed-amplitude and dominant-plus-Rayleigh targets is very poor, with 12 subpulses or less. Thus, from a discrimination point of view, the dominant-plus-Rayleigh target appears to be closer to the fixed-amplitude target than to the Rayleigh target.

3.5 Discrimination Example: Detection of Range Gate Pull Off

Range Gate Pull Off (RGPO) is a deceptive Electronic Countermeasure (ECM) that targets perform to cause the radar to break its track on the target. For a radar utilizing aperiodic revisit times and single-pulse dwells (*i.e.*, no pulse Doppler),
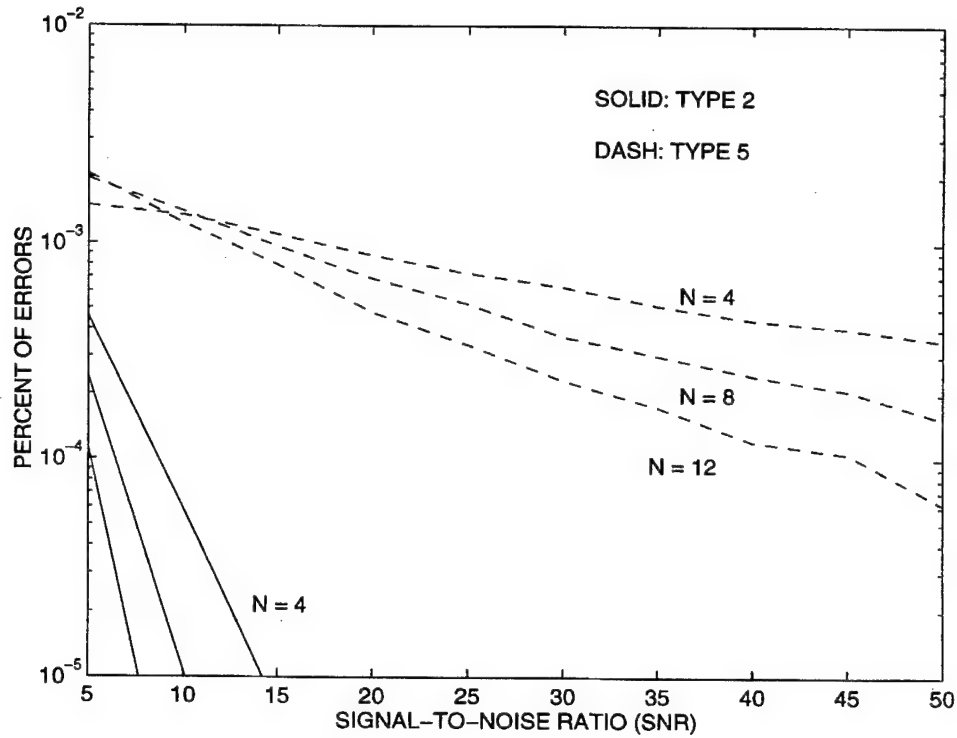
Figure 3.7 Percents of Types II and V Errors for Fixed-Amplitude Target
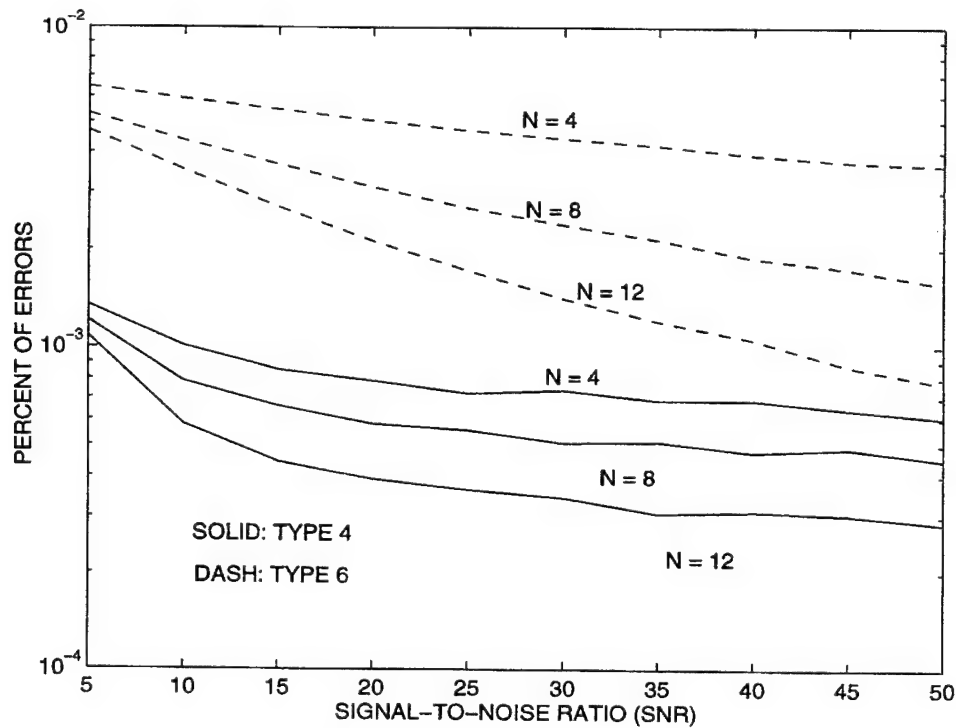
Figure 3.8 Percents of Types IV and VI Errors for Dominant-Plus-Rayleigh Target
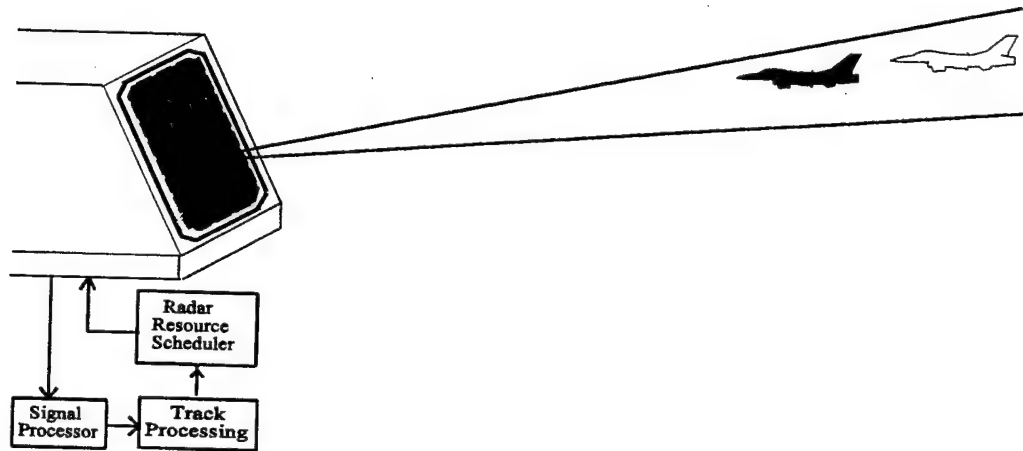
Figure 3.9   Illustration of RGPO

targets performing RGPO utilize Digital Radio Frequency Memory (DRFM) [23] to store the radar pulse and repeat the pulse at the radar with a controlled delay, so that the radar receives signals from the actual target and a false target at a longer range as illustrated by the dash target in Figure 3.9. The time delay of the repeated pulse is often controlled so that the false target is separated from the true target with either linear or quadratic motion, and the repeated pulse is typically amplified to produce a false target with an SNR higher than the actual target measurement. If the tracking algorithm uses the false target measurement instead of the actual target measurement, the track on the target will most likely be lost by the radar [24]. If the false target measurement is not associated with an existing track nor recognized as a RGPO echo, a new track is initiated on the RGPO, and radar resources are expended tracking the false target. Simple detection of RGPO by testing for a second target at a longer range can be problematic. For example, the target echo may not be detected, or the second echo could be a real target that is cooperating with the first target.

The use of frequency diversity to discriminate between actual target echoes and RGPO echoes is considered. For N radar subpulses at distinct frequencies, the amplitudes of the target echoes are modeled as Rayleigh distributed, while the amplitudes of the RGPO echoes are modeled as fixed, since the amplitudes of the repeated subpulses are expected to be fixed across the frequencies. A GLRT and variance test are

proposed for discriminating between echoes from Rayleigh targets and echoes from RGPO or a fixed-amplitude target. Results of Monte Carlo simulations are used to study the performances of the discrimination algorithms.

For discriminating between echoes from Rayleigh targets and echoes from RGPO or fixed-amplitude targets, let H_0 denote the hypothesis that a given set of subpulses originated with a Rayleigh target, and H_1 denote the hypothesis that a given set of subpulses originated from an RGPO or a fixed-amplitude target. The GML detection using the GLRT with N subpulses is given by

$$T(\{\Re_{ok}\}_{k=1}^N) = \prod_{k=1}^N \frac{f(\Re_{ok}|H_1, \Re_{F1} = \widehat{\Re}_{F1})}{f(\Re_{ok}|H_0, \Re_{R1} = \widehat{\Re}_{R1})} \tag{3.81}$$

Note that the conditioning on the measured amplitude of the signal associated with target detection has been omitted from (3.81). Thus, the presence of a target is assumed here. Using (3.24), (3.32), and (3.47) in (3.81); the first term of the series expansion of $I_0(\cdot)$; and taking the natural logarithm gives

$$\begin{aligned}
\overline{T}(\{\Re_{ok}\}_{k=1}^N) &= \ln(Y_N) - Y_N + 1 - \widehat{\Re}_{F1} + \frac{1}{N}\sum_{k=1}^N \ln I_0\left(2\sqrt{\Re_{ok}\widehat{\Re}_{F1}}\right) \\
&\approx \ln(Y_N) - \frac{1}{2}\ln(2\pi) + \frac{1}{N}\sum_{k=1}^N \left(2\sqrt{\Re_{ok}\widehat{\Re}_{F1}}\right) - Y_N + 1 - \widehat{\Re}_{F1} \\
&\quad - \frac{1}{2N}\sum_{k=1}^N \ln\left(2\sqrt{\Re_{ok}\widehat{\Re}_{F1}}\right)
\end{aligned} \tag{3.82}$$

where $\widehat{\Re}_{F1}$ is given by (3.54) or (3.57). Then the GML decision rule is given by

$$\delta(\{\Re_{ok}\}_{k=1}^N) = \begin{cases} H_0, & \overline{T}(\{\Re_{ok}\}_{k=1}^N) \le \lambda_1 \\ H_1, & \overline{T}(\{\Re_{ok}\}_{k=1}^N) > \lambda_1 \end{cases} \tag{3.83}$$

Comparing (3.26) with (3.49) suggests that the discrimination might be accomplished more simply by a variance test, which is defined by

$$\delta(\{\Re_{ok}\}_{k=1}^N) = \begin{cases} H_0, & \widetilde{T}(\{\Re_{ok}\}_{k=1}^N) \ge \lambda_2 \\ H_1, & \widetilde{T}(\{\Re_{ok}\}_{k=1}^N) < \lambda_2 \end{cases} \tag{3.84}$$

where

$$\widetilde{T}(\{\Re_{ok}\}_{k=1}^N) = \frac{1}{2\widehat{\Re}_{F1} + 1}\left[-\widehat{\Re}_{R1}^2 + \sum_{k=1}^N \Re_{ok}^2\right] \tag{3.85}$$

where $\widehat{\Re}_{F1}$ is given by (3.54) or (3.57).

The results of Monte Carlo simulations with 100,000 experiments are summarized in Figures 3.10 through 3.15, where the solid lines correspond to the GML discrimination of (3.83), and the dash lines correspond to the discrimination with the variance test of (3.84). Figures 3.10, 3.12, and 3.14 show the detection thresholds λ_1 and λ_2 versus the probability of false detection of RGPO or a fixed-amplitude target, P_{FDFA}. Figures 3.11, 3.13, and 3.15 show the probability of detection of RGPO or a fixed-amplitude target P_{DFA} versus P_{FDFA}. Figures 3.11, 3.13, and 3.15 show that the more complex GML provides a P_{DFA} that is approximately 0.1 to 0.2 greater than that of the variance test. Figure 3.11 shows that eight independent subpulses at 7 dB are required to achieve reasonable discrimination, while Figures 3.13 and 3.15 show that four subpulses at 10 or 13 dB provide rather reasonable discrimination.

Using GML detection with four subpulses at SNRs greater than 10 dB provides reliable discrimination between echoes from Rayleigh targets and echoes from an RGPO or a fixed-amplitude target. For example, four subpulses at 10 dB provide a probability of correctly discriminating a target as a fixed-amplitude of $P_{DFA} = 0.58$ with a false alarm rate of $P_{FDFA} = 0.05$, while four subpulses at 13 dB provides a $P_{DFA} = 0.82$ with $P_{FDFA} = 0.05$. If more reliable discrimination is needed or fewer frequencies are available for independent subpulses, the discrimination can be accomplished over multiple radar dwells by incorporating the target amplitude into the IMM algorithm [10, p. 209] as a feature by using (3.24) and (3.32) for a generalized likelihood for the Rayleigh target, and (3.47) and (3.57) for RGPO or fixed-amplitude target.

3.6 Rician Target

Considering target amplitude estimation for the Rician target, the in-phase and quadrature components of the sum signal for a Rician target is given by (3.1) and (3.2), with $\alpha_i = 0$ and $\beta_i = 0$ for all $i > 1$. Then

$$\bar{s}_I = E[s_I|\Theta_{Ri}, \phi_1] = \alpha_1 \cos \phi_1 \tag{3.86}$$

$$\bar{s}_Q = E[s_Q|\Theta_{Ri}, \phi_1] = \alpha_1 \sin \phi_1 \tag{3.87}$$

$$p_{11} = \text{VAR}[s_I|\Theta_{Ri}, \phi_1] = \text{VAR}[s_Q|\Theta_{Ri}, \phi_1] = \beta_{10}^2 + \sigma_S^2 \tag{3.88}$$

where Θ_{Ri} denotes the parameter set $\{\alpha_1, \beta_{10}, \sigma_S\}$. Using (3.86) through (3.88) for
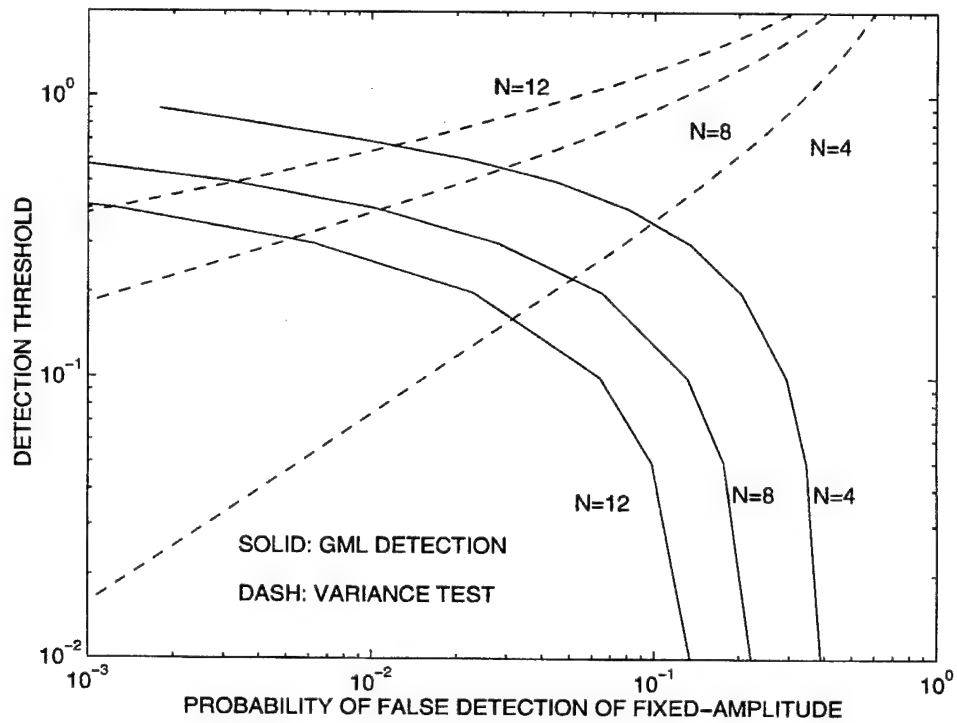
Figure 3.10   Detection Thresholds for $\Re_{R1} = \Re_{F1} = 7$ dB
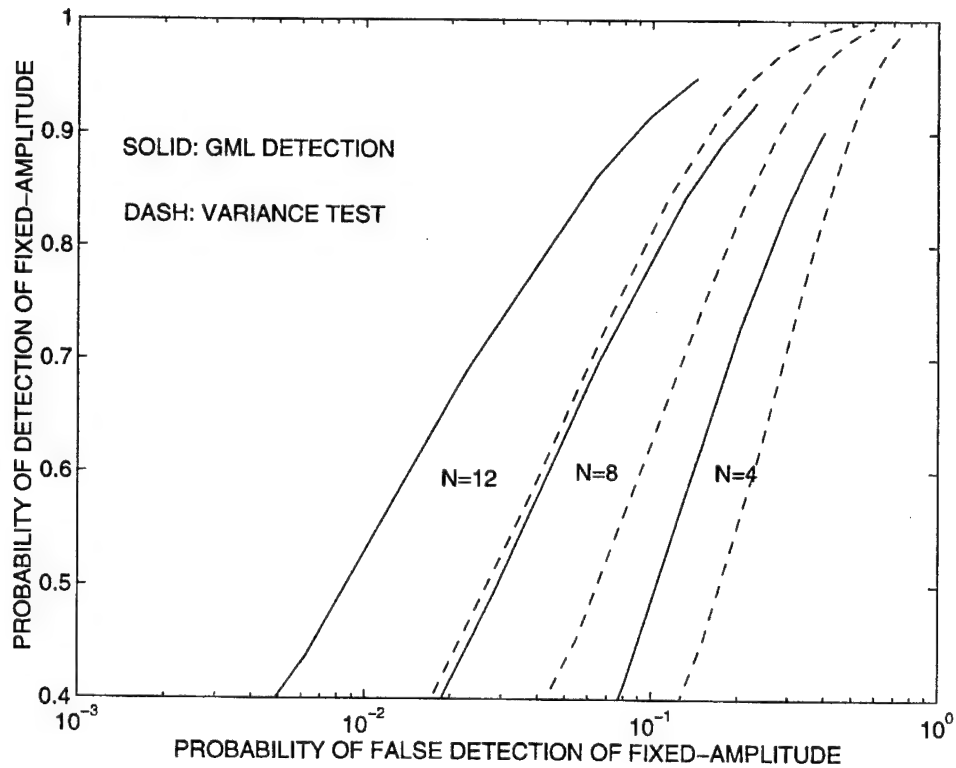
Figure 3.11   ROC Curves for $\Re_{R1} = \Re_{F1} = 7$ dB
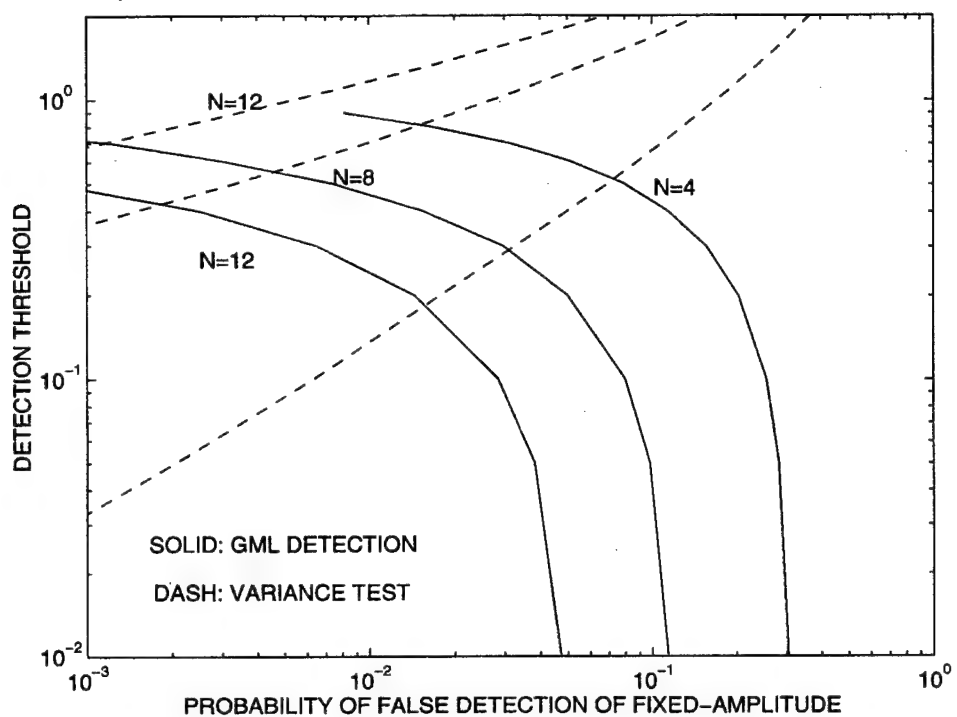
Figure 3.12   Detection Thresholds for $\Re_{R1} = \Re_{F1} = 10$ dB
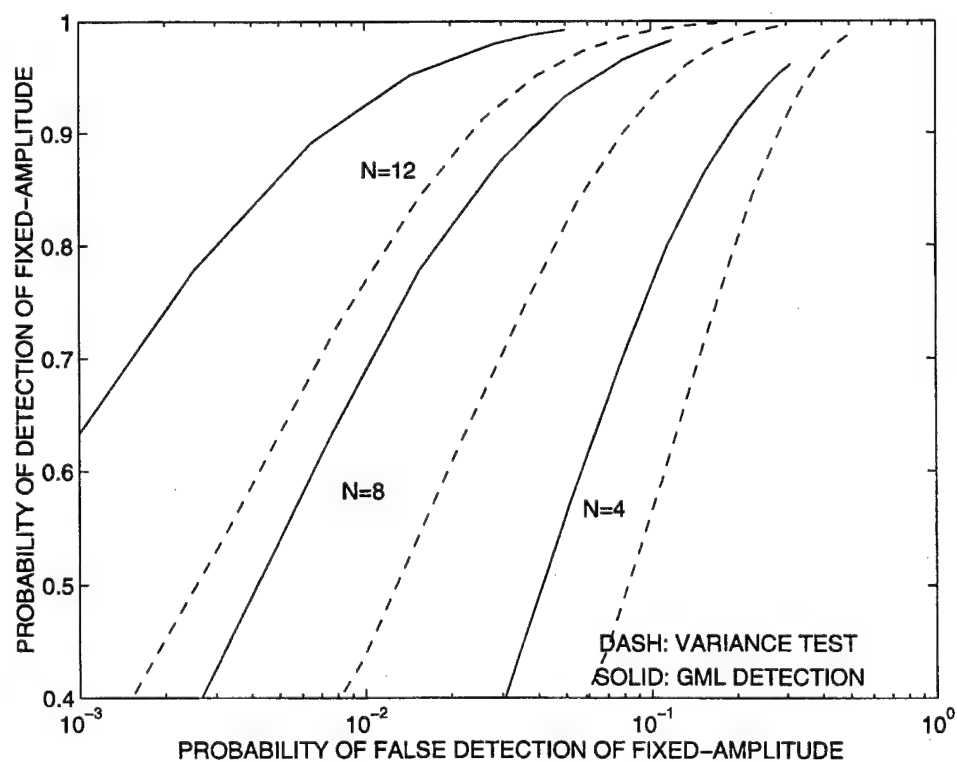
Figure 3.13   ROC Curves for $\Re_{R1} = \Re_{F1} = 10$ dB

57
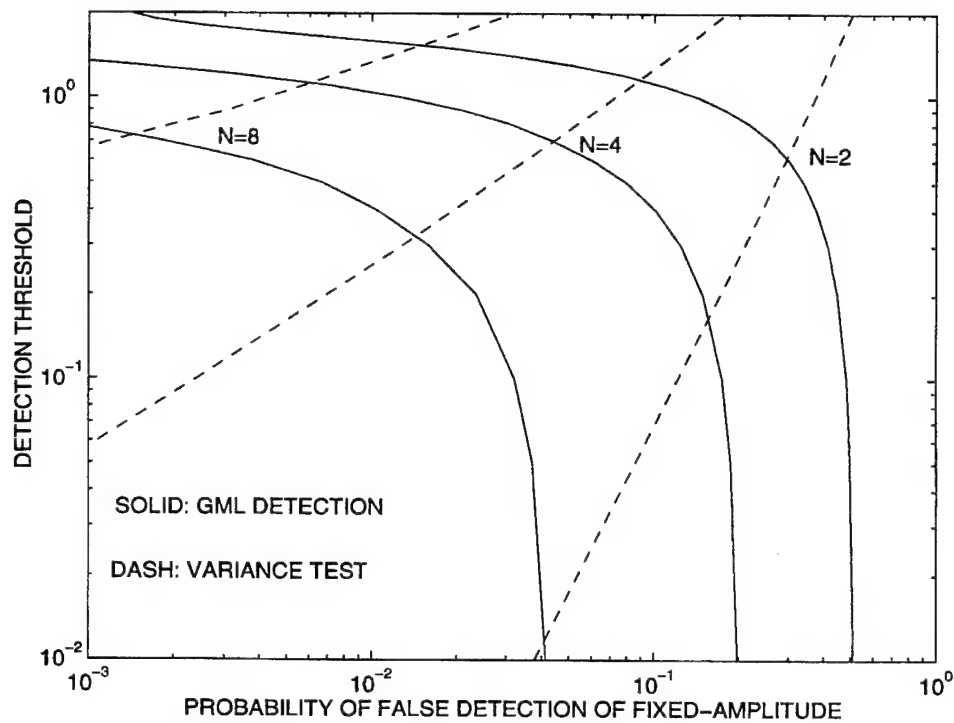
Figure 3.14   Detection Thresholds for $\Re_{R1} = \Re_{F1} = 13$ dB
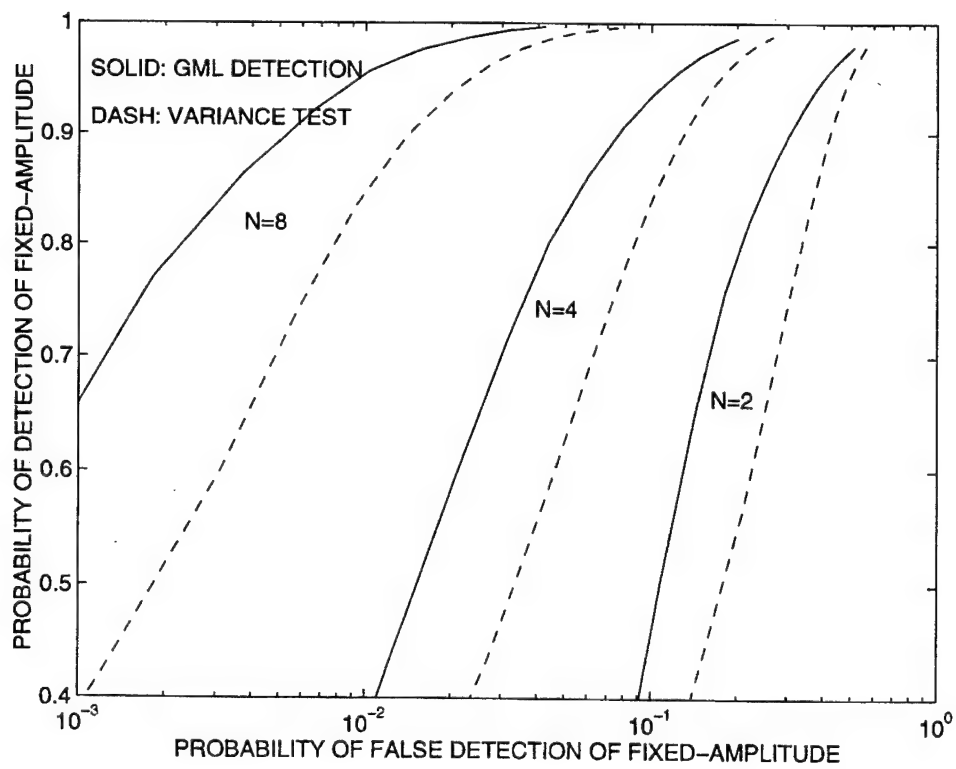
Figure 3.15   ROC Curves for $\Re_{R1} = \Re_{F1} = 13$ dB

$\bar{s}_I$, $\bar{s}_Q$, and p_{11} in (3.21) gives the PDF of the observed SNR for a Rican target as

$$f(\Re_o|\Theta_{Ri}) = \frac{1}{\Re_{R1}+1} I_0\left(\frac{2}{\Re_{R1}+1}\sqrt{\Re_o\Re_{F1}}\right)$$
$$\times \exp\left\{-\frac{1}{\Re_{R1}+1}\left(\Re_o + \Re_{F1}\right)\right\}, \quad \Re_o \geq 0 \qquad (3.89)$$

which agrees with that given in (2.61). Using (3.86) through (3.88) in (3.22) and (3.23) gives

$$E[\Re_o|\Theta_{Ri}] = \Re_{F1} + \Re_{R1} + 1 \qquad (3.90)$$
$$VAR[\Re_o|\Theta_{Ri}] = \left[\Re_{R1}+1\right]\left[2\Re_{F1}+\Re_{R1}+1\right] \qquad (3.91)$$

MM and ML estimators for the parameters of a Rician distribution were developed in [25], where the development of the ML estimator involved the use of a nondimensional PDF in order to reduce the optimization to a scalar problem. The nondimensional PDF was created by normalizing the random variables by the sample estimate of the second moment. The CRLB in [25] was also developed with the nondimensional PDF. However, in this section, the parameters of interest, $\Re_{F1}$ and $\Re_{R1}$, differ from the parameters in a standard Rician distribution. Setting (3.90) and (3.91) equal to their corresponding sample moments gives the MM estimators for $\Re_{F1}$ and $\Re_{R1}$ as

$$\widetilde{\Re}_{R1} = Y_N - 1 - \sqrt{\frac{2N-1}{N-1}Y_N^2 - V_N} \qquad (3.92)$$

$$\widetilde{\Re}_{F1} = \sqrt{\frac{2N-1}{N-1}Y_N^2 - V_N} \qquad (3.93)$$

where

$$V_N = \frac{1}{N-1}\sum_{k=1}^{N}\Re_{ok}^2 \qquad (3.94)$$

Monte Carlo simulations with 20,000 experiments were conducted to study the performances of the MM estimators of (3.92) and (3.93). The simulations are given in Figures 3.16 through 3.19 versus the SNR of the target for $N = 12$. In Figures 3.16 and 3.17, $\Re_{F1} = \Re_{R1}$ and $N = 12$ and 24. Figures 3.18 and 3.19 show the simulation results for $\Re_{F1} = 2\Re_{F2}$ and $N = 12$ and 24. Figures 3.16 and 3.18 show that the MM estimators are essentially unbiased for $N \geq 12$. Figures 3.16 and 3.17 show, for a target with $\Re_{R1} = \Re_{F1}$, that the estimation error in $\Re_{R1}$ is slightly less than the error in $\Re_{F1}$. Figures 3.18 and 3.19 show that the estimation errors in $\Re_{R1}$ and $\Re_{F1}$

are reduced when the percentage of the SNR that results from the Rayleigh part is reduced.

3.7 Two Rician Targets

The in-phase and quadrature components of the sum signal for two unresolved Rician targets are given by (3.1) and (3.2), with $\alpha_i = 0$ and $\beta_i = 0$ for all $i > 2$. Then

$$\bar{s}_I = E[s_I|\Theta_{2Ri}, \phi_1, \phi_2] = \alpha_1 \cos\phi_1 + \alpha_2 \cos\phi_2 \qquad (3.95)$$

$$\bar{s}_Q = E[s_Q|\Theta_{2Ri}, \phi_1, \phi_2] = \alpha_1 \sin\phi_1 + \alpha_2 \sin\phi_2 \qquad (3.96)$$

$$\text{VAR}[s_I|\Theta_{2Ri}, \phi_1, \phi_2] = \text{VAR}[s_Q|\Theta_{2Ri}, \phi_1, \phi_2] = \beta_{10}^2 + \beta_{20}^2 + \sigma_S^2 \qquad (3.97)$$

where Θ_{2Ri} denotes the parameter set $\{\alpha_1, \alpha_2, \beta_{10}, \beta_{20}, \sigma_S\}$. Then

$$\frac{\bar{s}_I^2 + \bar{s}_Q^2}{2\sigma_S^2} = \frac{\alpha_1^2}{2\sigma_S^2} + \frac{\alpha_2^2}{2\sigma_S^2} + 2\frac{\alpha_1\alpha_2}{2\sigma_S^2} \cos(\phi_1 - \phi_2)$$

$$= \Re_{F1} + \Re_{F2} + 2\sqrt{\Re_{F1}\Re_{F2}} \cos \Delta\phi$$

$$= \Re_F(1 + \sin 2\zeta \cos\Delta\phi) \qquad (3.98)$$

where

$$\Delta\phi = \phi_1 - \phi_2 \qquad (3.99)$$

$$\zeta = \tan^{-1}\left(\sqrt{\Re_{F2}\Re_{F1}^{-1}}\right) \qquad (3.100)$$

$$\Re_F = \Re_{F1} + \Re_{F2} \qquad (3.101)$$

Using (3.97) and (3.98) in (3.21) gives the PDF of the observed SNR for two Rician targets with fixed relative phase $\Delta\phi$ as

$$f(\Re_o|\Theta_{Ri}, \Delta\phi) = \frac{1}{\Re_R + 1} I_0\left(\frac{2\sqrt{\Re_o\Re_F}}{\Re_R + 1}\sqrt{1 + \sin 2\zeta \cos\Delta\phi}\right)$$

$$\times \exp\left\{-\frac{\Re_o + \Re_F(1 + \sin 2\zeta \cos\Delta\phi)}{\Re_R + 1}\right\}, \quad \Re_o \geq 0 \qquad (3.102)$$

where $\Re_R = \Re_{R1} + \Re_{R2}$. Then for a fixed $\Delta\phi$, the PDF of the observed SNR of two Rician targets is equivalent to the PDF of a single Rician target. Using (3.97) and (3.98) in (3.22) and (3.23) gives

$$E[\Re_o|\Theta_{2Ri}, \Delta\phi] = \Re_F(1 + \sin 2\zeta \cos\Delta\phi) + \Re_R + 1 \qquad (3.103)$$

$$E[\Re_o^2|\Theta_{2Ri}, \Delta\phi] = 2\left[\Re_F(1 + \sin 2\zeta \cos\Delta\phi) + \Re_R + 1\right]^2$$

$$- \left[\Re_F(1 + \sin 2\zeta \cos\Delta\phi)\right]^2 \qquad (3.104)$$

$$VAR[\Re_o|\Theta_{2Ri}, \Delta\phi] = \left[\Re_R + 1\right]\left[2\Re_F(1 + \sin 2\zeta \cos\Delta\phi) + \Re_R + 1\right] \qquad (3.105)$$
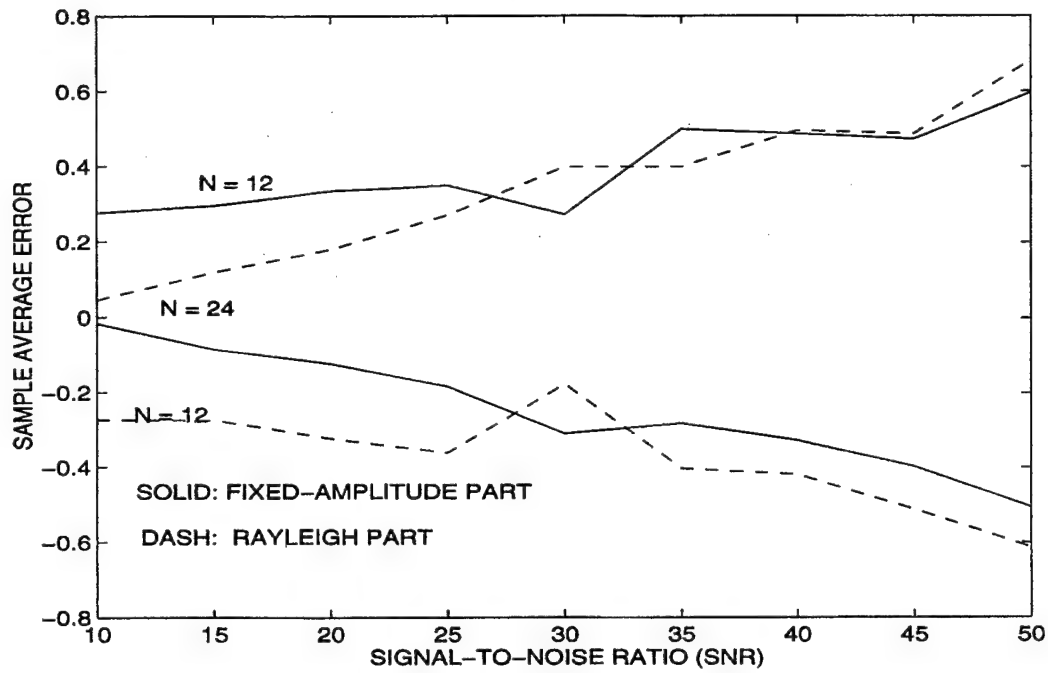
Figure 3.16   Sample Average of the Errors in the MM Estimates for $\Re_{F1} = \Re_{R1}$
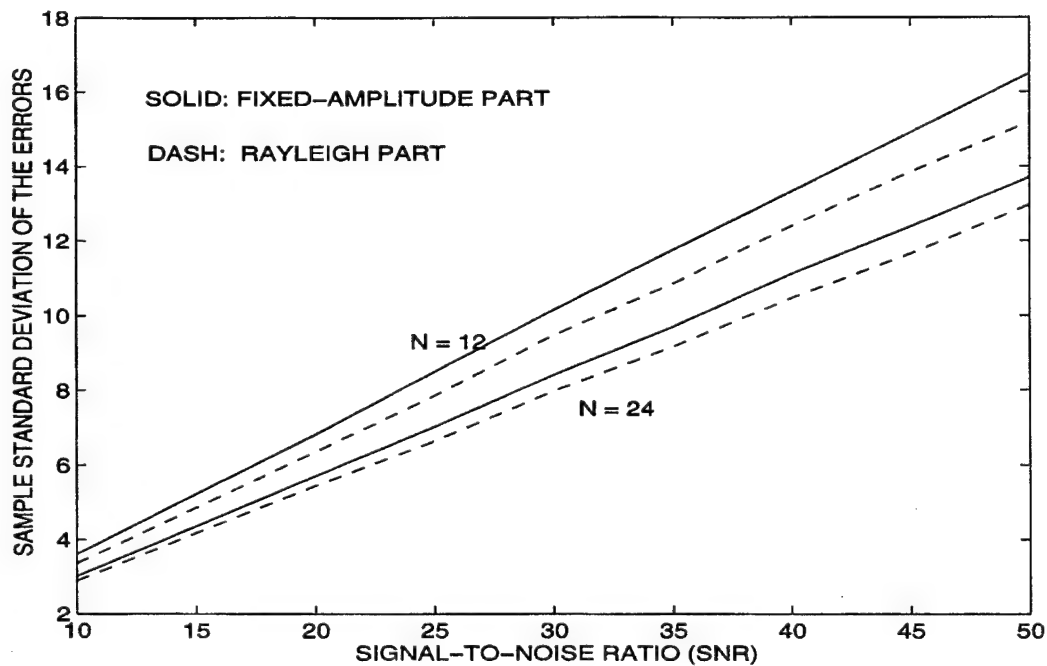
Figure 3.17   Sample Standard Deviation of the Errors in the MM Estimates for $\Re_{F1} = \Re_{R1}$
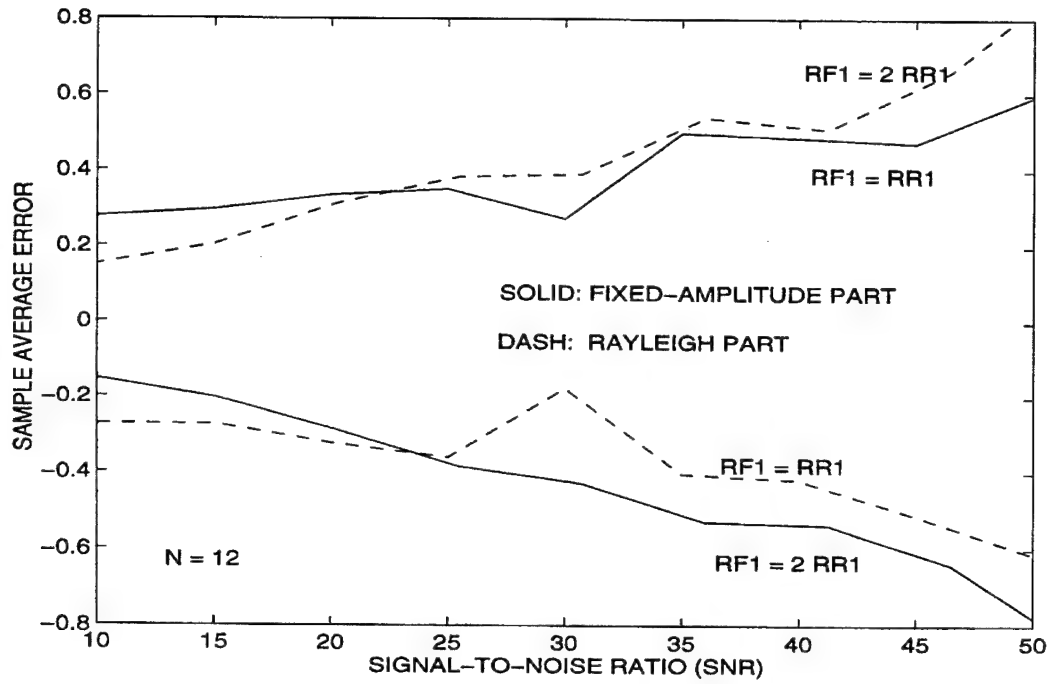
Figure 3.18   Sample Average of the Errors in the MM Estimates for $\Re_{F1} = 2\Re_{R1}$
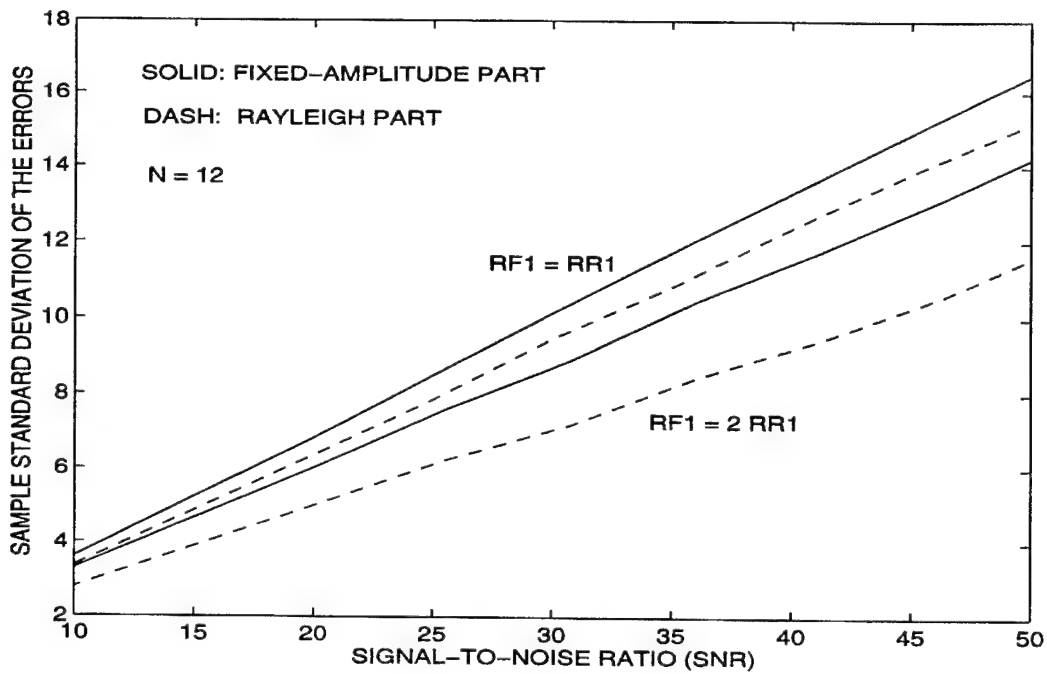
Figure 3.19   Sample Standard Deviation of the Errors in the MM Estimates for $\Re_{F1} = 2\Re_{R1}$

When the relative phase of two Rician targets $\Delta\phi$ is constant, only the composite quantities of $\Re_F(1 + \sin 2\zeta \cos\Delta\phi)$ and $\Re_R$ can be estimated, and the estimation problem is equivalent to that of a single Rician target as treated in Section 3.6. If $\Delta\phi$ is uniformly distributed between pulses, the PDF of the observed SNR of two Ricians is not available in a simple form for an arbitrary Θ_{2Ri}. If $\Delta\phi$ is treated as a random variable uniformly distributed on $(-\pi, \pi]$, then the PDF of $\Re_o$ is given by

$$f(\Re_o|\Theta_{2Ri}) = \frac{1}{\Re_R + 1}\exp\left\{ -\frac{\Re_o + \Re_F}{\Re_R + 1} \right\}\left[I_0\left(\frac{2\sqrt{\Re_o\Re_{F1}}}{\Re_R + 1}\right)I_0\left(\frac{2\sqrt{\Re_o\Re_{F2}}}{\Re_R + 1}\right)I_0\left(\frac{\Re_F \sin 2\zeta}{\Re_R + 1}\right)\right.$$
$$\left. + 2\sum_{m=1}^{\infty}(-1)^m I_m\left(\frac{2\sqrt{\Re_o\Re_{F1}}}{\Re_R + 1}\right)I_m\left(\frac{2\sqrt{\Re_o\Re_{F2}}}{\Re_R + 1}\right)I_m\left(\frac{\Re_F \sin 2\zeta}{\Re_R + 1}\right)\right] \quad (3.106)$$

where $\Re_o \geq 0$, and $I_m(\cdot)$ denotes the m-order modified Bessel function of the first kind. This PDF of $\Re_o$ is the result of using [13, 8.531.1] to express the Bessel function of (3.102) as an infinite series of Bessel functions and evaluating the integral of each term with respect to $\Delta\phi$.

Simplification of the PDF in (3.106) was considered, but none could be found at this time. However, the moments of $\Re_o$ can be obtained by taking the expected value of (3.103) and (3.104) with respect to $\Delta\phi$, which gives

$$E[\Re_o|\Theta_{2Ri}] = \Re_F + \Re_R + 1 \quad (3.107)$$
$$E[\Re_o^2|\Theta_{2Ri}] = \Re_F^2\left(1 + 0.5 \sin^2 2\zeta\right) + 2(\Re_R + 1)(2\Re_F + \Re_R + 1) \quad (3.108)$$
$$= \Re_F^2 + 2\Re_{F1}\Re_{F2} + 2(\Re_R + 1)(2\Re_F + \Re_R + 1)$$
$$VAR[\Re_o|\Theta_{2Ri}] = \frac{1}{2}\Re_F^2 \sin^2 2\zeta + \left(\Re_R + 1\right)\left[2\Re_F + \Re_R + 1\right] \quad (3.109)$$
$$= 2\Re_{F1}\Re_{F2} + \left(\Re_R + 1\right)\left[2\Re_F + \Re_R + 1\right]$$

Since $E[\Re_o|\Theta_{2Ri}]$ is independent of the ζ (i.e., the ratio of the values associated with the fixed-amplitude parts of the two targets), and the variance given in (3.109) is maximized when, $\Re_{F1} = \Re_{F2}$ (i.e., $\zeta = 1$), the probability of detection for the signal echoed from the two targets for a given false-alarm rate will be minimized when $\Re_{F1} = \Re_{F2}$. This assertion agrees with the conclusions drawn in [17]. However, Figure 2 of [17] is in error in that the PDF for $r = \infty$ has a singularity that does not allow the integral of the PDF to equal one. Thus, for various values of $\Re_F$, ζ, and $\Re_R$, (3.102) was integrated numerically with respect to $\Delta\phi$ form $-\pi$ to π to produce $f(\Re_o|\Theta_{2Ri})$. These PDFs of $\Re_o$ are shown in Figures 3.20 and 3.21. Figure 3.20 corresponds to two fixed-amplitude targets (i.e., $\Re_R = 0$), with $\Re_F = 16$ dB, and $\Re_{F1}\Re_{F2}^{-1} = 1, 4, 16$, and ∞. For the case of $\Re_{F1}\Re_{F2}^{-1} = 1$, the PDF achieves a maximum

of 0.1 at $\Re_o = 0$. Thus, Figure 3.20 indicates that for two fixed-amplitude targets with equal amplitudes, the most likely value of $\Re_o$ is 0. Figure 3.21 corresponds to two Rician targets with $\Re_F + \Re_R = 16$ dB, $\Re_R = 0.1\Re_F$, and $\Re_{F1}\Re_{F2}^{-1} = 1, 4, 16$, and ∞. Figure 3.21 shows that the presence of the Rayleigh component of the target amplitude results in unimodal PDFs, while the PDFs of Figure 3.20 are bimodal. However, when the fixed-amplitude parts of the two targets are equal, Figure 3.21 also indicates that the most likely value of $\Re_o$ is 0.

The PDFs presented in Figure 3.20 disagree with those presented in Figures 2 and 3 of [17] in that the maximum of PDFs in [17] occur at $\Re_o > \Re_F$, while in Figure 3.20 the maximums occur at $\Re_o < \Re_F$. The PDFs in Figure 3.20 were confirmed via Monte Carlo simulations. The observed SNRs were generated using (3.1) and (3.2), and the histograms of the observed SNRs closely agreed with the PDFs of Figure 3.20.

3.8 Two Fixed-Amplitude Targets

The in-phase and quadrature components of the sum signal for two unresolved fixed-amplitude targets is given by (3.1) and (3.2), with $\alpha_i = 0$ for $i > 2$, and $\beta_i = 0$ for $i > 0$. Then

$$\bar{s}_I = E[s_I | \Theta_F, \phi_1, \phi_2] = \alpha_1 \cos\phi_1 + \alpha_2 \cos\phi_2 \qquad (3.110)$$

$$\bar{s}_Q = E[s_Q | \Theta_F, \phi_1, \phi_2] = \alpha_1 \sin\phi_1 + \alpha_2 \sin\phi_2 \qquad (3.111)$$

$$\mathrm{VAR}[s_I | \Theta_F, \phi_1, \phi_2] = \mathrm{VAR}[s_Q | \Theta_F, \phi_1, \phi_2] = \sigma_S^2 \qquad (3.112)$$

where Θ_F denotes the parameter set $\{\alpha_1, \alpha_2, \sigma_S\}$. Then

$$\frac{\bar{s}_I^2 + \bar{s}_Q^2}{2\sigma_S^2} = \Re_F(1 + \sin 2\zeta \cos\Delta\phi) \qquad (3.113)$$

where

$$\Delta\phi = \phi_1 - \phi_2 \qquad (3.114)$$

$$\zeta = \tan^{-1}\left(\sqrt{\Re_{F2}\Re_{F1}^{-1}}\right) \qquad (3.115)$$

$$\Re_F = \Re_{F1} + \Re_{F2} \qquad (3.116)$$

Using (3.112) and (3.113) in (3.21) gives the PDF of the observed SNR for two fixed-amplitude targets with fixed relative phase $\Delta\phi$ as

$$f(\Re_o | \Theta_F, \Delta\phi) = I_0\left(2\sqrt{\Re_o\Re_F(1 + \sin 2\zeta \cos\Delta\phi)}\right)$$
$$\times \exp\left\{-\left(\Re_o + \Re_F(1 + \sin 2\zeta \cos\Delta\phi)\right)\right\}, \quad \Re_o \geq 0 \qquad (3.117)$$
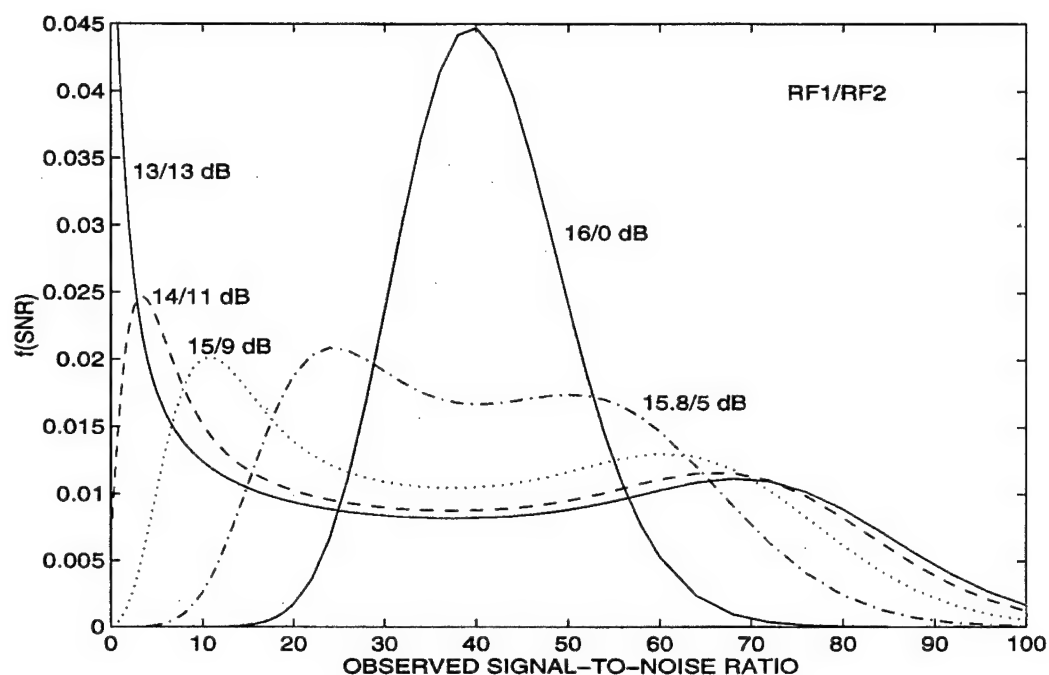
Figure 3.20   PDFs of the $\Re_o$ for Two Fixed-Amplitude Targets with $\Delta\phi$ Random, $\Re_F = 13$ dB and $\Re_{F1}\Re_{F2}^{-1}, = 1, 2, 4, 16$, and ∞
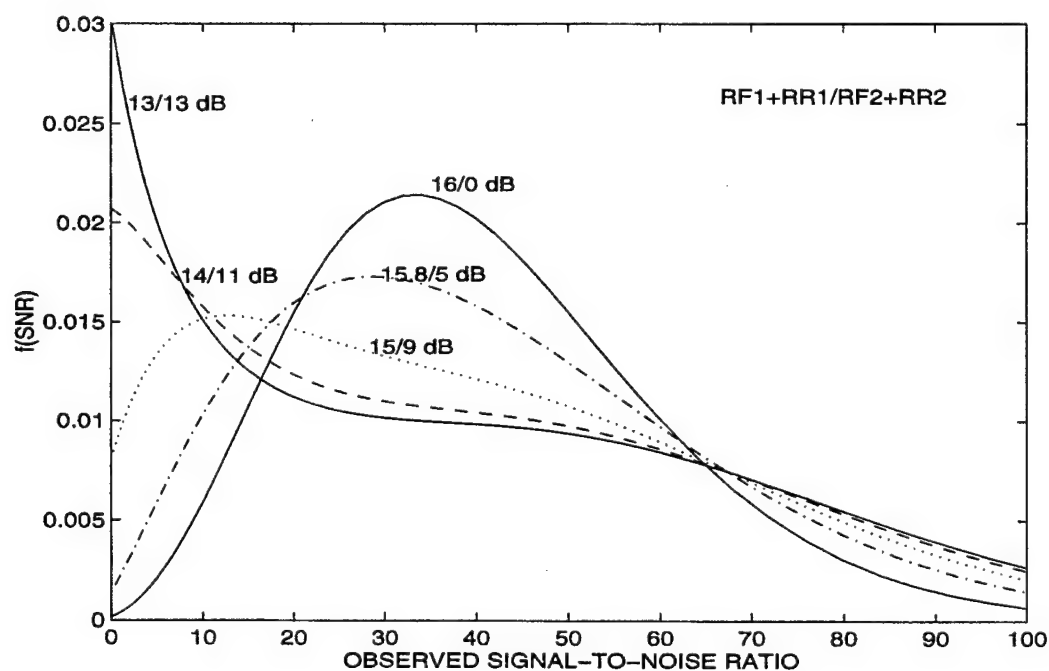
Figure 3.21   PDFs of $\Re_o$ for Two Rician Targets with $\Delta\phi$ Random, $\Re_F + \Re_R = 16$ dB, $\Re_R = 0.1\Re_F$, and $\Re_{F1}\Re_{F2}^{-1}, = 1, 2, 4, 16$, and ∞

Thus, if the relative phase $\Delta\phi$ between the two targets is fixed, $\Re_o$ is distributed the same as a single fixed-amplitude target that is treated in Section 3.2. Using (3.112) and (3.113) in (3.22) and (3.23) gives

$$E[\Re_o|\Theta_F, \Delta\phi] = \Re_F(1 + \sin 2\zeta \cos\Delta\phi) + 1 \tag{3.118}$$

$$E[\Re_o^2|\Theta_F, \Delta\phi] = 2\Big[\Re_F(1 + \sin 2\zeta \cos\Delta\phi) + 1\Big]^2 - \Big[\Re_F(1 + \sin 2\zeta \cos\Delta\phi)\Big]^2 \tag{3.119}$$

$$VAR[\Re_o|\Theta_F, \Delta\phi] = \Big[2\Re_F(1 + \sin 2\zeta \cos\Delta\phi) + 1\Big] \tag{3.120}$$

If the relative phase is random, the measured amplitude is not Rician. If $\Delta\phi$ is treated as a random variable uniformly distributed on $(-\pi, \pi]$, then

$$E[\Re_o|\Theta_F] = \Re_F + 1 \tag{3.121}$$

$$E[\Re_o^2|\Theta_F] = \Re_F^2\Big(1 + 0.5 \sin^2 2\zeta\Big) + 2(2\Re_F + 1) \tag{3.122}$$

$$= \Re_F^2 + 2\Re_{F1}\Re_{F2} + 2(2\Re_F + 1)$$

$$VAR[\Re_o|\Theta_F] = \frac{1}{2}\Re_F^2 \sin^2 2\zeta + \Big[2\Re_F + 1\Big] \tag{3.123}$$

$$2\Re_{F1}\Re_{F2} + \Big[2\Re_F + 1\Big]$$

When the relative phase $\Delta\phi$ of two fixed-amplitude targets is constant, only the composite quantity of $\Re_F(1 + \sin 2\zeta \cos\Delta\phi)$ can be estimated, and the estimation problem is equivalent to that of a single fixed-amplitude target, as treated in Section 3.2. However, if the relative phase is random, MM techniques can be used to develop estimators of $\Re_{F1}$ and $\Re_{F2}$ from (3.121) and (3.123). Setting (3.121) and (3.123) equal to their corresponding sample moments gives the MM estimators for $\Re_{F1}$ and $\Re_{F2}$ as

$$\widetilde{\Re}_{F1} = \frac{1}{2}(Y_N - 1) + \sqrt{\frac{5N-1}{4(N-1)}Y_N^2 + \frac{3}{2}Y_N - \frac{3}{4} - V_N} \tag{3.124}$$

$$\widetilde{\Re}_{F2} = \frac{1}{2}(Y_N - 1) - \sqrt{\frac{5N-1}{4(N-1)}Y_N^2 + \frac{3}{2}Y_N - \frac{3}{4} - V_N} \tag{3.125}$$

where

$$V_N = \frac{1}{N-1}\sum_{k=1}^{N}\Re_{ok}^2 \tag{3.126}$$

Note these MM estimators have been developed by assigning $\Re_{F1}$ to the stronger target and $\Re_{F2}$ to the weaker target.

Monte Carlo simulations with 10,000 experiments were conducted to study the performances of the MM estimators of (3.124) and (3.125). The simulation results are given in Figures 3.22 through 3.25 versus the SNR of target 1 for $N = 12$ and 24. In Figures 3.22 and 3.23, $\Re_{F1} = \Re_{F2}$, and $N = 12$ and 24. The large biases in the estimates, as shown by Figure 3.22, are the result of assigning the larger estimate to $\Re_{F1}$ and the smaller estimate to $\Re_{F2}$. Figure 3.23 shows that the standard deviations of the estimates are rather large compared to the size of the parameters. Figures 3.24 and 3.25 show the simulation results for $\Re_{F1} = \Re_{F2}$ and $\Re_{F1} = 2\Re_{F2}$ with $N = 12$. Figures 3.24 and 3.25 show that the biases in the estimates and the sample standard deviations of the estimation errors are reduced significantly when the SNR of one of the two targets is larger than that of other target. The reduction in the biases of the estimates can be attributed to the better assignment of estimates to targets that is implicit in (3.124) and (3.125). However, the reductions in the estimation error are consistent with the PDFs of the observed SNRs for two, fixed-amplitude targets, as shown in Figure 3.20.

3.9 Fixed-Amplitude Target in the Presence of Multipath

The signal received from a low elevation target in the presence of sea-surface-induced multipath includes four components [20, 21]. The first part travels directly to the target and returns directly to the radar, while the second part travels to the target via the sea surface and returns directly to the radar. The third part travels directly to the target and returns to the radar via the sea surface, while the fourth part travels to the target via the sea surface and returns to the radar via the sea surface. The in-phase and quadrature components of the sum signals for a fixed-amplitude target in the presence of sea-surface-induced multipath are given by (3.1) and (3.2), with

$$\alpha_1 = \alpha_t \tag{3.127}$$

$$\alpha_2 = g\rho_S\alpha_t \tag{3.128}$$

$$\alpha_3 = g\rho_S\alpha_t \tag{3.129}$$

$$\alpha_4 = (g\rho_S)^2\alpha_t \tag{3.130}$$

$$\phi_1 = \phi_t \tag{3.131}$$

$$\phi_2 = \phi_3 = \phi_t + \Delta\phi \tag{3.132}$$

$$\phi_4 = \phi_t + 2\Delta\phi \tag{3.133}$$

$$\beta_1 = 0 \tag{3.134}$$
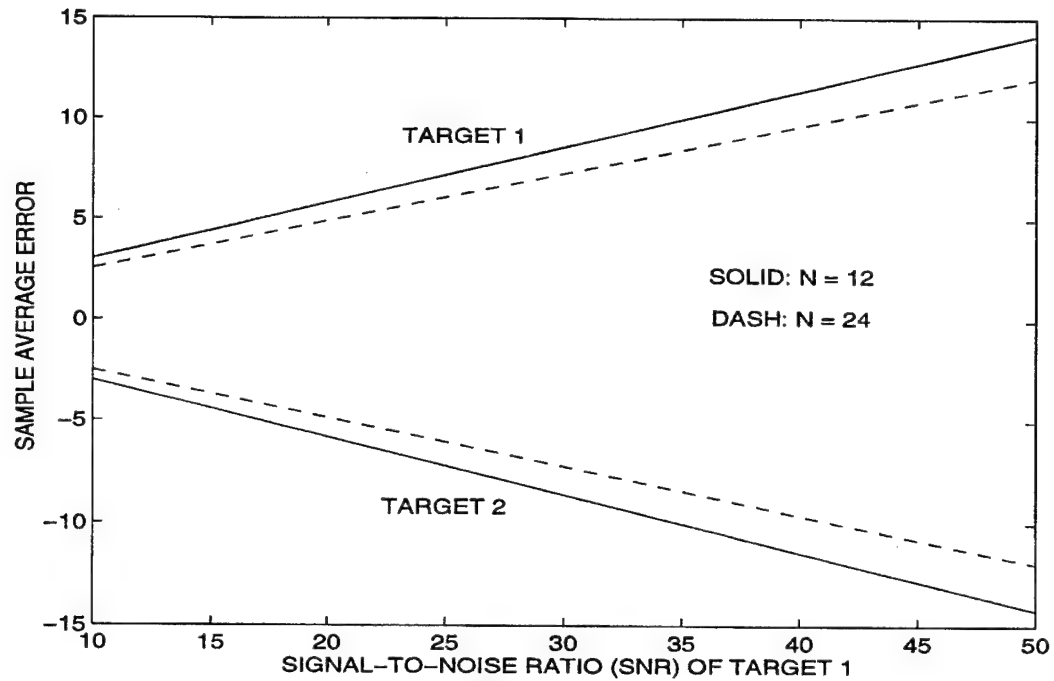
Figure 3.22 Sample Average of the Errors in the MM Estimates of $\Re_{F1}$ and $\Re_{F2}$ for $\Re_{F1} = \Re_{F2}$
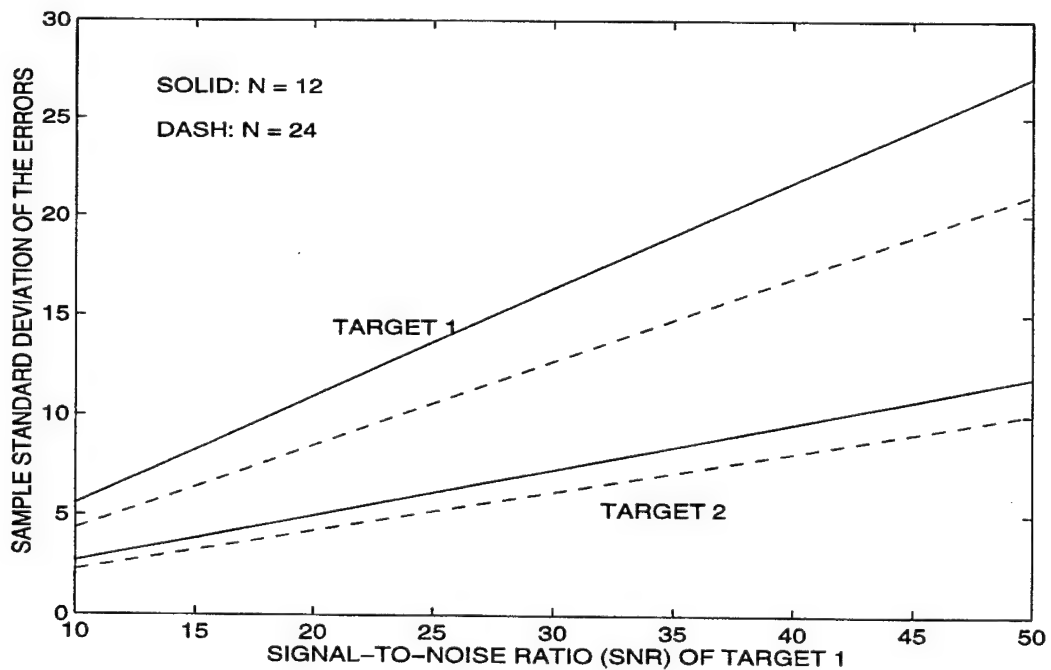
Figure 3.23 Sample Standard Deviation of the Errors in the MM Estimates of $\Re_{F1}$ and $\Re_{F2}$ for $\Re_{F1} = \Re_{F2}$

68
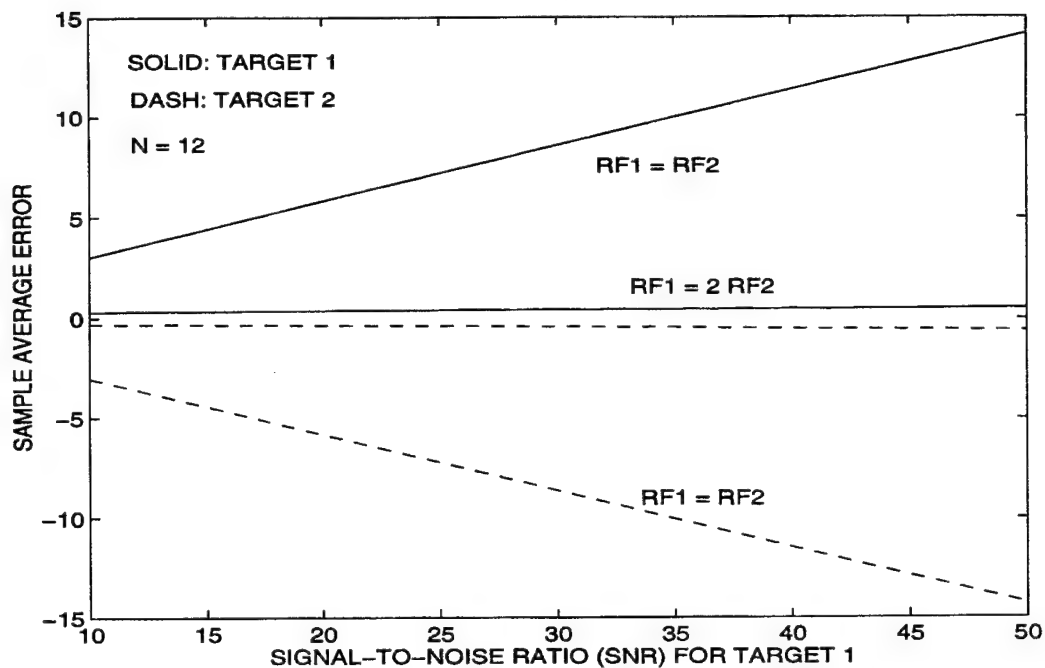
Figure 3.24   Sample Average of the Errors in the MM Estimates of $\Re_{F1}$ and $\Re_{F2}$ for $N = 12$
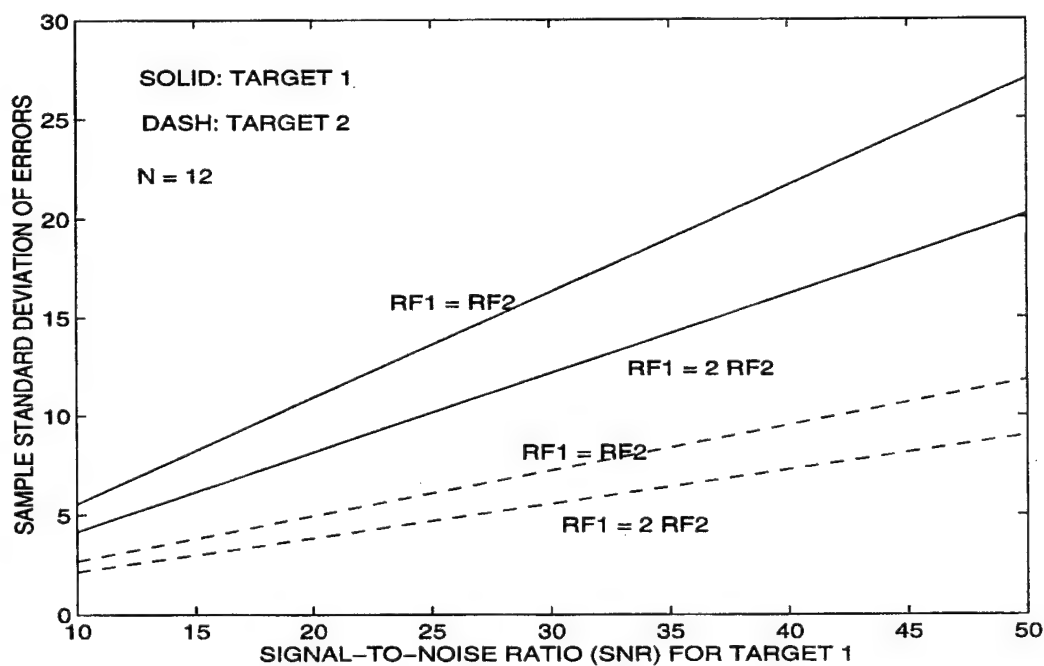
Figure 3.25   Sample Standard Deviation of the Errors in the MM Estimates of $\Re_{F1}$ and $\Re_{F2}$ for $N = 12$

$$\beta_2 = \beta_3 = g\rho_d\alpha_t \tag{3.135}$$

$$\beta_4 = (g\rho_d)^2\alpha_t \tag{3.136}$$

$$\varphi_2 = \varphi_3 = \phi_t + \phi_d + \Delta\phi \tag{3.137}$$

$$\varphi_4 = \phi_t + 2\phi_d + 2\Delta\phi \tag{3.138}$$

where α_t is the voltage amplitude of the target, and the remaining variables are defined in Section 2.6. The in-phase and quadrature portions of the sum signals can be rewritten as

$$s_I = \alpha_{tC}\,\cos\phi_t - \alpha_{tS}\,\sin\phi_t + \alpha_{IC}\,\cos(\phi_t + \Delta\phi) - \alpha_{IS}\,\sin(\phi_t + \Delta\phi)$$
$$2\alpha_t g\rho_d\,\cos(\phi_t + \phi_d + \Delta\phi) + \alpha_t(g\rho_d)^2\,\cos(\phi_t + 2\phi_d + 2\Delta\phi) + n_{SI} \tag{3.139}$$

$$s_Q = \alpha_{tC}\,\sin\phi_t + \alpha_{tS}\,\cos\phi_t + \alpha_{IC}\,\sin(\phi_t + \Delta\phi) + \alpha_{IS}\,\cos(\phi_t + \Delta\phi)$$
$$+ 2\alpha_t g\rho_d\,\sin(\phi_t + \phi_d + \Delta\phi) + \alpha_t(g\rho_d)^2\,\sin(\phi_t + 2\phi_d + 2\Delta\phi) + n_{SQ} \tag{3.140}$$

where

$$\alpha_{tC} = \alpha_t(1 + g\rho_S\,\cos\Delta\phi) \tag{3.141}$$

$$\alpha_{tS} = \alpha_t g\rho_S\,\sin\Delta\phi \tag{3.142}$$

$$\alpha_{IC} = \alpha_t g\rho_S(1 + g\rho_S\,\cos\Delta\phi) = g\rho_S\alpha_{tC} \tag{3.143}$$

$$\alpha_{IS} = \alpha_t(g\rho_S)^2\,\sin\Delta\phi = g\rho_S\alpha_{tS} \tag{3.144}$$

Let Θ_{MP} denote the parameter set $\{\alpha_t, \rho_S, \rho_{d0}, \sigma_S, \sigma_d\}$, and Φ_{MP} denote the parameter set $\{\phi_t, \Delta\phi\}$. Then

$$\bar{s}_I = \alpha_{tC}\,\cos\phi_t - \alpha_{tS}\,\sin\phi_t + \alpha_{IC}\,\cos(\phi_t + \Delta\phi) - \alpha_{IS}\,\sin(\phi_t + \Delta\phi) \tag{3.145}$$

$$\bar{s}_Q = \alpha_{tC}\,\sin\phi_t + \alpha_{tS}\,\cos\phi_t + \alpha_{IC}\,\sin(\phi_t + \Delta\phi) + \alpha_{IS}\,\cos(\phi_t + \Delta\phi) \tag{3.146}$$

and

$$p_{11} = 4\alpha_t^2\rho_{d0}^2 g^2[1 + \rho_{d0}^2 g^2] + \sigma_S^2 \tag{3.147}$$

While ρ_d is Rayleigh distributed, ϕ_d is uniformly distributed on $(-\pi, \pi]$, and the receiver errors are Gaussian, the sum signal of (3.145) and (3.146) is not a Gaussian signal because ρ_d^2 is exponentially distributed rather than Rayleigh. However, since typically $\rho_d < 0.5$ and $g < 1$, the effects of $(\rho_d g)^2$ should be small compared to that of $\rho_d g$. Thus, the sum signal will be approximated as Gaussian for the development of the PDFs of the measured amplitude of the sum signal and the observed SNR.

Approximating the sum signal of (3.139) and (3.140) as Gaussian and using (3.145) through (3.147) in (3.20) of Theorem 3.1 gives the PDF of the measured amplitude of the sum signal for low-elevation targets as

$$f(\Lambda|\Theta_{MP}, \Phi_{MP}) = \frac{\Lambda}{p_{11}} I_0\Big(\frac{\Lambda\alpha_t}{p_{11}}(1 + 2\rho_S g \, \cos\Delta\phi + \rho_S^2 g^2)\Big)$$
$$\times \exp\Big[-\frac{1}{2p_{11}}(\Lambda^2 + \alpha_t^2(1 + 2\rho_S g \, \cos\Delta\phi + \rho_S^2 g^2)^2)\Big] \quad (3.148)$$

where p_{11} is given by (3.150). Using (3.145) through (3.147) in (3.21) of Theorem 3.1 gives the PDF of the observed SNR for low-elevation targets as

$$f(\Re_o|\Theta_{MP}, \Phi_{MP}) = \frac{\sigma_S^2}{p_{11}} I_0\Big(\frac{2\sqrt{\Re_o \Re_F}(1 + 2\rho_S g \, \cos\Delta\phi + \rho_S^2 g^2)}{8\rho_{d0}^2 g^2[1 + \rho_{d0}^2 g^2]\Re_F + 1}\Big)$$
$$\times \exp\Big[-\frac{\Re_o + \Re_F(1 + 2\rho_S g \, \cos\Delta\phi + \rho_S^2 g^2)^2}{8\rho_{d0}^2 g^2[1 + \rho_{d0}^2 g^2]\Re_F + 1}\Big] \quad (3.149)$$

where

$$\Re_F = \frac{\alpha_t^2}{2\sigma_S^2} \quad (3.150)$$

Using (3.145) through (3.148) in (3.22) and (3.23) gives

$$E[\Re_o|\Theta_{MP}, \Phi_{MP}] = [(1 + 2\rho_S g \, \cos\Delta\phi + \rho_S^2 g^2)^2 + 8\rho_{d0}^2 g^2(1 + \rho_{d0}^2 g^2)]\Re_F + 1 \quad (3.151)$$

$$\text{VAR}[\Re_o^2|\Theta_{MP}, \Phi_{MP}] = \Big[8\rho_{d0}^2 g^2(1 + \rho_{d0}^2 g^2)\Re_F + 1\Big]$$
$$\times \Big[[2(1 + 2\rho_S g \, \cos\Delta\phi + \rho_S^2 g^2)^2 + 8\rho_{d0}^2 g^2(1 + \rho_{d0}^2 g^2)]\Re_F + 1\Big] \quad (3.152)$$

Given g, ρ_S, and ρ_{d0}, MM estimators of $\Re_F$ and $\cos\Delta\phi$ can be developed. Setting (3.151) and (3.152) equal to the corresponding sample moments gives MM estimates of $\Re_F$ and $\cos\Delta\phi$ as

$$\widetilde{\Re}_F = \frac{2Y_N - 1}{16\rho_{d0}^2 g^2(1 + \rho_{d0}^2 g^2)} - \frac{1}{8\rho_{d0}^2 g^2(1 + \rho_{d0}^2 g^2)}\sqrt{\frac{2N-1}{N-1}Y_N^2 - V_N} \quad (3.153)$$

$$\tilde{c} = -\frac{1 + \rho_S^2 g^2}{2\rho_S g} + \frac{1}{2\rho_S g}\sqrt{\frac{Y_N - 1}{\widetilde{\Re}_F} - 8\rho_{d0}^2 g^2(1 + \rho_{d0}^2 g^2)} \quad (3.154)$$

where V_N is given by (3.126), and $\tilde{c}$ denotes the MM estimate of $\cos\Delta\phi$.

Monte Carlo simulations with 10,000 experiments were conducted to study the performances of the MM estimators of (3.153) and (3.154). The results of the simulations are given in Figures 3.26 through 3.29 versus the SNR of the target for $N = 20$

and 40, and $\rho_S^2 g^2 = 0.7$. Figure 3.26 shows the sample averages of the errors in $\widetilde{\Re}_{F1}$ for $\rho_{d0}^2 g^2 = 0.1$ and 0.01, while Figure 3.28 shows the sample standard deviations of the errors. Figure 3.26 shows that the average errors in $\widetilde{\Re}_{F1}$ are more sensitive to the change in the diffuse parameter than the change in the number of samples, while Figure 3.28 shows that the sample deviations of the errors are more sensitive to the change in the number of samples than the change in the diffuse parameter. Figure 3.27 shows the sample averages of the errors in $\tilde{c}$, while Figure 3.29 shows the sample standard deviations of the errors. Figures 3.27 and 3.29 show that the performance of $\tilde{c}$ is rather sensitive to the parameters of the diffuse refection, $\rho_{d0}^2 g^2$. If the diffuse reflections are sufficiently weak (*e.g.*, $\rho_{d0}^2 g^2 < 0.05$) relative to the specular reflections, $\tilde{c}$ will not give acceptable estimates of $\cos\Delta\phi$. Additional simulation studies also showed that $\tilde{c}$ gives unacceptable estimates of $\cos\Delta\phi$ if the specular reflections are rather weak (*e.g.*, $\rho_S^2 g^2 < 0.6$). Therefore, since the MM estimators of (3.153) and (3.154) were found to require about 40 pulses (*i.e.*, independent samples) to achieve acceptable performances for a very restricted set of reflection parameters, the MM estimators are not recommended for the simultaneous estimation of the $\Re_{F1}$ and $\cos\Delta\phi$ in real-time tracking applications. However, ML estimators may provide better estimates of the parameters.
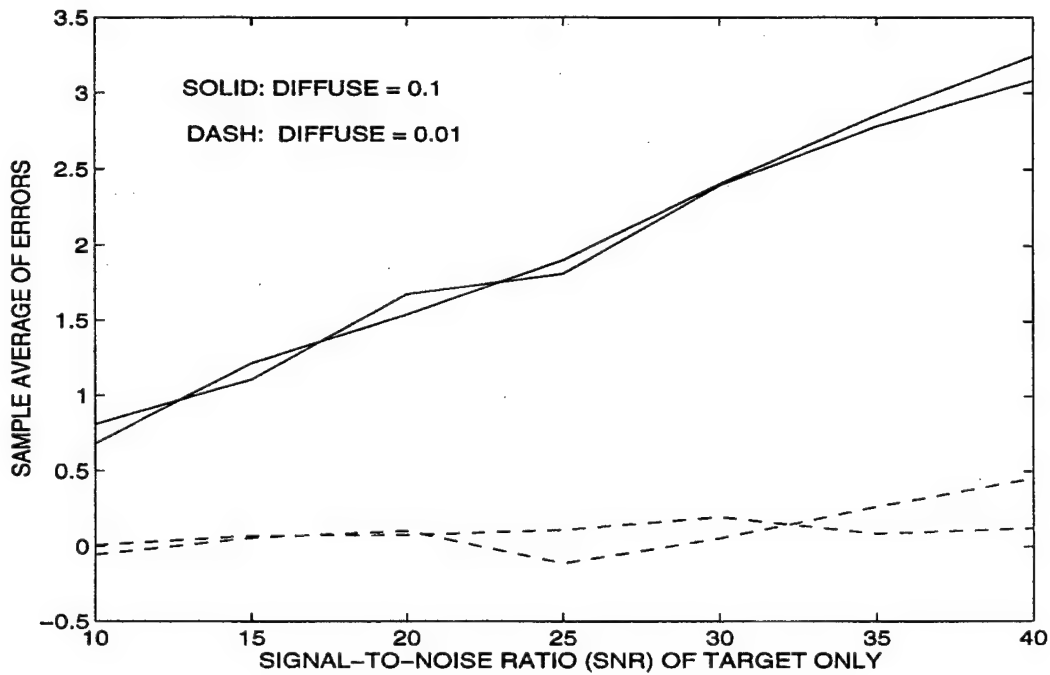
Figure 3.26 Sample Average of the Errors in the MM Estimates of $\Re_{F1}$ for $\Delta\phi = 90°$, $\rho_S^2 g^2 = 0.7$, and $\rho_{d0}^2 g^2 = 0.1$ and 0.01
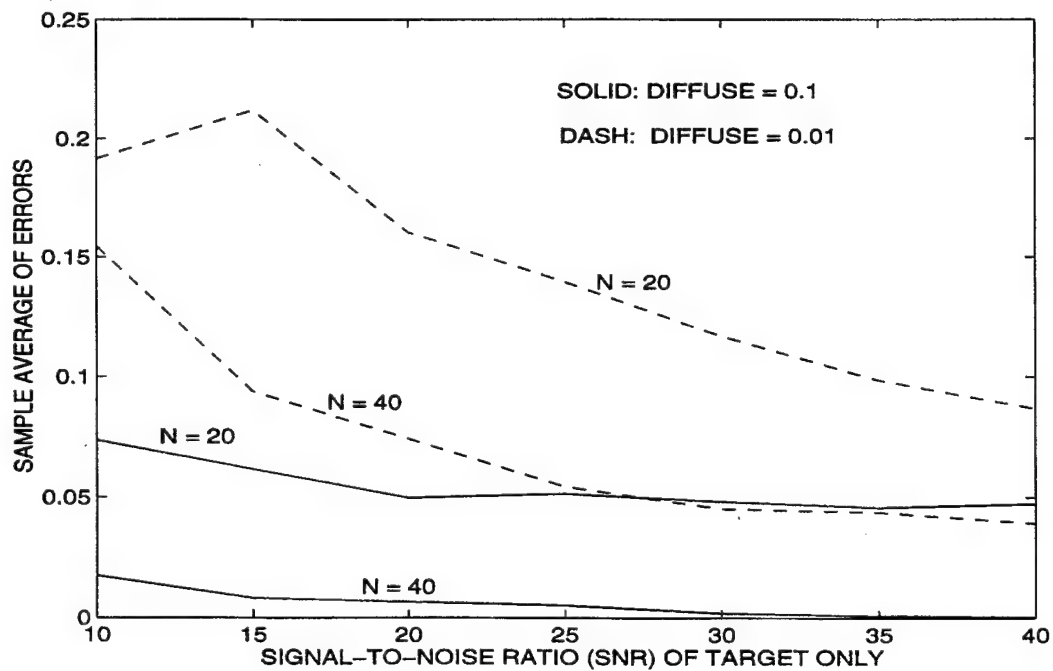
Figure 3.27 Sample Average of the Errors in the MM Estimates of $\cos\Delta\phi$ for $\Delta\phi = 90°$, $\rho_S^2 g^2 = 0.7$, and $\rho_{d0}^2 g^2 = 0.1$ and 0.01
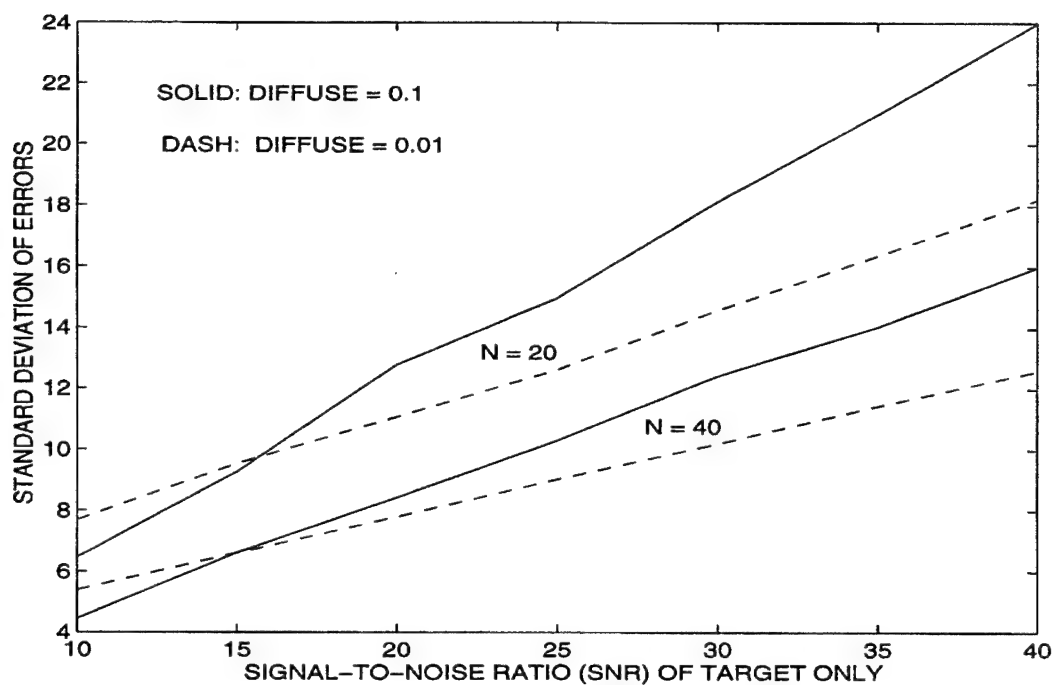
Figure 3.28 Sample Standard Deviation of the Errors in the MM Estimates of $\Re_{F1}$ for $\Delta\phi = 90°$, $\rho_S^2 g^2 = 0.7$, and $\rho_{d0}^2 g^2 = 0.1$ and 0.01
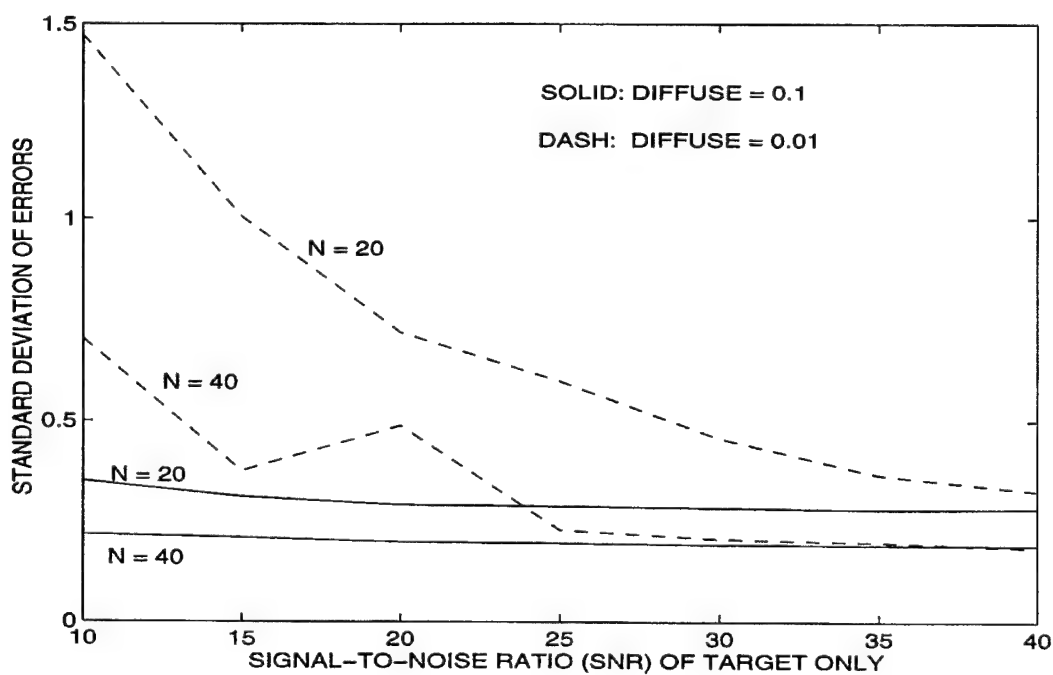
Figure 3.29 Sample Standard Deviation of the Errors in the MM Estimates of $\cos\Delta\phi$ for $\Delta\phi = 90°$, $\rho_S^2 g^2 = 0.7$, and $\rho_{d0}^2 g^2 = 0.1$ and 0.01

Chapter 4

PROBABILITY DISTRIBUTION OF
COMPLEX MONOPULSE RATIO

The probability distribution of the in-phase part (*i.e.*, real part)of the complex monopulse ratio has been studied rather extensively since 1960, while the probability distribution of the quadrature part (*i.e.*, imaginary part) of the monopulse ratio has been considered in only a couple of studies. However, as noted by Sherman in [1,4] and discussed in Chapter 1, the quadrature part of the monopulse ratio includes additional information when the measurements include unresolved targets. The probability distribution of the in-phase and quadrature parts of the monopulse ratio for M unresolved Rician targets is considered in this chapter. The PDF of the complex monopulse ratio is conditioned on the measured amplitude of the sum signal, and the conditional PDF is used to develop the first- and second-order statistics of the in-phase and quadrature monopulse ratios. Since the measured amplitude of the sum signal provides no information concerning the DOA of a target of unknown amplitude, the PDF of the monopulse ratios can be conditioned on the measured amplitude of the sum signal without any loss of information concerning the target DOA. However, conditioning the PDF on the measured amplitude gives the in-phase and quadrature monopulse ratios as Gaussian or approximately Gaussian random variables with first- and second-order statistics that are a function of the measured amplitude. Thus, the statistics of the monopulse ratios can be computed for each pulse.

After a survey of the literature concerned with probability distribution of the monopulse ratios, monopulse measurements of M unresolved Rician targets will be formulated, and the amplitude-conditioned PDF and statistics of the monopulse ratios will be presented in Theorem 4.1. In the remainder of this chapter, Theorem 4.1 will be used to develop the amplitude-conditioned PDF and statistics of the various special cases. In Section 4.1, a single Rayleigh target is considered for a monopulse system with real correlation in the receiver errors on the sum and difference channels. The case of two unresolved Rayleigh targets is considered in Section 4.2, while a

single fixed-amplitude target is considered in Section 4.3. Unresolved measurements of a fixed-amplitude target and Rayleigh target are considered in Section 4.4, and a single Rician target is considered in Section 4.5. Two unresolved targets with fixed-amplitudes are considered in Section 4.6, while a fixed-amplitude target in the presence of sea-surface-induced multipath is considered in Section 4.7.

Survey of the Literature

One of the first articles that considered the probability distribution of monopulse measurements was conducted in 1960 by Manasse [26]. Manasse considered the effects of thermal noise on the accuracy of an ACM system tracking a radio star with a *priori* known power, where the star is maintained near the antenna boresight. However, the results of Manasse are not applicable in typical radar tracking problems because the amplitude of the target is unknown. In 1962, Sharenson [27] considered the accuracy of an off-axis, single-return measurement for a monopulse radar. In his investigations, the monopulse system used the sum signal as a reference to detect the phase (*i.e.*, positive or negative) and estimate the corresponding amplitude of the difference signal, and the monopulse ratio was written as the ratio of two real Gaussian variables. Sharenson linearized the ratio about the sum-signal amplitude and indicated, under the assumption of SNR exceeding 12 dB, that the variance of the monopulse ratio of the two real numbers is inversely proposal to the SNR and increases as the off-axis angle increases. The results derived by Sharenson for the variance of this monopulse ratio of two real numbers are often reported in textbooks and courses for the variance of the in-phase part of the monopulse ratio. His results are particularly important in electronically steered radars that both search for new targets and maintain tracks on multiple targets because targets are detected at various off-axis angles. However, the variance of the monopulse ratio as developed by Sharenson is only approximately correct at high SNRs, and he concluded that the monopulse ratio is an unbiased estimate of the target DOA, which is known from later work to be inaccurate.

From 1977 through 1981, Kanter [28-32] developed the PDF and statistics of the in-phase monopulse ratio for various cases of unresolved targets. In [28], he derived the PDF of the monopulse ratio formed with N independent samples of the sum and difference signals, where each sample received a weight proportional to the sum-signal amplitude squared. Kanter's formulation included any combination of fixed-amplitude and Rayleigh targets. Since the PDF that Kanter developed represented an "average" distribution of the monopulse ratio over all possible sum-signal amplitudes,

he found the monopulse ratio to be a biased observation of the DOA for a fixed-amplitude target as given by (2.51) and to have an infinite variance when only a single observation is considered. Kanter showed in [29] for N independent samples of the monopulse ratio for Rayleigh targets that the central moments less than or equal to $2N - 1$ are finite. Thus, a monopulse ratio formed with two independent samples has a finite variance. Kanter also showed in [29] for Rayleigh targets that the bias in the monopulse ratio as an observation of the target DOA is independent of the number of samples N. In [30], Kanter derived the mean and first absolute central moment of the monopulse ratio without explicitly deriving the PDF of the monopulse ratio. He also showed that the single-pulse monopulse ratio has a finite variance if and only if the correlation coefficient of the sum and difference channels is ± 1. In [31], Kanter derived the PDF of the in-phase monopulse ratio for a fixed-amplitude target in the presence of a jammer (*i.e.*, a Rayleigh target) and numerically calculated the mean of the monopulse ratio for various signal-to-jamming ratios. In [32], Kanter developed the average monopulse response to two jammers or Rayleigh targets, two fixed-amplitude targets, and a fixed-amplitude target in the presence of a jammer. While Kanter has made numerous contributions to our understanding of the probability distribution of the in-phase monopulse ratio, his contributions were to "average" distribution of the monopulse ratio over all possible measured amplitudes of the sum signal. Thus, his results are applicable only to cases where the statistics of measured amplitude of the sum signal is ignored.

In 1981, Asseo [33] developed the PDF of the quadrature part of the monopulse ratio for one and two targets with either fixed or Rayleigh amplitudes. However, the PDFs that Asseo developed also represented the "average" distribution of the quadrature part of the monopulse ratio over all possible measured amplitudes of the sum signal. In 1991, Tullsson [34] considered the PDF for monopulse measurements of multiple unresolved Rayleigh targets and showed that conditioning the PDF on the measured amplitude of the sum signal gives the in-phase and quadrature monopulse ratios as Gaussian random variables, with the quadrature part having a mean of zero. Tullsson stated correctly without proof that the in-phase and quadrature parts of the monopulse ratio are independent. Tullsson also considered in [34] the effects of applying a threshold test to the sum-signal amplitude prior to computing the monopulse ratio. He showed for Rayleigh targets that the mean of the monopulse ratio is unaffected by thresholding, while the variance is inversely proportional to the SNR threshold.

In [35], Seifer noted the fact that every monopulse measurement that is considered

for processing has a sum-signal amplitude that exceeds a positive threshold. He showed that the variance of a monopulse ratio formed with a single pulse of the sum and difference signals is then finite when the thresholding of the amplitude of the sum signal is considered. Seifer also showed that amplitude thresholding of the sum signal increases the bias in the monopulse observations of the target DOA. Thus, the bias in the monopulse ratio as developed by Kanter and given by (2.51) is significantly less than the bias that will be seen in a system with a reasonable amplitude threshold. In [36] Seifer extended the results of [35] to targets that are offset from the null of the monopulse ratio. The focus of [35,36] is the average distribution of the monopulse ratio given that the measured amplitude of the sum signal exceeds a threshold. While Seifer's results are appropriate for the analysis and design of servo systems with filter designs based on stationary statistics, further analysis is needed to support filtering for nonstationary processes and decisions for control of modern sensor systems.

Groves, Blair, and Chow [37] developed the joint PDF of the in-phase and quadrature parts of the monopulse ratio for arbitrarily-correlated Gaussian errors and non-zero means in the sum and difference signals. The general result was used to consider the effects of amplitude thresholding of the sum signal for the special case of real correlation between the receiver errors in the sum and difference channels. However, the general result for the PDF represented the "average" distribution of the complex monopulse ratio over all possible measured amplitudes of the sum signal. In contrast to this average distribution, this chapter presents the amplitude-conditioned PDF and statistics for the in-phase and quadrature parts of the monopulse ratio.

Formulation of the Problem and General Result

In a typical monopulse radar system, the outputs of the receivers are match filtered, and the in-phase and quadrature portions of the sum and difference signals for the merged measurements from M Rician targets can be expressed as

$$s_I = \sum_{i=1}^{M} \left(\alpha_i \cos \phi_i + \beta_i \cos \varphi_i \right) + n_{SI} \tag{4.1}$$

$$s_Q = \sum_{i=1}^{M} \left(\alpha_i \sin \phi_i + \beta_i \sin \varphi_i \right) + n_{SQ} \tag{4.2}$$

$$d_I = \sum_{i=1}^{M} \left(\alpha_i \eta_i \cos \phi_i + \beta_i \eta_i \cos \varphi_i \right) + n_{dI} \tag{4.3}$$

$$d_Q = \sum_{i=1}^{M} \left(\alpha_i \eta_i \sin \phi_i + \beta_i \eta_i \sin \varphi_i \right) + n_{dQ} \tag{4.4}$$

where

α_i = amplitude from the fixed-amplitude part of target i

β_i = amplitude from the Rayleigh part of target i

ϕ_i = phase of the fixed-amplitude part of target i

φ_i = phase of the Rayleigh part of target i

η_i = DOA parameter of target i

$n_{SI} \sim N(0, \sigma_S^2)$

$n_{SQ} \sim N(0, \sigma_S^2)$

$n_{dI} \sim N(0, \sigma_d^2)$

$n_{dQ} \sim N(0, \sigma_d^2)$

with $N(\bar{x}, \sigma^2)$ denoting a Gaussian distribution with mean $\bar{x}$ and variance σ^2. Also, with $E[\cdot]$ denoting expected value,

$$E[n_{SI} n_{SQ}] = 0 \tag{4.5}$$

$$E[n_{dI} n_{dQ}] = 0 \tag{4.6}$$

$$E[n_{SI} n_{dI}] = \rho \sigma_S \sigma_d \tag{4.7}$$

$$E[n_{SQ} n_{dQ}] = \rho \sigma_S \sigma_d \tag{4.8}$$

where $\rho \neq 0$ represents a monopulse system with real correlation between the receiver errors in sum and difference channels. The phases, φ_i, are independent and uniformly distributed on $(-\pi, \pi]$. The Rayleigh parts of the target amplitudes are also independent.

Since β_i are Rayleigh distributed, and the φ_i are uniformly distributed on $(-\pi, \pi]$, s_I, s_Q, d_I, and d_Q are jointly Gaussian, independent random variables when the α_i and ϕ_i are given. Let

$$\bar{s}_I = E[s_I | \Psi, \Phi] = \sum_{i=1}^{M} \alpha_i \cos \phi_i \tag{4.9}$$

$$\bar{s}_Q = E[s_Q | \Psi, \Phi] = \sum_{i=1}^{M} \alpha_i \sin \phi_i \tag{4.10}$$

$$\bar{d}_I = E[d_I | \Psi, \Phi] = \sum_{i=1}^{M} \alpha_i \eta_i \cos \phi_i \tag{4.11}$$

$$\bar{d}_Q = E[d_Q | \Psi, \Phi] = \sum_{i=1}^{M} \alpha_i \eta_i \sin \phi_i \tag{4.12}$$

where Ψ is the parameter set $\{\alpha_1, \beta_{10}, \eta_1, \ldots, \alpha_M, \beta_{M0}, \eta_M, \sigma_S, \sigma_d\}$, Φ is the parameter set $\{\phi_1, \ldots, \phi_M\}$, and β_{i0} denotes the Rayleigh parameter of target i. Let

$$p_{11} = \text{VAR}[s_I|\Psi, \Phi] = \text{VAR}[s_Q|\Psi, \Phi] = \sum_{i=1}^{M} \beta_{i0}^2 + \sigma_S^2 \tag{4.13}$$

$$p_{22} = \text{VAR}[d_I|\Psi, \Phi] = \text{VAR}[d_Q|\Psi, \Phi] = \sum_{i=1}^{M} \eta_i^2 \beta_{i0}^2 + \sigma_d^2 \tag{4.14}$$

$$p_{12} = \text{COV}[s_I, d_I|\Psi, \Phi] = \text{COV}[s_Q, d_Q|\Psi, \Phi] = \sum_{i=1}^{M} \eta_i \beta_{i0}^2 + \rho \sigma_S \sigma_d \tag{4.15}$$

where $\text{VAR}[\cdot]$ denotes variance, and $\text{COV}[\cdot, \cdot]$ denotes covariance. Note that

$$\text{COV}[s_I, s_Q|\Psi, \Phi] = \text{COV}[d_I, d_Q|\Psi, \Phi] = 0 \tag{4.16}$$

and

$$\text{COV}[s_I, d_Q|\Psi, \Phi] = \text{COV}[d_I, s_Q|\Psi, \Phi] = 0 \tag{4.17}$$

Denoting $s = s_I + j s_Q$ and $d = d_I + j d_Q$, the in-phase and quadrature parts of the monopulse ratio are given by

$$y_I = \text{Re}\left(\frac{d}{s}\right) = \frac{d_I s_I + s_Q d_Q}{s_I^2 + s_Q^2} \tag{4.18}$$

$$y_Q = \text{Im}\left(\frac{d}{s}\right) = \frac{d_Q s_I - d_I s_Q}{s_I^2 + s_Q^2} \tag{4.19}$$

The joint PDF of y_I and y_Q is obtained by applying the one-to-one transformation of random variables defined by (3.9), (3.10), (4.18), and (4.19) into the PDF $f(s_I, s_Q, d_I, d_Q|\Psi, \Phi)$, integrating the result with respect to ψ, and conditioning the density on Λ, the measured amplitude of the sum signal. The following theorem gives the result in a general form.

Theorem 4.1 Let the in-phase and quadrature parts of the sum and difference signals be Gaussian signals with

$$\bar{s}_I = E[s_I|\Psi, \Phi] \tag{4.20}$$

$$\bar{s}_Q = E[s_Q|\Psi, \Phi] \tag{4.21}$$

$$\bar{d}_I = E[d_I|\Psi, \Phi] \tag{4.22}$$

$$\bar{d}_Q = E[d_Q|\Psi, \Phi] \tag{4.23}$$

$$p_{11} = E[(s_I - \bar{s}_I)^2|\Psi, \Phi] = E[(s_Q - \bar{s}_Q)^2|\Psi, \Phi] \tag{4.24}$$

$$p_{22} = E[(d_I - \bar{d}_I)^2|\Psi, \Phi] = E[(d_Q - \bar{d}_Q)^2|\Psi, \Phi] \tag{4.25}$$

$$p_{12} = E[(s_I - \bar{s}_I)(d_I - \bar{d}_I)|\Psi, \Phi] = E[(s_Q - \bar{s}_Q)(d_Q - \bar{d}_Q)|\Psi, \Phi] \tag{4.26}$$

and $E[(s_I - \bar{s}_I)(s_Q - \bar{s}_Q)|\Psi, \Phi] = E[(d_I - \bar{d}_I)(d_Q - \bar{d}_Q)|\Psi, \Phi] = 0$, where Ψ and Φ denote the sets of given parameters. Then the PDF of y_I and y_Q conditioned on the measured amplitude of the sum signal, Λ, is given by

$$f(y_I, y_Q | \Lambda, \Psi, \Phi) = \frac{\Lambda^2 p_{11}}{2\pi(p_{11}p_{22} - p_{12}^2)I_0\left(\frac{\Lambda}{p_{11}}\sqrt{\bar{s}_I^2 + \bar{s}_Q^2}\right)}$$

$$\times I_0\left(\frac{\Lambda p_{11}}{p_{11}p_{22} - p_{12}^2}\sqrt{A_1 + A_2 + A_3 + A_4}\right)$$

$$\times \exp\left[-\frac{p_{11}}{2(p_{11}p_{22} - p_{12}^2)}\left[\left(\bar{d}_I - \bar{s}_I\frac{p_{12}}{p_{11}}\right)^2 + \left(\bar{d}_Q - \bar{s}_Q\frac{p_{12}}{p_{11}}\right)^2\right]\right]$$

$$\times \exp\left[-\frac{\Lambda^2 p_{11}}{2(p_{11}p_{22} - p_{12}^2)}\left[\left(y_I - \frac{p_{12}}{p_{11}}\right)^2 + y_Q^2\right]\right] \qquad (4.27)$$

where

$$A_1 = \left[\left(\frac{p_{22}}{p_{11}} - \frac{p_{12}^2}{p_{11}^2} + \frac{p_{12}}{p_{11}}(1 - y_I)\right)^2 + \frac{p_{12}^2}{p_{11}^2}y_Q^2\right]\left(\bar{s}_I^2 + \bar{s}_Q^2\right) \qquad (4.28)$$

$$A_2 = \left[\left(y_I - \frac{p_{12}}{p_{11}}\right)^2 + y_Q^2\right]\left(\bar{d}_I^2 + \bar{d}_Q^2\right) \qquad (4.29)$$

$$A_3 = 2\left[\left(\frac{p_{22}}{p_{11}} - \frac{p_{12}^2}{p_{11}^2} + \frac{p_{12}}{p_{11}}(1 - y_I)\right)\left(y_I - \frac{p_{12}}{p_{11}}\right) - \frac{p_{12}}{p_{11}}y_Q^2\right]\left(\bar{s}_I\bar{d}_I + \bar{s}_Q\bar{d}_Q\right) \quad (4.30)$$

$$A_4 = 2\left[\frac{p_{22}}{p_{11}} - \frac{p_{12}^2}{p_{11}^2}(1 + y_Q) + \frac{p_{12}}{p_{11}}y_Q\right]\left(\bar{s}_I\bar{d}_Q - \bar{s}_Q\bar{d}_I\right) \qquad (4.31)$$

The first- and second-order moments of y_I and y_Q are given by

$$E[y_I | \Lambda, \Psi, \Phi] = \frac{p_{12}}{p_{11}} + I_{1|0}\left(\frac{\Lambda}{p_{11}}\sqrt{\bar{s}_I^2 + \bar{s}_Q^2}\right)$$

$$\times \left[\frac{\bar{s}_I\bar{d}_I + \bar{s}_Q\bar{d}_Q}{\Lambda\sqrt{\bar{s}_I^2 + \bar{s}_Q^2}} - \frac{p_{12}}{p_{11}\Lambda}\sqrt{\bar{s}_I^2 + \bar{s}_Q^2}\right] \qquad (4.32)$$

$$E[y_Q | \Lambda, \Psi, \Phi] = I_{1|0}\left(\frac{\Lambda}{p_{11}}\sqrt{\bar{s}_I^2 + \bar{s}_Q^2}\right)\left[\frac{\bar{s}_I\bar{d}_Q - \bar{s}_Q\bar{d}_I}{\Lambda\sqrt{\bar{s}_I^2 + \bar{s}_Q^2}}\right] \qquad (4.33)$$

$$\text{COV}[y_I, y_Q | \Lambda, \Psi, \Phi] = \left[\frac{\bar{d}_I\bar{d}_Q(\bar{s}_I^2 - \bar{s}_Q^2) - \bar{s}_I\bar{s}_Q(\bar{d}_I^2 - \bar{d}_Q^2)}{\Lambda^2(\bar{s}_I^2 + \bar{s}_Q^2)} - \frac{p_{12}}{\Lambda^2 p_{11}}[\bar{s}_I\bar{d}_Q - \bar{s}_Q\bar{d}_I]\right]$$

$$\times I_{1|0}^*\left(\frac{\Lambda}{p_{11}}\sqrt{\bar{s}_I^2 + \bar{s}_Q^2}\right) \qquad (4.34)$$

$$\text{VAR}[y_I | \Lambda, \Psi, \Phi] = \frac{p_{11}p_{22} - p_{12}^2}{\Lambda^2 p_{11}}$$

$$+ \frac{[\bar{s}_I\bar{d}_I + \bar{s}_Q\bar{d}_Q - p_{12}p_{11}^{-1}(\bar{s}_I^2 + \bar{s}_Q^2)]^2}{\Lambda^2(\bar{s}_I^2 + \bar{s}_Q^2)}I_{1|0}^*\left(\frac{\Lambda}{p_{11}}\sqrt{\bar{s}_I^2 + \bar{s}_Q^2}\right)$$

$$+ \left[\left(\bar{d}_I - \bar{s}_I \frac{p_{12}}{p_{11}} \right)^2 + \left(\bar{d}_Q - \bar{s}_Q \frac{p_{12}}{p_{11}} \right)^2 \right] \frac{p_{11}}{\Lambda^3 \sqrt{\bar{s}_I^2 + \bar{s}_Q^2}}$$

$$\times I_{1|0} \left(\frac{\Lambda}{p_{11}} \sqrt{\bar{s}_I^2 + \bar{s}_Q^2} \right) \tag{4.35}$$

$$\mathrm{VAR}[y_Q | \Lambda, \Psi, \Phi] = \frac{p_{11}p_{22} - p_{12}^2}{\Lambda^2 p_{11}} + I_{1|0}^* \left(\frac{\Lambda}{p_{11}} \sqrt{\bar{s}_I^2 + \bar{s}_Q^2} \right) \frac{[\bar{s}_I \bar{d}_Q - \bar{s}_Q \bar{d}_I]^2}{\Lambda^2 (\bar{s}_I^2 + \bar{s}_Q^2)}$$

$$+ \left[\left(\bar{d}_I - \bar{s}_I \frac{p_{12}}{p_{11}} \right)^2 + \left(\bar{d}_Q - \bar{s}_Q \frac{p_{12}}{p_{11}} \right)^2 \right] \frac{p_{11}}{\Lambda^3 \sqrt{\bar{s}_I^2 + \bar{s}_Q^2}}$$

$$\times I_{1|0} \left(\frac{\Lambda}{p_{11}} \sqrt{\bar{s}_I^2 + \bar{s}_Q^2} \right) \tag{4.36}$$

where

$$I_{1|0}(x) = \frac{I_1(x)}{I_0(x)} \tag{4.37}$$

$$I_{1|0}^*(x) = 1 - \frac{2}{x} I_{1|0}(x) - I_{1|0}^2(x) \tag{4.38}$$

and $I_1(\cdot)$ is the first-order modified Bessel function of the first kind.

Proof: See Theorem A.2 of Appendix A.

In the remainder of this chapter, the results of Theorem 4.1 will be used to develop the amplitude-conditioned PDF and statistics of the various special cases. First, a single Rayleigh target is considered for a monopulse system with real correlation in the receiver errors on the sum and difference channels.

4.1 Rayleigh Target and Real-Correlated Receiver Errors

The in-phase and quadrature components of the sum and difference signals for a Rayleigh target and real-correlated receiver errors are given by (4.1) through (4.4), with $\alpha_i = 0$ for all i, and $\beta_i = 0$ for all $i > 1$. Then $\bar{s}_I = \bar{s}_Q = \bar{d}_I = \bar{d}_Q = 0$, and (4.13) through (4.15) gives

$$p_{11} = \mathrm{VAR}[s_I | \Psi_R] = \mathrm{VAR}[s_Q | \Psi_R] = \beta_{10}^2 + \sigma_S^2 \tag{4.39}$$

$$p_{22} = \mathrm{VAR}[d_I | \Psi_R] = \mathrm{VAR}[d_Q | \Psi_R] = \eta_1^2 \beta_{10}^2 + \sigma_d^2 \tag{4.40}$$

$$p_{12} = \mathrm{COV}[s_I, d_I | \Psi_R] = \mathrm{COV}[s_Q, d_Q | \Psi_R] = \eta_1 \beta_{10}^2 \tag{4.41}$$

where Ψ_R is the parameter set $\{\beta_{10}, \eta_1, \sigma_S, \sigma_d\}$. Using these results in (4.27) through (4.31) gives the PDF of the in-phase and quadrature parts of the monopulse ratio for a Rayleigh target as

$$f(y_I, y_Q | \Lambda, \Psi_R) = \frac{\Lambda^2 p_{11}}{2\pi (p_{11}p_{22} - p_{12}^2)} \exp\left[- \frac{\Lambda^2 p_{11}}{2(p_{11}p_{22} - p_{12}^2)} \left[(y_I - \frac{p_{12}}{p_{11}})^2 + y_Q^2 \right] \right]$$

$$= f(y_I | \Re_o, \Psi_R) f(y_Q | \Re_o, \Psi_R) \tag{4.42}$$

where

$$f(y_I|\Re_o, \Psi_R) = N\left(\frac{\Re_{R1}\eta + \rho\sigma_d\sigma_S^{-1}}{\Re_{R1} + 1}, \frac{p}{2\Re_o}\right) \qquad (4.43)$$

$$f(y_Q|\Re_o, \Psi_R) = N\left(0, \frac{p}{2\Re_o}\right) \qquad (4.44)$$

$$p = \left[\frac{\sigma_d^2}{\sigma_S^2}\left(1 - \frac{\rho^2}{\Re_{R1} + 1}\right) + \frac{\Re_{R1}\eta(\eta - 2\rho\sigma_d\sigma_S^{-1})}{\Re_{R1} + 1}\right] \qquad (4.45)$$

with $\Re_{R1}$ given by (3.14), and $N(\bar{x}, \sigma^2)$ denoting the Gaussian distribution with mean $\bar{x}$ and variance σ^2. Thus, y_I and y_Q are conditionally Gaussian, independent random variables. Note that (4.43) shows that even for $\rho = 0$, y_I is a notably biased observation[3] of the DOA η for values of $\Re_{R1}$ less than about 13 dB. While the results of (4.43) through (4.45) can be shown to be equivalent to that developed by Tullsson in [34], Tullsson did not explicitly show the independence of y_I and y_Q given by (4.42).

For N independent samples or pulses, the ML estimate of $\bar{y}_I$, which is the mean of y_I given Λ, is given by

$$\hat{y}_I = \left[\sum_{j=1}^{N} \Re_{oj}\right]^{-1} \sum_{k=1}^{N} \Re_{ok} y_{Ik} = \frac{1}{NY_N} \sum_{k=1}^{N} \Re_{ok} y_{Ik} \qquad (4.46)$$

where $\Re_{ok}$ and y_{Ik} denote the observed SNR and in-phase monopulse ratio for pulse k and

$$Y_N = \frac{1}{N} \sum_{k=1}^{N} \Re_{ok} \qquad (4.47)$$

Thus, the estimate $\hat{y}_I$ is a "power" or "energy" weighted sum of the N monopulse ratios [28]. Since the y_{Ik} are Gaussian random variables, $\hat{y}_I$ is the minimum variance estimate of $\bar{y}_I$ and a Gaussian random variable with variance given by

$$\sigma_{\hat{y}_I}^2 = \left[\sum_{k=1}^{N} 2\Re_{ok}\right]^{-1} p = \frac{p}{2NY_N} \qquad (4.48)$$

However, note that $\hat{y}_I$ being the minimum variance estimate of $\bar{y}_I$ does not imply that $\hat{y}_I$ is the minimum variance estimate of η.

4.2 Two Rayleigh Targets

The in-phase and quadrature components of the sum and difference signals for two unresolved Rayleigh targets and independent receiver errors are given by (4.1) through (4.4), with $\alpha_i = 0$ for all i, $\beta_i = 0$ for all $i > 2$, and $\rho = 0$. The $\rho = 0$ is made

---

[3] Notably biased estimate is used here to denote a biased estimate with bias greater than 5% of the true value.

to simplify the following analysis. Then $\bar{s}_I = \bar{s}_Q = \bar{d}_I = \bar{d}_Q = 0$, and (4.13) through (4.15) gives

$$p_{11} = \text{VAR}[s_I|\Psi_{2R}] = \text{VAR}[s_Q|\Psi_{2R}] = \beta_{10}^2 + \beta_{20}^2 + \sigma_S^2 \tag{4.49}$$

$$p_{22} = \text{VAR}[d_I|\Psi_{2R}] = \text{VAR}[d_Q|\Psi_{2R}] = \eta_1^2\beta_{10}^2 + \eta_2^2\beta_{20}^2 + \sigma_d^2 \tag{4.50}$$

$$p_{12} = \text{COV}[s_I, d_I|\Psi_{2R}] = \text{COV}[s_Q, d_Q|\Psi_{2R}] = \eta_1\beta_{10}^2 + \eta_2\beta_{20}^2 \tag{4.51}$$

where Ψ_{2R} is the parameter set $\{\beta_{10}, \eta_1, \beta_{20}, \eta_2, \sigma_S, \sigma_d\}$. Using these results in (4.27) through (4.31) gives the PDF of the in-phase and quadrature parts of the monopulse ratio for two unresolved Rayleigh targets as

$$
\begin{aligned}
f(y_I, y_Q|\Lambda, \Psi_{2R}) &= \frac{\Lambda^2 p_{11}}{2\pi(p_{11}p_{22} - p_{12}^2)} \exp\left[-\frac{\Lambda^2 p_{11}}{2(p_{11}p_{22} - p_{12}^2)}\left[(y_I - \frac{p_{12}}{p_{11}})^2 + y_Q^2\right]\right] \\
&= f(y_I|\Re_o, \Psi_{2R})f(y_Q|\Re_o, \Psi_{2R})
\end{aligned} \tag{4.52}
$$

where

$$f(y_I|\Re_o, \Psi_{2R}) = N\left(\frac{\Re_{R1}\eta_1 + \Re_{R2}\eta_2}{\Re_{R1} + \Re_{R2} + 1}, \sigma_1^2\right) \tag{4.53}$$

$$f(y_Q|\Re_o, \Psi_{2R}) = N\left(0, \sigma_1^2\right) \tag{4.54}$$

$$\sigma_1^2 = \frac{q}{2\Re_o} \tag{4.55}$$

$$q = \left[\frac{\sigma_d^2}{\sigma_S^2} + \frac{\Re_{R1}\eta_1^2 + \Re_{R2}\eta_2^2 + \Re_{R1}\Re_{R2}(\eta_1 - \eta_2)^2}{\Re_{R1} + \Re_{R2} + 1}\right] \tag{4.56}$$

with $\Re_{R1}$ and $\Re_{R2}$ given by (3.14). Note that (4.53) through (4.56) can be shown to agree with the results of Tullsson in [34]. Thus, y_I and y_Q are conditionally Gaussian, independent random variables. The variance expression of (4.55) also shows that the DOA estimation for two unresolved targets is not directly improved by increasing the expected value of $\Re_o$ through the transmitted energy because increasing the transmitted energy also increases $\Re_{R1}$ and $\Re_{R2}$. The larger errors in the monopulse measurements occur when the two target echoes interfere to produce a value for $\Re_o$ that is small relative to $\Re_{R1}\Re_{R2}(\Re_{R1} + \Re_{R2} + 1)^{-1}$. These larger errors also occur when tracking a single, extended target, and the errors are referred to as glint [38].

For N independent samples or pulses, the ML estimate of $\bar{y}_I$, which is the mean of y_I given Λ, is given by (4.46). Since the y_{Ik} are Gaussian random variables, $\hat{y}_I$ is the minimum variance estimate of $\bar{y}_I$ and a Gaussian random variable with variance given by

$$\sigma_{\hat{y}_I}^2 = \left[\sum_{k=1}^{N} 2\Re_{ok}\right]^{-1} q = \frac{q}{2NY_N} \tag{4.57}$$

However, note that $\hat{y}_I$ being the minimum variance estimate of $\bar{y}_I$ does not imply that $\hat{y}_I$ is the minimum variance estimate of either η_1 or η_2.

4.3 Fixed-Amplitude Target

The in-phase and quadrature components of the sum and difference signals for a fixed-amplitude target and independent receiver errors are given by (4.1) through (4.4), with $\alpha_i = 0$ for all $i > 1$, $\beta_i = 0$ for all $i > 0$, and $\rho = 0$. Then

$$\bar{s}_I = E[s_I|\Psi_F, \Phi_F] = \alpha_1 \cos \phi_1 \tag{4.58}$$

$$\bar{s}_Q = E[s_Q|\Psi_F, \Phi_F] = \alpha_1 \sin \phi_1 \tag{4.59}$$

$$\bar{d}_I = E[d_I|\Psi_F, \Phi_F] = \alpha_1 \eta_1 \cos \phi_1 \tag{4.60}$$

$$\bar{d}_Q = E[d_Q|\Psi_F, \Phi_F] = \alpha_1 \eta_1 \sin \phi_1 \tag{4.61}$$

and (4.13) through (4.15) gives

$$p_{11} = \text{VAR}[s_I|\Psi_F, \Phi_F] = \text{VAR}[s_Q|\Psi_F, \Phi_F] = \sigma_S^2 \tag{4.62}$$

$$p_{22} = \text{VAR}[d_I|\Psi_F, \Phi_F] = \text{VAR}[d_Q|\Psi_F, \Phi_F] = \sigma_d^2 \tag{4.63}$$

$$p_{12} = \text{COV}[s_I, d_I|\Psi_F, \Phi_F] = \text{COV}[s_Q, d_Q|\Psi_F, \Phi_F] = 0 \tag{4.64}$$

where Ψ_F is the parameter set $\{\alpha_1, \eta_1, \sigma_S, \sigma_d\}$, and Φ_F is the parameter set $\{\phi_1\}$. Using these results in (4.28) through (4.31) gives

$$A_1 = \frac{\sigma_d^4}{\sigma_S^4} \alpha_1^2 \tag{4.65}$$

$$A_2 = [y_I^2 + y_Q^2]\alpha_1^2 \eta_1^2 \tag{4.66}$$

$$A_3 = 2y_I \frac{\sigma_d^2}{\sigma_S^2} \alpha_1^2 \eta_1 \tag{4.67}$$

$$A_4 = 0 \tag{4.68}$$

Using (4.58) through (4.68) in (4.27) gives the PDF of the in-phase and quadrature parts of the monopulse ratio for a fixed-amplitude target as

$$f(y_I, y_Q|\Lambda, \Psi_F) = \frac{\Lambda^2}{2\pi\sigma_d^2 I_0\left(\frac{\Lambda\alpha_1}{\sigma_S^2}\right)} I_0\left(\frac{\Lambda\alpha_1\eta_1}{\sigma_d^2}\sqrt{(y_I + \sigma_d^2\sigma_S^{-2}\eta_1^{-1})^2 + y_Q^2}\right)$$

$$\times \exp\left[-\frac{\Lambda^2}{2\sigma_d^2}\left[y_I^2 + y_Q^2 + \frac{\alpha_1^2\eta_1^2}{\Lambda^2}\right]\right] \tag{4.69}$$

Using (4.32) and (4.33) gives the first-order moments or expected values of y_I and y_Q as

$$E[y_I|\Lambda, \Psi_F] = \frac{\alpha_1}{\Lambda} I_{1|0}\left(\frac{\alpha_1\Lambda}{\sigma_S^2}\right) \eta_1 \tag{4.70}$$

$$E[y_Q|\Lambda, \Psi_F] = 0 \tag{4.71}$$

Using (4.34) through (4.35) gives the second central moments of y_I and y_Q as

$$\text{VAR}[y_I|\Lambda, \Psi_F] = \frac{\sigma_d^2}{\Lambda^2} + \frac{\alpha_1^2 \eta^2}{\Lambda^2}\left[1 - I_{1|0}^2\left(\frac{\alpha_1\Lambda}{\sigma_S^2}\right) - \frac{\sigma_S^2}{\alpha_1\Lambda}I_{1|0}\left(\frac{\alpha_1\Lambda}{\sigma_S^2}\right)\right] \quad (4.72)$$

$$\text{VAR}[y_Q|\Lambda, \Psi_F] = \frac{\sigma_d^2}{\Lambda^2} + \frac{\alpha_1\sigma_S^2}{\Lambda^3}I_{1|0}\left(\frac{\alpha_1\Lambda}{\sigma_S^2}\right)\eta^2 \quad (4.73)$$

$$\text{COV}[y_I, y_Q|\Lambda, \Psi_F] = 0 \quad (4.74)$$

While y_I and y_Q are not independent, (4.74) indicates the random variables are conditionally uncorrelated. Thus, any statistical processing of y_I and y_Q that is based on the first two moments can be accomplished independently.

The third and fourth central moments of y_I and y_Q were derived using (A.99) and (A.100) of Appendix A. The third central moments of y_I and y_Q are equal to the third marginal cumulants [12, p. 158] λ_{30} and λ_{03} as defined (A.88) in Appendix A. Thus, the third central moments are then given by

$$\mu_{30} = \lambda_{30}$$
$$= -\frac{\alpha_1^3\eta^3}{\Lambda^3}\left[\frac{\sigma_S^2}{\alpha_1\Lambda} + 2\left(1 - \frac{\sigma_S^4}{\alpha_1^2\Lambda^2}\right)I_{1|0}\left(\frac{\alpha_1\Lambda}{\sigma_S^2}\right) - \frac{3\sigma_S^2}{\alpha_1\Lambda}I_{1|0}^2\left(\frac{\alpha_1\Lambda}{\sigma_S^2}\right) - 2I_{1|0}^3\left(\frac{\alpha_1\Lambda}{\sigma_S^2}\right)\right]$$
$$= -\frac{\alpha_1^3\eta^3}{\Lambda^3}g_1\left(\frac{\alpha_1\Lambda}{\sigma_S^2}\right) \quad (4.75)$$

while the third central moment of y_Q was found to be zero or $\mu_{03} = \lambda_{03} = 0$. The function $g_1(2\Re_{F1})$ is shown for various $\Re_{F1}$ in Figure 4.1, where $\Re_{F1}$ is given by (3.13). Note that while the plot of $g_1(2\Re_{F1})$ in Figure 4.1 corresponds to $\Re_o = \Re_{F1}$, the effects of $\Re_o$ being larger or smaller than $\Re_{F1}$ can also be assessed by considering the function in the neighborhood of $\Re_{F1}$. Since $g_1(\cdot)$ is positive, the PDF of y_I is skewed toward zero, while the PDF of y_Q is symmetric about its mean of zero. Figure 4.1 also indicates the skewness of the PDF of y_I decreases as the SNR increases.

The forth marginal cumulants of y_I and y_Q are given by

$$\lambda_{40} = \frac{\alpha_1^4\eta^4}{\Lambda^4}\left[-2 + \frac{3\sigma_S^4}{\alpha_1^2\Lambda^2} + \frac{2\sigma_S^2}{\alpha_1\Lambda}\left(4 - \frac{3\sigma_S^4}{\alpha_1^2\Lambda^2}\right)I_{1|0}\left(\frac{\alpha_1\Lambda}{\sigma_S^2}\right)\right.$$
$$\left. + \left(8 - \frac{11\sigma_S^4}{\alpha_1^2\Lambda^2}\right)I_{1|0}^2\left(\frac{\alpha_1\Lambda}{\sigma_S^2}\right) - 12\frac{\sigma_S^2}{\alpha_1\Lambda}I_{1|0}^3\left(\frac{\alpha_1\Lambda}{\sigma_S^2}\right) - 6I_{1|0}^4\left(\frac{\alpha_1\Lambda}{\sigma_S^2}\right)\right]$$
$$= \frac{\alpha_1^4\eta^4}{\Lambda^4}g_2(\alpha_1\Lambda\sigma_S^{-2}) \quad (4.76)$$

$$\lambda_{04} = \frac{3\alpha_1^4\eta^4}{\Lambda^4}\left(\frac{\sigma_S^2}{\alpha_1\Lambda}\right)^2\left[1 - \frac{2\sigma_S^2}{\alpha_1\Lambda}I_{1|0}\left(\frac{\alpha_1\Lambda}{\sigma_S^2}\right) - I_{1|0}^2\left(\frac{\alpha_1\Lambda}{\sigma_S^2}\right)\right]$$
$$= -\frac{\alpha_1^4\eta^4}{\Lambda^4}g_3(\alpha_1\Lambda\sigma_S^{-2}) \quad (4.77)$$

where the scaling functions $g_2(2\Re_{F1})$ and $g_3(2\Re_{F1})$ are shown in Figure 4.1. The scaling functions suggest that PDFs of y_I and y_Q approach a Gaussian PDF as the SNR increases. The fourth central moments of y_I and y_Q are then given by

$$\mu_{40} = \lambda_{40} + 3\lambda_{20}^2 \tag{4.78}$$

$$\mu_{04} = \lambda_{04} + 3\lambda_{02}^2 \tag{4.79}$$

The kurtosis [39] will be used as a "measure" of the closeness of a PDF to a corresponding Gaussian PDF. The kurtosis for y_I is given by

$$K = \frac{\mu_{40}}{\mu_{20}^2} - 3 = \frac{\lambda_{40}}{\lambda_{20}^2} \tag{4.80}$$

The kurtosis for y_Q is given similarly. Since the fourth cumulant for a Gaussian random variable is zero, $K = 0$ for a Gaussian random variable. Figure 4.2 gives the maximum acceptable DOA versus SNR for a Gaussian approximation, with $|K| \leq 0.03$ and $|K| \leq 0.003$ as criteria for approximation. The solid lines correspond to y_I, while the dash lines correspond to y_Q. Since the kurtosis of y_I is positive by (4.76) and (4.80), the PDF of y_I is more peaked near the mean than the Gaussian PDF, while the PDF of y_Q is more flat near the mean than the Gaussian PDF, since the kurtosis is negative by (4.77) and (4.80). Also note that $\sigma_d = \sigma_S$ in Figure 4.2, and the SNR actually corresponds to $\sqrt{\Re_{F1}\Re_o}$. Thus, the appropriateness of using a Gaussian PDF for y_I and y_Q depends on the SNR and the observed SNR. For example, if $\sqrt{\Re_{F1}\Re_o} > 13$ dB, a Gaussian PDF for y_I satisfies the 0.003 criterion for $|\eta| < 1.0$. Figure 4.2 also indicates that, for a given $\Re_{F1}$ and η, a Gaussian PDF provides a better approximation to the peak of the PDF of y_I than for the PDF of y_Q.

4.4 Fixed-Amplitude Target and Rayleigh Target

The in-phase and quadrature components of the sum and difference signals for unresolved measurements of a fixed-amplitude target and a Rayleigh target and independent receiver errors are given by (4.1) through (4.4), with $\alpha_i = 0$ for all $i > 1$, $\beta_i = 0$ for all $i \neq 2$, and $\rho = 0$. Then

$$\bar{s}_I = E[s_I | \Psi_{FR}, \Phi_F] = \alpha_1 \cos \phi_1 \tag{4.81}$$

$$\bar{s}_Q = E[s_Q | \Psi_{FR}, \Phi_F] = \alpha_1 \sin \phi_1 \tag{4.82}$$

$$\bar{d}_I = E[d_I | \Psi_{FR}, \Phi_F] = \alpha_1 \eta_1 \cos \phi_1 \tag{4.83}$$

$$\bar{d}_Q = E[d_Q | \Psi_{FR}, \Phi_F] = \alpha_1 \eta_1 \sin \phi_1 \tag{4.84}$$
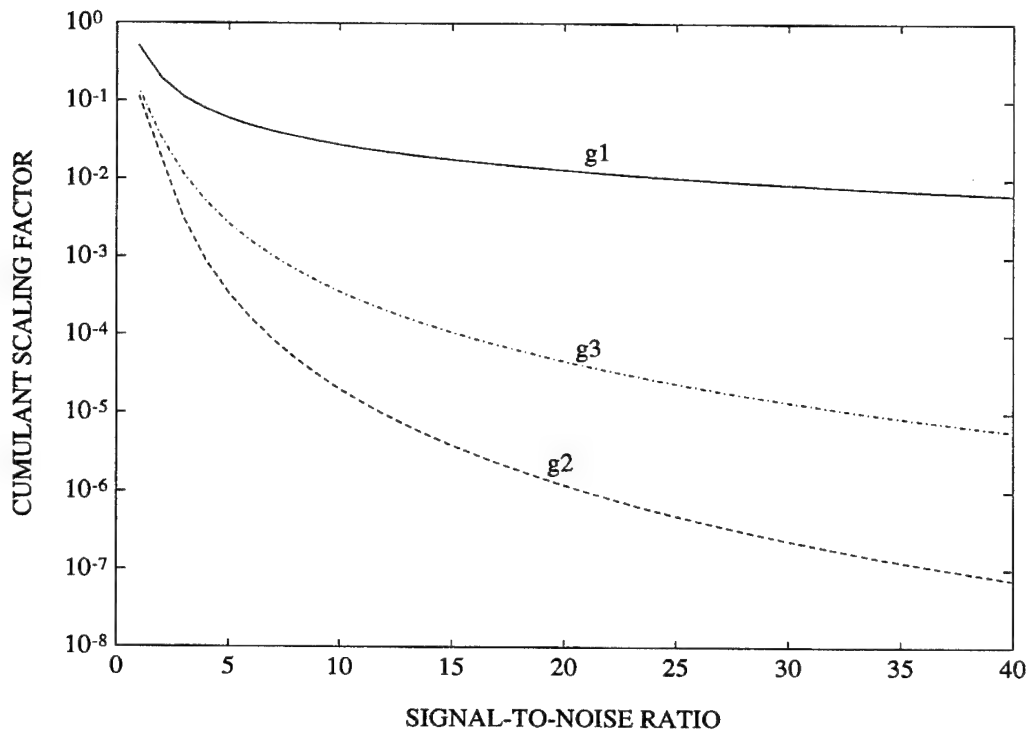
Figure 4.1   Scaling Functions for the Cumulants
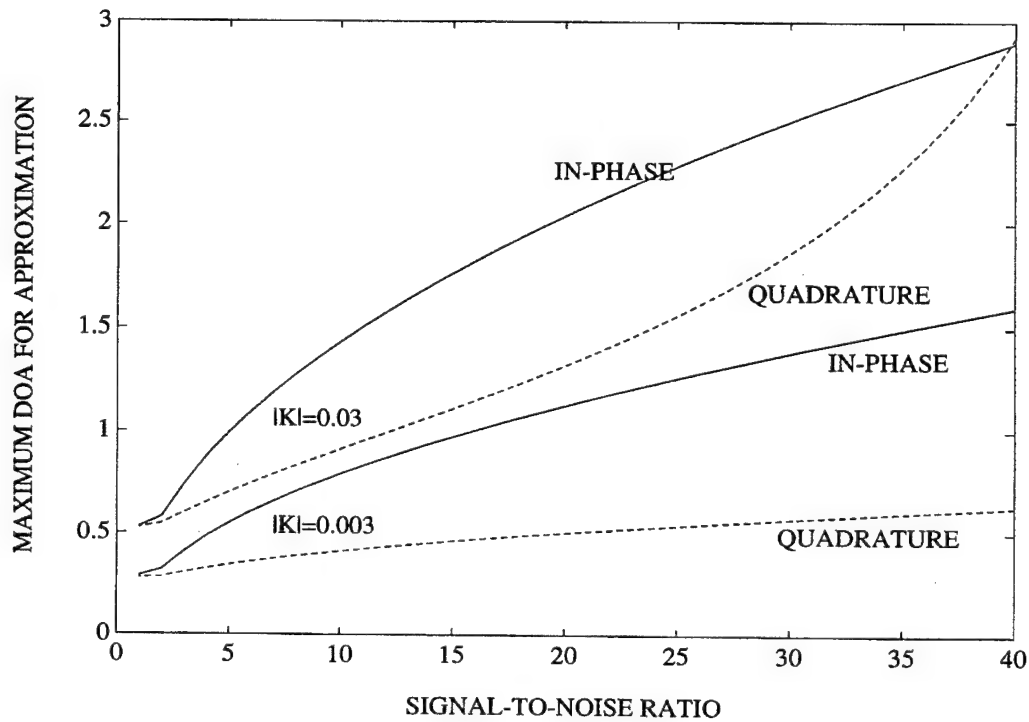
Figure 4.2   Maximum DOA Versus SNR for Gaussian Approximation

and (4.13) through (4.15) gives

$$p_{11} = \text{VAR}[s_I | \Psi_{FR}, \Phi_F] = \text{VAR}[s_Q | \Psi_{FR}, \Phi_F] = \beta_{20}^2 + \sigma_S^2 \qquad (4.85)$$

$$p_{22} = \text{VAR}[d_I | \Psi_{FR}, \Phi_F] = \text{VAR}[d_Q | \Psi_{FR}, \Phi_F] = \eta_2^2 \beta_{20}^2 + \sigma_d^2 \qquad (4.86)$$

$$p_{12} = \text{COV}[s_I, d_I | \Psi_{FR}, \Phi_F] = \text{COV}[s_Q, d_Q | \Psi_{FR}, \Phi_F] = \eta_2 \beta_{20}^2 \qquad (4.87)$$

where Ψ_{FR} is the parameter set $\{\alpha_1, \eta_1, \beta_{20}, \sigma_S, \sigma_d\}$, and Φ_F is the parameter set $\{\phi_1\}$. Using these results in (4.28) through (4.31) gives

$$A_1 = \alpha_1^2 \left[\left(\frac{\sigma_d^2}{\beta_{20}^2 + \sigma_S^2} + \frac{\eta_2^2 \beta_{20}^2 \sigma_S^2}{(\beta_{20}^2 + \sigma_S^2)^2} + \frac{\eta_2 \beta_{20}^2}{\beta_{20}^2 + \sigma_S^2}(1 - y_I) \right)^2 + \frac{\eta_2^2 \beta_{20}^4}{(\beta_{20}^2 + \sigma_S^2)^2} y_Q^2 \right] \quad (4.88)$$

$$A_2 = \alpha_1^2 \eta_1^2 \left[\left(y_I - \frac{\eta_2 \beta_{20}^2}{\beta_{20}^2 + \sigma_S^2} \right)^2 + y_Q^2 \right] \qquad (4.89)$$

$$A_3 = 2\alpha_1^2 \eta_1 \left[\left(\frac{\sigma_d^2}{\beta_{20}^2 + \sigma_S^2} + \frac{\eta_2^2 \beta_{20}^2 \sigma_S^2}{(\beta_{20}^2 + \sigma_S^2)^2} + \frac{\eta_2 \beta_{20}^2}{\beta_{20}^2 + \sigma_S^2}(1 - y_I) \right) \left(y_I - \frac{\eta_2 \beta_{20}^2}{\beta_{20}^2 + \sigma_S^2} \right) \right.$$
$$\left. - \frac{\eta_2^2 \beta_{20}^2}{\beta_{20}^2 + \sigma_S^2} y_Q^2 \right] \qquad (4.90)$$

$$A_4 = 0 \qquad (4.91)$$

Using (4.81) through (4.91) in (4.27) gives the PDF of the in-phase and quadrature parts of the monopulse ratio for unresolved measurements of a fixed-amplitude target and a Rayleigh as

$$f(y_I, y_Q | \Lambda, \Psi_{FR}) = \frac{\Lambda^2 \sigma_S^{-2}}{2\pi \left(\frac{\sigma_d^2}{\sigma_S^2} + \frac{\beta_{20}^2 \eta_2^2}{\beta_{20}^2 + \sigma_S^2} \right) I_0 \left(\frac{\Lambda \alpha_1}{\beta_{20}^2 + \sigma_S^2} \right)} I_0 \left(\frac{\Lambda \alpha_1 (\beta_{20}^2 + \sigma_S^2)\sqrt{C}}{\sigma_d^2 (\beta_{20}^2 + \sigma_S^2) + \eta_2^2 \beta_{20}^2 \sigma_S^2} \right)$$

$$\times \exp \left[- \frac{\Lambda^2 \alpha_1^2 (\beta_{20}^2 + \sigma_S^2)}{2(\sigma_d^2 (\beta_{20}^2 + \sigma_S^2) + \eta_2^2 \beta_{20}^2 \sigma_S^2)} \left[\frac{1}{\Lambda^2} \left(\eta_1 - \frac{\eta_2 \beta_{20}^2}{\beta_{20}^2 + \sigma_S^2} \right)^2 \right. \right.$$
$$\left. \left. + \left(y_I^2 - \frac{\eta_2 \beta_{20}^2}{\beta_{20}^2 + \sigma_S^2} \right)^2 + y_Q^2 \right] \right] \qquad (4.92)$$

where

$$C = \left[\frac{\sigma_d^2}{\beta_{20}^2 + \sigma_S^2} + \frac{\eta_2^2 \beta_{20}^2 \sigma_S^2}{(\beta_{20}^2 + \sigma_S^2)^2} + \frac{\eta_2 \beta_{20}^2}{\beta_{20}^2 + \sigma_S^2}(1 - y_I) + \eta_1 \left(y_I - \frac{\eta_2 \beta_{20}^2}{\beta_{20}^2 + \sigma_S^2} \right) \right]^2$$
$$+ \left[\eta_1 - \frac{\eta_2 \beta_{20}^2}{\beta_{20}^2 + \sigma_S^2} \right]^2 y_Q^2 \qquad (4.93)$$

Using (4.32) and (4.33) gives the first-order moments of y_I and y_Q as

$$E[y_I | \Lambda, \Psi_{FR}] = \frac{\beta_{20}^2}{\beta_{20}^2 + \sigma_S^2} \eta_2 + \frac{\alpha_1}{\Lambda} I_{1|0} \left(\frac{\alpha_1 \Lambda}{\beta_{20}^2 + \sigma_S^2} \right) \left(\eta_1 - \frac{\beta_{20}^2}{\beta_{20}^2 + \sigma_S^2} \eta_2 \right) \qquad (4.94)$$

$$E[y_Q | \Lambda, \Psi_{FR}] = 0 \qquad (4.95)$$

Using (4.34) through (4.35) gives the second central moments of y_I and y_Q as

$$\text{VAR}[y_I|\Lambda, \Psi_{FR}] = \frac{\sigma_S^2}{\Lambda^2}\left[\frac{\sigma_d^2}{\sigma_S^2} + \frac{\beta_{20}^2}{\beta_{20}^2 + \sigma_S^2}\right] + \frac{\alpha_1^2}{\Lambda^2}\left[\eta_1 - \frac{\beta_{20}^2}{\beta_{20}^2 + \sigma_S^2}\eta_2\right]^2$$

$$\times \left[1 - I_{1|0}^2\left(\frac{\alpha_1\Lambda}{\beta_{20}^2 + \sigma_S^2}\right) - \frac{\beta_{20}^2 + \sigma_S^2}{\alpha_1\Lambda}I_{1|0}\left(\frac{\alpha_1\Lambda}{\beta_{20}^2 + \sigma_S^2}\right)\right] \quad (4.96)$$

$$\text{VAR}[y_Q|\Lambda, \Psi_{FR}] = \frac{\sigma_S^2}{\Lambda^2}\left[\frac{\sigma_d^2}{\sigma_S^2} + \frac{\beta_{20}^2}{\beta_{20}^2 + \sigma_S^2}\right]$$

$$+ \frac{\alpha_1(\beta_{20}^2 + \sigma_S^2)}{\Lambda^3}\left[\eta_1 - \frac{\beta_{20}^2}{\beta_{20}^2 + \sigma_S^2}\eta_2\right]^2 I_{1|0}\left(\frac{\alpha_1\Lambda}{\beta_{20}^2 + \sigma_S^2}\right) \quad (4.97)$$

$$\text{COV}[y_I, y_Q|\Lambda, \Psi_{FR}] = 0 \quad (4.98)$$

While y_I and y_Q are not independent, (4.98) indicates the random variables are conditionally uncorrelated. Thus, any statistical processing of y_I and y_Q that is based on the first two moments can be accomplished independently.

4.5 Rician Target

The in-phase and quadrature components of the sum and difference signals for a Rician target and independent receiver errors are given by (4.1) through (4.4), with $\alpha_i = 0$ for all $i > 1$, $\beta_i = 0$ for all $i > 1$, and $\rho = 0$. Then

$$\bar{s}_I = E[s_I|\Psi_{Ri}, \Phi_{Ri}] = \alpha_1 \cos\phi_1 \quad (4.99)$$

$$\bar{s}_Q = E[s_Q|\Psi_{Ri}, \Phi_{Ri}] = \alpha_1 \sin\phi_1 \quad (4.100)$$

$$\bar{d}_I = E[d_I|\Psi_{Ri}, \Phi_{Ri}] = \alpha_1\eta_1 \cos\phi_1 \quad (4.101)$$

$$\bar{d}_Q = E[d_Q|\Psi_{Ri}, \Phi_{Ri}] = \alpha_1\eta_1 \sin\phi_1 \quad (4.102)$$

and (4.13) through (4.15) gives

$$p_{11} = \text{VAR}[s_I|\Psi_{Ri}, \Phi_{Ri}] = \text{VAR}[s_Q|\Psi_{Ri}, \Phi_{Ri}] = \beta_{10}^2 + \sigma_S^2 \quad (4.103)$$

$$p_{22} = \text{VAR}[d_I|\Psi_{Ri}, \Phi_{Ri}] = \text{VAR}[d_Q|\Psi_{Ri}, \Phi_{Ri}] = \eta_1^2\beta_{10}^2 + \sigma_d^2 \quad (4.104)$$

$$p_{12} = \text{COV}[s_I, d_I|\Psi_{Ri}, \Phi_{Ri}] = \text{COV}[s_Q, d_Q|\Psi_{Ri}, \Phi_{Ri}] = \eta_1\beta_{10}^2 \quad (4.105)$$

where Ψ_{Ri} is the parameter set $\{\alpha_1, \eta_1, \beta_{10}, \sigma_S, \sigma_d\}$, and Φ_{Ri} is the parameter set $\{\phi_1\}$. Using these results in (4.28) through (4.31) gives

$$A_1 = \alpha_1^2\left[\left(\frac{\sigma_d^2}{\beta_{10}^2 + \sigma_S^2} + \frac{\eta_1^2\beta_{10}^2\sigma_S^2}{(\beta_{10}^2 + \sigma_S^2)^2} + \frac{\eta_1\beta_{10}^2}{\beta_{10}^2 + \sigma_S^2}(1 - y_I)\right)^2 + \frac{\eta_1^2\beta_{10}^4}{(\beta_{10}^2 + \sigma_S^2)^2}y_Q^2\right] \quad (4.106)$$

$$A_2 = \alpha_1^2\eta_1^2\left[\left(y_I - \frac{\eta_1\beta_{10}^2}{\beta_{10}^2 + \sigma_S^2}\right)^2 + y_Q^2\right] \quad (4.107)$$

$$A_3 = 2\alpha_1^2 \eta_1 \left[\left(\frac{\sigma_d^2}{\beta_{10}^2 + \sigma_S^2} + \frac{\eta_1^2 \beta_{10}^2 \sigma_S^2}{(\beta_{10}^2 + \sigma_S^2)^2} + \frac{\eta_1 \beta_{10}^2}{\beta_{10}^2 + \sigma_S^2}(1 - y_I) \right) \left(y_I - \frac{\eta_1 \beta_{10}^2}{\beta_{10}^2 + \sigma_S^2} \right) \right.$$
$$\left. - \frac{\eta_1^2 \beta_{10}^2}{\beta_{10}^2 + \sigma_S^2} y_Q^2 \right] \tag{4.108}$$

and $A_4 = 0$. Using (4.99) through (4.108) in (4.27) gives the PDF of the in-phase and quadrature parts of the monopulse ratio for a Rician target as

$$f(y_I, y_Q | \Lambda, \Psi_{Ri}) = \frac{\Lambda^2 \sigma_S^{-2}}{2\pi \left(\frac{\sigma_d^2}{\sigma_S^2} + \frac{\beta_{10}^2 \eta_1^2}{\beta_{10}^2 + \sigma_S^2} \right) I_0 \left(\frac{\Lambda \alpha_1}{\beta_{10}^2 + \sigma_S^2} \right)} I_0 \left(\frac{\Lambda \alpha_1 (\beta_{10}^2 + \sigma_S^2) \sqrt{C}}{\sigma_d^2 (\beta_{10}^2 + \sigma_S^2) + \eta_1^2 \beta_{10}^2 \sigma_S^2} \right)$$
$$\times \exp \left[- \frac{\Lambda^2 \alpha_1^2 (\beta_{10}^2 + \sigma_S^2)}{2(\sigma_d^2 (\beta_{10}^2 + \sigma_S^2) + \eta_1^2 \beta_{10}^2 \sigma_S^2)} \left[\frac{\eta_1^2 \sigma_S^4}{\Lambda^2 (\beta_{10}^2 + \sigma_S^2)^2} \right. \right.$$
$$\left. \left. + \left(y_I^2 - \frac{\eta_1 \beta_{10}^2}{\beta_{10}^2 + \sigma_S^2} \right)^2 + y_Q^2 \right] \right] \tag{4.109}$$

where

$$C = \left[\frac{\sigma_d^2}{\beta_{10}^2 + \sigma_S^2} + \frac{\eta_1^2 \beta_{10}^2 \sigma_S^2}{(\beta_{10}^2 + \sigma_S^2)^2} + \frac{\eta_1 \beta_{10}^2}{\beta_{10}^2 + \sigma_S^2}(1 - y_I) + \eta_1 \left(y_I - \frac{\eta_1 \beta_{10}^2}{\beta_{10}^2 + \sigma_S^2} \right) \right]^2$$
$$+ \left[\eta_1 - \frac{\eta_1 \beta_{10}^2}{\beta_{10}^2 + \sigma_S^2} \right]^2 y_Q^2 \tag{4.110}$$

Using (4.32) and (4.33) gives the first-order moments of y_I and y_Q as

$$E[y_I | \Lambda, \Psi_{Ri}] = \left[\frac{\beta_{10}^2}{\beta_{10}^2 + \sigma_S^2} + \frac{\alpha_1 \sigma_S^2}{\Lambda (\beta_{10} + \sigma_S^2)} I_{1|0} \left(\frac{\alpha_1 \Lambda}{\beta_{10}^2 + \sigma_S^2} \right) \right] \eta_1 \tag{4.111}$$
$$E[y_Q | \Lambda, \Psi_{Ri}] = 0 \tag{4.112}$$

Using (4.34) through (4.35) gives the second central moments of y_I and y_Q as

$$\text{VAR}[y_I | \Lambda, \Psi_{Ri}] = \frac{\sigma_S^2}{\Lambda^2} \left[\frac{\sigma_d^2}{\sigma_S^2} + \frac{\beta_{10}^2}{\beta_{10}^2 + \sigma_S^2} \right] + \frac{\alpha_1^2 \eta_1^2 \sigma_S^4}{\Lambda^2 (\beta_{10}^2 + \sigma_S^2)^2}$$
$$\times \left[1 - I_{1|0}^2 \left(\frac{\alpha_1 \Lambda}{\beta_{10}^2 + \sigma_S^2} \right) - \frac{\beta_{10}^2 + \sigma_S^2}{\alpha_1 \Lambda} I_{1|0} \left(\frac{\alpha_1 \Lambda}{\beta_{10}^2 + \sigma_S^2} \right) \right] \tag{4.113}$$
$$\text{VAR}[y_Q | \Lambda, \Psi_{Ri}] = \frac{\sigma_S^2}{\Lambda^2} \left[\frac{\sigma_d^2}{\sigma_S^2} + \frac{\beta_{10}^2}{\beta_{10}^2 + \sigma_S^2} \right] + \frac{\alpha_1 \eta_1^2 \sigma_S^4}{\Lambda^3 (\beta_{10}^2 + \sigma_S^2)} I_{1|0} \left(\frac{\alpha_1 \Lambda}{\beta_{10}^2 + \sigma_S^2} \right) \tag{4.114}$$
$$\text{COV}[y_I, y_Q | \Lambda, \Psi_{Ri}] = 0 \tag{4.115}$$

While y_I and y_Q are not independent, (4.115) indicates the random variables are conditionally uncorrelated. Thus, any statistical processing of y_I and y_Q that is based on the first two moments can be accomplished independently.

4.6 Two Fixed-Amplitude Targets

The in-phase and quadrature components of the sum and difference signals for two unresolved fixed-amplitude targets and independent receiver errors are given by (4.1) through (4.4), with $\alpha_i = 0$ for all $i > 2$, $\beta_i = 0$ for all $i > 0$, and $\rho = 0$. Then

$$\bar{s}_I = E[s_I|\Psi_{2F}, \Phi_{2F}] = \alpha_1 \cos \phi_1 + \alpha_2 \sin \phi_2 \tag{4.116}$$

$$\bar{s}_Q = E[s_Q|\Psi_{2F}, \Phi_{2F}] = \alpha_1 \sin \phi_1 + \alpha_2 \sin \phi_2 \tag{4.117}$$

$$\bar{d}_I = E[d_I|\Psi_{2F}, \Phi_{2F}] = \alpha_1 \eta_1 \cos \phi_1 + \alpha_2 \eta_2 \sin \phi_2 \tag{4.118}$$

$$\bar{d}_Q = E[d_Q|\Psi_{2F}, \Phi_{2F}] = \alpha_1 \eta_1 \sin \phi_1 + \alpha_2 \eta_2 \sin \phi_2 \tag{4.119}$$

and (4.13) through (4.15) gives

$$p_{11} = \mathrm{VAR}[s_I|\Psi_{2F}, \Phi_{2F}] = \mathrm{VAR}[s_Q|\Psi_{2F}, \Phi_{2F}] = \sigma_S^2 \tag{4.120}$$

$$p_{22} = \mathrm{VAR}[d_I|\Psi_{2F}, \Phi_{2F}] = \mathrm{VAR}[d_Q|\Psi_{2F}, \Phi_{2F}] = \sigma_d^2 \tag{4.121}$$

$$p_{12} = \mathrm{COV}[s_I, d_I|\Psi_{2F}, \Phi_{2F}] = \mathrm{COV}[s_Q, d_Q|\Psi_{2F}, \Phi_{2F}] = 0 \tag{4.122}$$

where Ψ_{2F} is the parameter set $\{\alpha_1, \eta_1, \alpha_2, \eta_2, \sigma_S, \sigma_d\}$, and Φ_{2F} is the parameter set $\{\phi_1, \phi_2\}$. Using these results in (4.28) through (4.31) gives

$$A_1 = \frac{\sigma_d^4}{\sigma_S^4}\left[\alpha_1^2 + \alpha_2^2 + 2\alpha_1\alpha_2 \cos \Delta\phi\right] \tag{4.123}$$

$$A_2 = \left[y_I^2 + y_Q^2\right]\left[\alpha_1^2\eta_1^2 + \alpha_2^2\eta_2^2 + 2\alpha_1\alpha_2\eta_1\eta_2 \cos \Delta\phi\right] \tag{4.124}$$

$$A_3 = 2y_I\frac{\sigma_d^2}{\sigma_S^2}\left[\alpha_1^2\eta_1 + \alpha_2^2\eta_2 + \alpha_1\alpha_2(\eta_1 + \eta_2) \cos \Delta\phi\right] \tag{4.125}$$

$$A_4 = -2\alpha_1\alpha_2(\eta_1 - \eta_2)\frac{\sigma_d^2}{\sigma_S^2} \sin \Delta\phi \tag{4.126}$$

where $\Delta\phi = \phi_2 - \phi_1$. Using (4.116) through (4.126) in (4.27) gives the PDF of the in-phase and quadrature parts of the monopulse ratio for two unresolved fixed-amplitude targets as

$$f(y_I, y_Q|\Lambda, \Psi_{2F}, \Delta\phi) = \frac{\Lambda^2 I_0\left(\frac{\Lambda}{\sigma_d^2}\sqrt{A_1 + A_2 + A_3 + A_4}\right)}{2\pi\sigma_d^2 I_0\left(\frac{\Lambda}{\sigma_S^2}\sqrt{\alpha_1^2 + \alpha_2^2 + 2\alpha_1\alpha_2 \cos \Delta\phi}\right)}$$

$$\times \exp\left[-\frac{\Lambda^2}{2\sigma_d^2}\left[y_I^2 + y_Q^2 + \frac{1}{\Lambda^2}\left(\alpha_1^2\eta_1^2 + \alpha_2^2\eta_2^2 + 2\alpha_1\alpha_2\eta_1\eta_2 \cos \Delta\phi\right)\right]\right] \tag{4.127}$$

Using (4.32) and (4.33) gives the first-order moments of y_I and y_Q as

$$E[y_I|\Lambda, \Psi_{2F}, \Delta\phi] = I_{1|0}\left(\frac{\Lambda}{\sigma_S^2}\sqrt{\alpha_1^2 + \alpha_2^2 + 2\alpha_1\alpha_2 \cos \Delta\phi}\right)$$
$$\times \frac{\alpha_1^2\eta_1 + \alpha_2^2\eta_2 + \alpha_1\alpha_2(\eta_1 + \eta_2) \cos \Delta\phi}{\Lambda\sqrt{\alpha_1^2 + \alpha_2^2 + 2\alpha_1\alpha_2 \cos \Delta\phi}} \quad (4.128)$$

$$E[y_Q|\Lambda, \Psi_{2F}, \Delta\phi] = -I_{1|0}\left(\frac{\Lambda}{\sigma_S^2}\sqrt{\alpha_1^2 + \alpha_2^2 + 2\alpha_1\alpha_2 \cos \Delta\phi}\right)$$
$$\times \frac{\alpha_1\alpha_2(\eta_1 - \eta_2) \sin \Delta\phi}{\Lambda\sqrt{\alpha_1^2 + \alpha_2^2 + 2\alpha_1\alpha_2 \cos\Delta\phi}} \quad (4.129)$$

Using (4.34) through (4.35) gives the second central moments of y_I and y_Q as

$$\text{VAR}[y_I|\Lambda, \Psi_{2F}, \Delta\phi] = \frac{\sigma_d^2}{\Lambda^2} + \frac{[\alpha_1^2\eta_1 + \alpha_2^2\eta_2 + \alpha_1\alpha_2(\eta_1 + \eta_2) \cos \Delta\phi]^2}{\Lambda^2[\alpha_1^2 + \alpha_2^2 + 2\alpha_1\alpha_2 \cos \Delta\phi]}$$
$$\times I_{1|0}^*\left(\frac{\Lambda}{\sigma_S^2}\sqrt{\alpha_1^2 + \alpha_2^2 + 2\alpha_1\alpha_2 \cos \Delta\phi}\right)$$
$$+ \frac{\sigma_S^2(\alpha_1^2\eta_1^2 + \alpha_2^2\eta_2^2 + 2\alpha_1\alpha_2\eta_1\eta_2 \cos \Delta\phi)}{\Lambda^3\sqrt{\alpha_1^2 + \alpha_2^2 + 2\alpha_1\alpha_2 \cos \Delta\phi}}$$
$$\times I_{1|0}\left(\frac{\Lambda}{\sigma_S^2}\sqrt{\alpha_1^2 + \alpha_2^2 + 2\alpha_1\alpha_2 \cos \Delta\phi}\right) \quad (4.130)$$

$$\text{VAR}[y_Q|\Lambda, \Psi_{2F}, \Delta\phi] = \frac{\sigma_d^2}{\Lambda^2} + \frac{\alpha_1^2\alpha_2^2(\eta_1 - \eta_2)^2 \sin^2\Delta\phi}{\Lambda^2[\alpha_1^2 + \alpha_2^2 + 2\alpha_1\alpha_2 \cos \Delta\phi]}$$
$$\times I_{1|0}^*\left(\frac{\Lambda}{\sigma_S^2}\sqrt{\alpha_1^2 + \alpha_2^2 + 2\alpha_1\alpha_2 \cos \Delta\phi}\right)$$
$$+ \frac{\sigma_S^2(\alpha_1^2\eta_1^2 + \alpha_2^2\eta_2^2 + 2\alpha_1\alpha_2\eta_1\eta_2 \cos \Delta\phi)}{\Lambda^3\sqrt{\alpha_1^2 + \alpha_2^2 + 2\alpha_1\alpha_2 \cos \Delta\phi}}$$
$$\times I_{1|0}\left(\frac{\Lambda}{\sigma_S^2}\sqrt{\alpha_1^2 + \alpha_2^2 + 2\alpha_1\alpha_2 \cos \Delta\phi}\right) \quad (4.131)$$

$$\text{COV}[y_I, y_Q|\Lambda, \Psi_{2F}, \Delta\phi] = -\frac{[\alpha_1\alpha_2(\eta_1 - \eta_2) \sin \Delta\phi]}{\Lambda^2[\alpha_1^2 + \alpha_2^2 + 2\alpha_1\alpha_2 \cos \Delta\phi]}$$
$$\times I_{1|0}^*\left(\frac{\Lambda}{\sigma_S^2}\sqrt{\alpha_1^2 + \alpha_2^2 + 2\alpha_1\alpha_2 \cos \Delta\phi}\right)$$
$$\times [\alpha_1^2\eta_1 + \alpha_2^2\eta_2 + \alpha_1\alpha_2(\eta_1 + \eta_2) \cos \Delta\phi] \quad (4.132)$$

Then (4.132) shows that y_I and y_Q are not independent nor uncorrelated for a fixed relative phase $\Delta\phi \neq 0$ or $\pm\pi$. Since y_Q has a nonzero mean for a fixed relative phase $\Delta\phi \neq 0$ or $\pm\pi$, the sample mean of y_Q may prove useful in the detection of a fixed relative phase.

93

4.7 Fixed-Amplitude Target in Presence of Multipath

The in-phase and quadrature components of the sum and difference signals for a fixed-amplitude target in the presence of sea-surface-induced multipath are given by (4.1) through (4.4), with

$$\alpha_1 = \alpha_t \tag{4.133}$$

$$\alpha_2 = g\rho_S\alpha_t \tag{4.134}$$

$$\alpha_3 = g\rho_S\alpha_t \tag{4.135}$$

$$\alpha_4 = (g\rho_S)^2\alpha_t \tag{4.136}$$

$$\phi_1 = \phi \tag{4.137}$$

$$\phi_2 = \phi + \Delta\phi \tag{4.138}$$

$$\phi_3 = \phi + \Delta\phi \tag{4.139}$$

$$\phi_4 = \phi + 2\Delta\phi \tag{4.140}$$

$$\beta_1 = 0 \tag{4.141}$$

$$\beta_2 = g\rho_d\alpha_t \tag{4.142}$$

$$\beta_3 = g\rho_d\alpha_t \tag{4.143}$$

$$\beta_4 = (g\rho_d)^2\alpha_t \tag{4.144}$$

$$\varphi_2 = \phi + \phi_d + \Delta\phi \tag{4.145}$$

$$\varphi_3 = \phi + \phi_d + \Delta\phi \tag{4.146}$$

$$\varphi_4 = \phi + 2\phi_d + 2\Delta\phi \tag{4.147}$$

where α_t is the voltage amplitude of the target, and the remaining variables are defined in Section 2.6. Also, $\alpha_i = 0$, and $\beta_i = 0$ for all $i > 4$. The resulting equations correspond to (2.80) through (2.83). Note that $\Delta\phi$ includes the phase difference due to both the PLD and the specular reflection at the sea surface, which is approximately π. The errors n_{SI}, n_{SQ}, n_{dI}, and n_{dQ} are assumed independent so that $\rho = 0$.

Then (2.80) through (2.83) can be rewritten as

$$\begin{aligned} s_I = &\alpha_{tC}\,\cos\phi - \alpha_{tS}\,\sin\phi + \alpha_{IC}\,\cos(\phi + \Delta\phi) - \alpha_{IS}\,\sin(\phi + \Delta\phi) \\ &+ 2\alpha_t g\rho_d\,\cos(\phi_d + \Delta\phi) + \alpha_t(g\rho_d)^2\,\cos(2\phi_d + 2\Delta\phi) + n_{SI} \end{aligned} \tag{4.148}$$

$$\begin{aligned} s_Q = &\alpha_{tC}\,\sin\phi + \alpha_{tS}\,\cos\phi + \alpha_{IC}\,\sin(\phi + \Delta\phi) + \alpha_{IS}\,\cos(\phi + \Delta\phi) \\ &+ 2\alpha_t g\rho_d\,\sin(\phi_d + \Delta\phi) + \alpha_t(g\rho_d)^2\,\sin(2\phi_d + 2\Delta\phi) + n_{SQ} \end{aligned} \tag{4.149}$$

$$\begin{aligned} d_I = &\alpha_{tC}\eta_t\,\cos\phi - \alpha_{tS}\eta_t\,\sin\phi + \alpha_{IC}\eta_I\,\cos(\phi + \Delta\phi) - \alpha_{IS}\eta_I\,\sin(\phi + \Delta\phi) \\ &+ \alpha_t(\eta_t + \eta_I)g\rho_d\,\cos(\phi_d + \Delta\phi) + \alpha_t\eta_I(g\rho_d)^2\,\cos(2\phi_d + 2\Delta\phi) + n_{dI} \end{aligned} \tag{4.150}$$

$$d_Q = \alpha_{tC}\eta_t \sin\phi + \alpha_{tC}\eta_t \cos\phi + \alpha_{IC}\eta_I \sin(\phi + \Delta\phi) + \alpha_{IS}\eta_I \cos(\phi + \Delta\phi)$$
$$+ \alpha_t(\eta_t + \eta_I)g\rho_d \sin(\phi_d + \Delta\phi) + \alpha_t\eta_I(g\rho_d)^2 \sin(2\phi_d + 2\Delta\phi) + n_{dQ} \quad (4.151)$$

where

$$\alpha_{tC} = \alpha_t(1 + g\rho_S \cos\Delta\phi) \quad (4.152)$$

$$\alpha_{tS} = \alpha_t g\rho_S \sin\Delta\phi \quad (4.153)$$

$$\alpha_{IC} = \alpha_t g\rho_S(1 + g\rho_S \cos\Delta\phi) = g\rho_S\alpha_{tC} \quad (4.154)$$

$$\alpha_{IS} = \alpha_t(g\rho_S)^2 \sin\Delta\phi = g\rho_S\alpha_{tS} \quad (4.155)$$

Let Ψ_{MP} denote the parameter set $\{\alpha_t, \eta_t, \eta_I, \rho_S, \rho_{d0}, \sigma_S, \sigma_d\}$, and Φ_{MP} denote the parameter set $\{\phi, \Delta\phi, \}$. With $E[\cdot]$ denoting the expected value, let

$$\bar{s}_I = E[s_I|\Psi_{MP}, \Phi_{MP}] = \alpha_{tC} \cos\phi - \alpha_{tS} \sin\phi + \alpha_{IC} \cos(\phi + \Delta\phi)$$
$$- \alpha_{IS} \sin(\phi + \Delta\phi) \quad (4.156)$$

$$\bar{s}_Q = E[s_Q|\Psi_{MP}, \Phi_{MP}] = \alpha_{tC} \sin\phi + \alpha_{tS} \cos\phi + \alpha_{IC} \sin(\phi + \Delta\phi)$$
$$+ \alpha_{IS} \cos(\phi + \Delta\phi) \quad (4.157)$$

$$\bar{d}_I = E[d_I|\Psi_{MP}, \Phi_{MP}] = \alpha_{tC}\eta_t \cos\phi - \alpha_{tS}\eta_t \sin\phi + \alpha_{IC}\eta_I \cos(\phi + \Delta\phi)$$
$$- \alpha_{IS}\eta_I \sin(\phi + \Delta\phi) \quad (4.158)$$

$$\bar{d}_Q = E[d_Q|\Psi_{MP}, \Phi_{MP}] = \alpha_{tC}\eta_t \sin\phi + \alpha_{tC}\eta_t \cos\phi + \alpha_{IC}\eta_I \sin(\phi + \Delta\phi)$$
$$+ \alpha_{IS}\eta_I \cos(\phi + \Delta\phi) \quad (4.159)$$

Also,

$$p_{11} = E[(s_I - \bar{s}_I)^2|\Psi_{MP}, \Phi_{MP}] = E[(s_Q - \bar{s}_Q)^2|\Psi_{MP}, \Phi_{MP}]$$
$$= 4\alpha_t^2\rho_{d0}^2g^2[1 + \rho_{d0}^2g^2] + \sigma_S^2 \quad (4.160)$$

$$p_{22} = E[(d_I - \bar{d}_I)^2|\Psi_{MP}, \Phi_{MP}] = E[(d_Q - \bar{d}_Q)^2|\Psi_{MP}, \Phi_{MP}]$$
$$= \alpha_t^2\rho_{d0}^2g^2[(\eta_t + \eta_I)^2 + 4\rho_{d0}^2g^2\eta_I^2] + \sigma_d^2 \quad (4.161)$$

$$p_{12} = E[(d_I - \bar{d}_I)(s_I - \bar{s}_I)|\Psi_{MP}, \Phi_{MP}] = E[(d_Q - \bar{d}_Q)(s_Q - \bar{s}_Q)|\Psi_{MP}, \Phi_{MP}]$$
$$= 2\alpha_t^2\rho_{d0}^2g^2[\eta_t + (1 + 2\rho_{d0}^2g^2)\eta_I] \quad (4.162)$$

While ρ_d is Rayleigh distributed, ϕ_d is uniformly distributed on $(-\pi, \pi]$, and the receiver errors are Gaussian, the sum and difference signals of (4.148) through (4.151) are not Gaussian signals because ρ_d^2 is exponentially distributed rather than Rayleigh. However, since typically $\rho_d < 0.5$ and $g < 1$, the effects of $(\rho_d g)^2$ should be small compared to that of $\rho_d g$. Thus, the sum and difference signals will be approximated

as Gaussian for the development of the statistics of monopulse measurements of low-elevation targets.

Using (4.156) through (4.162) in (4.27) gives the PDF of the in-phase and quadrature parts of the monopulse ratio for a fixed-amplitude target in multipath, where

$$\bar{s}_I^2 + \bar{s}_Q^2 = \alpha_t^2(1 + 2\rho_S g \cos\Delta\phi + \rho_S^2 g^2)^2 \tag{4.163}$$

$$\bar{d}_I^2 + \bar{d}_Q^2 = \alpha_t^2(1 + 2\rho_S g \cos\Delta\phi + \rho_S^2 g^2)(\eta_t^2 + 2\rho_S g \eta_t \eta_I \cos\Delta\phi + \rho_S^2 g^2 \eta_I^2) \tag{4.164}$$

$$\bar{s}_I \bar{d}_I + \bar{s}_Q \bar{d}_Q = \alpha_t^2(1 + 2\rho_S g \cos\Delta\phi + \rho_S^2 g^2)$$

$$\times (\eta_t + \rho_S g(\eta_t + \eta_I) \cos\Delta\phi + \rho_S^2 g^2 \eta_I) \tag{4.165}$$

$$\bar{s}_I \bar{d}_Q - \bar{s}_Q \bar{d}_I = -\rho_S g \alpha_t^2(1 + 2\rho_S g \cos\Delta\phi + \rho_S^2 g^2)(\eta_t - \eta_I)) \sin\Delta\phi \tag{4.166}$$

Using (4.32) and (4.33) gives approximately the expected values of y_I and y_Q as

$$E[y_I|\Lambda, \Psi_{MP}, \Delta\phi] = \frac{p_{12}}{p_{11}} + I_{1|0}\left(\frac{\Lambda\alpha_t}{p_{11}}(1 + 2\rho_S g \cos\Delta\phi + \rho_S^2 g^2)\right)\frac{\alpha_t}{\Lambda} \tag{4.167}$$

$$\times \left[\left(\eta_t - \frac{p_{12}}{p_{11}}\right) + (\rho_S g)^2\left(\eta_I - \frac{p_{12}}{p_{11}}\right) + \left(\eta_t + \eta_I - 2\frac{p_{12}}{p_{11}}\right)\rho_S g \cos\Delta\phi\right]$$

$$E[y_Q|\Lambda, \Psi_{MP}, \Delta\phi] = I_{1|0}\left(\frac{\Lambda\alpha_t}{p_{11}}(1 + 2\rho_S g \cos\Delta\phi + \rho_S^2 g^2)\right)$$

$$\times \frac{\alpha_t \rho_S g}{\Lambda}\left(\eta_I - \eta_t\right) \sin\Delta\phi \tag{4.168}$$

where

$$\frac{p_{12}}{p_{11}} = \frac{2\alpha_t^2 \rho_{d0}^2 g^2[\eta_t + (1 + 2\rho_{d0}^2 g^2)\eta_I]}{4\alpha_t^2 \rho_{d0}^2 g^2[1 + \rho_{d0}^2 g^2] + \sigma_S^2} \tag{4.169}$$

Using (4.34) gives approximately the covariance of the in-phase and quadrature monopulse ratios as

$$\text{COV}[y_I, y_Q|\Lambda, \Psi_{MP}, \Delta\phi] = \left[(\eta_I - \eta_t)\frac{\alpha_t^2 \rho_S g}{\Lambda^2} \sin\Delta\phi\right]$$

$$\times I_{1|0}^*\left(\frac{\Lambda\alpha_t}{p_{11}}(1 + 2\rho_S g \cos\Delta\phi + \rho_S^2 g^2)\right)$$

$$\times \left[\left(\eta_t - \frac{p_{12}}{p_{11}}\right) + (\rho_S g)^2\left(\eta_I - \frac{p_{12}}{p_{11}}\right) + \left(\eta_t + \eta_I - 2\frac{p_{12}}{p_{11}}\right)\rho_S g \cos\Delta\phi\right] \tag{4.170}$$

Using (4.35) gives approximately the variance of y_I as

$$\text{VAR}[y_I|\Lambda, \Psi_{MP}, \Delta\phi] = \frac{p_{11}p_{22} - p_{12}^2}{\Lambda^2 p_{11}} + \frac{\alpha_t p_{11}}{\Lambda^3}I_{1|0}\left(\frac{\Lambda\alpha_t}{p_{11}}(1 + 2\rho_S g \cos\Delta\phi + \rho_S^2 g^2)\right)$$

$$\times \left[\left(\eta_t - \frac{p_{12}}{p_{11}}\right)^2 + (\rho_S g)^2\left(\eta_I - \frac{p_{12}}{p_{11}}\right)^2\right.$$

$$\left. + 2\rho_S g\left(\eta_t - \frac{p_{12}}{p_{11}}\right)\left(\eta_I - \frac{p_{12}}{p_{11}}\right) \cos\Delta\phi\right]$$

96

$$+ \left[\left(\eta_t - \frac{p_{12}}{p_{11}}\right) + (\rho_S g)^2\left(\eta_I - \frac{p_{12}}{p_{11}}\right) + \left(\eta_t + \eta_I - 2\frac{p_{12}}{p_{11}}\right)\rho_S g \, \cos\Delta\phi\right]^2 \cdot$$

$$\times \frac{\alpha_t^2}{\Lambda^2} I_{1|0}^* \left(\frac{\Lambda\alpha_t}{p_{11}}(1 + 2\rho_S g \, \cos\Delta\phi + \rho_S^2 g^2)\right) \tag{4.171}$$

where

$$\frac{p_{11}p_{22} - p_{12}^2}{\Lambda^2 p_{11}} = \frac{1}{2\Re_o}\left[\frac{\sigma_d^2}{\sigma_S^2} + \frac{16\Re_F^2\rho_{d0}^6 g^6[\eta_t - \eta_I]^2 + 2\Re_F\rho_{d0}^2 g^2[(\eta_t + \eta_I)^2 + 4\rho_{d0}^2 g^2\eta_I^2]}{8\Re_F\rho_{d0}^2 g^2[1 + \rho_{d0}^2 g^2] + 1}\right]$$
$$\tag{4.172}$$

$$\Re_F = \frac{\alpha_t^2}{2\sigma_S^2} \tag{4.173}$$

Using (4.36) gives approximately the variance of y_Q as

$$\mathrm{VAR}[y_Q|\Lambda, \Psi_{MP}, \Delta\phi] = \frac{p_{11}p_{22} - p_{12}^2}{\Lambda^2 p_{11}} + \frac{\alpha_t p_{11}}{\Lambda^3} I_{1|0}\left(\frac{\Lambda\alpha_t}{p_{11}}(1 + 2\rho_S g \, \cos\Delta\phi + \rho_S^2 g^2)\right)$$

$$\times \left[\left(\eta_t - \frac{p_{12}}{p_{11}}\right)^2 + (\rho_S g)^2\left(\eta_I - \frac{p_{12}}{p_{11}}\right)^2 + 2\rho_S g\left(\eta_t - \frac{p_{12}}{p_{11}}\right)\left(\eta_I - \frac{p_{12}}{p_{11}}\right)\cos\Delta\phi\right]$$

$$+ \left(\eta_I - \eta_t\right)^2\left[\frac{\alpha_t^2\rho_S^2 g^2}{\Lambda^2}\sin^2\Delta\phi\right] I_{1|0}^*\left(\frac{\Lambda\alpha_t}{p_{11}}(1 + 2\rho_S g \, \cos\Delta\phi + \rho_S^2 g^2)\right) \tag{4.174}$$

Using the $\Re_o = E[\Re_o|\Theta_{MP}, \Phi_{MP}]$ of (3.151) and the sea-surface reflection model given in Section 2.6, trajectories of $E[y_I|\Lambda, \Psi_{MP}, \Delta\phi]$, $E[y_Q|\Lambda, \Psi_{MP}, \Delta\phi]$, and the variances were generated for low-elevation targets, with the antenna boresight pointing directly at the target. Trajectories were generated for radars operating at 4 GHz in S band, 10 GHz in X band, and 16 GHz in Ku band. For all cases, the sea surface was assumed to have a RMS wave height of 0.25 m, and the radar is vertically polarized and 20 m above the sea surface.

For the S band case, the radar was modeled to have a one-way beamwidth of 2.5° and a squint angle of 1.05°. The target travels from a range of 20 km to a range of 5 km at an altitude 80 m. The means of y_I and y_Q and the associated standard deviations are shown in Figures 4.3 and 4.4 for a 16-dB target (i.e., 16 dB in the absence of multipath), and Figure 4.5 gives the covariance of y_I and y_Q. Again, note that $\Re_o = E[\Re_o|\Theta_{MP}, \Phi_{MP}]$ of (3.151) has been used in (4.167) through (4.174). Figure 4.6 compares the expected standard deviations for the in-phase monopulse ratios for a 16-dB target with that for a 13 dB target. Note that the standard deviation for the monopulse ratios in the absence of multipath is about 0.11 for a 16-dB target and 0.14 for a 13-dB target. Thus, the presence of multipath severely corrupts the means and variances of the in-phase and quadrature monopulse ratios.
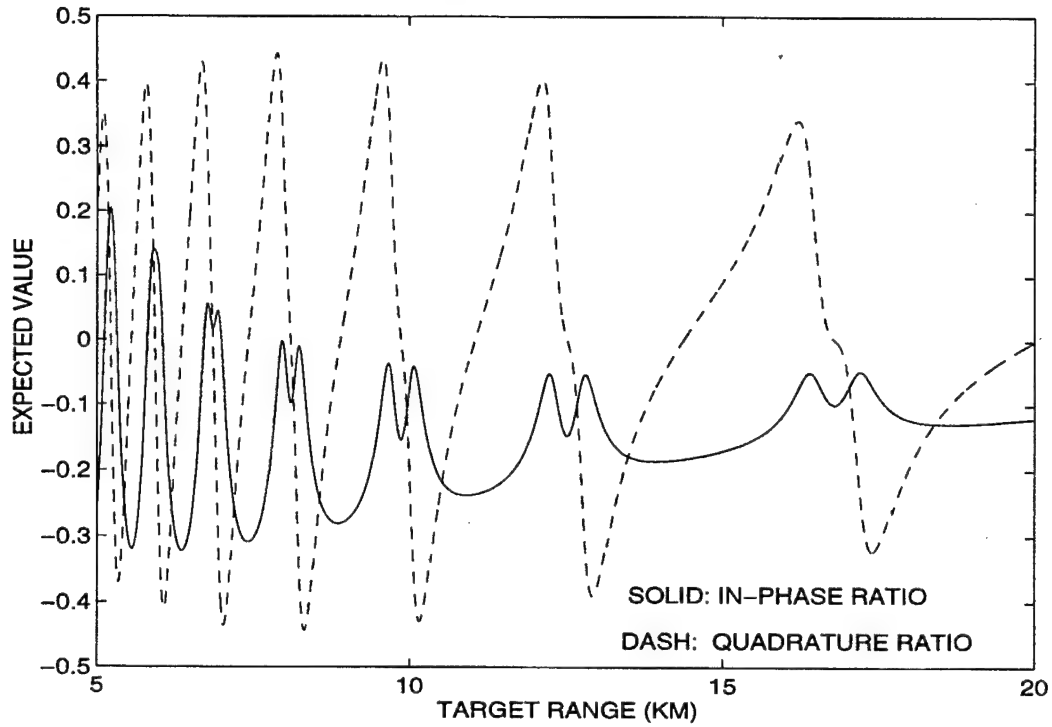
Figure 4.3 Means of Monopulse Ratios for 16-dB Target at an Altitude of 80 m and S Band Radar
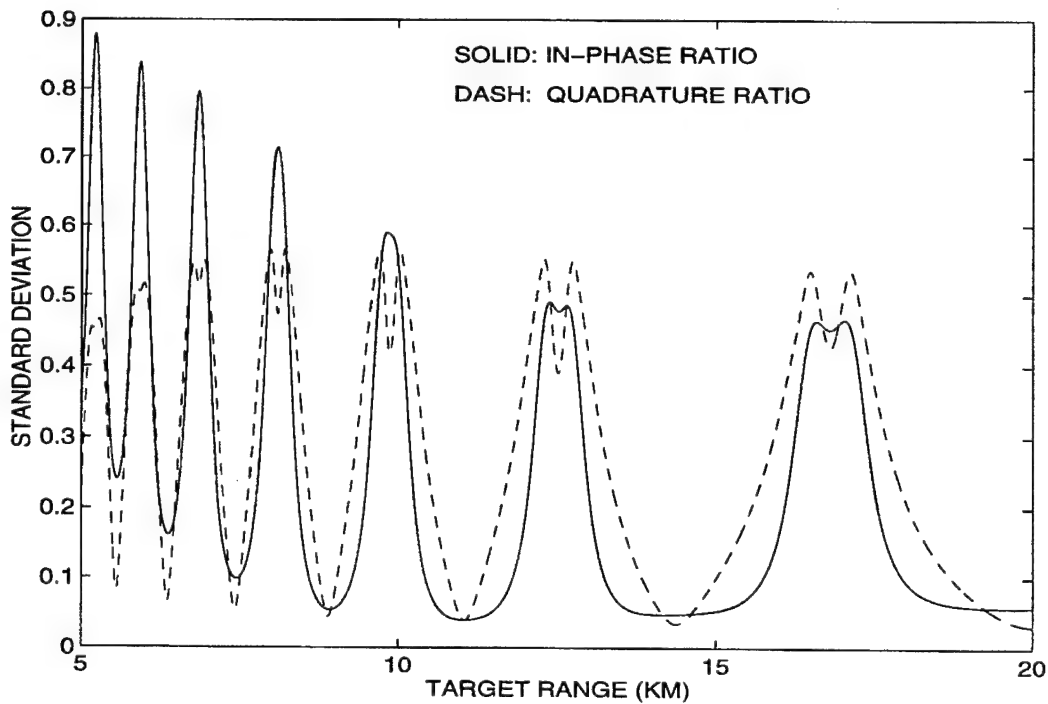
Figure 4.4 Standard Deviations of Monopulse Ratios for 16-dB Target at an Altitude of 80 m and S Band Radar

However, Figure 4.4 shows that the standard deviation of the in-phase monopulse ratio is reduced significantly when the target is out of the multipath nulls (*i.e.*, peaks in the expected value of the in-phase monopulse ratios) and at longer ranges, where the specular reflections are relatively strong, and the angles between the target and the image are rather small. Figure 4.6 shows that the larger amplitudes of the target reduce the measurement errors at longer ranges where the specular reflections are relatively strong and increases the measurement errors at the shorter ranges where the diffuse reflections are relatively strong. The results of Figure 4.3 are given in the complex plane in Figure 4.7 along with the same results for $\rho_{d0} = 0$. Note that Figure 4.7 gives only the results for the target ranges of 15 km to 8 km. The dash lines in Figure 4.7 give the means of y_I and y_Q for specular-only reflections at the sea surface. Figure 4.7 shows that ignoring the effects of the diffuse reflections will result in significant errors in the DOA estimation for a target in the presence of sea-surface-induced multipath. The expected values of the in-phase monopulse ratios for a target at an altitude of 40 m are shown in Figure 4.8 for specular and diffuse reflections and specular-only reflections. Figure 4.8 indicates that the presence of the diffuse reflections reduces the effects of the multipath nulls. Note that fewer multipath nulls occur when tracking a target at altitude of 40 m than when tracking a target at an altitude of 80 m.

For the X band case, the radar was modeled to have a one-way beamwidth of 1.5° and a squint angle of 0.63°. The target travels from a range of 20 km to a range 5 km at an altitude 30 m. The expected values of y_I are shown in Figures 4.9 and 4.10 for a 16-dB target at altitudes of 40 m and 25 m, respectively. The dash lines of Figures 4.9 and 4.10 give the means of y_I for specular-only reflections at the sea surface. Note that ignoring the effects of the diffuse reflections in X band will result in larger errors in the DOA estimation than ignoring the diffuse reflections at S band. Figure 4.11 gives the expected values of y_I and y_Q plotted in the complex plane for specular and diffuse reflections, and specular-only reflections at the sea surface.

For the Ku band case, the radar was modeled to have a one-way beamwidth of 1.0° and a squint angle of 0.42°. Two 16-dB targets are considered. Both targets travel from a range of 20 km to range 5 km, while the first target travels at an altitude of 25 m, and the second target travels at an altitude of 10 m. The expected values of y_I for both targets are plotted in Figures 4.12 and 4.13. The dash lines in Figures 4.12 and 4.13 give the expected values of y_I for specular-only reflections at the sea surface. Note that effects of ignoring the diffuse reflections are even greater in Ku band than in X band or S band.
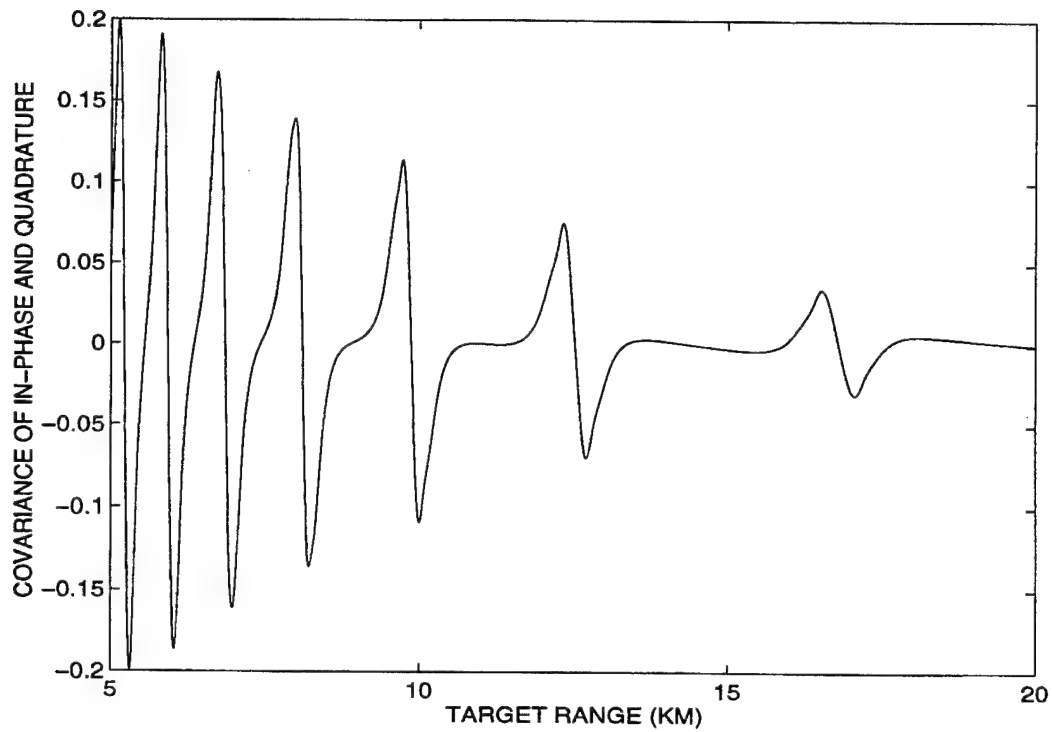
Figure 4.5 Covariance of the In-Phase and Quadrature Monopulse Ratios for 16-dB Target at an Altitude of 80 m and S Band Radar
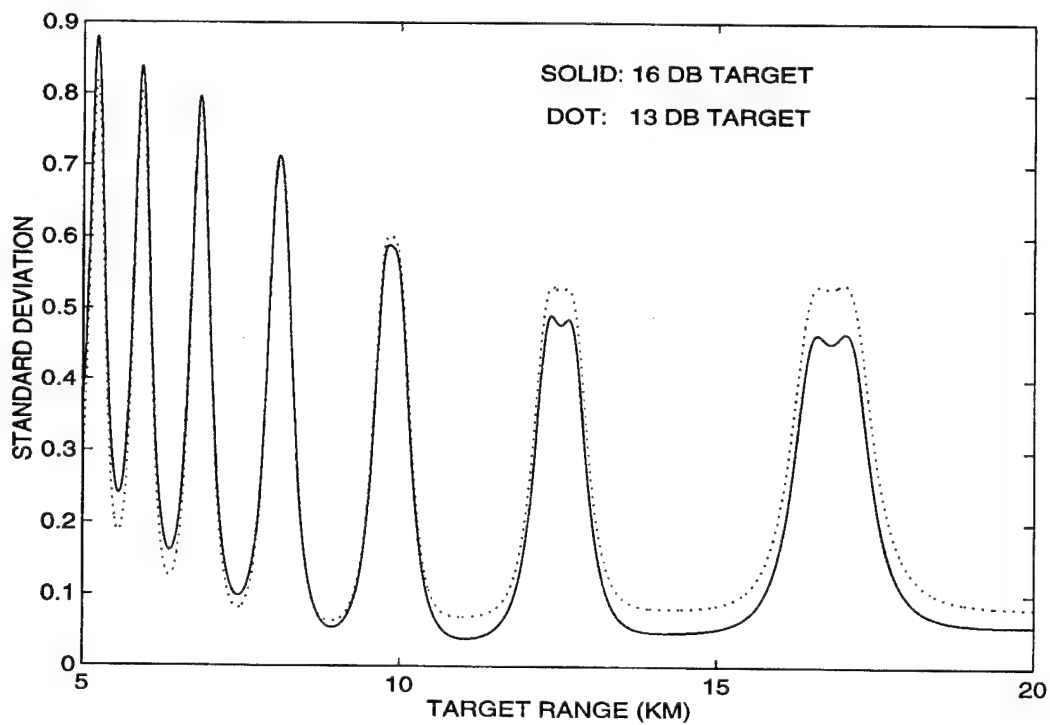
Figure 4.6 Standard Deviations of the In-Phase Monopulse Ratios for 13-dB and 16-dB Targets at an Altitude of 80 m and S Band Radar
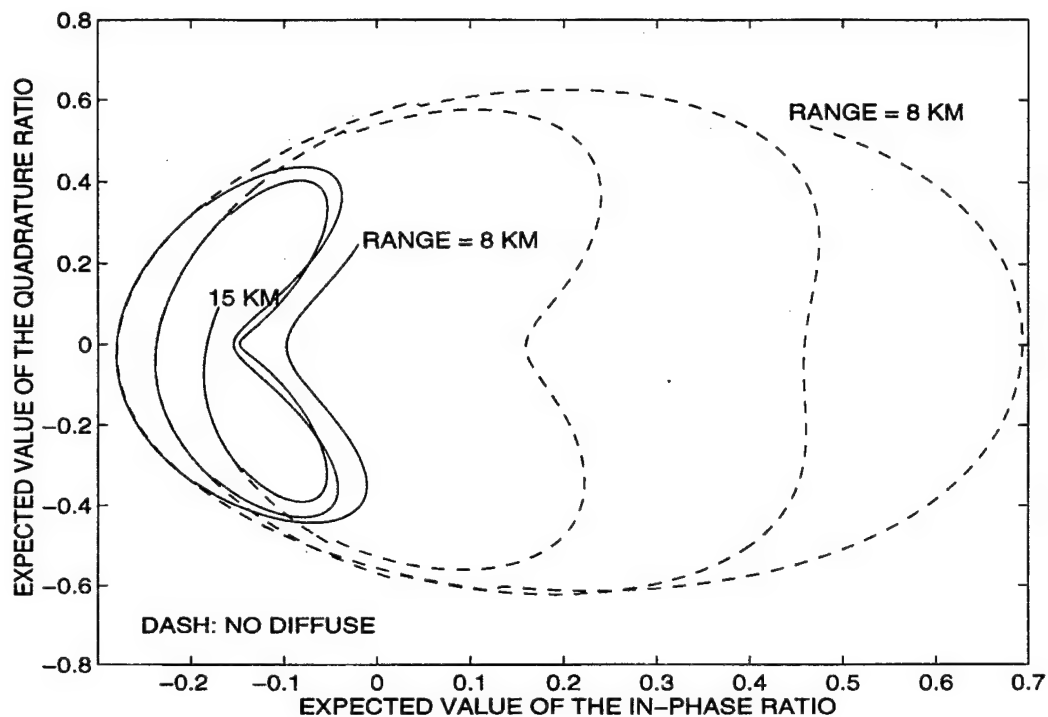
Figure 4.7 Means of the Complex Monopulse Ratios for 16-dB Target at an Altitude of 80 m and S Band Radar
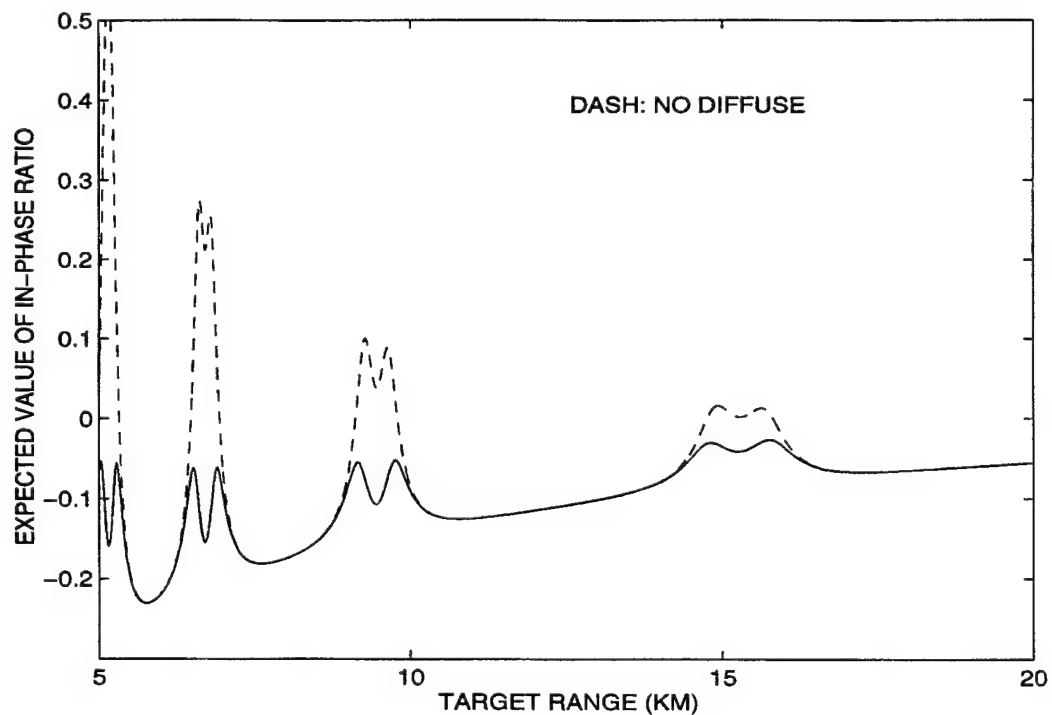
Figure 4.8 Means of the In-Phase Monopulse Ratios for 16-dB Target at an Altitude of 40 m and S Band Radar
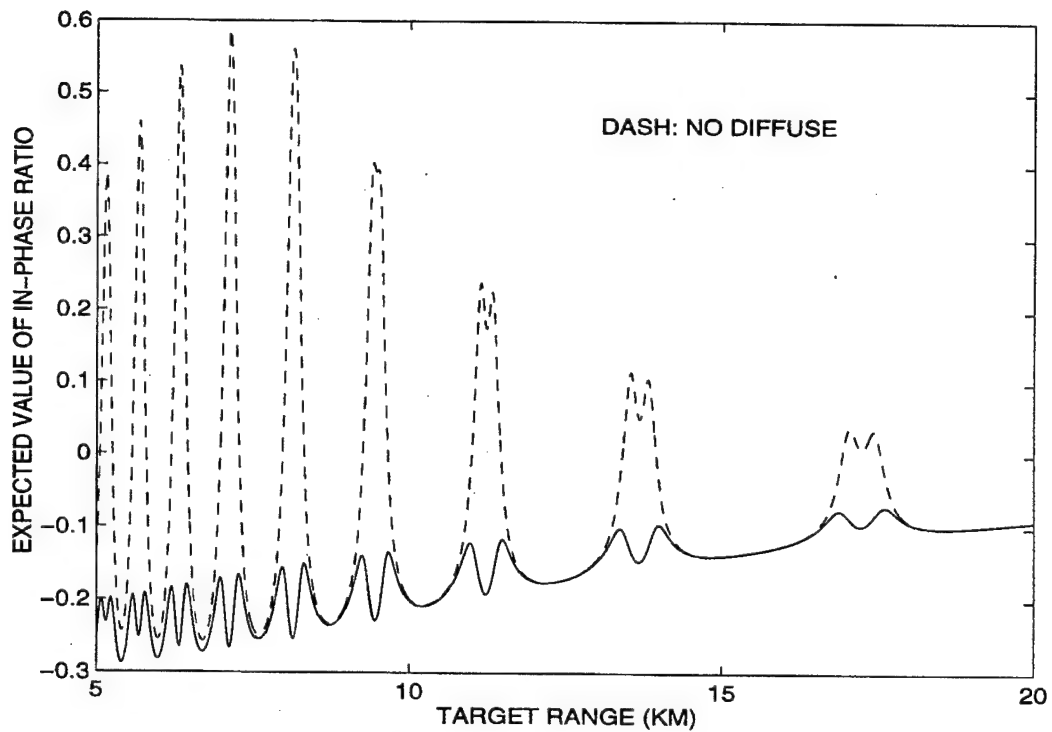
Figure 4.9 Means of the In-Phase Monopulse Ratios for 16-dB Target at an Altitude of 40 m and X Band Radar
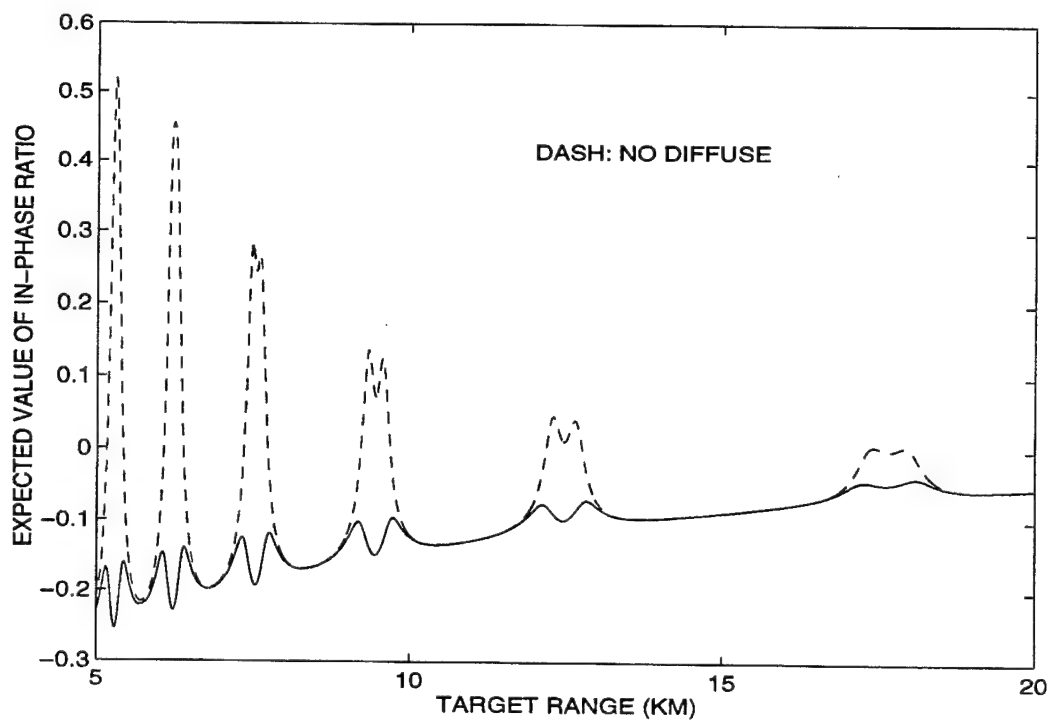
Figure 4.10 Means of the In-Phase Monopulse Ratios for 16-dB Target at an Altitude of 25 m and X Band Radar
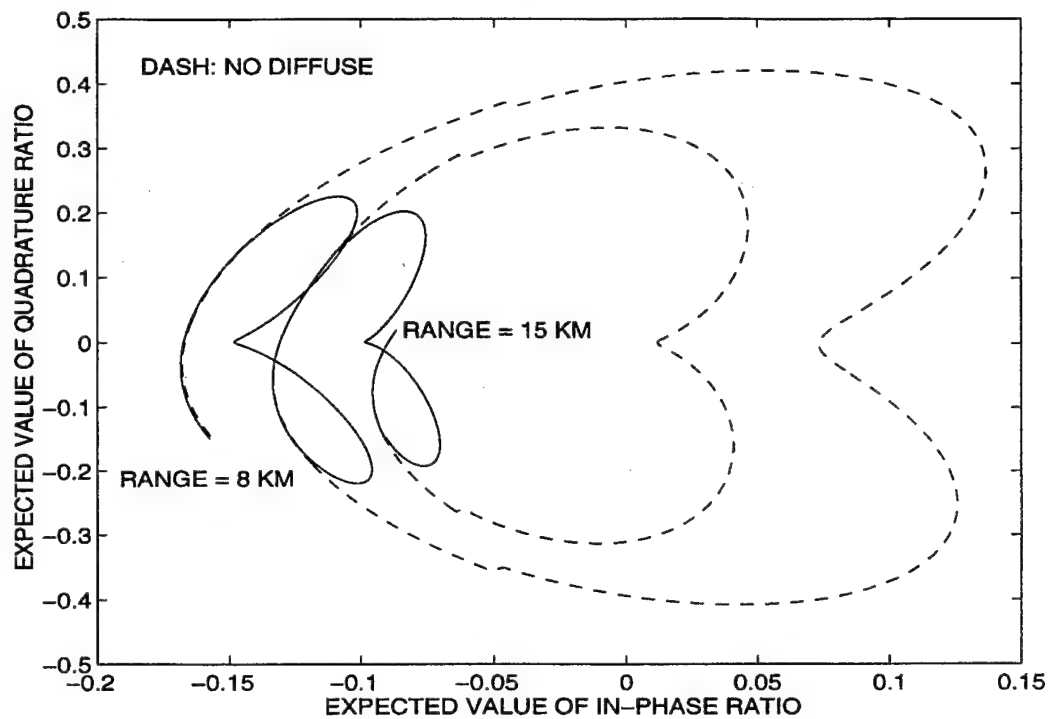
Figure 4.11 Means of the Complex Monopulse Ratios for 16-dB Target at an Altitude of 25 m and X Band Radar
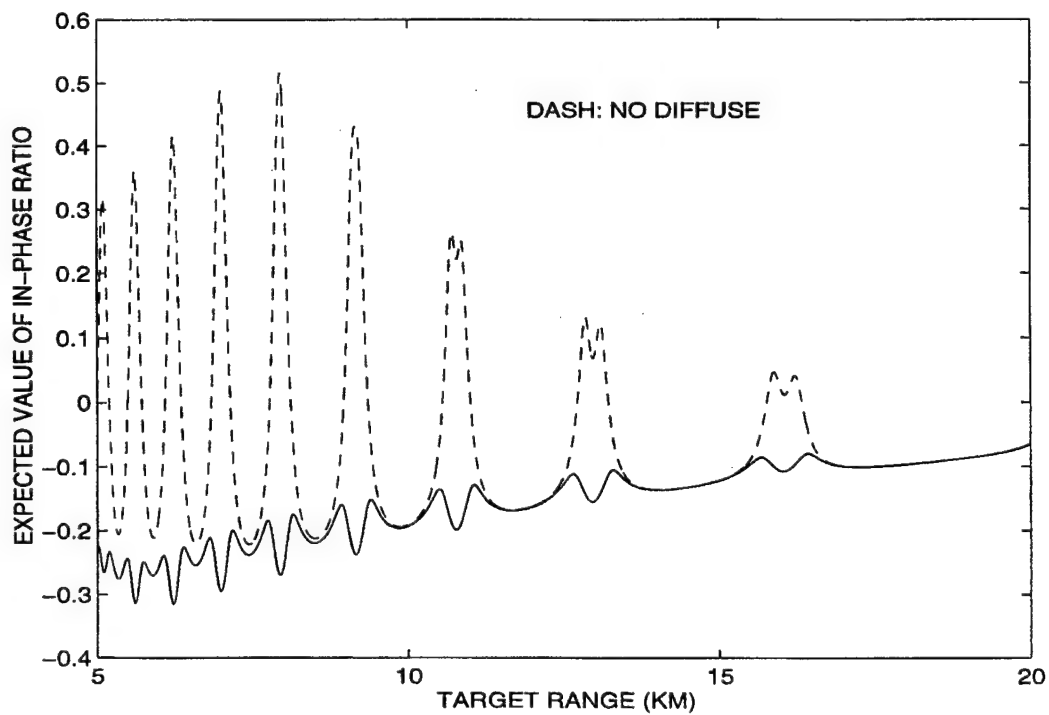
Figure 4.12 Means of the In-Phase Monopulse Ratios for 16-dB Target at an Altitude of 25 m and Ku Band Radar
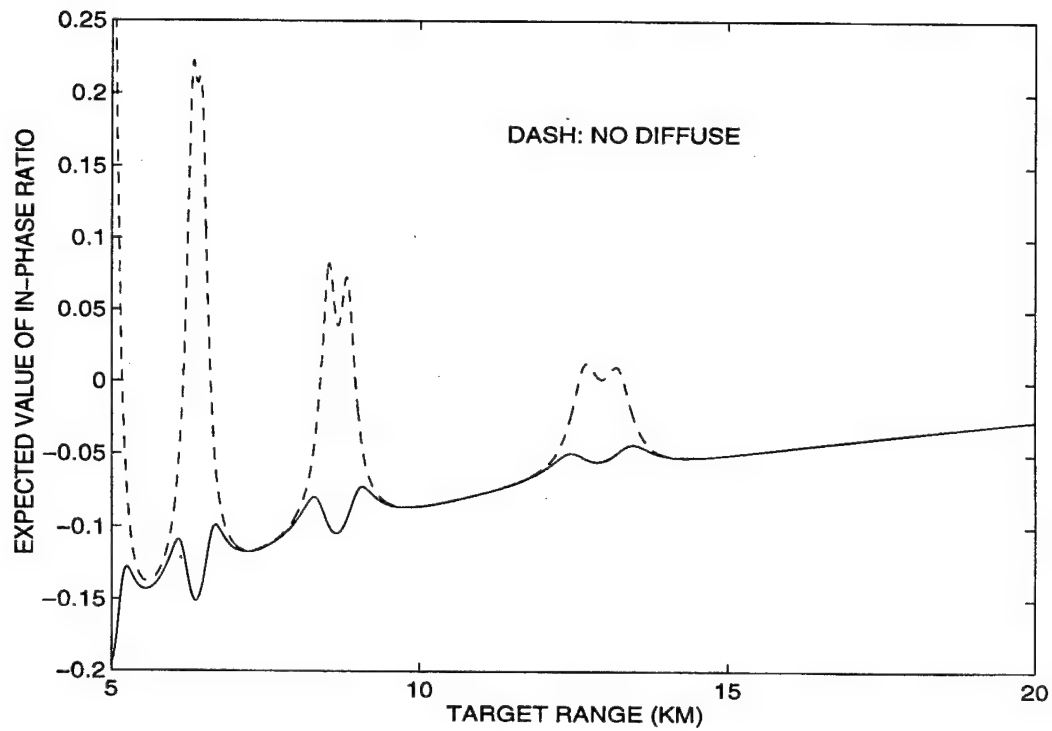
Figure 4.13 Means of the In-Phase Monopulse Ratios for 16-dB Target at an Altitude of 10 m and Ku Band Radar

Chapter 5

DIRECTION-OF-ARRIVAL (DOA) ESTIMATION

As discussed in Section 2.3, the monopulse ratio is typically used as the DOA estimate. However, the results of Chapter 4 show that the monopulse ratio is not the ML estimate [11, p. 65] nor MM estimate [11,p. 151] of the DOA for a single, resolved target. The use of the monopulse ratio is the result of physical insight into the problem and the work of Mosca in [40,41]. In [40], Mosca showed that the ML estimate of the DOA for a single pulse and unknown target amplitude and phase is given approximately by the in-phase monopulse ratio for a high SNR and a small DOA (*i.e.*, a target very near the antenna boresight). In [41], Mosca derived the ML estimator for the DOA for N pulse returns from a pulse-to-pulse Rayleigh fluctuating target. Mosca concluded that the estimator was too complicated and showed that for a high SNR and a small DOA, the ML estimate is closely approximated by the in-phase part of the monopulse ratio. When the target amplitude and/or phase are jointly estimated, Mosca showed in [40,41] that at moderate and low SNRs, the monopulse ratio is a biased estimate of the DOA as given by (2.51). A slightly different approach to the DOA estimation for a single target is taken in this chapter to relax the restrictions of a high SNR and small DOA. The amplitude-conditioned[4] PDFs and statistics developed in Chapter 4 are used to develop ML estimators and/or MM estimators of the DOA for a single resolved target with a known target amplitude. The amplitude-conditioned PDFs are also used to develop the CRLBs for any unbiased estimator of the DOA. When the target amplitude is unknown, the ML estimate of the target amplitude, as developed in Chapter 3, is used in the ML estimators and MM estimators to form GML estimators and Generalized Method of Moments (GMM)

---

[4] Since the conditional PDF corresponds to a PDF that is defined on a restricted probability space that is specified by the measured amplitude of the sum signal, statistical quantities developed on the restricted probability space have the same properties as their unconditional counterparts. Since all of the estimators and CRLBs developed in the chapter are conditional estimators and CRLBs, the term "conditional" will not be used explicitly to denote the estimators and CRLBs developed in this chapter.

estimators, respectively. The DOA estimates and the target amplitude estimates are also used to develop estimates of the variance of the DOA estimates that are required to support Kalman filter tracking of the targets.

When target echoes are not resolved in the frequency or time domains, the results of Chapter 4 clearly show that the in-phase monopulse ratio is not an appropriate estimate of the DOA of either target. While the problem of DOA estimation of unresolved targets has been addressed in several studies involving array signal processing [8] and multiple-beam monopulse (i.e., more than two beams per angular coordinate) [6,7], the work of Sherman in [1,4,42] is the only technique that utilizes a standard monopulse system in the DOA estimation of two unresolved targets. Sherman proposed the use of complex monopulse ratios from two pulses separated sufficiently in time so that the relative phase of the two targets changes, but sufficiently close in time so that the amplitudes of the two targets remain fixed. Sherman then used the five measured quantities, the two complex monopulse ratios and the ratio of the measured amplitudes of the sum signal, to compute the DOAs of the two targets, the two relative phases, and the ratio of the target amplitudes. In [43], Daum studied the angular estimation accuracies of a standard monopulse radar system for two unresolved targets and showed that the estimation accuracies decline significantly as the variance of the target amplitude fluctuations increases. Sherman also showed in [44] under similar assumptions that the in-phase monopulse ratios from the two angular coordinates and the ratio of the measured amplitudes from two pulses can be used to estimate the centroid of the two targets and the slope of the line connecting them. However, achieving two pulses with echoes that satisfy the requirements of Sherman's technique is not very likely. Furthermore, Sherman utilized a deterministic formulation of the problem to develop his approach. Thus, to date, the results of Sherman have not been further developed and reported in the literature.

In this chapter, a stochastic approach is taken to the DOA estimation for two unresolved targets. The Fisher Information Matrix (FIM) and CRLBs are developed for the DOA estimation of two unresolved Rayleigh targets using a standard monopulse radar. The FIM and CRLBs are used to study the effects of beam pointing on the DOA estimation. For two unresolved Rayleigh targets as considered in Section 4.2, the mean of the in-phase monopulse ratio is used to estimate the DOA of the centroid of the two targets, while the variance of the in-phase and quadrature monopulse ratios is used to estimate the difference of the DOAs of the two targets. The DOAs of both targets can be computed from the DOA of the centroid and the difference of the two DOAs. Expressions for estimating the variances of both DOA estimates are developed.

While Sherman's approach to DOA estimation for two unresolved targets has received very little attention since its publication, his approach to the DOA estimation for a target in the presence of multipath [1,4,42] has received considerable attention [5,45-47]. Sherman proposed the use of the complex monopulse ratio from a single pulse and the geometric constraint imposed by the sea surface to estimate the DOA of the target. Peeblez and Goldman [45] compared the performance of Sherman's technique with that of conventional tracking and concluded that it provides significant reductions in the errors, even when knowledge of the surface-reflection coefficient is imperfect. Symonds and Smith [46] extended Sherman's technique to multiple frequencies and conducted some simulation studies to assess the performance of the DOA estimation. The results of their simulation studies indicated that Sherman's technique provides significant improvement in conventional tracking over smooth surfaces (*i.e.*, no diffuse reflections) but only marginal improvement over rough surfaces. These conclusions of Symonds and Smith also agree with the conclusions of the experiment conducted by Howard [47] and the analysis of Barton in [5]. Again, Sherman utilized a deterministic formulation of the problem to develop his DOA estimation for a target in the presence of multipath. A stochastic approach could taken to the DOA estimation for a target in the presence of sea-surface-induced multipath. The diffuse reflections are included explicitly in the model of the sum and difference channel voltages as discussed in Section 2.6. The complex monopulse ratios from multiple pulses, target amplitude estimate, and the geometric constraint imposed by the sea surface could be used to estimate the DOA of the target and $\Delta\phi$. The variances of the monopulse ratios in Section 4.7 could also be utilized to develop an estimator for the variances of the DOA estimates.

DOA estimation for a single Rayleigh target and real-correlation in the receiver errors is considered in Section 5.1, while single-pulse DOA estimation is considered in Section 5.2. DOA estimation of a Rayleigh target in the presence of a Gaussian jammer is considered in Section 5.3. Since the jammer signals enter into all the range bins, the DOA estimate of the jammer, which is estimated with the monopulse measurements that do not include the target, is utilized with the results of Section 4.2 to estimate the DOA of the Rayleigh target. DOA estimation of two unresolved Rayleigh targets with known relative RCS is developed in Section 5.4, along with a strategy for pointing the antenna boresight when two targets are unresolved.

5.1 Rayleigh Target

CRLBs for any unbiased estimator of the DOA for Rayleigh targets are developed using the amplitude-conditioned PDF of the complex monopulse ratio developed in Section 4.1. While only the in-phase part of the monopulse ratio is typically used to estimate the DOA, CRLBs are developed for DOA estimators that utilize the in-phase and/or quadrature parts of the monopulse ratio in order to illustrate the value of the quadrature part in the estimation of the DOA. Using the amplitude-conditioned PDF of the complex monopulse ratio, ML and MM estimators are developed for the target DOA, and the estimates are used to form estimates of the variance of the DOA estimate. For an unknown target amplitude parameter, ML and MM estimates of the DOA are computed using the ML estimate of the target amplitude parameter that is computed from the measured amplitudes of the sum signal as discussed in Section 3.1. The performances of these estimators are compared to that of the monopulse ratio for DOA estimation, which does not require knowledge of the target amplitude. The MM estimate of the DOA and the ML estimate of the target amplitude are used to form an estimate of the variance of the DOA estimate. Using simulation results, the performances of the ML and MM estimators are compared with that of the monopulse ratio, and the performances of the variance estimators are studied.

Cramer-Rao Lower Bounds (CRLBs) for DOA Estimates

Since the CRLB gives the lower bound for the variance of any unbiased estimate, the performances of the ML and MM estimators of the DOA will be compared to the CRLB to assess the potential for alternate estimators that are better. Furthermore, the value of the quadrature monopulse ratio to the DOA estimation is assessed by comparing the CRLBs for estimators that utilize either the in-phase or quadrature monopulse ratio or both ratios.

The CRLB [11, p. 66] associated with $\hat{\eta}_1$ based on N observations of y_I and y_Q is given by

$$J_{y_I, y_Q}(\hat{\eta}_1 | N, \{\Re_{ok}\}_{k=1}^N, \Psi_R) = \left[-\sum_{k=1}^N E\left[\frac{\partial^2 \ln f(y_{Ik}, y_{Qk} | \Re_{ok}, \Psi_R)}{\partial \eta_1^2} \Bigg| \Re_{ok}, \Psi_R \right] \right]^{-1}$$

(5.1)

where $\Re_{ok}$ is the observed SNR of (2.23) for pulse k, and y_{Ik} and y_{Qk} are the in-phase and quadrature monopulse ratios for pulse k, respectively. Using (4.42) in (5.1) gives

$$J_{y_I, y_Q}(\hat{\eta}_1 | N, \{\Re_{ok}\}_{k=1}^N, \Psi_R) = \frac{p}{2NY_N}\left[1 + \frac{1}{\Re_{R1}} \right]^2 \left[1 + \frac{2(\eta_1 - \rho\sigma_d\sigma_S^{-1})^2}{pY_N} \right]^{-1}$$

(5.2)

where p is given by (4.45). Using the marginal PDF of y_{Ik} from (4.43) in (5.1) gives the CRLB associated with $\hat{\eta}_1$ based on N observations of y_I only as

$$J_{y_I}(\hat{\eta}_1|N, \{\Re_{ok}\}_{k=1}^N, \Psi_R) = \frac{p}{2NY_N}\left[1 + \frac{1}{\Re_{R1}}\right]^2 \left[1 + \frac{(\eta_1 - \rho\sigma_d\sigma_S^{-1})^2}{pY_N}\right]^{-1} \quad (5.3)$$

Comparing (5.2) and (5.3) shows that the use of y_I and y_Q gives a smaller CRLB for $\hat{\eta}_1$ than the use of only y_I, when $\eta_1 \neq \rho\sigma_d\sigma_S$. Therefore, y_Q provides some information concerning the value of η_1. Using the marginal PDF of y_{Qk} from (4.44) in (5.1) gives the CRLB associated with $\hat{\eta}_1$ based on N observations of y_Q only as

$$J_{y_Q}(\hat{\eta}_1|N, \{\Re_{ok}\}_{k=1}^N, \Psi_R) = \frac{p^2}{2N(\eta_1 - \rho\sigma_d\sigma_S^{-1})^2}\left[1 + \frac{1}{\Re_{R1}}\right]^2 \quad (5.4)$$

Comparing (5.2) with (5.3) and examining (5.4) indicates that y_Q provides essentially no information concerning the value of η_1 when $\eta_1 \approx \rho\sigma_d\sigma_S^{-1}$. Therefore, for $\rho = 0$ and a target near the center of the beam (i.e., $\eta_1 \approx 0$), the observations of y_Q provide essentially no information toward the estimation of η_1. Thus, the typical practice of ignoring the observations of y_Q makes perfect sense when the antenna boresight is maintained near the target. However, the observations of y_Q should be considered when off-boresight (i.e., $\eta_1 \not\approx \rho\sigma_d\sigma_d$) measurements occur rather often, as in phased array radar tracking many targets or off-boresight tracking.

Unconditional CRLBs that were developed from $f(y_I, y_Q|\Psi_R)$ are given in Appendix B. Unconditional CRLBs were also developed from $f(\Lambda, y_I, y_Q|\Psi_R)$, and those unconditional CRLBs are given by setting $Y_N = E[Y_N|\Psi_R] = \Re_{R1}+1$ in (5.2) through (5.4). The conditional CRLBs are shown in Appendix B to be less than the unconditional CRLBs for $\Re_{R1} > 3$ dB. Thus, DOA estimators utilizing monopulse processing should be developed from the conditional PDF or the conditional statistics.

Estimation of DOA and Variances

The development of the ML estimator will be followed by the development of the MM estimator and the estimators of the variances. The ML estimator of a parameter maximizes the likelihood function for a given set of observations of random variables. Any estimate that satisfies the CRLB with equality is called an efficient estimate, and if an efficient estimate exists, it is given by the unique solution to the likelihood function [11, p. 65].

The ML estimate of η_1 is given by

$$\hat{\eta}_{ml} = arg\max_{\eta_1} \prod_{k=1}^N f(y_{Ik}, y_{Qk}|\Re_{ok}, \Psi_R) \quad (5.5)$$

109

Taking the derivative of (5.5), the extrema and reflection points are given by $\bar{\eta}$ satisfying

$$\bar{\eta}_{ml}^3 + a_2\bar{\eta}_{ml}^2 + a_1\bar{\eta}_{ml} + a_0 = 0 \tag{5.6}$$

where

$$a_2 = X_N - \rho\frac{\sigma_d}{\sigma_S}\left(3 + Y_N\right) \tag{5.7}$$

$$a_1 = \left[1 + \frac{1 - \rho^2}{\Re_{R1}} + 2\rho^2 + \left(1 - \frac{\rho^2}{\Re_{R1} + 1}\right)Y_N\right]\frac{\sigma_d^2}{\sigma_S^2} - \left[1 + \frac{1}{\Re_{R1}}\right]Z_N \tag{5.8}$$

$$a_0 = \frac{\sigma_d^2}{\sigma_S^2}\left[1 + \frac{1 - \rho^2}{\Re_{R1}}\right]\left[\frac{\rho}{\Re_{R1} + 1}\frac{\sigma_d}{\sigma_S}Y_N - X_N - \rho\frac{\sigma_d}{\sigma_S}\right] + \left[1 + \frac{1}{\Re_{R1}}\right]\rho\frac{\sigma_S}{\sigma_d}Z_N \tag{5.9}$$

$$X_N = \frac{1}{N}\sum_{k=1}^{N}\Re_{ok}y_{Ik} \tag{5.10}$$

$$Y_N = \frac{1}{N}\sum_{k=1}^{N}\Re_{ok} \tag{5.11}$$

$$Z_N = \frac{1}{N}\sum_{k=1}^{N}\Re_{ok}\left[\left(y_{Ik} - \frac{\rho}{\Re_{R1} + 1}\frac{\sigma_d}{\sigma_S}\right)^2 + y_{Qk}^2\right] \tag{5.12}$$

Since (5.6) does not have a unique solution, an efficient estimator of η_1 does not exist for finite values of N. One of the $\bar{\eta}$ that satisfies (5.6) is the ML estimate $\hat{\eta}_{ml}$, which can be computed using Newton's method with $\hat{y}_I$ of (4.46) as the initial value, or using a root-finding algorithm and selecting the root closest to $\hat{y}_I$. As an alternative to solving the cubic expression in (5.6), (5.5) can be maximized numerically. Also, if $\bar{\eta}$ is sufficiently small so that $\bar{\eta}^3$ and $a_2\bar{\eta}^2$ can be ignored, then $\hat{\eta}_{ml} \approx -a_0a_1^{-1}$, which corresponds to the monopulse ratio if the SNR is sufficiently high so that $1 + \Re_{R1}^{-1} \approx 1$.

When the target amplitude parameter $\Re_{R1}$ is not known, as is the case in most radar tracking problems, $\Re_{R1}$ in (5.5) can be replaced by its ML estimate $\widehat{\Re}_{R1}$, given by (3.32), to form a generalized likelihood function. Then, $\hat{\eta}_{ml}$ that satisfies (5.5) with $\Re_{R1} = \widehat{\Re}_{R1}$ in (5.7), (5.8), and (5.12) will be referred to as $\hat{\eta}_{gml}$, the GML estimate of η_1. However, the use of small values for $\widehat{\Re}_{R1}$ for small N may not be realistic since target detection will be required before monopulse processing is used. Thus, the GML estimate is given by

$$\hat{\eta}_{gml} = \hat{\eta}_{ml} \quad \text{for} \quad \Re_{R1} = \widehat{\Re}_{R1} > \frac{\Re_{th}}{N} \tag{5.13}$$

where $\Re_{th}$ is the SNR detection threshold. Thus, if $N\widehat{\Re}_{R1} \le \Re_{th}$, a monopulse ratio is not formed and used for DOA estimation. Note that the use of $\Re_{R1} = \widehat{\Re}_{R1}$ will

increase the RMS error in the DOA estimate, and later in this section, simulation results show that for certain DOAs and SNRs the monopulse ratio should be used as the DOA estimate rather than the GML estimate. Since no analytical expression is available for $\hat{\eta}_{ml}$, the computation of variance of the $\hat{\eta}_{ml}$ is not considered in this section.

MM estimation is accomplished for K parameters by setting the first K sample moments to the actual moments, which are functions of the parameters of interest, and solving for the parameter estimates. Noting that the observations y_{Ik} are not stationary and that by using $\hat{y}_I$, the ML estimate of the conditional mean of y_I, of (4.46) to estimate η_1 gives

$$\hat{\eta}_{mm} = \left[1 + \frac{1}{\Re_{R1}}\right]\hat{y}_I - \frac{\rho}{\Re_{R1}}\frac{\sigma_d}{\sigma_S} \tag{5.14}$$

which is an unbiased estimate of the DOA when $\Re_{R1}$ is known. When the target amplitude parameter $\Re_{R1}$ is not known, $\Re_{R1}$ in (5.14) can be replaced by its ML estimate $\widehat{\Re}_{R1}$. However, the use of small values for $\widehat{\Re}_{R1}$ in (5.14) can introduce large errors. Thus, the GMM estimate, as it will be referred to in this report, is given by

$$\hat{\eta}_{gmm} = \left[1 + \frac{1}{\widehat{\Re}_{R1}}\right]\hat{y}_I - \frac{\rho}{\widehat{\Re}_{R1}}\frac{\sigma_d}{\sigma_S} \quad \text{for} \quad \Re_{R1} = \widehat{\Re}_{R1} > \frac{\Re_{th}}{N} \tag{5.15}$$

where $\Re_{th}$ is the SNR detection threshold as discussed above. The use of an estimate for $\Re_{R1}$ will increase the RMS error in the DOA estimate, and later in this section, simulation results show, for certain DOAs and SNRs, that the monopulse ratio or the GML estimate should be used as the DOA estimate rather than the GMM estimate.

Using (4.43), (4.48), and (5.14) gives the variance of the MM estimate as

$$\sigma_{\hat{\eta}}^2 = \left[1 + \frac{1}{\Re_{R1}}\right]^2\sigma_{\hat{y}_I}^2 = \left[1 + \frac{1}{\Re_{R1}}\right]^2\left[\sum_{k=1}^{N}2\Re_{ok}\right]^{-1}p = \left[1 + \frac{1}{\Re_{R1}}\right]^2\frac{p}{2NY_N} \tag{5.16}$$

When using the DOA estimates developed above or the monopulse ratio for tracking targets with a monopulse radar, an estimate of the variance of each DOA estimate is required for the Kalman filter. Using an estimate of the conditional mean of y_I in (4.45) to reduce the dependency of p on $\Re_{R1}$ and form an estimate of p gives an estimate of the variance of the in-phase monopulse ratio as

$$\hat{\sigma}_{\hat{y}_I}^2 = \left[\sum_{k=1}^{N}2\Re_{ok}\right]^{-1}\hat{p} = \frac{\hat{p}}{2NY_N} \tag{5.17}$$

where

$$\hat{p} = \left[\frac{\sigma_d^2}{\sigma_S^2}\left(1 - \frac{\rho}{\Re_{R1}+1}\right) + \left(\hat{y}_I - \frac{\rho\sigma_d^2\sigma_S^{-2}}{\Re_{R1}+1}\right)(\hat{\eta}_1 - 2\rho\sigma_d^1\sigma_S^{-1})\right] \tag{5.18}$$

111

When the target amplitude is known, the variance of the monopulse ratios can be estimated by using the ML or MM estimate for $\hat{\eta}_1$ in (5.18). When the target amplitude is unknown, the variance of the monopulse ratios can be estimated by using the monopulse ratio, the GML estimate, or the GMM estimate for η_1. Using the resulting $\hat{p}$, an estimate of $\sigma_{y_{Ik}}^2$, the variance of the monopulse ratios of pulse k, can be computed using the N pulses according to

$$\hat{\sigma}_{y_{Ik}}^2 = \hat{\sigma}_{y_{Qk}}^2 = \frac{\hat{p}}{2\Re_{ok}} \qquad (5.19)$$

Using (5.16) and (5.18) gives an estimate of the variance of $\hat{\eta}_{mm}$ as

$$\hat{\sigma}_{\hat{\eta}}^2 = \Big[1 + \frac{1}{\Re_{R1}}\Big]^2 \hat{\sigma}_{\hat{y}_I}^2 = \Big[1 + \frac{1}{\Re_{R1}}\Big]^2 \Big[\sum_{k=1}^{N} 2\Re_{ok}\Big]^{-1} \hat{p} = \Big[1 + \frac{1}{\Re_{R1}}\Big]^2 \frac{\hat{p}}{2NY_N} \qquad (5.20)$$

where $\hat{\eta}_1 = \hat{\eta}_{mm}$ in $\hat{p}$. When the target amplitude is unknown, the variance of $\hat{\eta}_{gmm}$ can be estimated by using $\hat{\eta}_1 = \hat{\eta}_{gmm}$ and $\Re_R = \widehat{\Re}_R$ in $\hat{p}$ and setting a minimum value for the estimated SNR as in (5.15).

Since no analytical expression is available for $\hat{\eta}_{ml}$, no estimator is developed for the variance of the estimate. However, considering the CRLB of (5.2) indicates that (5.20) may provide a good estimate of the variance associated with $\hat{\eta}_{ml}$ by using $\hat{\eta}_1 = \hat{\eta}_{ml}$ in $\hat{p}$ when the target amplitude is known or $\hat{\eta}_1 = \hat{\eta}_{gml}$ in $\hat{p}$ when the target amplitude is unknown. The performance of the variance estimators developed in this section will be considered next through simulation studies.

Simulation Results

The results of Monte Carlo simulation studies are presented to give insight into the relative performances of the estimators. Each result is the average from 20,000 experiments with averaging over the conditioning random variable Λ (*i.e.*, Λ is random between experiments). When a threshold test is applied to the estimated SNR, as in the GML and GMM estimators, the results are the average from 20,000 experiments with the estimated SNR exceeding the threshold. Since Λ is random, the DOA estimation errors were normalized by the corresponding conditional CRLB prior to computing the sample standard deviations. Similarly, the variance estimators were studied by normalizing each error in the DOA estimate by the standard deviation estimate for that pulse and then computing the sample statistics. The performances of the monopulse ratio, ML estimator, and MM estimator of the DOA are compared for the cases of known and unknown target amplitude, and the performances of the variance estimators are then compared.
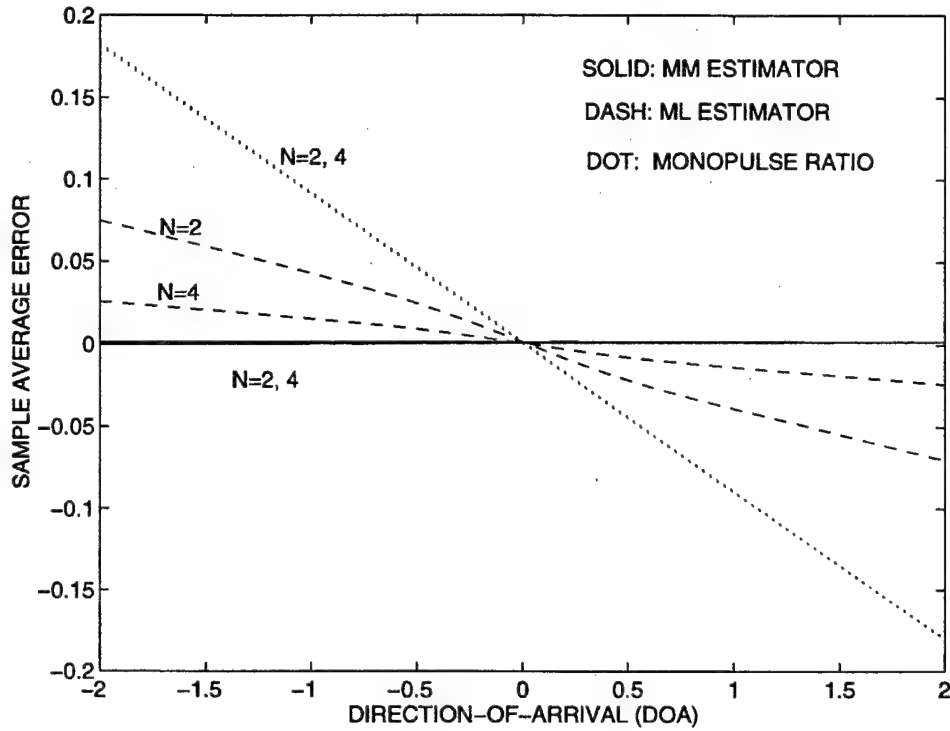
Figure 5.1 Sample Average Error for Known Target Amplitude with $N = 2$ and 4, $\rho = 0$, and $\Re_{R1} = 10$ dB
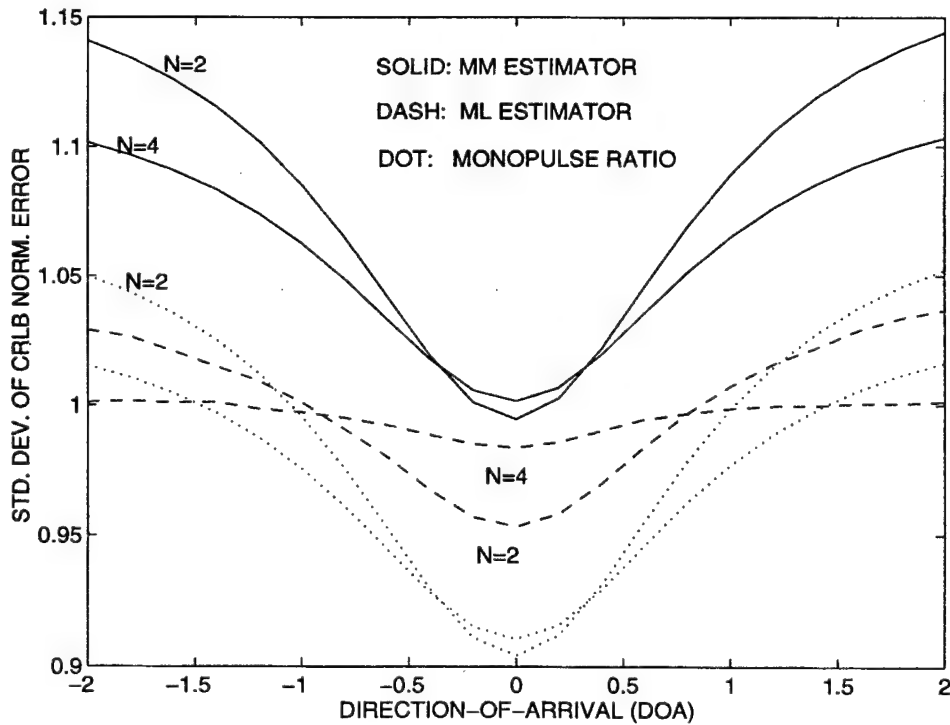
Figure 5.2 Sample Standard Deviation of CRLB Normalized Error for Known Target Amplitude with $N = 2$ and 4, $\rho = 0$, and $\Re_{R1} = 10$ dB
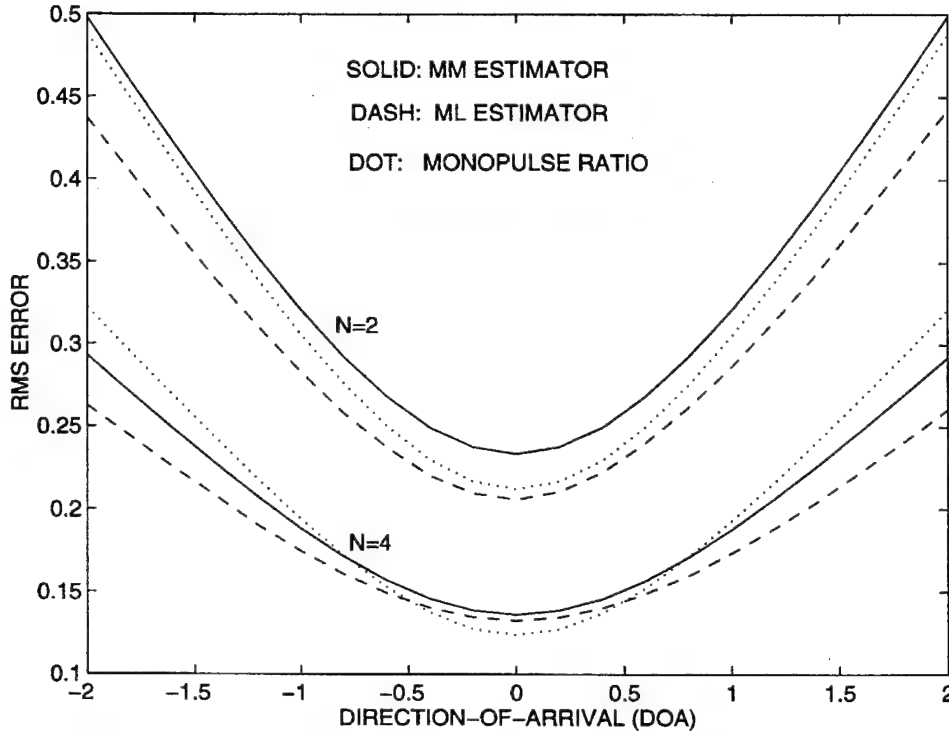
Figure 5.3 RMS Error for Known Target Amplitude with $N = 2$ and 4, $\rho = 0$, and $\Re_{R1} = 10$ dB

Monte Carlo simulations with 20,000 experiments were conducted for $N = 2$ and 4, $\Re_{R1} = 10$ dB, and $\rho = 0$ to compare the performances of the ML and MM estimators and the monopulse ratio. Figure 5.1 shows the sample average errors in the DOA estimates, while Figure 5.2 shows the sample standard deviations of the errors normalized by the CRLBs of (5.2). Figure 5.1 shows that, as expected, the monopulse ratio and ML estimate are biased estimators of η_1, while the MM estimate is unbiased. Furthermore, the bias of the monopulse ratio is independent of N, as indicated by (4.43), while the bias in the ML estimate decreases with increases in N, as expected due to the consistency of ML estimates. However, Figure 5.2 shows that the monopulse ratio provides a smaller variance relative to the CRLB than either the ML estimator or MM estimator for $|\eta_1| < 1.0$ and $\Re_{R1} = 10$. Note that since the monopulse ratio and ML estimators are biased, the variance of the estimates can be less than the CRLB as shown in Figure 5.2. Figure 5.2 also indicates that the variance of the ML estimate approaches the CRLB with increases in N as required by the asymptotically efficient property of ML estimates. Figure 5.3 shows that the RMS error for the ML estimator is about 10 percent less than that for the MM estimator. Figure 5.3 also shows for the cases considered that the $\hat{\eta}_{ml}$ is superior to using the
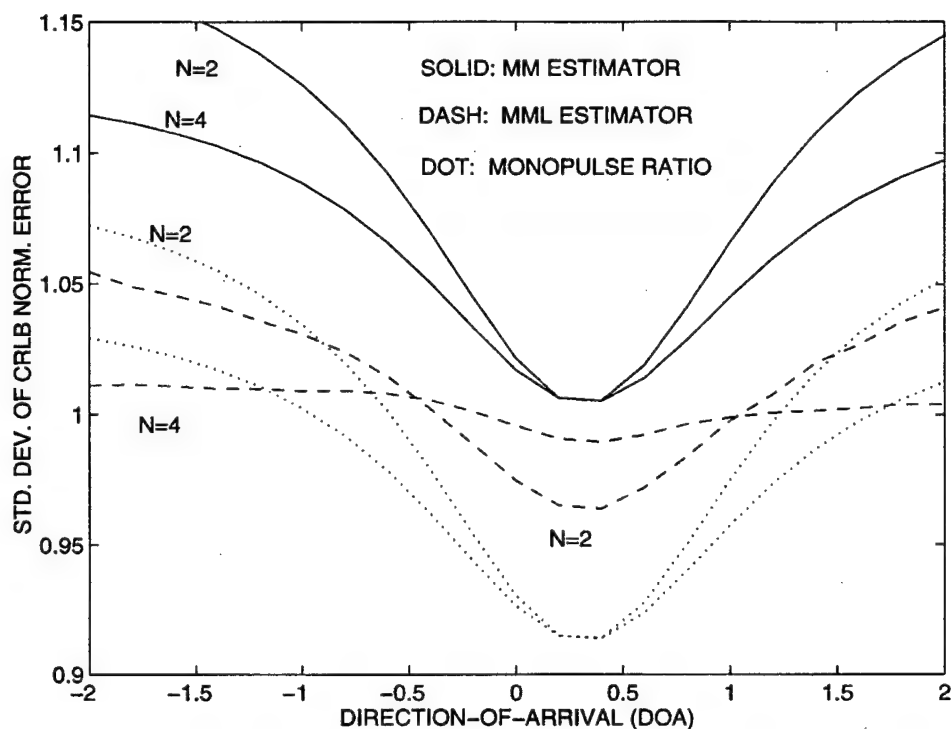
Figure 5.4 Sample Standard Deviation of CRLB Normalized Error for Known Target Amplitude with $N = 2$ and 4, $\rho = 0.3$, and $\Re_{R1} = 10$ dB
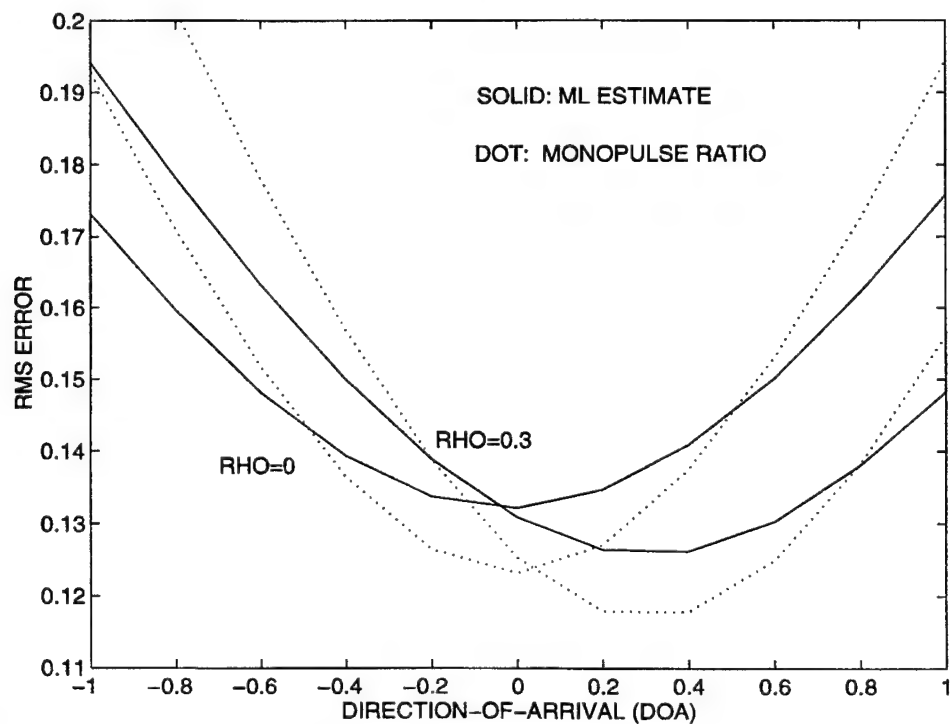
Figure 5.5 RMS Error for Known Target Amplitude with $N = 2$ and 4, $\rho = 0.3$, and $\Re_{R1} = 10$ dB
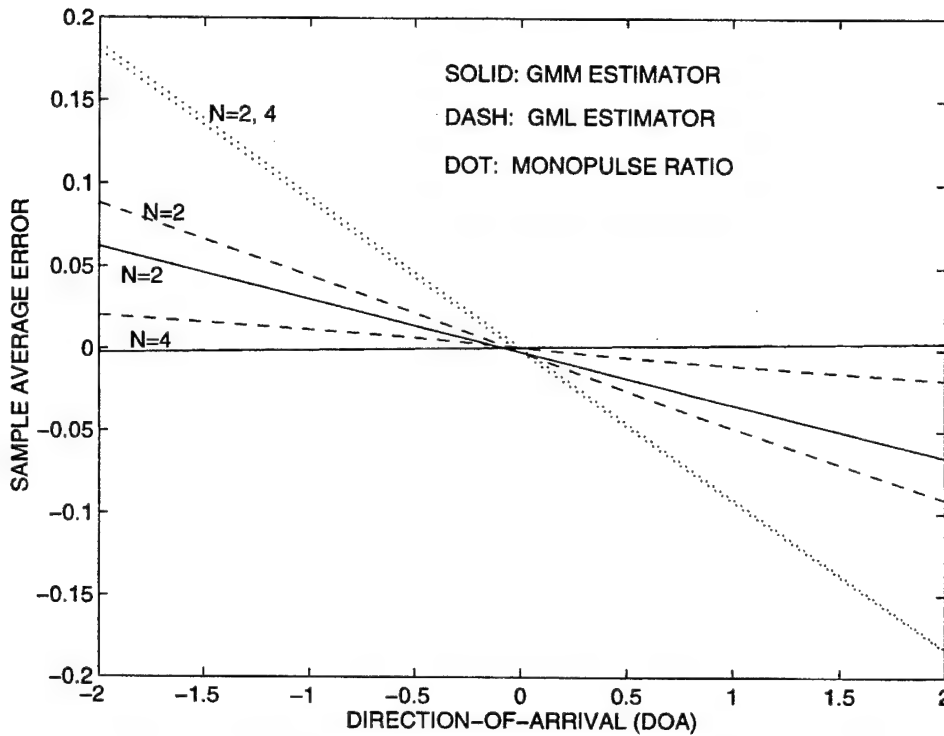
Figure 5.6 Sample Average Error for Unknown Target Amplitude with $N = 2$ and 4, $\rho = 0$, and $\Re_{R1} = 10$ dB

monopulse ratio, except for $N = 4$ and $|\eta_1| < 0.5$. The interval of η_1 for which the monopulse ratio is superior to $\hat{\eta}_{ml}$ decreases as N increases, because the bias in the monopulse ratio becomes a larger percent of the RMS error as N increases.

Another simulation was conducted for $\rho = 0.3$, and the results are shown in Figures 5.4 and 5.5. The results in Figure 5.4 are similar to those of Figure 5.2 with two notable differences. The minimum of the sample standard deviations are shifted from $\eta = 0$ in Figure 5.2 to $\eta = 0.3$ in Figure 5.4, and the DOA estimates for $\rho = 0.3$ are slightly less efficient than the DOA estimates for $\rho = 0$. However, Figure 5.5 shows that the RMS errors in the DOA estimates for $\rho = 0.3$ do achieve an overall lower value than the RMS errors in the DOA estimates for $\rho = 0$. Figure 5.4 also shows that the RMS errors in the DOA estimates are equal for $\rho = 0$ and 0.3 at $\eta = 0$.

Figure 5.6 shows the sample average error in the DOA estimates for an unknown target amplitude, while Figure 5.7 shows the RMS error for $N = 2$ and 4, $\Re_{R1} = 10$ dB, $\Re_{th} = 13$ dB in (5.13) and (5.15), and $\rho = 0$. Figure 5.6 shows that the monopulse ratio, GML estimates, and GMM estimates are biased estimators of η_1 when the target amplitude is unknown. Furthermore, the bias of the monopulse ratio is independent of N as indicated by (4.43), while the biases in the GML estimates and

GMM estimates decrease as N increases. Figure 5.7 shows that the RMS error for the monopulse ratio is less than the RMS error of the GML estimator for $|\eta_1| < 0.5$ and the RMS error of the GMM estimator for $|\eta_1| < 0.7$. However, for $|\eta_1| > 1$ the RMS error in the monopulse ratio is much larger than that of the GML estimates or GMM estimates. Note that Figure 5.7 indicates that the bias in the monopulse ratio estimate is about 50 percent of the total RMS error for a 10-dB target. Also, note that the restrictions placed on $\widehat{\Re}$ by (5.13) and (5.15) resulted in the RMS errors for $N = 2$ in Figure 5.7 being similar to the RMS errors for $N = 4$ in Figure 5.3. Since the threshold test of $\widehat{\Re}$ in (5.13) and (5.15) removed less informative measurements (i.e., measurements with the large variances) from consideration, the RMS errors in Figure 5.7 are less than those in Figure 5.3. In an actual scenario, the threshold test reduces the number of usable pulses (or sets of pulses) which, in effect, increases the variance of the estimator.

DOA estimation was also considered for a 7-dB Gaussian noise jammer, and the results are shown in Figure 5.8. The monopulse measurements of the jammer are made with a track gate containing 16 range bins. Each range bin provides a monopulse measurement, and the amplitude of the jammer is Rayleigh. Figure 5.8 shows that for a 7-dB jammer, the monopulse ratio provides less RMS error than the GML estimate or GMM estimate for $|\eta_1| < 0.4$. Thus, as $\Re_{R1}$ decreases, the range of η_1 for which the monopulse ratio provides better estimates than the GML estimator or GMM estimator also decreases. Therefore, the GML estimator or GMM estimator should be considered for DOA estimation of low SNR targets when many pulses are available for processing.

Simulation studies were conducted for various values of N and $\Re_{R1}$ to identify the DOAs at which the RMS error in the monopulse ratio estimate exceeds that of the GML estimate, and these critical DOAs (i.e., for DOAs greater than the critical DOA, the GML estimate should be used rather than the monopulse ratio) are shown graphically in Figure 5.9. For example, Figure 5.9 shows that for $\Re_{th} = 13$ dB, $\Re_{R1} = 10$ dB, $N = 4$, and $|\eta_1| > 0.6$, the GML estimator should be used rather than the monopulse ratio. Due to the low probability of processing for $\Re_{th} = 13$ dB, no results were compiled for $N = 2$ and $\Re_{R1} < 10$ dB. Also, for $N = 8$ and $|\eta_1| > 0.5$, the GML estimate should be used rather than the monopulse ratio, and for $N = 16$ and $|\eta_1| > 0.3$, the GML estimate should be used rather than the monopulse ratio. Similar results were obtained for the GMM estimator, and the critical DOAs for the GMM estimator were found to be 0.1 to 0.2 greater than that for the GML estimator for $N = 2$, 4, and 8. For $N = 16$, the critical DOA for the GMM estimator was also
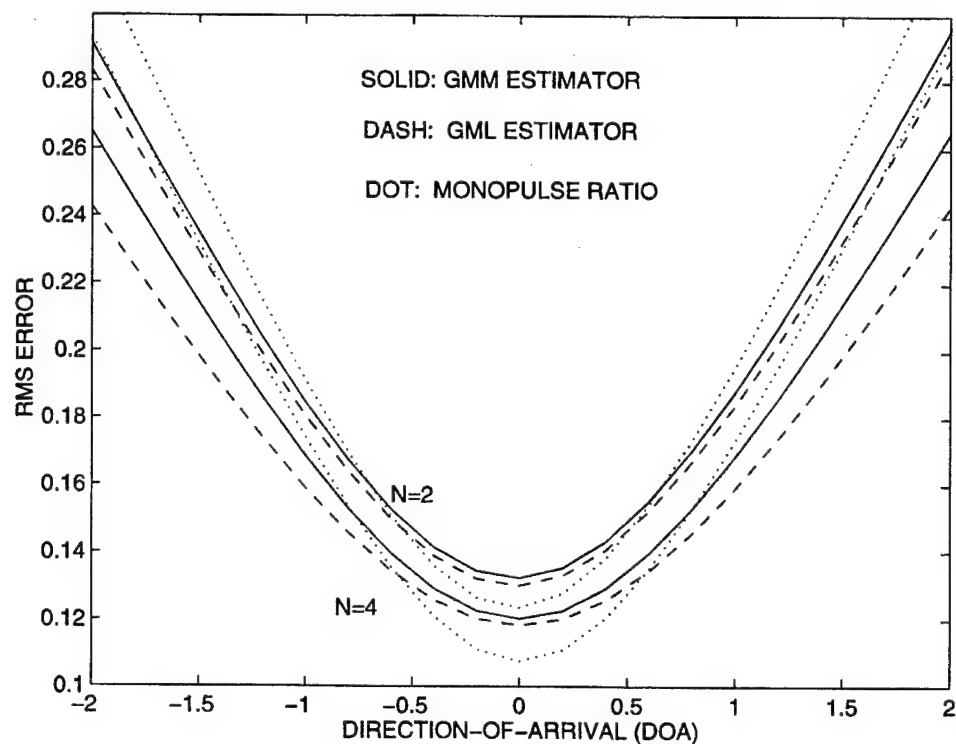
Figure 5.7 RMS Error in DOA Estimate for Unknown Target Amplitude with $N = 2$ and 4, $\rho = 0$, and $\Re_{R1} = 10$ dB
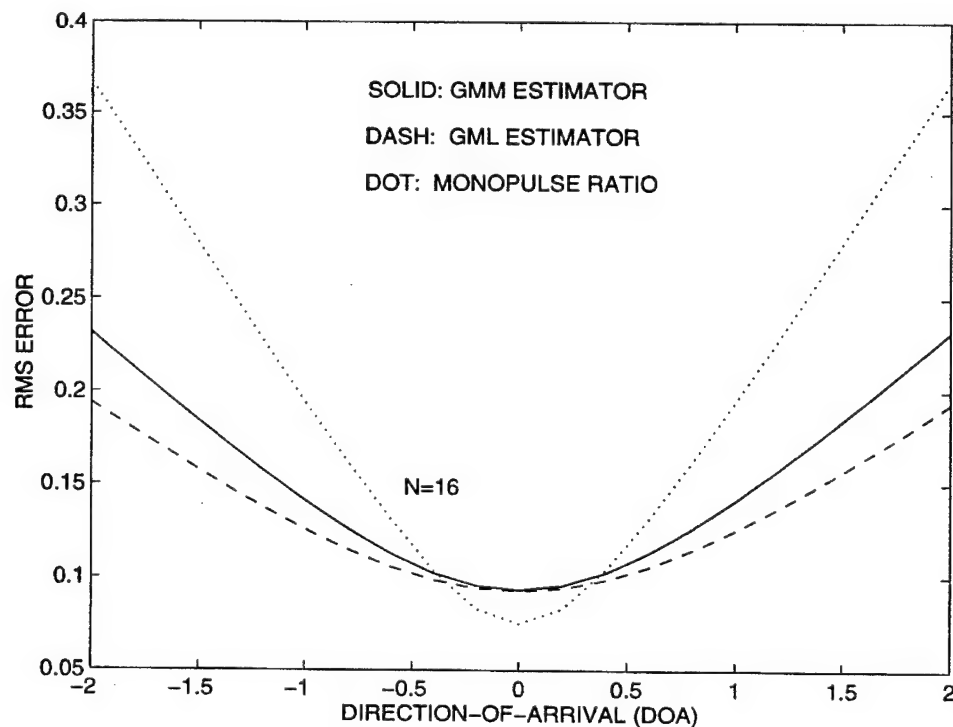
Figure 5.8 RMS Error in DOA Estimate for $\Re_{R1} = 7$-dB Jammer with $N = 16$ Range Cells and $\rho = 0$
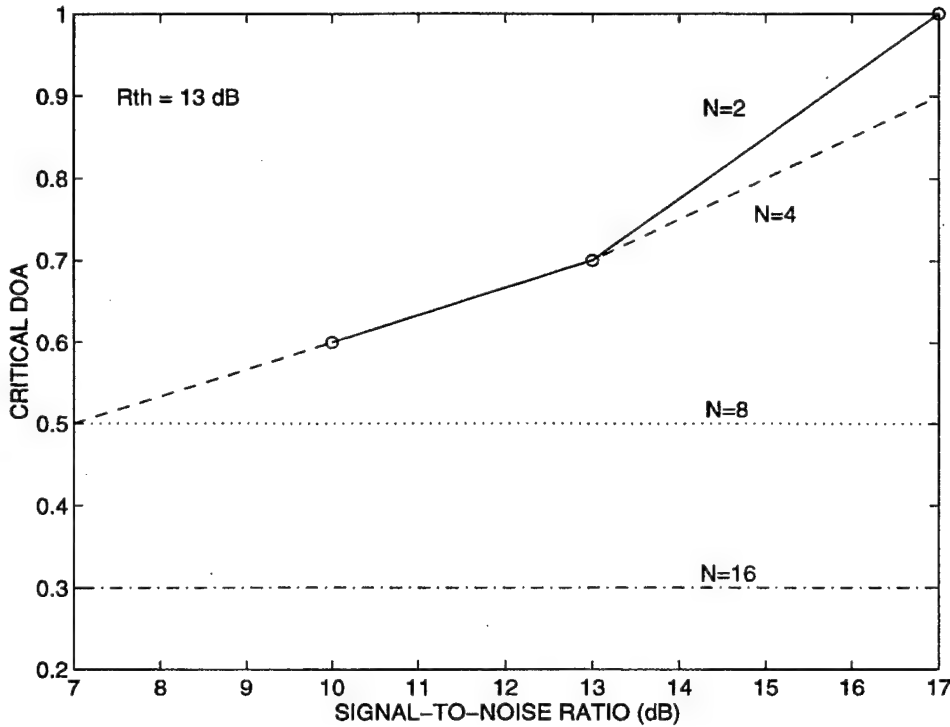
Figure 5.9 Critical DOAs for Use of the GML Estimator Rather Than the Monopulse Ratio with $\rho = 0$

0.3. The effects of decreasing $\Re_{th}$ to 10 dB were to increase the critical DOAs by 0.1 to 0.2 for $N = 2$ and 4, while leaving the critical DOAs for $N = 8$ and 16 unchanged.

The performance of the estimators for the variance for the monopulse ratios was analyzed through simulation studies. Estimates of the variance of the monopulse ratios were generated with (5.17) by using $\hat{y}_I$, $\hat{\eta}_{gml}$, and $\hat{\eta}_{gmm}$ for $\hat{\eta}_1$ in (5.18) along with $\Re_{R1} = \widehat{\Re}_{R1}$ and $\rho = 0$. The sample standard deviation of each estimate of the mean of the monopulse ratio normalized by the estimate of its standard deviation was computed using each DOA estimate, and the results are given in Figure 5.10 for $\Re_{R1} = 10$ dB and $\rho = 0$. The variance estimates are notably low for $|\eta_1| > 1.0$ as shown by Figure 5.10. The variance estimators that used $\hat{\eta}_1 = \hat{\eta}_{gml}$ or $\hat{\eta}_{gmm}$ provided slightly better results for $|\eta_1| > 0.5$ than the variance estimator that used $\hat{\eta}_1 = \hat{y}_I$. For $|\eta_1| < 1.0$, all of the estimators provide standard deviations that are in error by less than 10 percent.

The performance of the estimators for the variance for the DOA estimates was also analyzed through simulation studies. Estimates of the variance were generated with (5.20) for the GML estimates and GMM estimates by using $\hat{\eta}_{gml}$ and $\hat{\eta}_{gmm}$, respectively, for $\hat{\eta}_1$ in (5.18) along with $\Re_{R1} = \widehat{\Re}_{R1}$ and $\rho = 0$. Estimates of the

variance for the monopulse ratio as the DOA estimate were generated with (5.17) by using $\hat{y}_I$ for $\hat{\eta}$ in (5.18) along with $\Re_{R1} = \widehat{\Re}_{R1}$ and $\rho = 0$. The error in each DOA estimate was normalized by the estimate of its standard deviation, and the RMS values of these normalized errors are given in Figure 5.11 for $\Re_{R1} = 10$ dB and $\rho = 0$. Figure 5.11 shows that the variance estimates are notably small for $|\eta_1| > 1.0$. The variance estimators that used $\hat{\eta}_1 = \hat{\eta}_{gml}$ or $\hat{\eta}_{gmm}$ provided significantly better estimates for $|\eta_1| > 0.5$ than the variance estimator that used $\hat{\eta}_1 = \hat{y}_I$. Figure 5.11 also indicates that the use of the monopulse ratio as the DOA estimate and the variance of the monopulse ratio as the variance of the DOA estimate will result in significant error (*i.e.*, standard deviations of the DOA estimate that are in error by more than 20 percent) for $|\eta_1| > 1$.

Concluding Remarks

CRLBs were computed for unbiased estimators of the DOA that utilize either the in-phase monopulse ratio, the quadrature monopulse ratio, or both, and the results showed that the quadrature ratio provides information for estimating the DOA when the DOA is not equal to zero for independent receiver errors (*i.e.*, $\rho = 0$). ML estimator and MM estimator of the DOA were developed for a single Rayleigh target, and the performances of these estimators were compared through simulation results to that of the in-phase monopulse ratio as the DOA estimate. For a target with a known amplitude parameter, the ML estimates were shown to be the solution of a cubic equation, while the MM estimates were shown to be a bias-compensated version of the in-phase monopulse ratio. While the MM estimate provides an unbiased estimate of the DOA, the ML estimator was found to provide estimates with smaller RMS error than those of the MM estimator. For four or more independent samples or pulses and small DOAs, the monopulse ratio was found to provide the DOA estimate with the smallest RMS error. For targets with an unknown amplitude, the ML estimate of the amplitude parameter was used in the ML estimator and MM estimator to form the GML and GMM estimators, respectively. While the GMM estimators provide DOA estimates with less bias than the GML estimator, the GML estimator was found to provide estimates with a smaller RMS errors than the GMM estimator. However, for small DOAs, the monopulse ratio was found to provide DOA estimates with the smallest RMS error. Simulation studies for various sample sizes and SNRs identified the DOAs at which the RMS errors in the monopulse ratio estimates exceed that of the GML estimates. For example, the GML estimate should be used as the DOA estimate rather than monopulse ratio for $N = 8$ and $|\eta_1| > 0.5$, and for $N = 16$ and
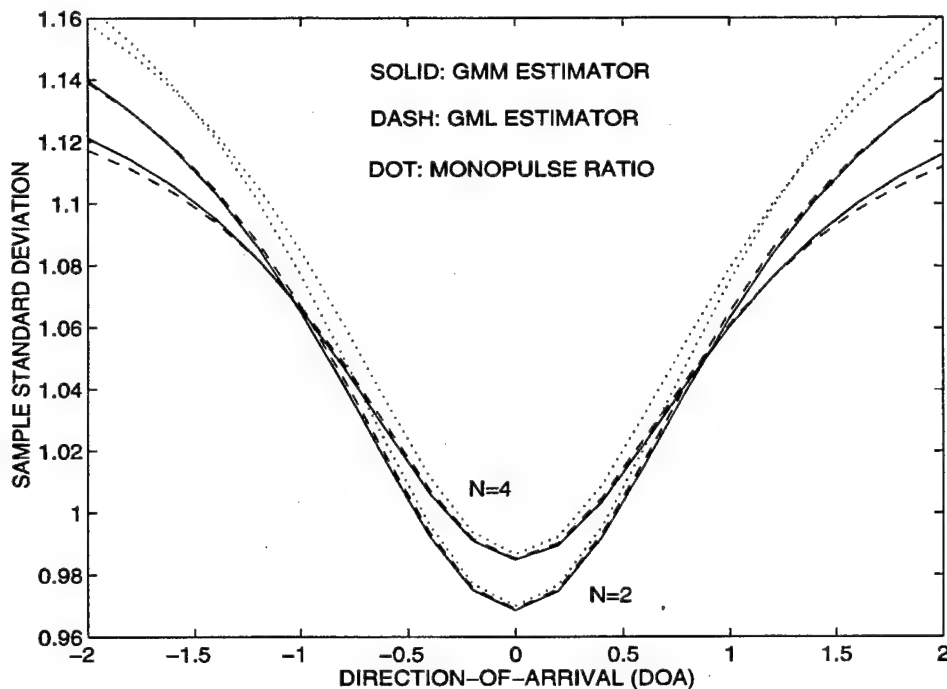
Figure 5.10 Sample Standard Deviation of Monopulse Ratio Normalized with the Standard Deviation Estimate and $\hat{\eta}_1 = \hat{y}_I, \hat{\eta}_{gml}$, or $\hat{\eta}_{gmm}$ in $\hat{p}$ with $\Re_{R1} = 10$ dB and $\rho = 0$
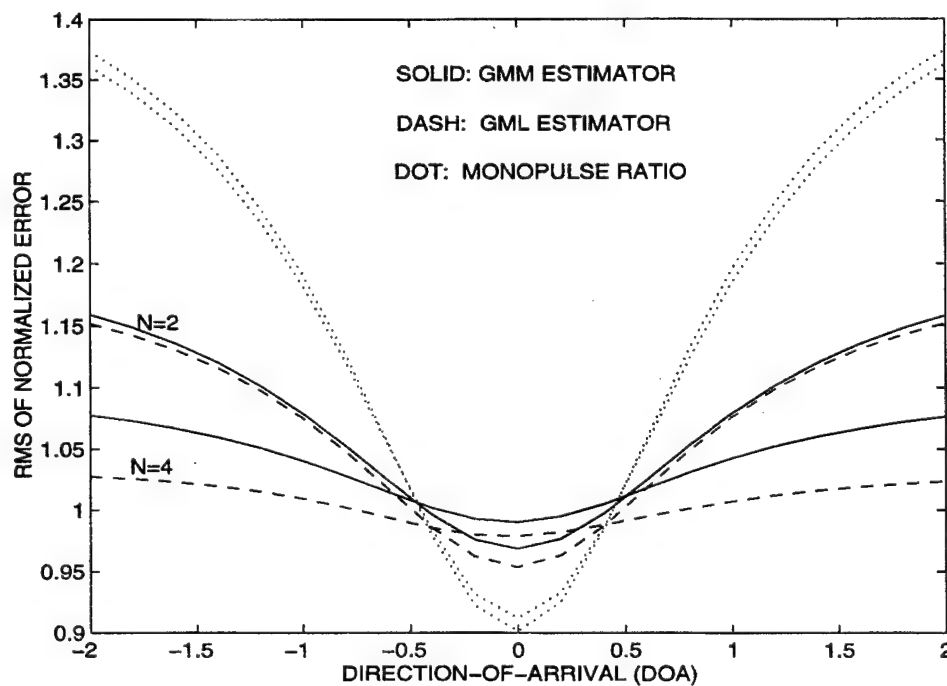
Figure 5.11 RMS of the DOA Estimation Errors Normalized with the Variance Estimate and $\hat{\eta}_1 = \hat{y}_I, \hat{\eta}_{gml}$, or $\hat{\eta}_{gmm}$ in $\hat{p}$ with $\Re_{R1} = 10$ dB and $\rho = 0$

121

$|\eta_1| > 0.3$, the GML estimate should be used rather than the monopulse ratio.

Estimators of the variances of the monopulse ratio and the DOA estimates were also developed, and the results of simulation studies of the performance of the estimators were given. While the results show that variance estimators for the monopulse ratio using η_{gml} and η_{gmm} provide slightly better estimates of the variance at DOAs greater than 0.5, all of the variance estimators for the monopulse ratio were in error by more than 5 percent for DOAs greater than 1.0. The results also showed that the variance estimators for the DOA estimate using η_{gml} and η_{gmm} provided significantly better estimates of the variance at DOAs greater than 0.5, and the use of the monopulse ratio as the DOA estimate and the variance of the monopulse ratio as the variance of the DOA estimate could be problematic for $|\eta_1| > 1$.

5.2 Single-Pulse DOA Estimation

Since the RCS of targets and propagation factors can change between scans or revisits to a target, the target amplitude is usually treated as an unknown between revisits, while it may be treated as fixed during the dwell period as for a fixed-amplitude target. In this section, the cases of both known and unknown target amplitudes are considered. Since small displacements of the target generate ambiguity in the phase, the phase is assumed unknown and uniformly distributed on $(-\pi, \pi]$.

Using the results of Section 4.3, the PDF of the in-phase and quadrature parts of the monopulse ratio for a fixed-amplitude target are given prior to integration with respect to the measured phase ψ as

$$f(y_I, y_Q, \psi | \Lambda, \Psi_F, \Phi_F) = \frac{\Lambda^2}{4\pi^2 \sigma_d^2 I_0\left(\frac{\Lambda \alpha_1}{\sigma_S^2}\right)} \exp\left[-\frac{\Lambda^2}{2\sigma_d^2}\left[(y_I - \frac{\alpha_1 \eta_1}{\Lambda}\cos(\psi - \phi_1))^2\right.\right.$$
$$\left.\left. + (y_Q - \frac{\alpha_1 \eta_1}{\Lambda}\sin(\psi - \phi_1))^2\right]\right] \tag{5.21}$$

Since (4.71) indicates that the location of the PDF of y_Q is independent of η_1, a single observation of y_Q provides essentially no information concerning the value of η_1. Note that while the variance of y_Q depends on η_1, single sample estimation of the variance is not considered viable. Noting that the ML value of y_Q is zero and using $y_Q = 0$ in (5.21) gives $\psi - \phi_1 = 0$. Thus, under this assumption, the ML estimate of η_1 for a known target amplitude α_1 is given by

$$\hat{\eta}_1 = \frac{\Lambda}{\alpha_1} y_I = \sqrt{\frac{\Re_o}{\Re_{F1}}} y_I \tag{5.22}$$

where $\Re_{F1}$ is given by (3.13), and $\Re_o$ is the observed SNR given by (3.11). Note that (5.22) is similar to the results for known amplitude and phase in [40], where the case of known amplitude and unknown phase is not considered. Then (4.70) indicates that (5.22) gives a biased estimate of η_1. While an unbiased estimate of η_1 can be computed with (4.70), the estimate will not be ML. Using $\hat{\eta}_1$ of (5.22) in (4.72) and (4.73) gives an estimate of the variance of y_I and y_Q as

$$\hat{\sigma}_{y_I}^2 = \frac{\sigma_d^2}{\Lambda^2} + y_I^2 \left[1 - I_{1|0}^2(\alpha_1 \Lambda \sigma_S^{-2}) - \frac{\sigma_S^2}{\alpha_1 \Lambda} I_{1|0}(\alpha_1 \Lambda \sigma_S^{-2}) \right]$$

$$= \frac{1}{2\Re_o} \left[\frac{\sigma_d^2}{\sigma_S^2} + 2y_I^2 \Re_o \left[1 - I_{1|0}^2(2\sqrt{\Re_{F1}\Re_o}) - \frac{1}{2\sqrt{\Re_{F1}\Re_o}} I_{1|0}(2\sqrt{\Re_{F1}\Re_o}) \right] \right] \quad (5.23)$$

$$\hat{\sigma}_{y_Q}^2 = \frac{\sigma_d^2}{\Lambda^2} + y_I^2 \frac{\sigma_S^2}{\alpha_1 \Lambda} I_{1|0}(\alpha_1 \Lambda \sigma_S^{-2}) = \frac{1}{2\Re_o} \left[\frac{\sigma_d^2}{\sigma_S^2} + \frac{y_I^2}{2\sqrt{\Re_{F1}\Re_o}} I_{1|0}(2\sqrt{\Re_{F1}\Re_o}) \right] \quad (5.24)$$

Using (5.22) and (5.23) gives an estimate of the variance of $\hat{\eta}_1$ as

$$\hat{\sigma}_{\hat{\eta}_1}^2 = \frac{\Lambda^2}{\alpha_1^2} \hat{\sigma}_{y_I}^2 = \frac{\Re_o}{\Re_{F1}} \hat{\sigma}_{y_I}^2 \quad (5.25)$$

When the target amplitude is unknown to the signal processor, an ML estimate of the target amplitude will be used along with the monopulse ratios to estimate the DOA. Since the target amplitude is observed through the sum signal, the estimation of the target amplitude will be decoupled from the monopulse processing. Given an observation of the sum-signal amplitude Λ and (3.54), the ML estimate $\hat{\alpha}_1$ of the target amplitude satisfies

$$\frac{\hat{\alpha}_1}{\Lambda} = I_{1|0}(\hat{\alpha}_1 \Lambda \sigma_S^{-2}) \quad (5.26)$$

Note that Λ is a biased estimate or observation of α_1 for low and moderate observed SNRs $\Re_o$. An approximation of the ML estimate is given by

$$\frac{\hat{\alpha}_1}{\sigma_S} \approx \frac{\Lambda}{\sigma_S} \left[\frac{\Lambda^2}{\Lambda^2 + \sigma_S^2} \right] \qquad \text{for} \quad \Re_o \geq 3 \text{ dB} \quad (5.27)$$

where the maximum percent of error in the approximation was found numerically to be 5 percent at $\Re_o = 3$ dB. Note that σ_S is included on both sides of the equation to emphasize that the approximation is about scaled values of α_1 and Λ. The limitation of $\Re_o \geq 3$ dB is not a particular problem since the detection threshold is often greater than 3 dB, and a single observation with a smaller amplitude provides essentially no error reduction relative to the beamwidth of the sum pattern. Thus, using $\hat{\alpha}_1$ for α_1 in (5.22) gives an approximately ML estimate of η_1 for a monopulse measurement of target with amplitude unknown as

$$\hat{\eta}_1 = \left[1 + \frac{\sigma_S^2}{\Lambda^2} \right] y_I = \left[1 + \frac{1}{2\Re_o} \right] y_I \quad \text{for} \quad \Re_o > 3 \text{ dB} \quad (5.28)$$

This estimate differs from the results of [40], where the monopulse ratio is given as the ML estimate for a high SNR. While (5.28) provides a biased estimate of η_1, the bias will be less than that provided by the standard monopulse ratio. An estimate with less bias can be computed by using (5.26) and (5.27) in (4.70), but the estimate will not be ML. Under the ML conditions of (5.26)

$$\frac{\sigma_S^4}{2\Lambda^4} \approx 1 - I_{1|0}^2(\alpha_1\Lambda\sigma_S^{-2}) - \frac{\sigma^2}{\alpha_1\Lambda}I_{1|0}(\alpha_1\Lambda\sigma_S^{-2}) \tag{5.29}$$

Using (5.29) in (5.23) and (5.26) in (5.24) with $\alpha_1 = \hat{\alpha}_1$ gives an estimate of the variance of y_I and y_Q as

$$\hat{\sigma}_{y_I}^2 = \frac{\sigma_d^2}{\Lambda^2} + \frac{y_I^2\sigma_S^4}{8\Lambda^4} = \frac{1}{2\Re_o}\left[\frac{\sigma_d^2}{\sigma_S^2} + \frac{y_I^2}{4\Re_o}\right] \quad \text{for} \quad \Re_o > 3 \text{ dB} \tag{5.30}$$

$$\hat{\sigma}_{y_Q}^2 = \frac{\sigma_d^2}{\Lambda^2} + \frac{y_I^2\sigma_S^2}{\Lambda^2} = \frac{1}{2\Re_o}\left[\frac{\sigma_d^2}{\sigma_S^2} + y_I^2\right] \quad \text{for} \quad \Re_o > 3 \text{ dB} \tag{5.31}$$

While (5.31) is similar to (2.49), (5.30) differs significantly from (2.49), which is commonly reported in the literature as the variance of monopulse ratio.

A Monte Carlo simulation of 5,000 experiments was conducted for various values of $\Re_{F1}$ and η_1 to assess the validity of (5.30) and (5.31) for estimating the variances of the corresponding monopulse ratios. For each experiment, the measured amplitude was restricted so that $\Re_o \geq 3$ dB and $\sigma_d^2 = \sigma_S^2$, and y_I and y_Q were normalized by the corresponding standard deviation of (5.30) or (5.31) before computing the sample standard deviation. The results of the simulation study for y_I are summarized in Figure 5.12, where the dash lines correspond to (5.30), and the solid line corresponds to the variance calculation of (2.49) with $\Re = \Re_o$ and $\eta = y_I$. Thus, the variance estimates of (5.30) appear valid for $3 \leq \Re_{F1} \leq 12$ dB and $|\eta_1| < 2$, while the variance estimates for $\Re_{F1} \geq 15$ dB are valid for $|\eta_1| < 3$. Note that the variance estimates produced with (2.49) are valid for $\Re_{F1} \geq 12$ dB and $|\eta_1| < 0.25$. The results for y_Q are given in Figure 5.13 and indicate that (5.31) is valid for $3 \leq \Re_{F1} \leq 9$ dB and $|\eta_1| < 1$, and $\Re_{F1} \geq 12$ dB and $|\eta_1| < 3$.

Using (5.28) and (5.30) gives an estimate of the variance of $\hat{\eta}_1$ as

$$\hat{\sigma}_{\hat{\eta}_1}^2 = \left[1 + \frac{\sigma_S^2}{\Lambda^2}\right]^2 \left[\frac{\sigma_d^2}{\Lambda^2} + \frac{y_I^2\sigma_S^4}{2\Lambda^4}\right]$$

$$= \frac{1}{2\Re_o}\left[1 + \frac{1}{2\Re_o}\right]^2 \left[\frac{\sigma_d^2}{\sigma_S^2} + \frac{y_I^2}{4\Re_o}\right] \quad \text{for} \quad \Re_o > 3 \text{ dB} \tag{5.32}$$
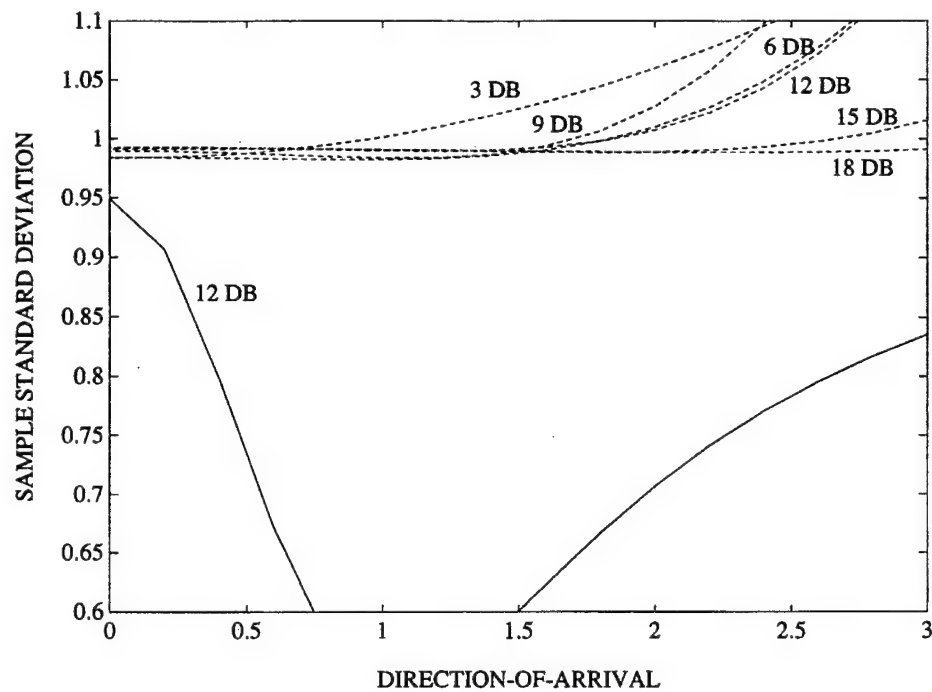
Figure 5.12 Simulation Results of Consistency Study of Variance Estimate for the In-Phase Monopulse Ratio
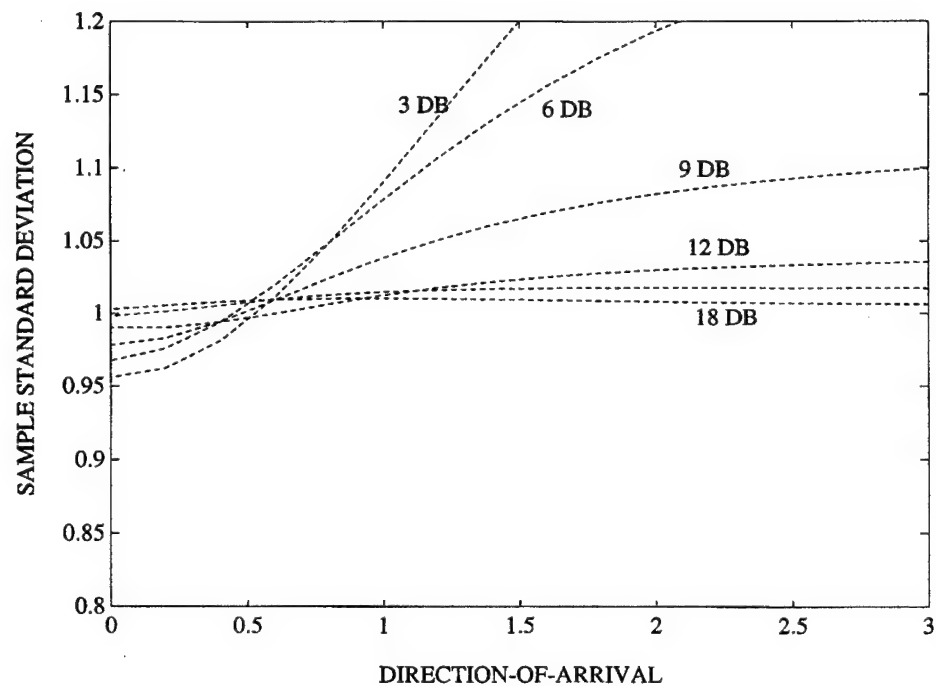
Figure 5.13 Simulation Results of Consistency Study of Variance Estimate for the Quadrature Monopulse Ratio

125

Single-pulse ML estimators for the DOA were presented for the cases of known and unknown target amplitudes. The single-pulse DOA estimator for a target with unknown amplitude is important because it characterizes any given monopulse measurement without assumptions regarding the distribution of the target amplitude. While the approximate ML estimators are biased for low to moderate SNRs, the bias of the DOA estimate is less than that provided by the monopulse ratio alone. An unbiased DOA estimator could be developed with (4.70), (5.26), and (5.27). Simulation results indicate that the variance estimator developed in this section for the in-phase part of the monopulse measurement of a target with unknown amplitude is much closer to being consistent than (2.49), which is commonly presented in the literature.

5.3 Rayleigh Target in the Presence of a Gaussian Jammer

Since jammer signals enter into all the range bins, the DOA estimate of the jammer and the amplitude of the jammer signal can be estimated with the monopulse measurements that do not include the target. The DOA of the jammer can be estimated as discussed in Section 5.1 for a Rayleigh target. The variance of the DOA estimate for the jammer is also estimated as discussed in Section 5.1. These estimates of the DOA and the amplitude of the jammer are used in conjunction with the results of Section 4.2 to develop an MM approach to the DOA estimation for the target.

Let $\widehat{\Re}_J$ and $\hat{\eta}_J$ be estimates of the amplitude and DOA of the jammer, and let $\sigma_{\hat{\eta}J}^2$ be the estimated variance of $\hat{\eta}_J$. Also, let $\rho = 0$. Using (3.16) and (3.32) gives an estimate of $\Re_{R1}$ for N subpulses that include both the target and jammer echoes as

$$\widehat{\Re}_{R1} = Y_N - 1 - \widehat{\Re}_J \tag{5.33}$$

Setting the estimate of the conditional mean $\hat{y}_I$ in (4.46) equal to the mean of (4.53) and using (5.33) in the result gives an estimate of η_1 as

$$\hat{\eta}_1 = \left[\frac{Y_N}{Y_N - 1 - \widehat{\Re}_J}\right]\hat{y}_I - \left[\frac{\widehat{\Re}_J}{Y_N - 1 - \widehat{\Re}_J}\right]\hat{\eta}_J \tag{5.34}$$

Assuming that the errors in $\hat{y}_I$ and $\hat{\eta}_J$ are uncorrelated, ignoring the variance of $\widehat{\Re}_J$, and using (4.55) and (4.56) gives an estimate of the variance of $\hat{\eta}_1$ as

$$\hat{\sigma}_{\hat{\eta}1}^2 = \left[\frac{Y_N}{Y_N - 1 - \widehat{\Re}_J}\right]^2 \frac{\hat{q}}{2NY_N} + \left[\frac{\widehat{\Re}_J}{Y_N - 1 - \widehat{\Re}_J}\right]^2 \sigma_{\hat{\eta}J}^2 \tag{5.35}$$

where

$$\hat{q} = \frac{\sigma_d^2}{\sigma_S^2} + \left[1 - \frac{\widehat{\Re}_J + 1}{Y_N}\right]\hat{\eta}_1^2 + \left[\frac{\widehat{\Re}_{R2}}{Y_N}\right]\hat{\eta}_J^2 + \left[1 - \frac{\widehat{\Re}_J + 1}{Y_N}\right]\left[\frac{\widehat{\Re}_J}{Y_N}\right](\hat{\eta}_1 - \hat{\eta}_J)^2 \tag{5.36}$$

Thus, when tracking a Rayleigh target in the presence of a Gaussian noise jammer, (5.33) gives an estimate of the target amplitude in the presence of the jammer, and (5.34) gives an estimate of the DOA of the target that is "compensated" for the bias in the monopulse ratios that results from the jammer.

5.4 Two Unresolved Rayleigh Targets with Known Relative RCS

The FIM and CRLBs are developed for the DOA estimation of two unresolved Rayleigh targets using a standard monopulse radar. The FIM and CRLBs are used to study the effects of beam pointing on the DOA estimation. Using the results of Section 4.2 for two unresolved Rayleigh targets, an MM approach is taken to the DOA estimation for two unresolved Rayleigh targets. The mean of the in-phase monopulse ratio is used to estimate the DOA of the centroid of the two targets, while the variance of the in-phase and quadrature monopulse ratios is used to estimate the difference of the DOAs of the two targets. Simulation results that illustrate the performance of the DOA estimators are given along with some simulation results for a simple tracking example.

Fisher Information and CRLBs

The FIM and CRLBs associated with η_1 and η_2 are developed. The FIM will be used to study the effects of antenna pointing on the DOA estimation, while the CRLBs will be used later in this section to assess the performance of the DOA estimators.

The FIM [11, p. 79] associated with $\hat{\eta}_1$ and $\hat{\eta}_2$, based on N observations of y_I and y_Q, is found by using (4.53) and (4.54). The FIM is given by

$$I_{y_I,y_Q}(\hat{\eta}_1,\hat{\eta}_2|N,\{\Re_{ok}\}_{k=1}^N,\Psi_{2R}) = \frac{2NY_N\Re_{R1}\Re_{R2}}{q(\Re_{R1}+\Re_{R2}+1)^2} \tag{5.37}$$

$$\times \begin{bmatrix} \dfrac{\Re_{R1}}{\Re_{R2}}\left[1+\dfrac{2}{qY_N}(\eta_1+\Re_{R2}\Delta\eta)^2\right] & 1+\dfrac{2}{qY_N}\dfrac{(\eta_1+\Re_{R2}\Delta\eta)}{(\eta_1-\Re_{R1}\Delta\eta)^{-1}} \\ 1+\dfrac{2}{qY_N}\dfrac{(\eta_1+\Re_{R2}\Delta\eta)}{(\eta_1-\Re_{R1}\Delta\eta)^{-1}} & \dfrac{\Re_{R2}}{\Re_{R1}}\left[1+\dfrac{2}{qY_N}(\eta_2-\Re_{R1}\Delta\eta)^2\right] \end{bmatrix}$$

where $\Delta\eta = \eta_1 - \eta_2 > 0$.

The FIM of (5.37) was used to study the effects of sensor pointing on the DOA estimation. The dependence of $I_{y_I,y_Q}(\hat{\eta}_1,\hat{\eta}_2|N,\{\Re_{ok}\}_{k=1}^N,\Psi_{2R})$ on Y_N was removed by setting $Y_N = E[Y_N|\Psi_{2R}] = \Re_{R1} + \Re_{R2} + 1$ in (5.37). The effects of the antenna gain pattern are not assumed to be included in λ, the relative RCS of the two targets. The effects of the antenna gain pattern were included in the analysis of the FIM by using

$$\overline{\Re}_{R1} = \Re_{R1}\cos^4\left(\frac{\eta_1\pi}{4\eta_{bw}}\right) \qquad \overline{\Re}_{R2} = \Re_{R2}\cos^4\left(\frac{\eta_2\pi}{4\eta_{bw}}\right) \tag{5.38}$$

in (5.37) for $\Re_{R1}$ and $\Re_{R2}$, respectively. The η_{bw} denotes the DOA value at the one-way, half-power point on the antenna gain pattern of the sum channel. Thus, at $\eta_1 = \eta_{bw}$, $\overline{\Re}_{R1} = \Re_{R1} - 6$ dB. For a monopulse error slope, k_m, in units of beamwidth, $2\eta_{bw} \approx k_m$. For all of the examples in this section, $\eta_{bw} = 0.8$.

Figure 5.14 shows the FIM for two 13-dB targets (*i.e.*, $\Re_{R1} = \Re_{R2} = 13$ dB) separated by one-half beamwidth (*i.e.*, $\Delta\eta = \eta_{bw} = 0.8$) versus the DOA of target 1, η_1, for $N = 4$, 8, and 12 subpulses. The DOA for target 2 is given by $\eta_2 = \eta_1 - \Delta\eta$. Thus, $\eta_1 = 0$ in Figure 5.14 corresponds to target 1 on the antenna boresight, while $\eta_1 = 0.8$ corresponds to target 2 on the antenna boresight. The trace of the FIM in Figure 5.14 shows that pointing the antenna boresight exactly between the two targets (*i.e.*, $\eta_1 = 0.4$) is the least informative angle for sensor pointing. Considering the Fisher information for the two targets separately shows that one radar dwell with eight subpulses between the two targets (*i.e.*, $\eta_1 = 0.4$) gives Fisher information for the individual targets of 55 each for a total of 110, while two consecutive radar dwells with four subpulses each at the individual targets (*i.e.*, $\eta_1 = 0$ and 0.8) gives a total Fisher information of about 125. Thus, when two Rayleigh targets with equal RCSs are separated by about one-half beamwidth, the most informative beam-pointing strategy involves pointing directly at the two targets on consecutive dwells. The DOAs and target amplitudes would then be estimated jointly with approximate knowledge of the antenna patterns.

Figure 5.15 shows the FIM for two 13-dB targets separated by one-fourth beam-width (*i.e.*, $\Delta\eta = 0.5\eta_{bw} = 0.4$) versus η_1 for $N = 4$, 8, and 12 subpulses. Thus, $\eta_1 = 0$ in Figure 5.15 corresponds to target 1 on the antenna boresight, while $\eta_1 = 0.4$ corresponds to target 2 on the antenna boresight. The trace of the FIM in Figure 5.15 shows that pointing the antenna boresight between the two targets (*i.e.*, $0 \leq \eta_1 \leq 0.4$) maximizes the information. Considering the Fisher information for the two targets separately shows that one radar dwell with eight subpulses between the two targets (*i.e.*, $\eta_1 = 0.2$) gives Fisher information of about 250, while two consecutive radar dwells with four subpulses each at the individual targets gives Fisher information of about 240. Thus, when two Rayleigh targets with equal RCS are separated by less than one-fourth beamwidth, pointing between the two targets maximizes the information. The DOAs and target amplitudes are then estimated jointly, with approximate knowledge of the antenna patterns and the relative RCS of the targets as discussed later in this section. Note that reducing the separation of the two targets from one-half beamwidth to one-fourth beamwidth increases the Fisher information from 125 to 250.

Figure 5.16 shows the FIM for a 16-dB target and a 10-dB target (*i.e.*, $\Re_{R1} = $

Figure 5.14 Fisher Information for η_1 and η_2 with $Y_N = E[Y_N|\Psi_{2R}] = \Re_{R1} + \Re_{R2} + 1$, $\Re_{R1} = \Re_{R2}$, and $\Delta\eta = \eta_{bw}$
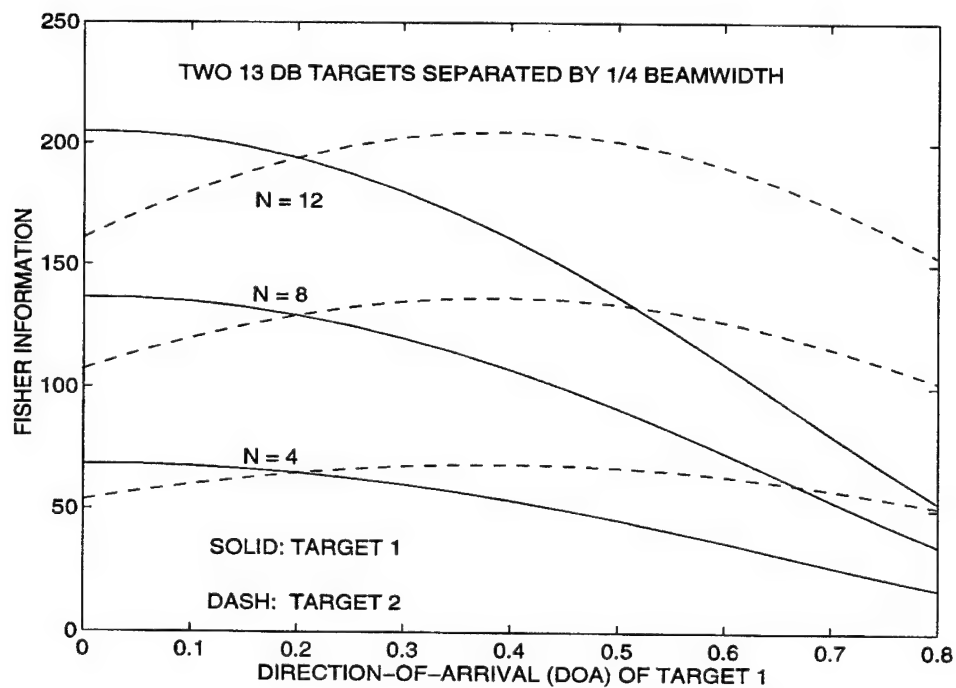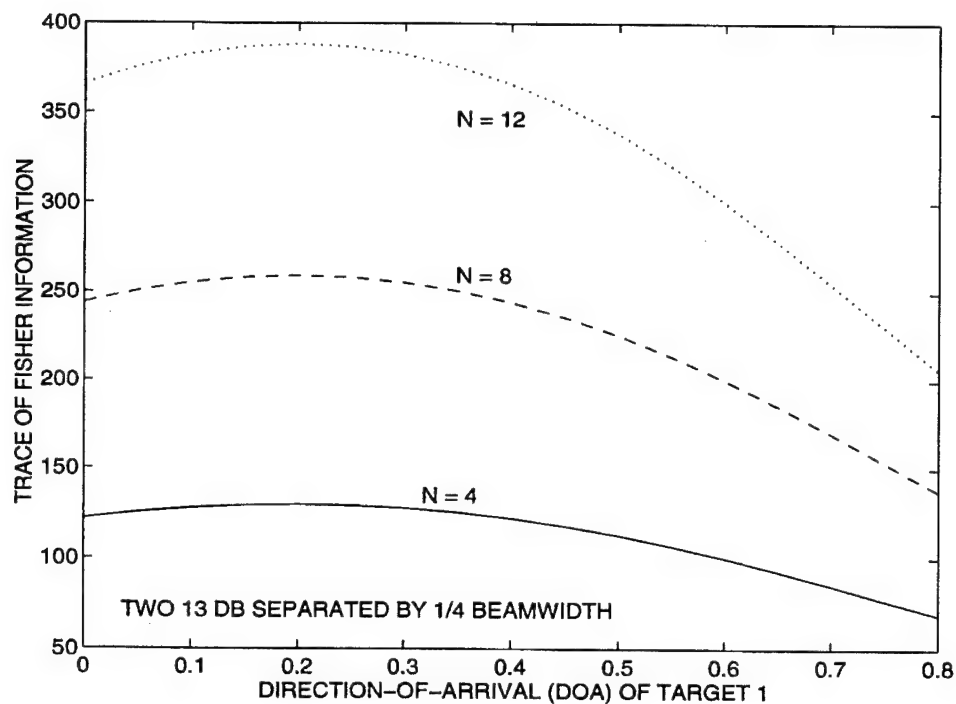
Figure 5.15 Fisher Information for η_1 and η_2 with $Y_N = E[Y_N|\Psi_{2R}] = \Re_{R1} + \Re_{R2} + 1$, $\Re_{R1} = \Re_{R2}$, and $\Delta\eta = 0.5\eta_{bw}$

130

$4\Re_{R2} = 16$ dB) separated by one-fourth beamwidth versus η_1 for $N = 4$, 8, and 12 subpulses. Thus, $\eta_1 = 0$ in Figure 5.16 corresponds to target 1 on the antenna boresight, while $\eta_1 = 0.4$ corresponds to target 2 on the antenna boresight. The trace of the FIM in Figure 5.16 shows that pointing the antenna boresight at target 2 (i.e., $\eta_1 \approx 0.4$) gives the maximum Fisher information for target 2. Considering the Fisher information for the two targets separately shows that one radar dwell with eight subpulses between the two targets (i.e., $\eta_1 = 0.2$) gives Fisher information of about 350, while two consecutive radar dwells with four subpulses each at the individual targets gives Fisher information of about 275. However, the difference in the Fisher information is an information gain on the larger target. Thus, when two Rayleigh targets with significantly different RCSs are separated by about one-fourth beamwidth, the most informative beam-pointing strategy appears to be pointing directly at the stronger target and using the results for the stronger target to estimate the DOA of the weaker target. While joint estimation of the DOAs and targets amplitudes would be appropriate, the DOAs and target amplitudes could be estimated for the stronger target first and the weaker target second.

A bound on the covariance of the error of any unbiased estimator of $[\,\eta_1 \quad \eta_2\,]$ [11, p. 79] is given by

$$\text{COV}\begin{bmatrix} \hat{\eta}_1 \\ \hat{\eta}_2 \end{bmatrix} \geq J_{y_I,y_Q}(\hat{\eta}_1, \hat{\eta}_2 | N, \{\Re_{ok}\}_{k=1}^N, \Psi_{2R}) = \left[I_{y_I,y_Q}(\hat{\eta}_1, \hat{\eta}_2 | N, \{\Re_{ok}\}_{k=1}^N, \Psi_{2R}) \right]^{-1}$$

$$(5.39)$$

where

$$J_{y_I,y_Q}(\hat{\eta}_1, \hat{\eta}_2 | N, \{\Re_{ok}\}_{k=1}^N, \Psi_{2R}) = \frac{q^2(\Re_{R1} + \Re_{R2} + 1)^2}{8N\Re_{R1}\Re_{R2}[(\eta_1 + \Re_{R2}\Delta\eta)^2 + (\eta_2 - \Re_{R1}\Delta\eta)^2]}$$

$$\times \begin{bmatrix} \dfrac{\Re_{R2}}{\Re_{R1}}\left[1 + \dfrac{2}{qY_N}(\eta_1 - \Re_{R1}\Delta\eta)^2\right] & -1 - \dfrac{2}{qY_N}\dfrac{(\eta_1 + \Re_{R2}\Delta\eta)}{(\eta_1 - \Re_{R1}\Delta\eta)^{-1}} \\ -1 - \dfrac{2}{qY_N}\dfrac{(\eta_1 + \Re_{R2}\Delta\eta)}{(\eta_1 - \Re_{R1}\Delta\eta)^{-1}} & \dfrac{\Re_{R1}}{\Re_{R2}}\left[1 + \dfrac{2}{qY_N}(\eta_2 + \Re_{R2}\Delta\eta)^2\right] \end{bmatrix} \quad (5.40)$$

The diagonal elements of $J_{y_I,y_Q}(\hat{\eta}_1, \hat{\eta}_2 | N, \{\Re_{ok}\}_{k=1}^N, \Psi_{2R})$ give the CRLBs for $\hat{\eta}_1$ and $\hat{\eta}_2$. These CRLBs will be used to assess the efficiency [11, p. 71] of the DOA estimators later in this section.
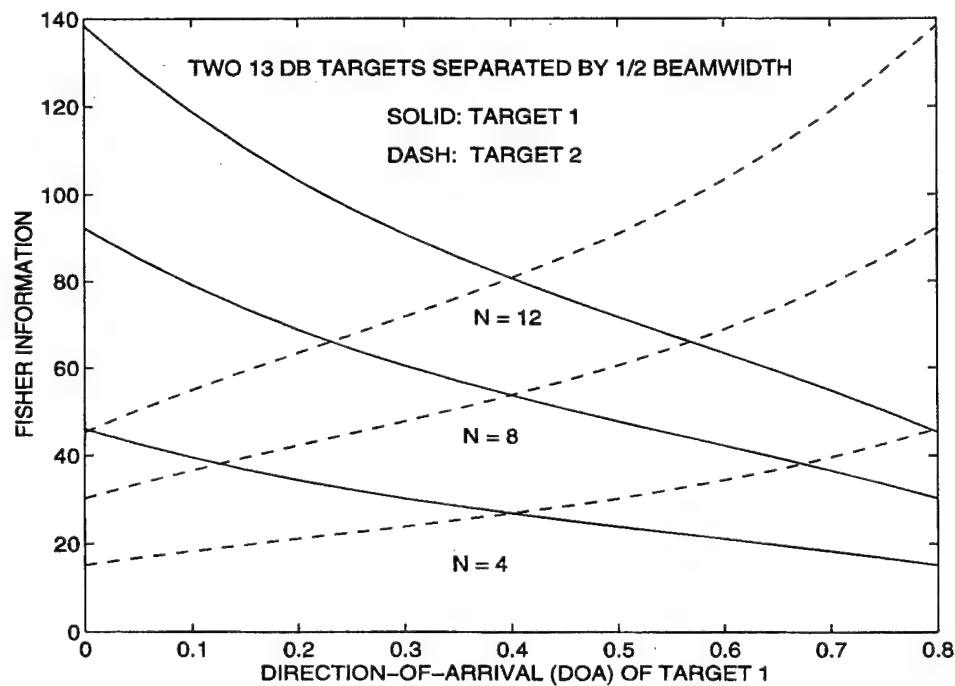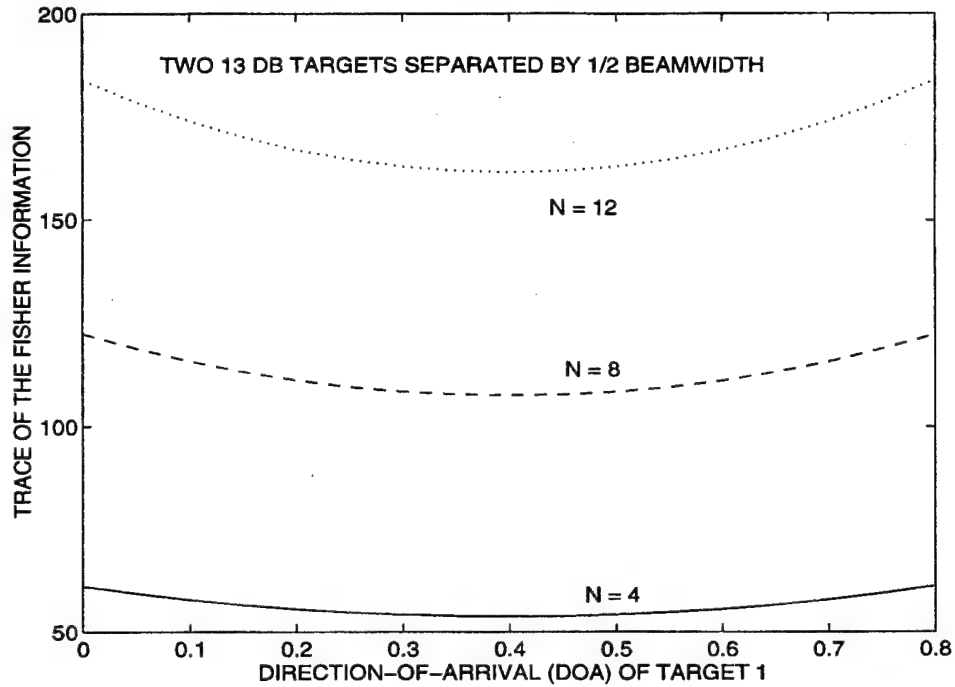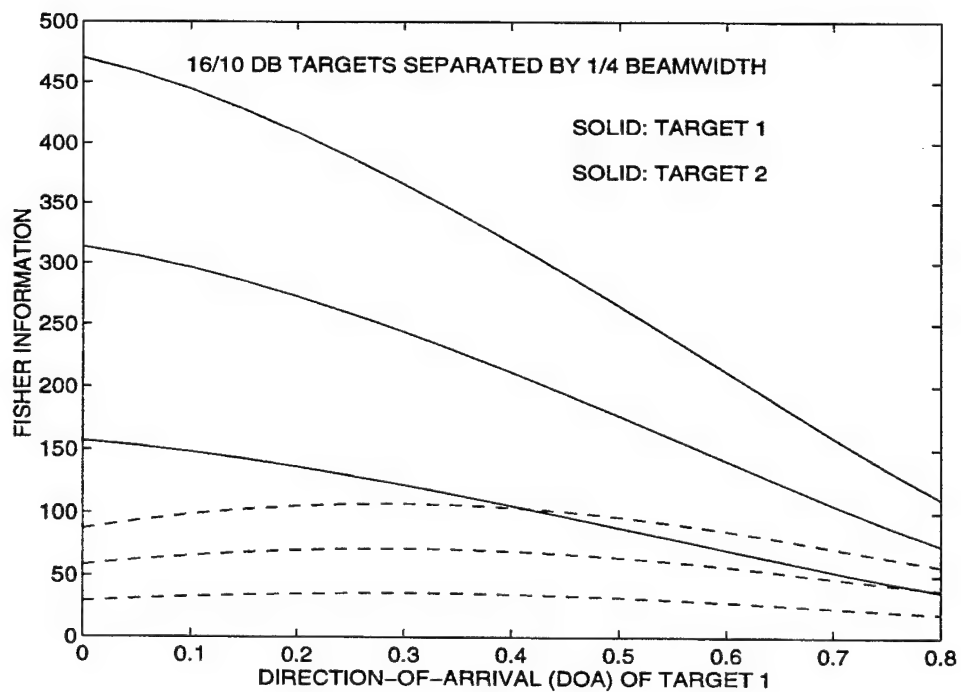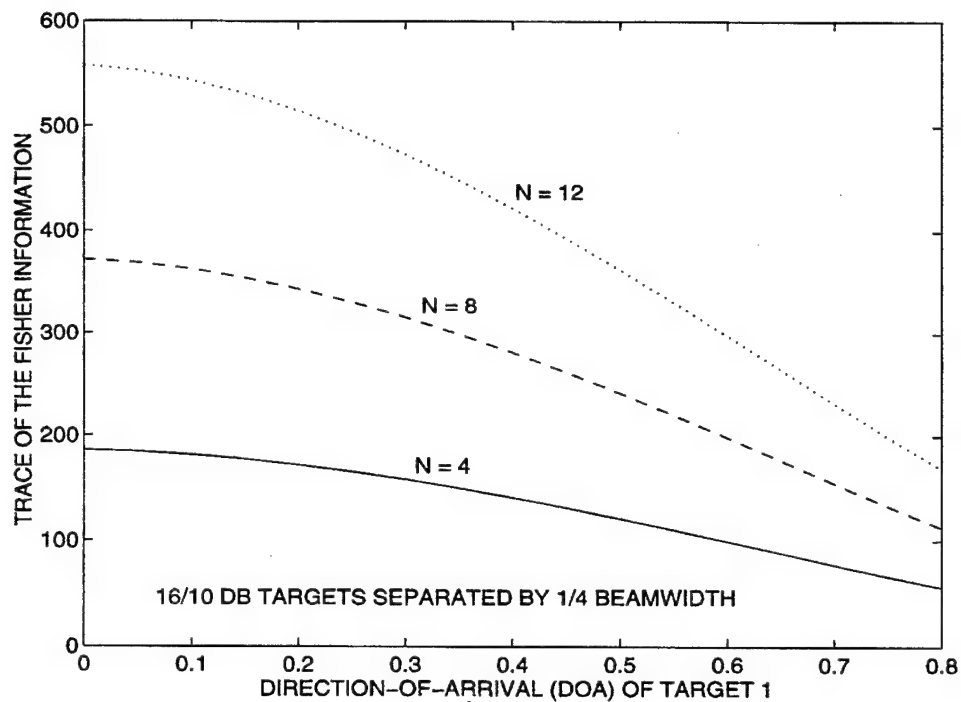
Figure 5.16 Fisher Information for η_1 and η_2 with $Y_N = E[Y_N|\Psi_{2R}] = \Re_{R1} + \Re_{R2} + 1$, $\Re_{R1} = \Re_{R2}$, and $\Delta\eta = 0.5\eta_{bw}$

DOA Estimation

An MM approach is taken to the DOA estimation for two unresolved Rayleigh targets. Since two DOAs are to be estimated, two expressions are needed for the MM estimation. Since the observations y_{Ik} of y_I are not stationary, $\hat{y}_I$, the ML estimate of the amplitude-conditioned mean of y_I, and (4.53) provide the first expression as

$$\hat{y}_I = \frac{\Re_{R1}\eta_1 + \Re_{R2}\eta_2}{\Re_{R1} + \Re_{R2} + 1} \tag{5.41}$$

Let $\Delta\eta = \eta_1 - \eta_2 > 0$, so that $\eta_1 > \eta_2$. Also, since the relative RCS of the two targets is assumed known, let $\Re_{R2} = \lambda\Re_{R1}$, where $\lambda > 0$. Then

$$\eta_1 \approx \hat{y}_I + \frac{\lambda}{1+\lambda}\Delta\eta \tag{5.42}$$

$$\eta_2 \approx \hat{y}_I - \frac{1}{1+\lambda}\Delta\eta \tag{5.43}$$

Since the y_{Ik} are nonstationary, Gaussian random variables, the second expression for DOA estimation will be obtained by forming a Chi-squared random variable with $2N - 1$ degrees of freedom from y_{Ik}, $\Re_{ok}$, and $\hat{y}_I$, and setting the random variable equal to its mean[5]. Thus, for $N > 1$, let

$$X_N = \begin{bmatrix} y_{I1} - \hat{y}_I & \cdots & y_{IN} - \hat{y}_I & y_{Q1} & \cdots & y_{QN} \end{bmatrix} \tag{5.44}$$

$$R_N = 2 \, \text{diag} \begin{bmatrix} \Re_{o1} & \cdots & \Re_{oN} & \Re_{o1} & \cdots & \Re_{oN} \end{bmatrix} \tag{5.45}$$

Since for $N = 1$, $\hat{y}_I = y_{I1}$, let $X_1 = y_{Q1}$ and $R_1 = 2\Re_{o1}$. Also let

$$v_N = X_N^T R_N X_N q^{-1} \tag{5.46}$$

where q is given by (4.56). Since the amplitude-conditioned PDF of the in-phase and quadrature monopulse ratios are Gaussian, as given by (4.53) through (4.56), v_N is a Chi-squared random variable with $2N - 1$ degrees of freedom, where one degree of freedom has been lost due to the estimation of the conditional mean of y_I [48, p. 320]. Then

$$E[v_N] = 2N - 1 \tag{5.47}$$

$$\text{VAR}[v_N] = 2(2N - 1) \tag{5.48}$$

Setting v_N equal to its mean gives

$$\hat{q} = \frac{X_N^T R_N X_N}{2N - 1}, \qquad N \geq 1 \tag{5.49}$$

---

[5] The use of the ML value of the Chi-squared random variable, which is 2N-3, was found to give a significantly larger bias in the DOA estimates than the mean.

Since for a typical monopulse radar $\Delta \eta > 1.5$ would allow the targets to be resolved by placing one target at a time in the null of the antenna pattern, assume that $\Delta \eta < 1.5$. Thus, pointing the antenna boresight between the targets allows the approximation of q by

$$q \approx \frac{\sigma_d^2}{\sigma_S^2} + \frac{\lambda \Re_{R1}}{1 + \lambda} \Delta \eta^2 \tag{5.50}$$

Inserting $\hat{q}$ in (5.49) for q and using the result in (5.42) and (5.43) gives the DOA estimates as

$$\hat{\eta}_1 = \hat{y}_I + \sqrt{\frac{\lambda \tilde{q}}{\widehat{\Re}_R}} \tag{5.51}$$

$$\hat{\eta}_2 = \hat{y}_I - \sqrt{\frac{\tilde{q}}{\lambda \widehat{\Re}_R}} \tag{5.52}$$

where

$$\tilde{q} = \begin{cases} 0, & \hat{q} \leq \sigma_d^2 \sigma_S^{-2} \\ \frac{4\eta_{bw}^2 \lambda}{(1 + \lambda)^2} \widehat{\Re}_R, & \hat{q} \geq \frac{4\eta_{bw}^2 \lambda}{(1 + \lambda)^2} \widehat{\Re}_R + \sigma_d^2 \sigma_S^{-2} \\ \hat{q} - \sigma_d^2 \sigma_S^{-2}, & \text{otherwise} \end{cases} \tag{5.53}$$

$$\widehat{\Re}_R = Y_N - 1 \quad \text{for} \quad Y_N = \frac{1}{N} \sum_{k=1}^{N} \Re_{ok} \tag{5.54}$$

with η_{bw} denoting the DOA value at the one-way, half-power point on the antenna gain pattern of the sum channel. For a monopulse error slope, k_m, in units of beamwidth, $2\eta_{bw} \approx k_m$. The first case of (5.53) is introduced to ensure that the DOA estimates are real numbers, while the second case is introduced to prevent the difference of the two DOA estimates from being unreasonably large. Limiting the difference of the two DOA estimates was found to be critical when correcting the known relative RCS λ for the effects of the antenna gain pattern of the sum channel as discussed below.

Note that $\tilde{q}$ can be expressed as a function of v_N and that for a twice differentiable function $g(x)$,

$$E[g(x)] \approx g(\bar{x}) + g''(\bar{x})\sigma_x^2 \tag{5.55}$$

where $\bar{x} = E[x]$, $\sigma_x^2 = \text{VAR}[x]$, and $g''(\bar{x})$ is the second derivative of $g(x)$ with respect to x evaluated at $x = \bar{x}$. Using (5.55) with (5.51) and (5.52) gives approximations of the variances of the DOA estimates for $q \gg \sigma_d^2 \sigma_S^{-2}$ as

$$\text{VAR}[\hat{\eta}_1 | \Psi_{2R}] \approx q \left[\frac{1}{2NY_N} + \frac{\lambda q}{\Re_R(2N-1)(q - \sigma_d^2 \sigma_S^{-2})} \right] \tag{5.56}$$

$$\text{VAR}[\hat{\eta}_2 | \Psi_{2R}] \approx q \left[\frac{1}{2NY_N} + \frac{q}{\lambda \Re_R(2N-1)(q - \sigma_d^2 \sigma_S^{-2})} \right] \tag{5.57}$$

where $\Re_R = \Re_{R1} + \Re_{R2}$. Setting $q = \hat{q}$ in (5.56) and (5.57), and by analysis of simulation results, $q(q - \sigma_d^2 \sigma_S^{-2})^{-1} = 1.5$ was found to provide relatively good estimates of the variances for the DOA estimates, which are given by

$$\sigma_{\hat{\eta}_1}^2 = \hat{q}\left[\frac{1}{2NY_N} + \frac{1.5\lambda}{\hat{\Re}_R(2N-1)}\right] \tag{5.58}$$

$$\sigma_{\hat{\eta}_2}^2 = \hat{q}\left[\frac{1}{2NY_N} + \frac{1.5}{\lambda\hat{\Re}_R(2N-1)}\right] \tag{5.59}$$

Simulation Results

Monte Carlo simulations with 40,000 experiments were conducted to study the performances of the DOA estimators for various values of N, $\Delta\eta$, and λ. While the relative RCS of the two targets is assumed to be known, the effect of the antenna gain pattern is not assumed to be included in λ. The effects of the antenna gain pattern were included in the simulation of (4.1) through (4.4) by using

$$\tilde{\beta}_1 = \beta_1 \cos\left(\frac{\eta_1 \pi}{4\eta_{bw}}\right) \tag{5.60}$$

$$\tilde{\beta}_2 = \beta_2 \cos\left(\frac{\eta_2 \pi}{4\eta_{bw}}\right) \tag{5.61}$$

for β_1 and β_2, respectively. The effects of the antenna gain pattern were addressed in the DOA estimation by using a modified λ in (5.51) and (5.52), which is given by

$$\tilde{\lambda} = \lambda \frac{\cos^4\left(\dfrac{\tilde{\eta}_2 \pi}{4\eta_{bw}}\right)}{\cos^4\left(\dfrac{\tilde{\eta}_1 \pi}{4\eta_{bw}}\right)} \tag{5.62}$$

where $\tilde{\eta}_1$ and $\tilde{\eta}_2$ are the DOA estimates that result from ignoring the effects of the antenna gain pattern. The multiplier modification to λ was restricted to greater than 0.25 and less than 4. During the simulations, only measurements with $NY_N > 17$ dB were utilized in the DOA estimation, and $\eta_{bw} = 0.8$.

The effect of N on the DOA estimation was studied using $\Delta\eta = 0.4$ and setting $N\Re_{R1} = N\Re_{R2} = 26$ dB (*i.e.*, without the effects of the antenna pattern). The averages and standard deviations of the errors in the DOA estimates for target 1 are shown versus the DOA of target 1 in Figures 5.17 and 5.18. The DOA for target 2 is given by $\eta_2 = \eta_1 - \Delta\eta$. Thus, $\eta_1 = 0$ in Figures 5.17 and 5.18 corresponds to target 1 on the antenna boresight, while $\eta_1 = 0.4$ corresponds to target 2 on the antenna boresight. For each case of N, the average error and standard deviation decreases as

N increases. Figure 5.19 shows the sample standard deviations of the CRLB normalized errors in the estimates of η_1. Since Λ is random, the DOA estimation errors were normalized by the corresponding CRLB prior to computing the sample standard deviations. For $N = 12$, the simulated performance of the DOA estimators approaches the performance predicted with the CRLB, while for $N = 4$ or 8 the simulated performance of the DOA estimators differs significantly from the performance predicted with the CRLB. Figure 5.19 also shows that a radar pulse with a specific energy provides better DOA estimation with more subpulses at distinct frequencies.

The effect of $\Delta\eta$ on the DOA estimation was studied using $N = 8$ and setting $\Re_{R1} = \Re_{R2} = 17$ dB. The averages and standard deviations of the errors in the DOA estimates for target 1 are shown in Figures 5.20 and 5.21 for various DOAs of target 1 and $\Delta\eta = 0.2$, 0.4, 0.6, and 0.8. The DOA estimation for $\Delta\eta = 0.8$ is significantly degraded when compared to that for $\Delta\eta = 0.2$ or 0.4. Thus, when two targets are separated by about one-half of the one-way beamwidth, DOA estimation with two consecutive dwells at the individual targets may be better than a single dwell between them. This observation agrees with those made earlier in this chapter.

The effect of λ on the DOA estimation was studied using $N = 8$, $\Delta\eta = 0.4$, and $\Re_{R1} = 17$ dB. The averages and standard deviations of the errors in the DOA estimates for targets 1 and 2 are shown in Figures 5.22 and 5.23 for the positive DOAs of target 1; the corresponding negative DOAs of target 2; and $\lambda = 1$, 0.5, and 0.25 (i.e., $\Re_{R2} = 17$, 14, and 11 dB). The $\eta_1 = 0$ in Figures 5.22 and 5.23 corresponds to target 1 on the antenna boresight and $\eta_2 = -0.4$, while $\eta_1 = 0.4$ corresponds to $\eta_2 = 0$, target 2 on the antenna boresight. The DOA estimation for target 1 improves as $\Re_{R2}$ decreases, while DOA estimation for target 2 degrades as $\Re_{R2}$ decreases as expected. The errors were also normalized by the standard deviation estimates of (5.58) and (5.59), and the sample standard deviations of those errors are given in Figure 5.24, which indicates that the variance estimates of (5.58) and (5.59) are reasonably good.

Results of 20 experiments for a simple tracking example are given to illustrate the concept of tracking unresolved targets with monopulse measurements. The computer simulation program of [24] was modified to include multiple targets and processing measurements of unresolved targets. The target trajectories, as shown in Figure 5.25, are constant speed and height, and are initially separated by 1.4 km. The targets converge to a separation of about one beamwidth at $x = 50$ km. The solid lines show the true bearing of the two targets, while the dashed lines denote one beamwidth with the antenna boresight pointed directly at a bearing of zero. When the targets are separated by more than one beamwidth, measurements are easily associated with the
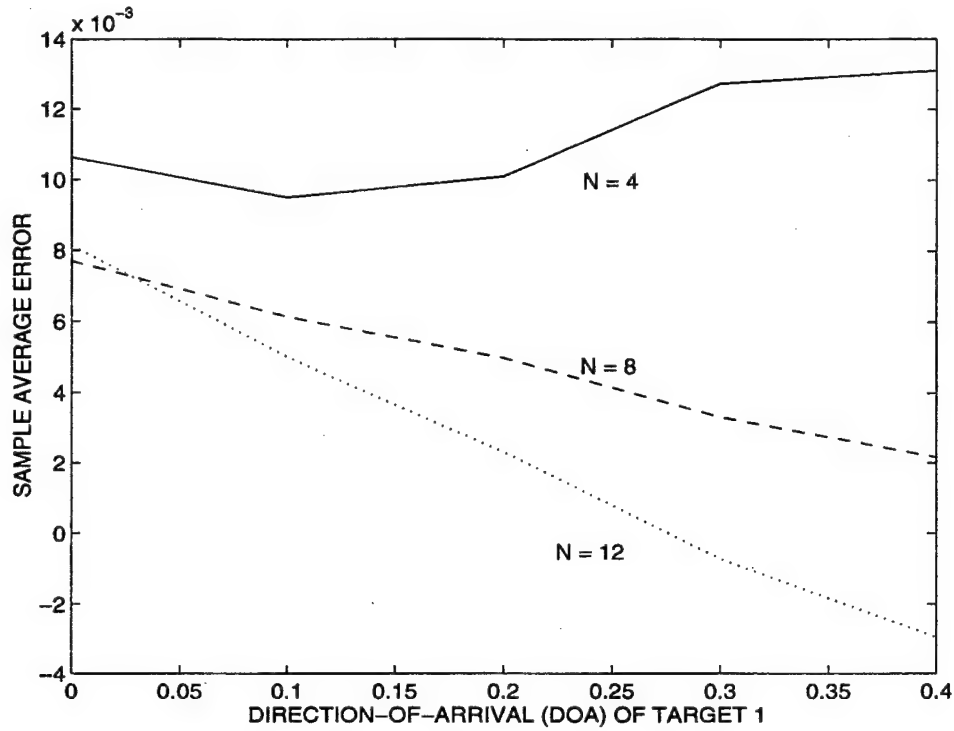
Figure 5.17 Average Errors in DOA Estimates for $\Delta\eta = 0.5\eta_{bw}$ and $\lambda = 1$
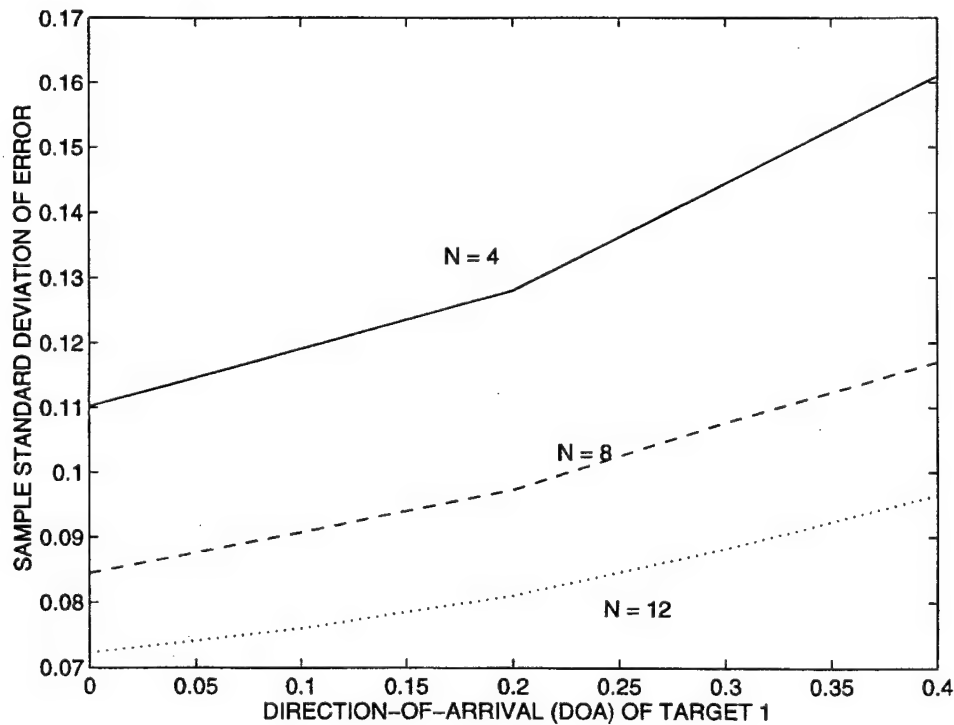
Figure 5.18 Standard Deviation of Errors in DOA Estimates for $\Delta\eta = 0.5\eta_{bw}$ and $\lambda = 1$
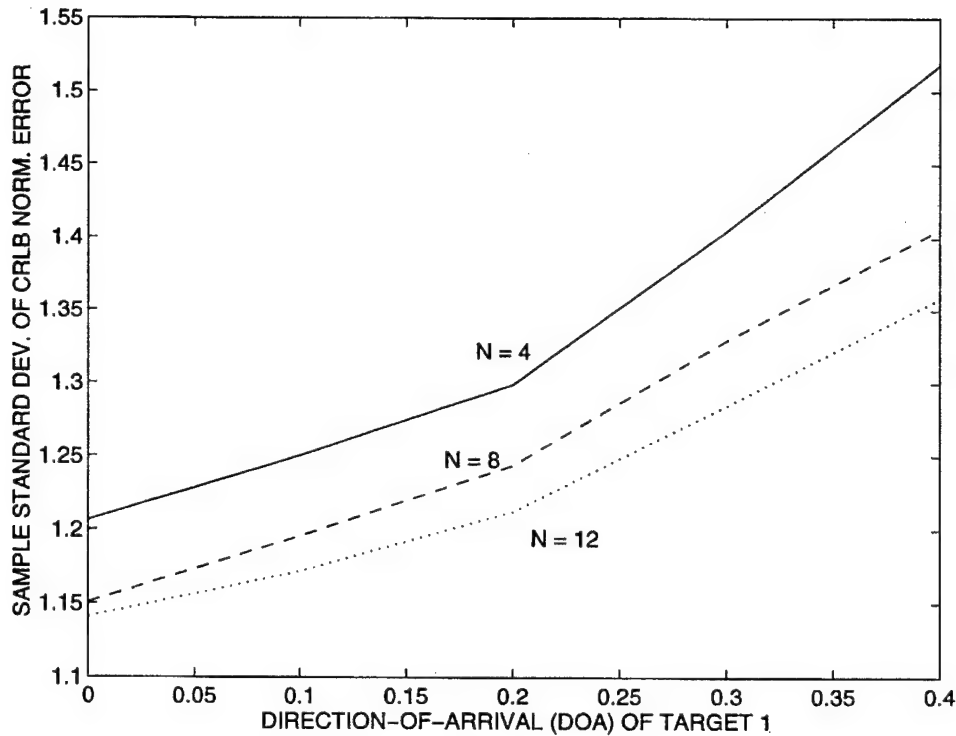
Figure 5.19 Standard Deviations of CRLB Normalized Errors in DOA Estimates for $\Delta\eta = 0.5\eta_{bw}$ and $\lambda = 1$

correct target, and conventional DOA estimation and tracking works fine. At about one beamwidth separation of the two targets (i.e., $x = 50$ km), the presence of the other target adversely effects the monopulse measurements, and when the presence of the second target was not taken into consideration in the DOA estimation and tracking, most tracks were lost at this point in the trajectories. A target track was declared lost after four consecutive measurements failed to statistically associate with the target or when the relative positions of the two targets inverted. At this point in the tracking, the DOA and amplitude estimates of the other track filter were used in the DOA and variance estimation in a manner similar to that in Section 5.3 for a Rayleigh target in the presence of a Gaussian jammer. As the targets continued to converge, most tracks were declared lost by about $x = 70$ km if the processing of unresolved measurements as developed in this section was not employed. For the processing of unresolved targets, the antenna boresight was pointed at the estimated centroid of the two equal RCS targets, and two dwells of six subpulses were used. The average tracking errors of the two-target scenario are shown in Figure 5.25, and the RMS errors are shown in Figure 5.26. In Figure 5.25, the dashed lines denote one beamwidth with the antenna boresight pointed directly at a bearing of zero. The
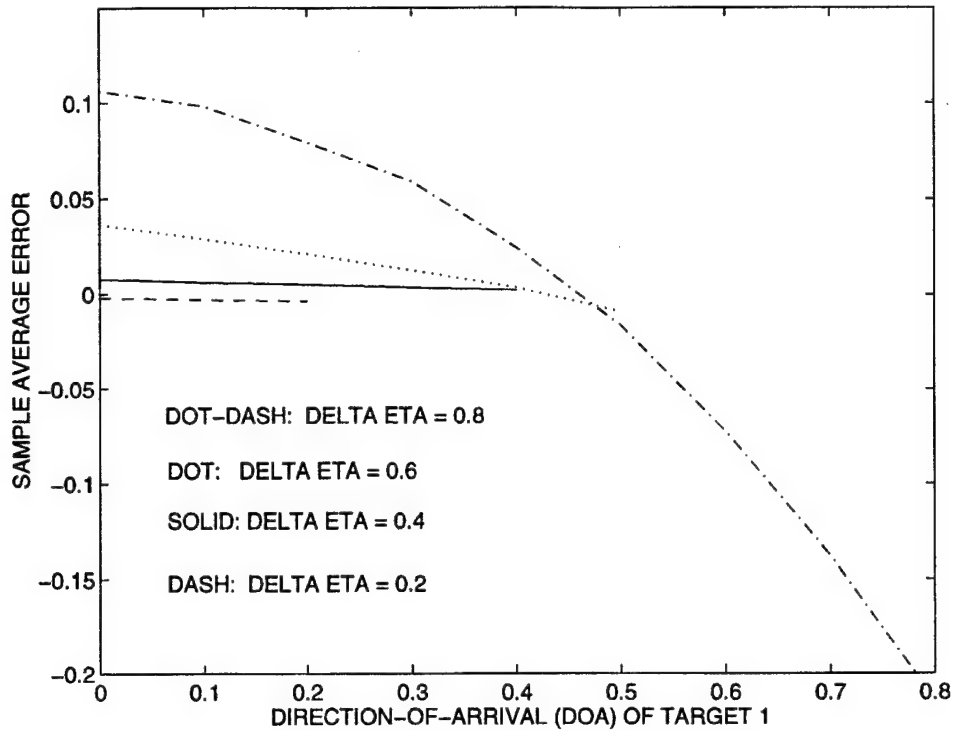
Figure 5.20 Average Errors in DOA Estimates for $N = 8$ and $\lambda = 1$
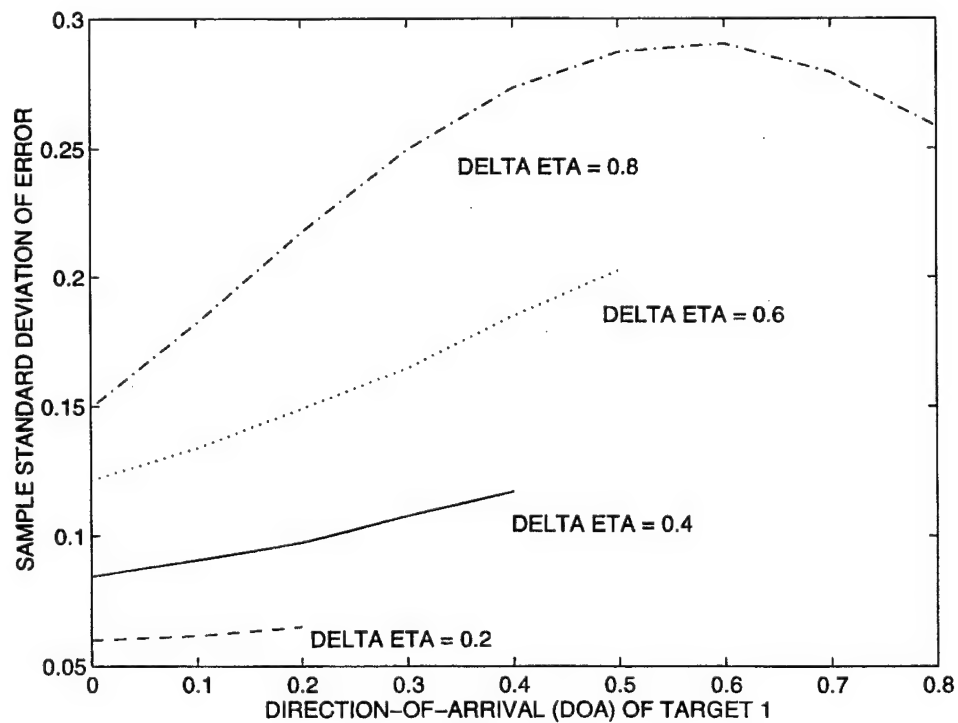
Figure 5.21 Standard Deviations of Errors in DOA Estimates for $N = 8$ and $\lambda = 1$
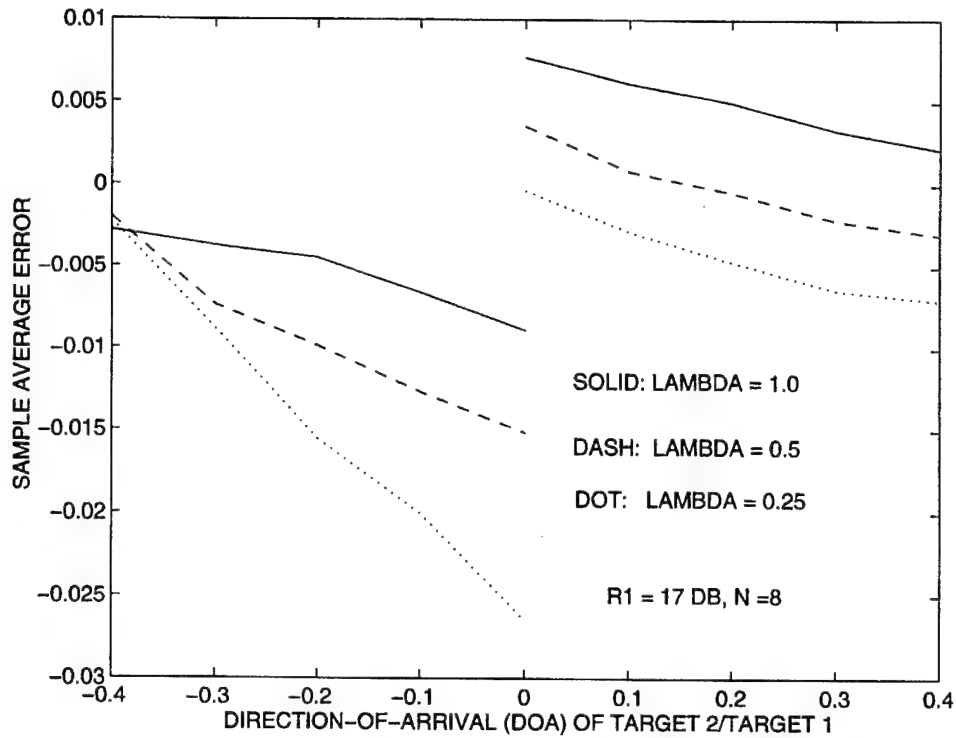
Figure 5.22 Average Errors in DOA Estimates for $N = 8$ and $\Delta\eta = 0.5\eta_{bw}$
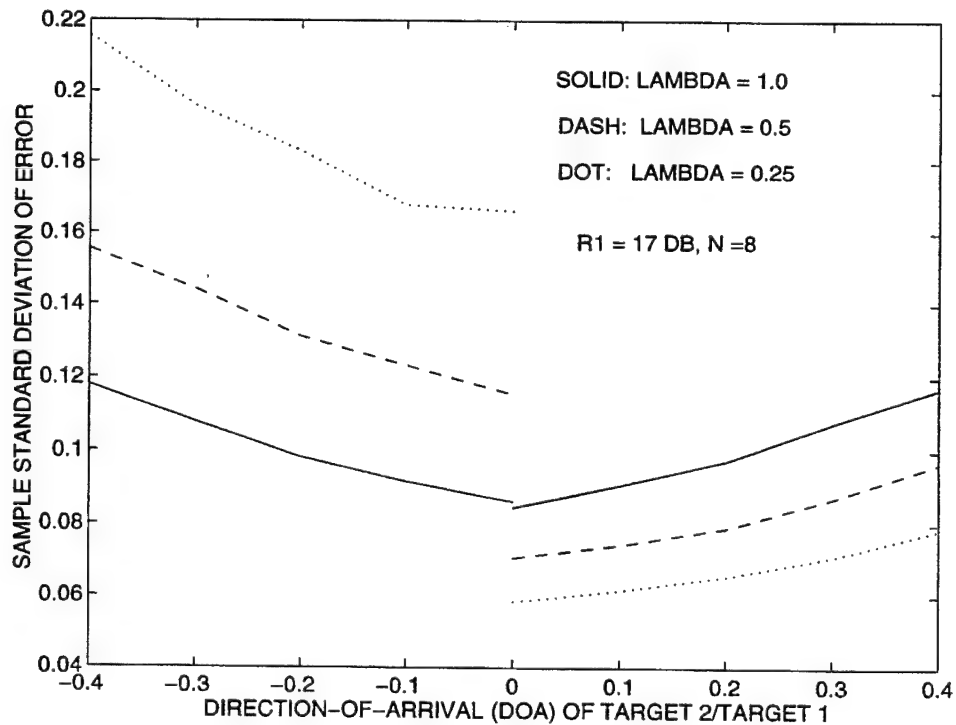
Figure 5.23 Standard Deviations of Errors in the DOA Estimates for $N = 8$ and $\Delta\eta = 0.5\eta_{bw}$
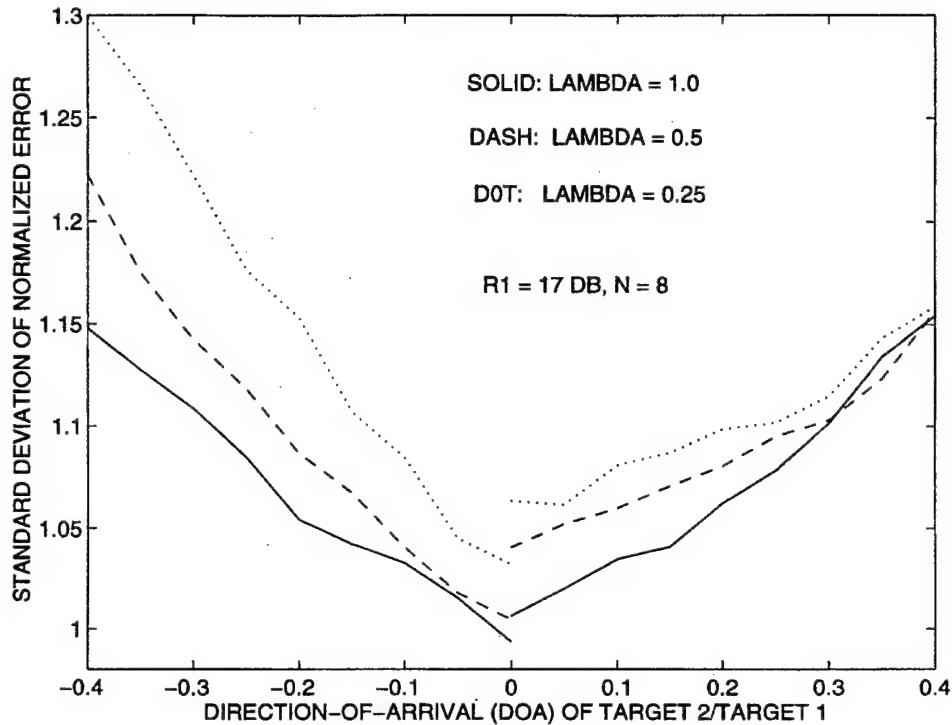
Figure 5.24 Standard Deviations of Errors in the DOA Estimates Normalized by the Estimates of Standard Deviation for $N = 8$ and $\Delta\eta = 0.5\eta_{bw}$

large bias in the estimates is the result of the upper limit of half a beamwidth imposed on $\hat{\eta}_1 - \hat{\eta}_2$ through $\tilde{q}$.

The initial results of the simple tracking example demonstrate the potential of tracking two unresolved Rayleigh targets, since the track estimates were maintained and did not coalesce. The use of conventional measurement processing and tracking resulted in the loss of both targets in every experiment. Further investigations are needed to reduce the bias in the estimates and improve the transition between tracking resolved targets and tracking unresolved targets.
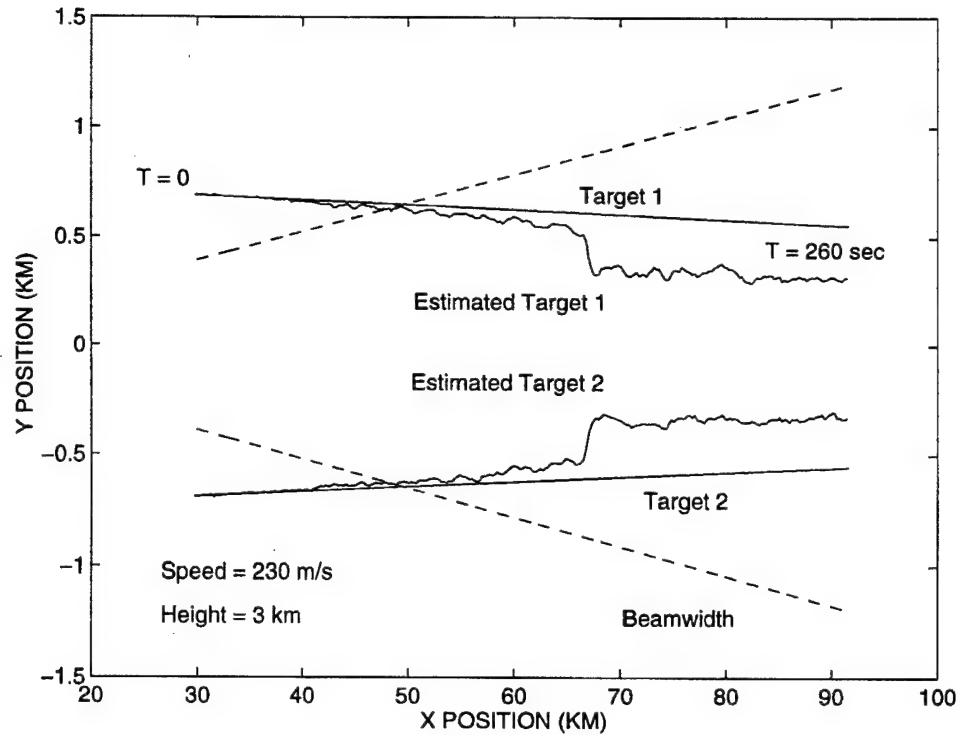
Figure 5.25 Average Tracking Errors of Unresolved Processing for Two Targets
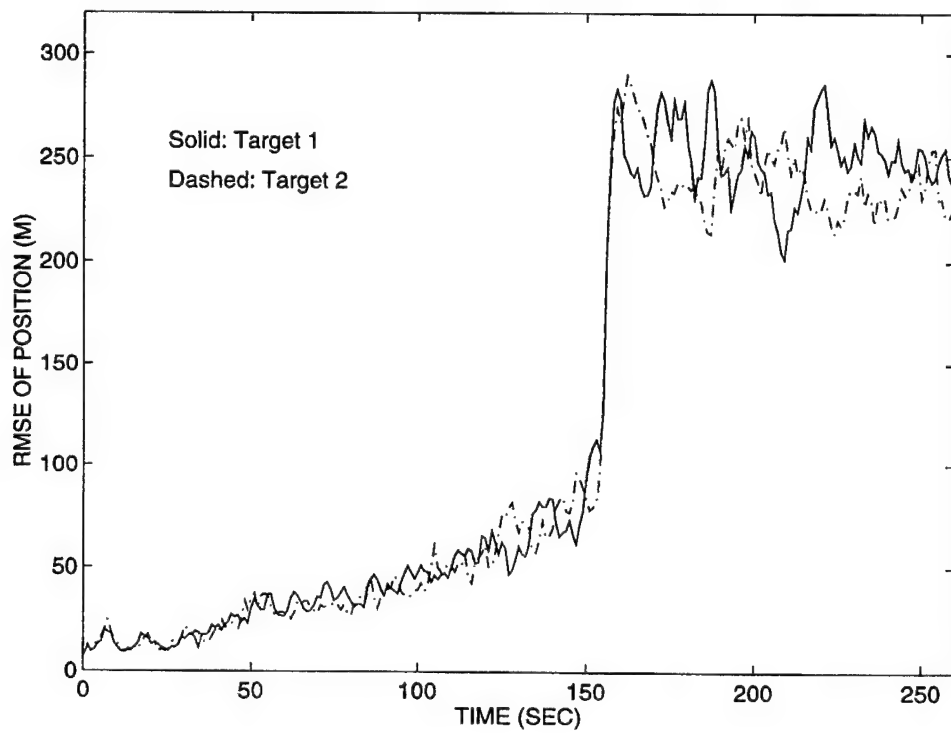
Figure 5.26 RMS of Tracking Errors of Unresolved Processing for Two Targets

142

Chapter 6

DETECTION OF THE PRESENCE OF TWO UNRESOLVED RAYLEIGH TARGETS

When target echoes interfere (*i.e.*, the echoes are not resolved in the frequency or time domains), the DOA estimate indicated by the in-phase monopulse ratio can wander far beyond the angular separation of the targets [1,4,42]. The failure to detect the presence of this interference can be catastrophic to the performance of the tracking algorithm, since its position and velocity estimates determine the association of any subsequent measurements to the target. This chapter addresses the detection of the presence of two unresolved Rayleigh targets. The detection of the presence of two unresolved, fixed-amplitude targets is not considered in this research due the intractable statistics. However, this chapter includes results of simulation studies of performance of the detection algorithm for unresolved Rayleigh targets when two fixed-amplitude targets are present.

In order to reduce the catastrophic effects of this target multiplicity, a threshold test of either the measured amplitude of the sum signal or the magnitude of the quadrature part of the monopulse ratio was considered in [49]. In the amplitude threshold test, a DOA estimate was considered unreliable when the measured amplitude of the sum signal failed to exceed a threshold value, and the DOA estimate was not used for tracking. In the quadrature monopulse test, a DOA estimate was not used for tracking when the magnitude of the quadrature ratio exceeded a threshold value. Using either of these tests will tend to make the tracking more stable and follow the stronger target if the amplitudes are fixed and the amplitude of one target is 3 to 5 dB stronger than that of the other target. However, both of these tests require knowledge of the amplitude of at least one of the two targets in the absence of the other target. While in some cases the amplitudes could be estimated prior to the occurrence of the target multiplicity, the reliability of the amplitude estimates may be a problem since the RCS of typical targets can be very sensitive to the aspect angle of the radar. Furthermore, target multiplicity can occur with targets of approx-

imately the same amplitude. In [50], a maximum-likelihood detection algorithm was developed for detecting target multiplicity or interference using the complex voltage outputs of the antenna lobes. However, the algorithm in [50] was developed for signals with a high postdetection SNR and targets with fixed amplitudes that differ by more than 3 dB. Furthermore, in many monopulse systems, the sum and difference of the two antenna lobes are formed in the waveguide prior to the receivers. Thus, only the sum and difference signals are available for signal processing. This is particularly true in array antennas with constrained feeds [1, p. 288].

The detection of the presence of unresolved targets was considered in [33] with an M out of N threshold test of the magnitude of the quadrature monopulse measurements. The threshold value for each quadrature monopulse measurement was derived to be a function of the SNR and DOA with the marginal PDF for the quadrature monopulse measurements. The detection of unresolved Rayleigh targets was further considered in [51], where the power centroid and angular extent of a set of measurements were estimated from the sum and difference signals, and target multiplicity was declared when the estimated angular extent exceeded that expected from a single target. The algorithm of [51] was shown to give significantly improved detection over the algorithm of [33] for two or more (independent) observations (*i.e.*, $N > 1$) and to be equivalent to the algorithm of [33] for one observation (*i.e.*, $N = 1$). While an improvement in the detection of unresolved Rayleigh targets was realized in [51], the detection threshold value remained a function of the SNR and DOA. In this chapter, amplitude-conditioned PDFs of Sections 4.1 and 4.2 are used to develop a GLRT for detection of the presence of unresolved Rayleigh targets with a Neyman-Pearson algorithm. Conditioning the PDF of the monopulse measurements on the measured amplitude of the sum signal gives the in-phase and quadrature monopulse ratios as conditionally independent, Gaussian random variables so that the PDF is fully specified by the means and variances. Since the SNR of neither target is assumed known, the measured amplitude of the sum signal provide no information concerning the DOA of either target or the presence of two targets. Thus, the PDF of the monopulse measurements can be conditioned on the measurement amplitude to obtain a Gaussian distribution without any loss of information.

A Neyman-Pearson algorithm for GML detection of target multiplicity is developed in this chapter. The algorithm is developed for a single radar dwell that includes multiple noncoherent pulses at slightly different frequencies so that independence of the target amplitudes is achieved. When utilizing the conditional PDF in the detection of target multiplicity, the test statistic is shown to be a chi-square random

variable with $2N - 1$ degrees of freedom for N pulses. The test utilizes the observed SNRs and estimates of the SNR and DOA. Thus, the test requires no specification of the SNR or DOA of either target. Of course, the probability of detecting target multiplicity is dependent on the relative amplitudes and locations of the two targets. ROC curves are given to illustrate the performance of the new detection algorithm, and specific comparisons are made between the predicted performances of the new algorithm and the algorithm developed in [51]. Simulation results that confirm the performance predictions of the ROC curves are given along with concluding remarks.

Detection of Target Multiplicity

Let H_0 denote the hypothesis of no unresolved targets (*i.e.*, Target 1 only), and H_1 denote the hypothesis of two unresolved targets (*i.e.*, Targets 1 and 2). Then, Section 4.2 gives the PDFs of y_I and y_Q for two unresolved Rayleigh targets as

$$f(y_I|H_1, \Re_o, \Psi_{2R}) = N\Big(\frac{\Re_{R1}\eta_1 + \Re_{R2}\eta_2}{\Re_{R1} + \Re_{R2} + 1}, \sigma_1^2\Big) \tag{6.1}$$

$$f(y_Q|H_1, \Re_o, \Psi_{2R}) = N\Big(0, \sigma_1^2\Big) \tag{6.2}$$

where

$$\sigma_1^2 = \frac{q}{2\Re_o} \tag{6.3}$$

$$q = \Big[\frac{\sigma_d^2}{\sigma_s^2} + \frac{\Re_{R1}\eta_1^2 + \Re_{R2}\eta_2^2 + \Re_{R1}\Re_{R2}(\eta_1 - \eta_2)^2}{\Re_{R1} + \Re_{R2} + 1}\Big] \tag{6.4}$$

with q being introduced for later reference. The $\Re_{R1}$ and $\Re_{R2}$ are the SNRs of target 1 and target 2, respectively, while η_1 and η_2 are the DOAs for target 1 and target 2, respectively. The variance expression of (6.3) also shows that the DOA estimation for two unresolved targets is not directly improved by increasing the expected value of $\Re_o$ through the transmitted energy because increasing the transmitted energy also increases $\Re_{R1}$ and $\Re_{R2}$. The larger errors in the monopulse measurements occur when the two target echoes interfere to produce a value for $\Re_o$ that is small relative to $\Re_{R1}\Re_{R2}(\Re_{R1} + \Re_{R2} + 1)^{-1}$.

Using the results of Section 4.1, the PDFs of y_I and y_Q for a single target are given by

$$f(y_I|H_0, \Re_o, \Psi_R) = N\Big(\frac{\Re_{R1}}{\Re_{R1} + 1}\eta_1, \sigma_0^2\Big) \tag{6.5}$$

$$f(y_Q|H_0, \Re_o, \Psi_R) = N\Big(0, \sigma_0^2\Big) \tag{6.6}$$

where

$$\sigma_0^2 = \frac{p}{2\Re_o} \tag{6.7}$$

$$p = \left[\frac{\sigma_d^2}{\sigma_s^2} + \frac{\Re_{R1}}{\Re_{R1} + 1}\eta_1^2\right] \tag{6.8}$$

Since the receiver errors are assumed to be independent, p of (6.8) was obtained by setting $\rho = 0$ in (4.45).

Since y_I is a conditional Gaussian random variable under H_0 or H_1, the ML estimate [11, p. 65] of $\bar{y}_I$, which is the conditional mean of y_I under H_0 or H_1, is given for N independent pulses by

$$\hat{y}_I = \left[\sum_{j=1}^{N} \Re_{oj}\right]^{-1} \sum_{k=1}^{N} \Re_{ok} y_{Ik} = \left[NY_N\right]^{-1} \sum_{k=1}^{N} \Re_{ok} y_{Ik} \tag{6.9}$$

where the y_{Ik} denotes the in-phase monopulse ratio for pulse k, and $\Re_{ok}$ denotes the observed SNR given by (3.11) for pulse k. Thus, the estimate $\hat{y}_I$ is a "power" weighted sum of the N monopulse ratios. Since the y_{Ik} are Gaussian random variables, $\hat{y}_I$ is also the minimum variance estimate of $\bar{y}_I$ and a Gaussian random variable with variance given by

$$\sigma_{\hat{y}_I}^2 = \frac{p}{2}\left[\sum_{k=1}^{N} \Re_{ok}\right]^{-1} = \frac{p}{2NY_N} \tag{6.10}$$

Using

$$\hat{y}_I \approx \frac{\Re_{R1}}{\Re_{R1} + 1}\eta_1 \tag{6.11}$$

from (6.5) and $\Re_{R1} = \widehat{\Re}_{R1}$ in (6.8) gives an estimate of σ_{0k}^2, which is the variance the monopulse ratio of pulse k under hypothesis H_0, as

$$\hat{\sigma}_{0k}^2 = \frac{\hat{p}}{2\Re_{ok}} \tag{6.12}$$

$$\hat{p} = \left[\frac{\sigma_d^2}{\sigma_S^2} + \left(1 + \frac{1}{\widehat{\Re}_{R1}}\right)\hat{y}_I^2\right] \tag{6.13}$$

where $\widehat{\Re}_{R1}$ is the ML estimate of $\Re_{R1}$ under H_0 (i.e., $\Re_{R2} = 0$). Then $\widehat{\Re}_{R1}$ is given by (3.32) with $\widehat{\Re}_{R1} = \widehat{\Re}_R$. An estimate of the variance of the $\hat{y}_I$ can be achieved by using $\hat{p}$ in (6.10).

Comparing (6.1) through (6.4) with (6.5) through (6.8) suggests that the presence of unresolved Rayleigh targets can be detected using the GLRT [11, p. 92], where the ML estimate of $\bar{y}_I$, the conditional mean of y_I under H_0 and H_1, is used for the

means since η_1 nor η_2 is known *a priori*. Since the monopulse measurements are conditionally Gaussian distributed under H_0 and H_1, (6.9) gives the ML estimate of the conditional mean $\bar{y}_I$ under both hypotheses. Thus, using (6.1) through (6.8) and generalizing directly over the conditional mean under each hypothesis gives the generalized likelihood ratio [11, p. 92] for N independent pulses as

$$
L(\{y_{Ik}\}_{k=1}^N, \{y_{Qk}\}_{k=1}^N | \{\Re_{ok}\}_{k=1}^N, \Psi_{2R}) = \frac{\displaystyle\max_{\bar{y}_I} \prod_{k=1}^N f(y_{Ik}, y_{Qk}|H_1, \Re_{ok}, \Psi_{2R})}{\displaystyle\max_{\bar{y}_I} \prod_{k=1}^N f(y_{Ik}, y_{Qk}|H_0, \Re_{ok}, \Psi_R)}
$$

$$
= \frac{\displaystyle\prod_{k=1}^N f(y_{Ik}, y_{Qk}|H_1, \bar{y}_I = \hat{y}_I, \Re_{ok}, \Psi_{2R})}{\displaystyle\prod_{k=1}^N f(y_{Ik}, y_{Qk}|H_0, \bar{y}_I = \hat{y}_I, \Re_{ok}, \Psi_R)}
$$

$$
= \left(\frac{p}{q}\right)^N \exp\left[-\frac{1}{2}(q^{-1} - p^{-1})X_N^T R_N X_N\right] \quad (6.14)
$$

where for $N > 1$,

$$
X_N = \begin{bmatrix} y_{I1} - \hat{y}_I & \cdots & y_{IN} - \hat{y}_I & y_{Q1} & \cdots & y_{QN} \end{bmatrix}^T \quad (6.15)
$$

$$
R_N = 2\,\text{diag}\begin{bmatrix} \Re_{o1} & \cdots & \Re_{oN} & \Re_{o1} & \cdots & \Re_{oN} \end{bmatrix} \quad (6.16)
$$

and for $N = 1$, $X_1 = y_{Q1}$ and $R_1 = 2\Re_{o1}$. The y_{Ik} and y_{Qk} are the in-phase and quadrature monopulse ratios for pulse k, while $\Re_{ok}$ is the observed SNR of (3.11) for pulse k. Taking the logarithm of (6.14) gives the test statistic for the GLRT as

$$
T_N = X_N^T R_N X_N \quad (6.17)
$$

This T_N is related to the test statistic $\widehat{C}^2$ of [51] according to

$$
T_N = Y_N \widehat{C}^2 \quad (6.18)
$$

where Y_N is the sample mean of the observed SNRs as given by (3.29). The use of the amplitude-conditioned PDFs of the y_{Ii} and y_{Qi} in the GLRT gives the test statistic T_N, which is proportional to a chi-square distributed random variable, while the test statistic $\widehat{C}^2$ used in [51] is F-distributed [52, p. 946]. The performance predictions of this section and the simulation results of the next section indicate that the use of T_N gives better detection of target multiplicity than the use of $\widehat{C}^2$.

Since the conditional densities for the in-phase and quadrature monopulse ratios are Gaussian for H_0 with variance given by (6.7), $T_N p^{-1}$ is a chi-square random variable with $2N - 1$ degrees of freedom under H_0, where one degree of freedom has been lost due to the estimation of the conditional mean of y_I [48, p. 320]. Taking a Neyman-Pearson approach to the detection problem, the probability of false detection of multiple targets (*i.e.*, the probability of detecting the presence of unresolved targets when only one target is present) for a detection threshold λ_d is given by

$$P_{FDMT} = P\{T_N p^{-1} > \lambda_d | H_0, \{\Re_{ok}\}_{k=1}^N, \Psi_R\} = \frac{1}{2^{N-\frac{1}{2}} \Gamma(N - \frac{1}{2})} \int_{\lambda_d}^{+\infty} t^{N-\frac{3}{2}} e^{-\frac{t}{2}} dt$$
(6.19)

where $P\{\cdot\}$ denotes probability of an event, and $\Gamma(\cdot)$ is the gamma function [52, p. 253]. Figure 6.1 shows the normalized detection threshold λ_d versus P_{FDMT} for $N = 2, 3, 4$, and 5. Note that the P_{FDMT} can also be determined with a table for the chi-square distribution that can be found in various books (*e.g.*, [52, p. 984]).

Since no assumptions are made regarding the DOAs or SNRs of the targets, a Neyman-Pearson approach will be taken to the detection problem so that an estimate of only p is required. Thus, for a specified P_{FDMT} and corresponding λ_d, the decision rule δ is given by

$$\delta = \begin{cases} H_0, & T_N \le \hat{p}\lambda_d \\ H_1, & T_N > \hat{p}\lambda_d \end{cases}$$
(6.20)

where

$$\hat{p} = \frac{\sigma_S^2}{\sigma_d^2} + \left[1 + \frac{1}{\widehat{\Re}_{R1}}\right] \hat{y}_I^2 = \frac{\sigma_S^2}{\sigma_d^2} + \left[1 + \frac{1}{Y_N - 1}\right] \left[\frac{1}{NY_N} \sum_{k=1}^N \Re_{ok} y_{Ik}\right]^2$$
(6.21)

with Y_N given by (4.47), and the MM estimate of η_1 has been used in p of (6.8) to form $\hat{p}$. Note that predictions of detection performance given in this section are only approximations, since $\hat{p}$ is used for p. However, the predictions of performance are shown to agree rather well with the results of simulation studies.

Since the conditional densities for the in-phase and quadrature monopulse ratios are Gaussian for H_1 with variance given by (6.3), $T_N q^{-1}$ is a chi-squared random variable with $2N - 1$ degrees of freedom under H_1. The probability of detection of multiple targets (*i.e.*, the probability of detecting the presence of unresolved targets when two unresolved targets are present) is given by

$$P_{DMT} = P\{T_N q^{-1} > \lambda_d \hat{p} q^{-1} | H_1, \{\Re_{ok}\}_{k=1}^N, \Psi_{2R}\}$$
$$= \frac{1}{2^{N-\frac{1}{2}} \Gamma(N - \frac{1}{2})} \int_{\lambda_d \hat{p} q^{-1}}^{+\infty} t^{N-\frac{3}{2}} e^{-\frac{t}{2}} dt$$
(6.22)
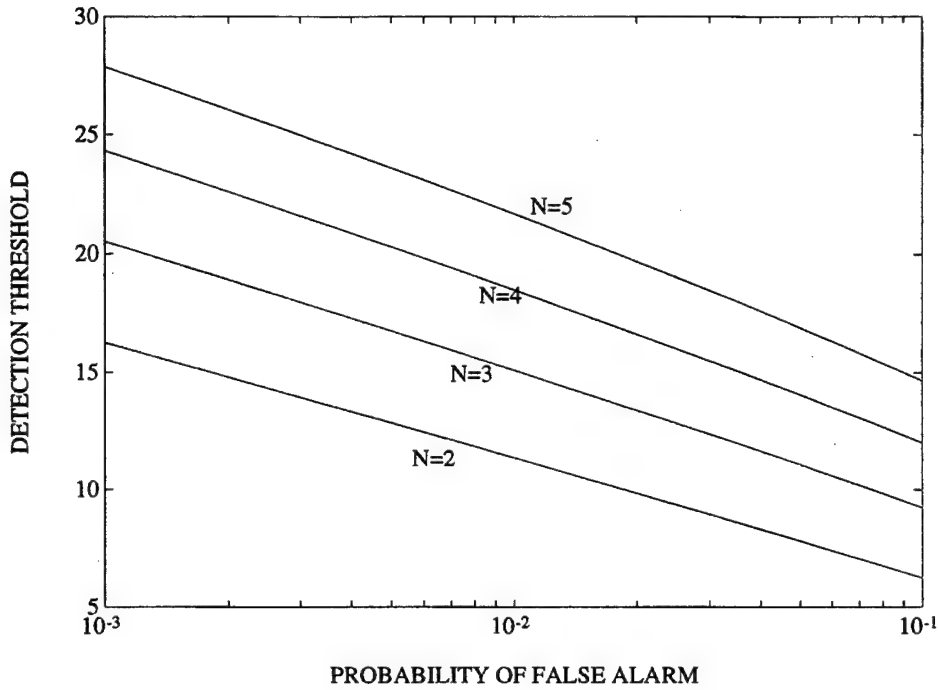
Figure 6.1 Detection Thresholds Versus Probability of False Alarm for $N = 2, 3, 4$, and 5 Pulses

Figure 6.2 shows approximate ROC curves for the detection algorithm for target 1 and target 2 situated symmetrically about the boresight of the antenna (*i.e.*, $\eta_1 = -\eta_2$), $\Re_{R1} = \Re_{R2} = 13$ dB, and $\sigma_d^2 = \sigma_S^2$. The solid lines denote cases where $\eta_1 = -\eta_2 = 0.4$, while the dashed lines denote cases where $\eta_1 = -\eta_2 = 0.2$. Thus, for Figure 6.2 and monopulse error slope $k_m = 1.6$ (see (2.45)), the solid lines correspond to two targets situated about one-fourth of a beamwidth from the antenna boresight, while the dashed lines correspond to two targets situated about one-eighth of a beamwidth from the antenna boresight. The P_{FDMT} were generated for a $2N - 1$ degree-of-freedom chi-square random variable for various values of λ_d. The P_{DMT} were generated by using

$$\hat{y}_I = \frac{\Re_{R1}\eta_1 + \Re_{R2}\eta_2}{\Re_{R1} + \Re_{R2} + 1} \tag{6.23}$$

and the true values of Ψ_{2R} in $\hat{p}$ and q. For the solid lines, $\hat{p} = 1.0$ and $q = 7.4$, and for the dashed lines, $\hat{p} = 1.0$ and $q = 2.6$. Figure 6.2 indicates that a $P_{DMT} = 0.92$ with $P_{FDMT} = 0.01$ can be achieved with four pulses at 13 dB when the two targets are separated symmetrically about the antenna boresight by one-half of a beamwidth. Four 13-dB pulses correspond to a total SNR of about 19 dB, which is not an unreasonable SNR for tracking. The detection performance drops to $P_{DMT} = 0.4$

with $P_{FDMT} = 0.01$ when the two targets are separated by one-fourth of a beamwidth. Comparing the solid and dash lines of Figure 6.2 indicates that the difficulty of the detection problem increases as the angle of separation decreases.

Figure 6.3 shows the ROC curves for the detection algorithm for target 1 at the boresight of the antenna (*i.e.*, $\eta_1 = 0$) and target 2 off the boresight by one-half of the beamwidth (*i.e.*, $\eta_2 = 0.8$). The solid lines denote cases where $\Re_{R1} = \Re_{R2} = 13$ dB, while the dashed lines denote cases where $\Re_{R1} = 4\Re_{R2} = 13$ dB. Thus, for Figure 6.3, the solid lines correspond to $\hat{p} = 1.1$ and $q = 7.6$, and the dashed lines correspond to $\hat{p} = 1.0$ and $q = 3.6$. Comparing the solid lines from Figures 6.2 and 6.3 indicates that pointing between two targets provides slightly better detection of the target multiplicity than pointing directly at one of the two targets. Comparing Figures 6.2 and 6.3 also suggests that the probability of detection is more sensitive to the angular separation of the targets than to the relative amplitudes.

Simulation Results

Since $\hat{p}$ is used for p in the decision rule of (6.19), the decision rule was applied to simulated measurements to confirm the performance predictions given in the previous section. Radar dwells with four pulses ($N = 4$) were considered, and $\lambda_d = 18.4$ was chosen in order to achieve a false alarm rate of 0.01. Table 6.1 provides the percents of false alarms for various DOAs and SNRs that occurred during Monte Carlo simulations with 25,000 experiments for each entry. The measurements were simulated with (4.1) through (4.2) by setting $\alpha_i = 0$ for all i, and $\beta_i = 0$ for all $i > 1$. For $\eta_1 = \pm 0.75$ and $k_m = 1.6$, the target is about one-half a beamwidth off the antenna boresight (*i.e.*, $\theta = \pm 0.47\theta_{BW}$). Note that with the exception of $\eta_1 = \pm 0.75$ and ± 1.0, and $\Re_{R1} = 7$ dB, the false alarm rates found with the simulation studies agree well with the design value of 1.0 percent. This poor performance for $\Re_{R1}$ and $\eta_1 = \pm 1.0$ is the result of using an estimated value for p at a low SNR with only a few pulses. Note that the total expected SNR of four pulses at 7 dB is 13 dB (*i.e.*, $4E[\Re_o] = 20$).

The probabilities of detection that occurred during 25,000 experiments for each entry are shown in Figure 6.4. The measurements included four independent pulses that were simulated using (4.1) through (4.4) for one target at the boresight and the second target at various off-axis angles. The decision rule was implemented with $\lambda_d = 18.5$ to achieve a $P_{FDMT} = 0.01$. The solid lines correspond to simulation results with $\Re_{R1} = \Re_{R2} = 13$ dB, $\Re_{R1} = \Re_{R2} = 10$, and $\Re_{R1} = 4\Re_{R2} = 13$ dB, while the dotted lines correspond to the predicted performance based on the results of the
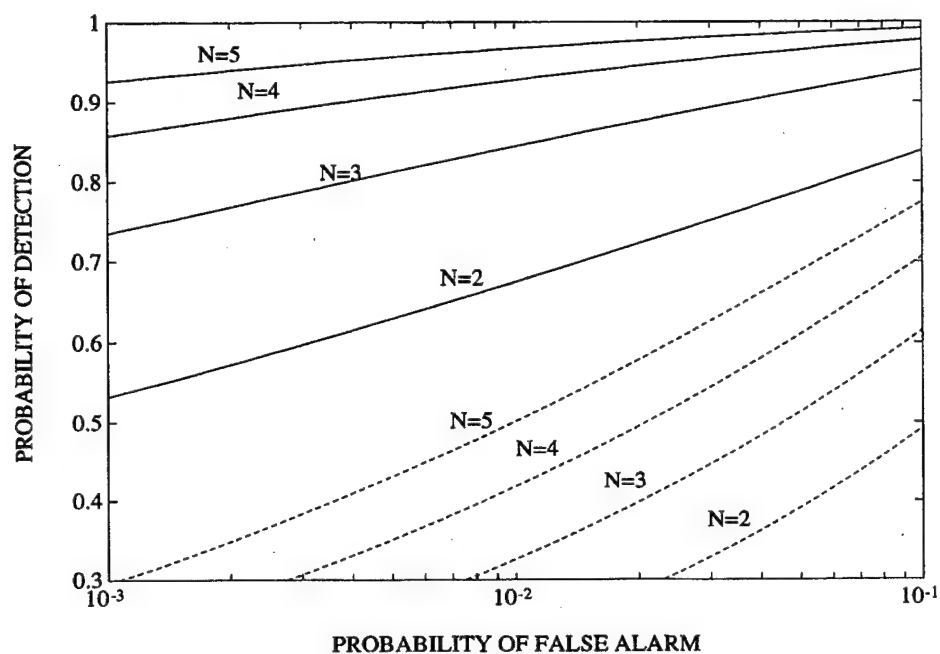
Figure 6.2 ROC Curves for Two 13-dB Targets Symmetric About the Antenna Boresight (solid: one-half beamwidth separation, dashed: one-fourth beamwidth separation)
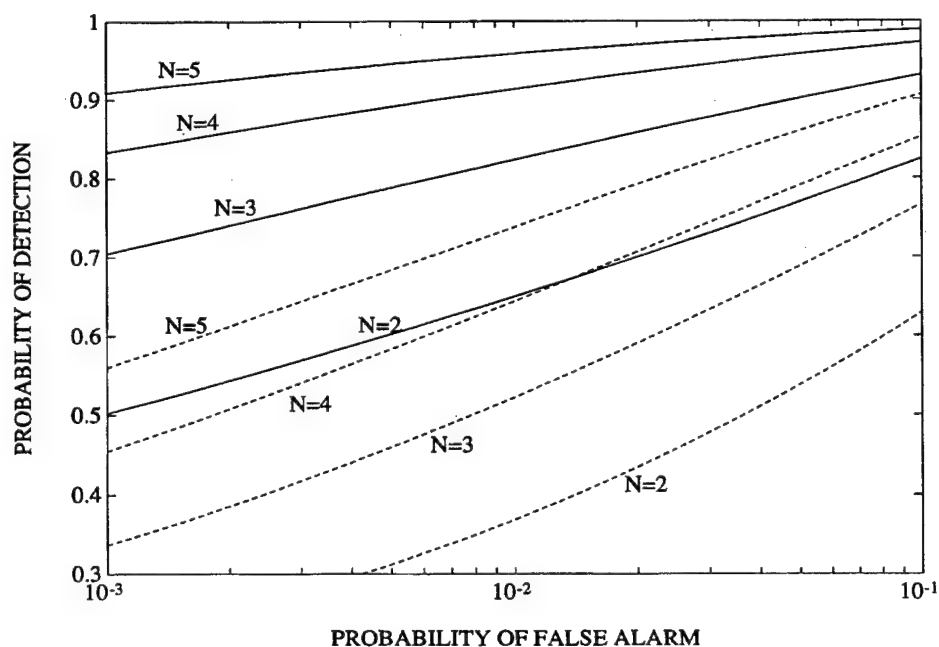
Figure 6.3 ROC Curves for Two Targets Separated By One-Half Beamwidth with One 13-dB Target at the Antenna Boresight (solid: 13 dB second target, dashed: 7 dB second target)

Table 6.1 Percents of False Alarms for Detection of Target Multiplicity

η_1	Percent of False Alarms (%)		
	$\Re_{R1} = 7$ dB	$\Re_{R1} = 10$ dB	$\Re_{R1} = 13$ dB
-1.00	2.1	1.6	1.3
-0.75	1.8	1.3	1.2
-0.50	1.4	1.2	1.1
-0.25	1.1	1.0	1.0
0.00	1.0	0.9	0.9
0.25	1.1	1.0	1.0
0.50	1.4	1.2	1.1
0.75	1.8	1.3	1.2
1.00	2.1	1.6	1.3

previous section. Figure 6.4 shows that the simulated performance of the detection algorithm agrees very well with the performance predictions based on (6.19) and (6.22). For two 13-dB targets and four pulses, Figure 6.3 predicts $P_{DMT} = 0.92$ for $P_{FDMT} = 0.01$, while the simulations results give $P_{DMT} = 0.89$. Figure 6.4 suggests that the probability of detection depends on the total SNR (*i.e.,* $\Re_{R1} + \Re_{R2}$). Figure 6.4 also indicates that the probability of detection depends strongly on the angle of separation.

Figure 6.5 shows the probabilities of detection that occurred during 25,000 experiments for each entry. The measurements included four independent pulses that were simulated using (4.1) through (4.4) for two targets symmetrically located about the antenna boresight at various off-axis angles. The decision rule was implemented with $\lambda_d = 18.5$ to achieve a $P_{FDMT} = 0.01$. The solid lines correspond to simulation results with $\Re_{R1} = \Re_{R2} = 10$ dB, $\Re_{R1} = \Re_{R2} = 13$ dB, and $\Re_{R1} = \Re_{R2} = 16$ dB, while the dot lines correspond to the predicted performance based on the results of the previous section. Figure 6.5 shows that the simulated performance of the detection algorithm agrees well with the performance predictions.

The simulation studies that were conducted for Figure 6.5 were also conducted for two fixed-amplitude targets to assess the performance of the algorithm when the targets are fixed-amplitude rather than Rayleigh. The results of that simulation study are given in Figure 6.6. Thus, for two fixed-amplitude targets, the simulated performance of the detection algorithm exceeds the performance predictions for two unresolved Rayleigh targets. Note that the GML detection algorithm in this chapter was developed for Rayleigh targets, and a better algorithm may exist for the detection of the presence of unresolved targets with fixed-amplitudes. In fact, if the targets are known to have only amplitudes that are fixed and with random relative phases, the results of Section 3.8 indicate clearly that the measured amplitude of the sum signal can be used to detect the presence of unresolved targets with fixed-amplitudes.

The predicted performance of the detection algorithm in [51] with five pulses is cited for two 15-dB Rayleigh targets (*i.e.*, SNR = 18 dB) situated symmetrically about the boresight as $P_{DMT} = 0.77$ and $P_{FDMT} = 0.05$. Note that the performance predictions in [51] are based on the use of the true SNR and DOA in the selection of the detection threshold, while the detection threshold for the GML algorithm developed in this chapter does not require this knowledge. The case[6] considered in [51] corresponds to $\eta_1 = -\eta_2 = 0.25$ and $\Re_{R1} = \Re_{R2} = 15$ dB, which gives $\hat{p} = 1.0$ and $q = 4.94$. For this case, the predicted performance of the GML detection algorithm with five pulses is $P_{FDMT} = 0.05$ and $P_{DMT} = 0.94$. A Monte Carlo simulation with 25,000 experiments was conducted to confirm the performance improvement. The decision rule was implemented with $\lambda_d = 16.9$ to achieve a $P_{FDMT} = 0.05$. The percent of detections in the Monte Carlo simulations was 94 percent. Thus, the predicted performance agrees with that of the simulations as shown in Figure 6.5. Also, for this case, the predicted performance of the GML detection algorithm with three pulses is $P_{FDMT} = 0.05$ and $P_{DMT} = 0.81$. The decision rule was implemented with $\lambda = 11.1$ to achieve a $P_{FDMT} = 0.05$, and the percent of detections in the Monte Carlo simulations was 81 percent. Thus, the simulation results confirm the superior performance of the GML algorithm. Furthermore, the GML algorithm without a *priori* knowledge of SNR and DOA provides better detection than the algorithm in [51] with knowledge of the SNR and DOA. This improvement in detection performance can be attributed to the use of the amplitude-conditioned PDF of the monopulse ratios and the use of the likelihood ratio for the detection [22, p. 64].

---

[6] Since $\frac{\pi}{2}$ was omitted from the trigonometric functions in [51], this case does not correspond to two targets separated by one-half beamwidth as stated in [51].
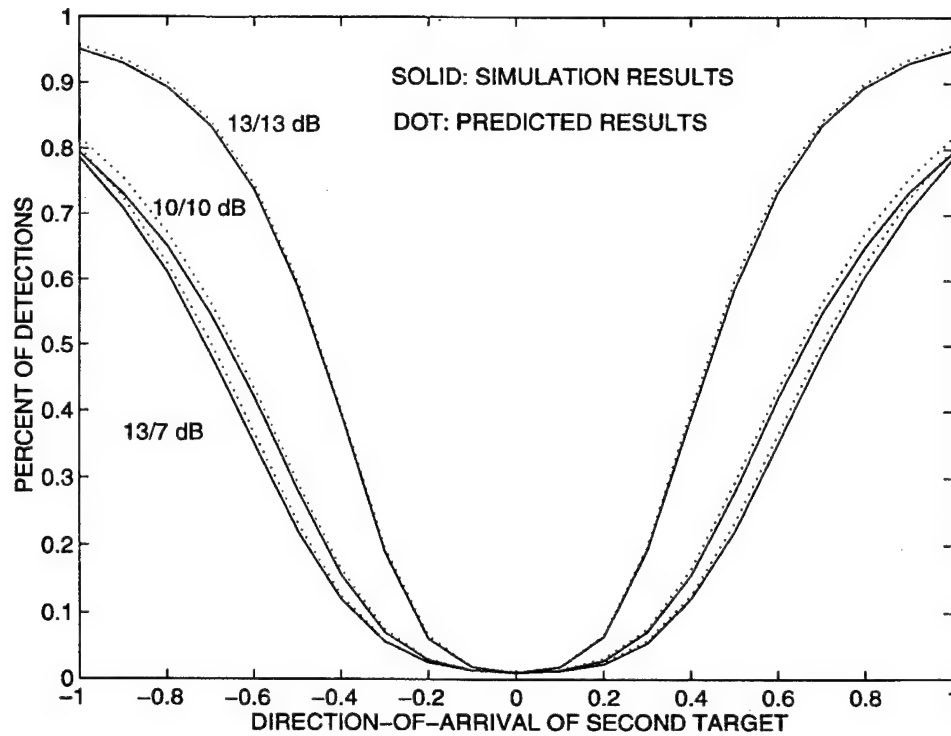
Figure 6.4 Simulation Results for Target 1 at the Antenna Boresight
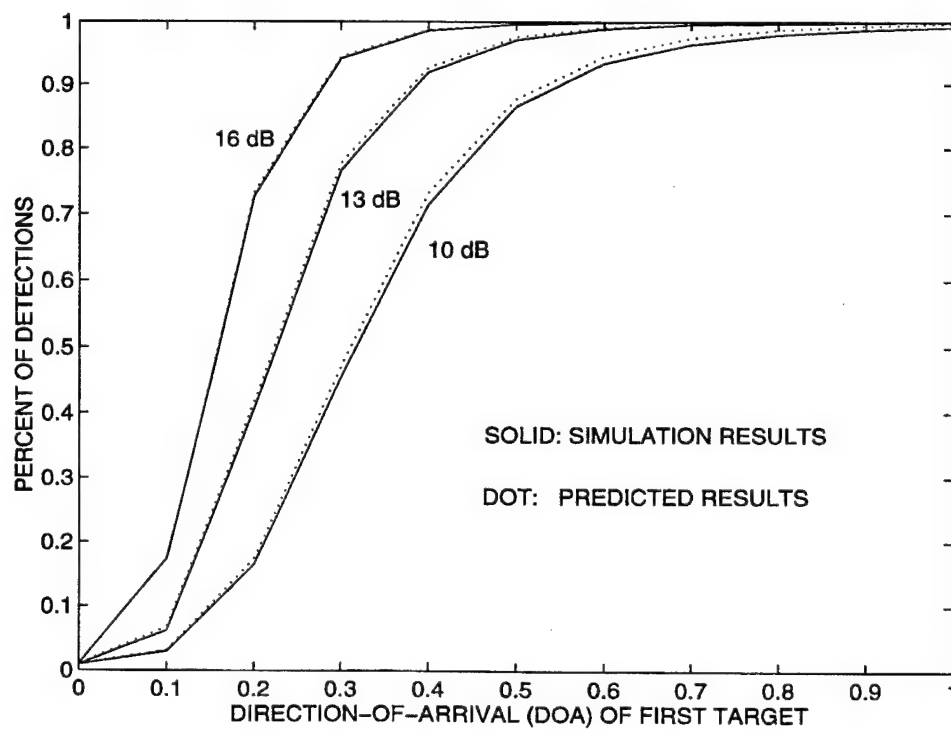
Figure 6.5 Simulation Results for Two Targets Symmetric About the Boresight
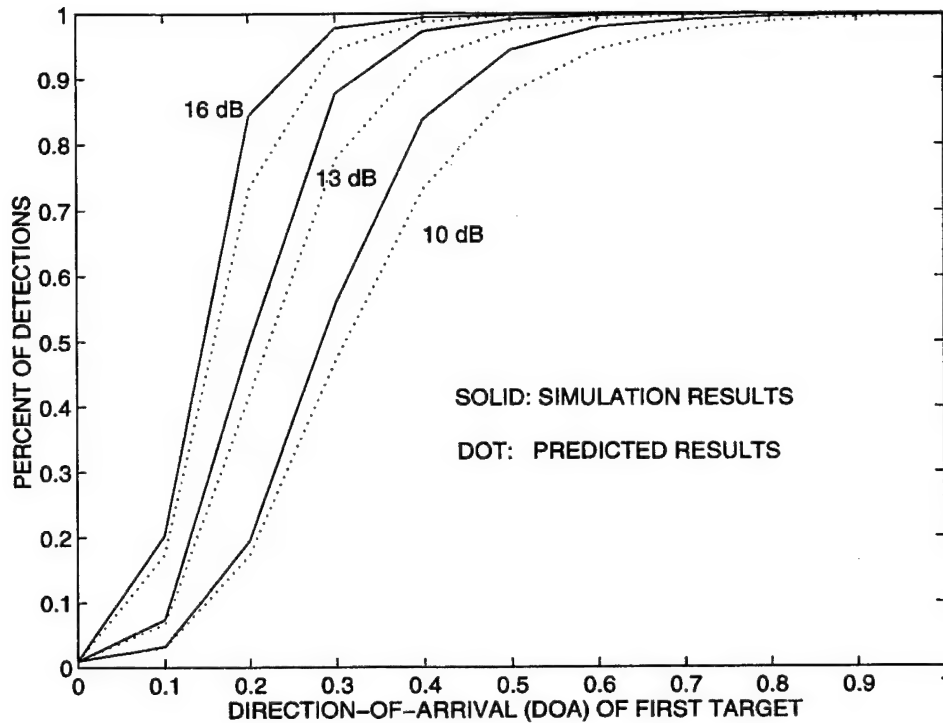
Figure 6.6 Simulation Results for Two Fixed-Amplitude Targets Symmetric About the Boresight

Concluding Remarks

The Neyman-Pearson algorithm for GML detection of the presence of multiple unresolved Rayleigh targets requires no *a priori* specifications of the SNR or DOA of the target of interest. However, the design value of the false-alarm rate is not necessarily achieved with four pulses when the SNR is 7 dB and below, and the DOA is near one-half of a beamwidth off the antenna boresight. Also, the probability of detecting target multiplicity with fewer than six pulses and targets of moderate SNRs (*i.e.*, 13 dB or less) is shown by Figure 6.2 to be very low when the targets are separated by less than one-fourth of a beamwidth. The performance predictions that were found agree very well with the results of Monte Carlo simulations.

The GML detection algorithm without knowledge of the SNR and DOA was shown via simulations to be superior to the detection algorithm developed in [51] that requires knowledge of the SNR and DOA to set the detection threshold. For two unresolved Rayleigh targets separated by one-half of a beamwidth, the new algorithm with five pulses provides $P_{DMT} = 0.94$ for a $P_{FDMT} = 0.05$, while the algorithm of [51] provides $P_{DMT} = 0.77$ for a $P_{FDMT} = 0.05$. Also, for this case from [51], the performance of the GML detection algorithm with three pulses was $P_{FDMT} = 0.05$

and $P_{DMT} = 0.81$. Thus, the GML detection algorithm with three pulses provides better detection than the algorithm of [51] with five pulses. Also, the design of the GML detection algorithm is easier than the design of the algorithm in [51] in that the design of the GML algorithm involves the chi-square distribution, while the design of the algorithm in [51] involves the F-distribution [52, p. 946].

The statistics associated with detection of the presence of two unresolved, fixed-amplitude targets is intractable. However, the simulations results showed that the GML detection algorithm provides detection of the presence of unresolved targets with fixed amplitudes that exceeds the predicted performance for two unresolved Rayleigh targets.

Chapter 7

CONCLUSIONS AND FUTURE RESEARCH

When target echoes interfere in a monopulse radar system, the DOA estimate indicated by the in-phase monopulse ratio can wander far beyond the angular separation of the targets. In addition to closely-spaced targets, the problem of unresolved or merged measurements also occurs when targets are observed in the presence of jammer signals or sea-surface-induced multipath. The failure to detect the presence of this interference and address it in the DOA estimation can be catastrophic to the performance of the tracking algorithm, since its position and velocity estimates determine the association of any subsequent measurements to the target. Monopulse processing for tracking unresolved targets was addressed through amplitude estimation and discrimination, probability distribution of the complex monopulse ratio, DOA estimation, and detection of the presence of unresolved targets.

Estimation of the target amplitude parameters and discrimination between various models for the target amplitude fluctuations were considered in Chapter 3. The PDF of the measured amplitude of the sum signal was developed for M unresolved Rician targets. CRLBs, ML estimators, and MM estimators were developed for the amplitude parameters of Rayleigh, fixed-amplitude, new dominant-plus-Rayleigh, and Rician targets. The waveform requirements for reliable discrimination between Rayleigh, fixed-amplitude, and dominant-plus-Rayleigh targets were also be considered. The PDF of the measured amplitude of two unresolved Rician targets was studied and shown to conflict with the results of [17]. MM estimators were developed for the target amplitudes of two unresolved, fixed-amplitude targets, and the target amplitude and the cosine of the phase difference between the target and specular reflections from the sea surface. Future research includes the development of ROC curves for the detection of the new dominant-plus-Rayleigh target and the extension of the results for a fixed-amplitude target in multipath to a Rayleigh target in multipath. Other research opportunities include the extension of the technique for target

amplitude discrimination to multiple radar dwells and optimal allocation of radar resources for discrimination.

The amplitude-conditioned PDF and the statistics of the complex monopulse ratio are developed in Chapter 4 for M unresolved Rician targets. Conditioning the PDF of the monopulse ratio on the measured amplitude of the sum signal gives in-phase and quadrature monopulse ratios that are approximately Gaussian random variables so that the PDF is specified approximately by the means and variances. The amplitude-conditioned PDF and the statistics were developed for various cases of a single target and two unresolved targets, and a fixed-amplitude target in the presence of sea-surface-induced multipath. For a single pulse and a resolved target, the in-phase and quadrature monopulse ratios were shown to be uncorrelated, non-Gaussian random variables for a nonzero DOA, and the marginal PDF of the quadrature ratio was shown to have a mean of zero and be symmetric about zero for all DOAs. For M unresolved Rayleigh targets, the in-phase and quadrature monopulse ratios were shown to be conditionally independent, Gaussian random variables with equal variances, and the quadrature monopulse ratio was shown to have a mean of zero. The PDF and statistics of the monopulse ratios were also developed for the case of two unresolved, fixed-amplitude targets with a given relative phase. Future research will involve the development of the statistics of the monopulse ratios for a random relative phase and two fixed-amplitude targets. These statistics for a random phase could be used to detect the presence of two unresolved, fixed-amplitude targets and estimate the DOAs. The PDF and statistics of the monopulse ratios were also developed for a fixed-amplitude target in the presence of sea-surface-induced multipath. Further research will involve the extension of the statistics for a fixed-amplitude target to a Rayleigh target in the presence of sea-surface-induced multipath.

DOA estimation was considered in Chapter 5 for single resolved targets and two unresolved targets. For a single target, the DOA estimation with multiple pulses from a Rayleigh target was considered along with single-pulse DOA estimation. DOA estimation was also considered for a Rayleigh target in the presence of a Gaussian noise jammer and two unresolved Rayleigh targets with known relative RCS. Further research is needed to relax this requirement for a known relative RCS. One potential approach to relaxing this requirement involves the use of two spatially-offset radar dwells. However, development of the DOA estimation algorithm is not considered in this report, because the estimation algorithm and the associated analysis will

be quite cumbersome. Further research is needed to develop a technique for DOA estimation for two unresolved, fixed-amplitude targets and a fixed-amplitude target in the presence of multipath. Further research is also needed to identify the system-level benefits of array signal processing [2] versus monopulse processing for DOA estimation of unresolved targets.

The detection of the presence of two unresolved Rayleigh targets was considered in Chapter 6. A GLRT was used to develop a Neyman-Pearson algorithm for the detection of the presence of unresolved Rayleigh targets, and performance predictions of the new algorithm were shown to agree closely with the results of simulation studies. Further research is needed to develop a technique for detecting the presence of two unresolved, fixed-amplitude targets. This effort will again require the development of the PDF and statistics for two unresolved, fixed-amplitude targets with random relative phase as discussed above. However, simulations results showed that the GML detection algorithm developed in Chapter 6 provides detection of the presence of unresolved targets with fixed amplitudes that exceeds the predicted performance for two unresolved Rayleigh targets.

While additional research is needed to develop the algorithms for supporting the tracking of unresolved targets with fixed amplitudes, the basic algorithms needed to support the tracking of two unresolved Rayleigh targets has been completed in this report. These basic algorithms involve the detection of the presence of unresolved Rayleigh targets and DOA estimation for two unresolved Rayleigh targets. Previous approaches to DOA estimation of unresolved targets require a *priori* knowledge of the number of targets present (usually restricted to two), a very high SNR (often 40 to 50 dB), and the absence of irregular or diffuse reflections. Through a stochastic approach to the tracking of unresolved targets, these restrictions have been relaxed for Rayleigh targets. The requirement for a *priori* knowledge of the number of targets has been relaxed to one or two targets, where the presence of unresolved targets is detected, not known a *priori*. The required SNR is relaxed from 40 dB to near 20 dB, which is achievable with conventional monopulse radars. The required absence of irregular or diffuse reflections has been relaxed through the inclusion of models for the target amplitude fluctuations in the problem formulations (*e.g.*, a Rayleigh target). However, to fully utilize the results of this report, the results must be incorporated into the tracking (*i.e.*, state estimation) and data association algorithms [53]. One approach to the state estimation and data association involves the Nearest-Neighbor

Probabilistic Data Association (NNPDA) algorithm [54]. The NNPDA algorithm assigns measurements to tracks under the hypotheses of one target or two targets. The addition of a hypothesis of unresolved targets will allow the NNPDA algorithm to address the tracking of closely-spaced or unresolved targets. This NNPDA Merged Measurements (NNPDAMM) algorithm would utilize the PDFs used in Chapter 6 as measures of the likelihood of a merged measurement (*i.e.*, unresolved targets) for the data association.

REFERENCES

1. S. M. Sherman, *Monopulse Principles and Techniques,* Artech House, Inc., Dedham, MA, 1984.

2. S. Haykin, Ed., *Array Signal Processing,* Prentice-Hall, Inc., Englewood Cliffs, NJ, 1985.

3. I. Kanter, "Multiple Gaussian Targets: The Track-on-Jam Problem," *IEEE Trans. Aero. Elect. Sys.,* Nov 1977, pp. 620-623.

4. S. M. Sherman, *Complex Indicted Angles in Monopulse Radar,* Ph.D. Dissertation, University of Pennsylvania, 1965.

5. D. K. Barton, "Low-Angle Radar Tracking," *Proc. of IEEE,* Jun 1974, pp. 687-704.

6. P. Z. Peebles and R. S. Berkowitz, "Multiple-Target Monopulse Radar Processing Techniques," *IEEE Trans. Aero. Elect. Sys.,* Nov 1968, pp. 845-854.

7. W. D. White, "Low Angle Radar Tracking in the Presence of Multipath," *IEEE Trans. Aero. Elect. Sys.,* Nov 1974, pp. 835-852.

8. A. A. Ksienski and R. B. McGhee, "A Decision Theoretic Approach to the Angular Resolution and Parameter Estimation Problem for Multiple Targets," *IEEE Trans. Aero. Elect. Sys.,* May 1968, pp. 443-455.

9. D. K. Barton, Ed., *Radar Resolution & Multipath Effects,* Artech House, Inc., Dedham, MA, 1975.

10. Y. Bar-Shalom, and X.R. Li *Estimation and Tracking: Principles, Techniques, and Software,* Artech House, Inc., Norwood, MA, 1993.

11. H. L., Van Trees, *Detection, Estimation, and Modulation Theory,* John Wiley & Sons, Inc., 1968.

12. A. Papoulis, *Probability, Random Variables, and Stochastic Processes, 2nd Ed.,* McGraw-Hill, Inc., New York, NY, 1984.

13. I. S. Gradshteyn and I.M. Ryzhik, A. Jeffrey, Ed., *Table of Integrals, Series, and Products,* Fifth Edition, A. Jeffrey, Ed., Academic Press, Inc., San Diego, CA, 1990.

14. M. I. Skolnik, *Introduction to Radar Systems,* McGraw-Hill, Inc., New York, NY, 1980.

15. J.V. DiFranco and W.L. Rubin, *Radar Detection,* Artech House, Inc., Dedham, MA, 1980.

16. W. D. Blair and M. Brandt-Pearce, "Estimation and Discrimination for Swerling Targets, *Proc. of 28th IEEE Southeastern Symp. on Sys. Theory*, Baton Rouge, LA, Apr 1996, pp. 280-284.

17. J. K. Jao and M. Elbaum, "First-Order Statistics of a Non-Rayleigh Fading Signal and Its Detection," *Proc. of the IEEE*, Jul 1978, pp. 781-789.

18. S. O. Rice, "Mathematical Analysis of Random Noise," *Selected Papers on Noise and Stochastic Processes*, N. Wax, Ed., Dover, New York, NY, 1954.

19. H. Stark and J. W. Woods, *Probability, Random Processes, and Estimation Theory for Engineers*, Prentice-Hall, Inc., Englewood Cliffs, NJ, 1986.

20. E. Daeipour, W. D. Blair, and Y. Bar-Shalom, "Bias Compensation and Tracking With Monopulse Radars in the Presence of Multipath," *IEEE Trans. Aero. Elect. Sys.*, Jul 1997.

21. G. W. Groves, W. D. Blair, and J. E. Conte, *Monopulse Radar and Tracking Simulation for Study of Multipath Effects*, Naval Surface Warfare Center Dahlgren Division, Technical Report NSWCDD/TR-97/30, Mar 1997.

22. D. Kazakos and P. Papantoni-Kazakos, *Detection and Estimation*, Computer Science Press, New York, NY, 1990.

23. E. Koos, "Digital RF Memories Enter Second Decade," *Journal of Electronic Defense*, Aug 1985, pp. 49-51.

24. W. D. Blair and G. A. Watson, *Benchmark Problem for Radar Resource Allocation and Tracking Maneuvering Targets in the Presence of ECM*, Naval Surface Warfare Center Dahlgren Divison Technical Report NSWCDD/TR-96/10, Sep 1996.

25. K. K. Talukdar and W. D. Lawing, "Estimation of the Parameters of the Rice Distribution," *Journal of Acoustical Society of America*, Mar 1991, pp. 1193-1197.

26. R. Manasse, "Maximum Angular Accuracy of Tracking a Radio Star by Lobe Comparison," *IRE Trans. Ant. and Prop.*, Jan 1960, pp. 50-56.

27. S. Sharenson, "Angle Estimation Accuracy With a Monopulse Radar in the Search Mode," *IRE Trans. Aero. and Nav. Elect.*, Sep 1962, pp. 175-179.

28. I. Kanter, "The Probability Density Function of the Monopulse Ratio for N Looks at a Combination of Constant and Rayleigh Targets," *IEEE Trans. Infor. Theory*, Sep 1977, pp. 643-648.

29. I. Kanter, "Multiple Gaussian Targets: The Track-on-Jam Problem," *IEEE Trans. Aero. Elect. Sys.*, Nov 1977, pp. 620-623.

30. I. Kanter, "Three Theorems on the Moments of the Monopulse Ratio," *IEEE Trans. Infor. Theory*, Mar 1978, pp. 272-276.

31. I. Kanter, "The Effect of Jamming on Monopulse Accuracy," *IEEE Trans. Aero. Elect. Sys.*, Sep 1979, pp. 738-741.

32. I. Kanter, "Varieties of Average Monopulse Responses to Multiple Targets," *IEEE Trans. Aero. Elect. Sys.*, Jan 1981, pp. 25-28.

33. S. J. Asseo, "Detection of Target Multiplicity Using Quadrature Monopulse Angle," *IEEE Aero. Elect. Sys.*, Mar 1981, pp. 271-280.

34. B. E. Tullsson, "Monopulse Tracking of Rayleigh Targets: A Simple Approach," *IEEE Trans. Aero. Elect. Sys.*, May 1991, pp. 520-531.

35. A. D. Seifer, "Monopulse-Radar Angle Tracking In Noise or Noise Jamming," *IEEE Trans. Aero. Elect. Sys.*, Jul 1992, pp. 622-637.

36. A. D. Seifer, "Monopulse-Radar Angle Measurement in Noise," *IEEE Trans. Aero. Elect. Sys.*, Jul 1994, pp. 950-957..

37. G. W. Groves, W. D. Blair, and W. C. Chow, "Probability Distribution of the Complex Monopulse Ratio with Arbitrary Correlation Between the Channels," *IEEE Trans. Aero. Elect. Sys.*, Oct 1997.

38. B. H. Borden, and M. L. Mumford, "A Statistical Glint/Radar Cross Section Model," *IEEE Trans. Aero. Elect. Sys.*, Apr 1983, pp. 781-785.

39. A. M. Mood, F. A. Graybill, and D. C. Boes, *Introduction to the Theory of Statistics, 3rd Ed.*, McGraw-Hill, Inc., New York, NY, 1974.

40. E. Mosca, "Maximum Likelihood Angle Estimation in Amplitude Comparison Monopulse Systems Operation On a Signal Pulse Bias," *Alta Frequenza* (English Issue), May 1968, pp. 408-414.

41. E. Mosca, "Angle Estimation in Amplitude Comparison Monopulse Systems," *IEEE Trans. Aero. and Elect. Sys.*, Mar 1969, pp. 205-212.

42. S. M. Sherman, "Complex Indicated Angles Applied To Unresolved Targets and Multipath," *IEEE Trans. Aero. and Elect. Sys.*, Jan 1971, pp. 160-170.

43. F. E. Daum, "Angular Estimation Accuracy for Unresolved Targets," *Proc. of 1987 American Control Conference*, Minneapolis, MN, Jun 1987, pp. 1135-36.

44. R. S. Berkowitz and S. M. Sherman, "Information Derivable from Monopulse Radar Measurements of Two Unresolved Targets," *IEEE Trans. Aero. and Elect. Sys.*, Sep 1971, pp. 1011-1013.

45. P. Z. Peebles, and L. Goldman, "Radar Performance with Multipath Using Complex Angle," *IEEE Trans. Aero. and Elect. Sys.*, Jan 1971, pp. 171-178.

46. M. D. Symonds and J. M. Smith, "Multifrequency Complex-Angle Tracking of Low-Level Targets," *Proc. of IEE International Radar Conf.*, London, England, Oct 23-25, 1973, pp. 166-171.

47. D. D. Howard, S. M. Sherman, and D. N. Thomson, "Experimental Results of the Complex Indicated Angle Technique for Elevation Measurements in the Multipath Region," *IEEE Trans. Aero. Elect. Sys.*, Nov 1974, pp. 779-784.

48. Y. Bar-Shalom and T. E. Fortmann, *Tracking and Data Association*, Academic Press, Inc., Orlando, FL, 1988.

49. S. J. Asseo, "Effect of Monopulse Signal Thresholding on Tracking Multiple Targets," *IEEE Trans. Aero. Elect. Sys.*, Jul 1974, pp. 504-509.

50. R. J. McAulay and T. P. McGarty, "Maximum-Likelihood Detection of Unresolved Radar Targets and Multipath," *IEEE Trans. Aero. Elect. Sys.*, Nov 1974, pp. 821-829.

51. P. L. Bogler, "Detecting the Presence of Target Multiplicity," *IEEE Trans. Aero. Elect. Sys.*, Mar 1986, pp. 197-203.

52. M. Abramowitz and I. A. Stegun, Ed., *Handbook of Mathematical Functions, with Formulas, Graphs, and Mathematical Tables*, U.S. Government Printing Office, Washington, DC, 1972, and John Wiley & Sons, Inc. 1972.

53. Y. Bar-Shalom and X. R. Li, *Multitarget-Multisensor Tracking: Principles and Techniques*, YBS Publishers, Box U-157, Storrs, CT, 1995.

54. R. J. Fitzgerald, "Development of Practical PDA Logic for Multitarget Tracking by Multiprocessor," in *Multitarget-Multisensor Tracking: Advanced Applications*, Y. Bar-Shalom, Ed., Artech House, Inc., Norwood, MA, 1990.

Appendix A

DERIVATION OF THE PDF AND STATISTICS
OF THE COMPLEX MONOPULSE RATIO FOR
UNRESOLVED RICIAN TARGETS

In a typical monopulse radar system, the outputs of the receivers are match filtered, and the in-phase and quadrature portions of the sum and difference signals for the merged measurements from M Rician targets can be expressed as

$$s_I = \sum_{i=1}^{M} \left(\alpha_i \cos \phi_i + \beta_i \cos \varphi_i \right) + n_{SI} \qquad (A.1)$$

$$s_Q = \sum_{i=1}^{M} \left(\alpha_i \sin \phi_i + \beta_i \sin \varphi_i \right) + n_{SQ} \qquad (A.2)$$

$$d_I = \sum_{i=1}^{M} \left(\alpha_i \eta_i \cos \phi_i + \beta_i \eta_i \cos \varphi_i \right) + n_{dI} \qquad (A.3)$$

$$d_Q = \sum_{i=1}^{M} \left(\alpha_i \eta_i \sin \phi_i + \beta_i \eta_i \sin \varphi_i \right) + n_{dQ} \qquad (A.4)$$

where

$\alpha_i =$ amplitude from the fixed-amplitude part of target i

$\beta_i =$ amplitude from the Rayleigh part of target i

$\phi_i =$ phase of the fixed-amplitude part of target i

$\varphi_i =$ phase of the Rayleigh part of target i

$\eta_i =$ Direction-Of-Arrival (DOA) parameter of target i

$n_{SI} \sim N(0, \sigma_S^2)$

$n_{SQ} \sim N(0, \sigma_S^2)$

$n_{dI} \sim N(0, \sigma_d^2)$

$n_{dQ} \sim N(0, \sigma_d^2)$

with $N(\bar{x}, \sigma^2)$ denoting a Gaussian distribution with mean $\bar{x}$ and variance σ^2. Also, with $E[\cdot]$ denoting expected value,

$$E[n_{SI}n_{SQ}] = 0 \qquad (A.5)$$

$$E[n_{dI}n_{dQ}] = 0 \qquad (A.6)$$

$$E[n_{SI}n_{dI}] = \rho\sigma_S\sigma_d \qquad (A.7)$$

$$E[n_{SQ}n_{dQ}] = \rho\sigma_S\sigma_d \qquad (A.8)$$

The phases, φ_i, are independent and uniformly distributed on $(-\pi, \pi]$. The Rayleigh parts of the target amplitudes are also independent, and the PDF of the Rayleigh part of target i is given by

$$f(\beta_i|\beta_{i0}) = \frac{\beta_i}{\beta_{i0}^2} \exp\left[-\frac{\beta_i^2}{2\beta_{i0}^2}\right], \quad \beta_i \geq 0 \qquad (A.9)$$

Since β_i are Rayleigh distributed and the φ_i are uniformly distributed on $(-\pi, \pi]$, s_I, s_Q, d_I, and d_Q are jointly Gaussian, independent random variables, when the α_i and ϕ_i are given. Let

$$\bar{s}_I = E[s_I|\Theta] = \sum_{i=1}^{M} \alpha_i \cos \phi_i \qquad (A.10)$$

$$\bar{s}_Q = E[s_Q|\Theta] = \sum_{i=1}^{M} \alpha_i \sin \phi_i \qquad (A.11)$$

$$\bar{d}_I = E[d_I|\Theta] = \sum_{i=1}^{M} \alpha_i\eta_i \cos \phi_i \qquad (A.12)$$

$$\bar{d}_Q = E[d_Q|\Theta] = \sum_{i=1}^{M} \alpha_i\eta_i \sin \phi_i \qquad (A.13)$$

where Θ is the parameter set $\{\alpha_1, \phi_1, \beta_{10}, \eta_1, \ldots, \alpha_M, \phi_M, \beta_{M0}, \eta_M, \sigma_S, \sigma_d\}$. Also, let

$$p_{11} = \text{VAR}[s_I|\Theta] = \text{VAR}[s_Q|\Theta] = \sum_{i=1}^{M} \beta_{i0}^2 + \sigma_S^2 \qquad (A.14)$$

$$p_{22} = \text{VAR}[d_I|\Theta] = \text{VAR}[d_Q|\Theta] = \sum_{i=1}^{M} \eta_i^2\beta_{i0}^2 + \sigma_d^2 \qquad (A.15)$$

$$p_{12} = \text{COV}[s_I, d_I|\Theta] = \text{COV}[s_Q, d_Q|\Theta] = \sum_{i=1}^{M} \eta_i\beta_{i0}^2 + \rho\sigma_S\sigma_d \qquad (A.16)$$

where $\text{VAR}[\cdot]$ denotes variance and $\text{COV}[\cdot, \cdot]$ denotes covariance. Note that

$$\text{COV}[s_I, s_Q|\Theta] = \text{COV}[d_I, d_Q|\Theta] = 0 \qquad (A.17)$$

A-2

and

$$\text{COV}[s_I, d_Q|\Theta] = \text{COV}[d_I, s_Q|\Theta] = 0 \qquad (A.18)$$

Letting Λ and ψ denote the measured amplitude and phase of the sum signal gives

$$s_I = \Lambda \cos \psi \qquad (A.19)$$

$$s_Q = \Lambda \sin \psi \qquad (A.20)$$

where $-\pi < \psi \leq \pi$. Writing the measured amplitude of the sum signal in terms of SNR gives

$$\Re_o = \frac{\Lambda^2}{2\sigma_S^2} \qquad (A.21)$$

where $\Re_o$ is referred to as the observed SNR.

The SNR of Rician target i is given by

$$\Re_i = E[\Re_o|\Theta] = \Re_{Fi} + \Re_{Ri} \qquad (A.22)$$

where

$$\Re_{Fi} = \frac{\alpha_i^2}{2\sigma_S^2} \qquad (A.23)$$

$$\Re_{Ri} = \frac{\beta_{i0}^2}{\sigma_S^2} \qquad (A.24)$$

Thus, $\Re_{Fi}$ denotes the SNR associated with the fixed-amplitude part of target i, and $\Re_{Ri}$ denotes the SNR associated with the Rayleigh part of target i. Also, let

$$\Re_F = \sum_{i=1}^{M} \Re_{Fi} \qquad (A.25)$$

$$\Re_R = \sum_{i=1}^{M} \Re_{Ri} \qquad (A.26)$$

The development of the PDF of the observed SNR $\Re_o$ utilizes the PDF of the measured amplitude Λ, which is derived by applying the transformation of random variables in (A.19) and (A.20) to the PDF of s_I and s_Q and integrating the results with respect to ψ. The following theorem gives the results in a general form.

Theorem A.1 Let the in-phase and quadrature signals s_I and s_Q be Gaussian signals with

$$\bar{s}_I = E[s_I|\Theta] \tag{A.27}$$

$$\bar{s}_Q = E[s_Q|\Theta] \tag{A.28}$$

$$p_{11} = E[(s_I - \bar{s}_I)^2|\Theta] = E[(s_Q - \bar{s}_Q)^2|\Theta] \tag{A.29}$$

and $E[(s_I - \bar{s}_I)(s_Q - \bar{s}_Q)|\Theta] = 0$, where Θ denotes the set of given parameters. Then the PDF of the measured amplitude of the signal is given by

$$f(\Lambda|\Theta) = \frac{\Lambda}{p_{11}} I_0\left(\frac{\Lambda}{p_{11}}\sqrt{\bar{s}_I^2 + \bar{s}_Q^2}\right) \exp\left[-\frac{1}{2p_{11}}(\Lambda^2 + \bar{s}_I^2 + \bar{s}_Q^2)\right] \tag{A.30}$$

where $I_0(\cdot)$ is the zero-order modified Bessel function of the first kind. The PDF of the observed SNR of the signal is given by

$$f(\Re_o|\Theta) = \frac{1}{\Re_R + 1} I_0\left(\frac{2\sqrt{\Re_o}}{\Re_R + 1}\sqrt{\frac{\bar{s}_I^2}{2\sigma_S^2} + \frac{\bar{s}_Q^2}{2\sigma_S^2}}\right) \exp\left[-\frac{1}{\Re_R + 1}\left(\Re_o + \frac{1}{2\sigma_S^2}(\bar{s}_I^2 + \bar{s}_Q^2)\right)\right] \tag{A.31}$$

and

$$E[\Re_o|\Theta] = \frac{1}{2\sigma_S^2}(\bar{s}_I^2 + \bar{s}_Q^2) + \Re_R + 1 \tag{A.32}$$

$$\text{VAR}[\Re_o|\Theta] = \left(\Re_R + 1\right)\left(\frac{1}{\sigma_S^2}(\bar{s}_I^2 + \bar{s}_Q^2) + \Re_R + 1\right) \tag{A.33}$$

Proof:

The PDF of s_I and s_Q is given by

$$f(s_I, s_Q|\Theta) = \frac{1}{2\pi p_{11}} \exp\left[-\frac{1}{2p_{11}}\left((s_I - \bar{s}_I)^2 + (s_Q - \bar{s}_Q)^2\right)\right] \tag{A.34}$$

Applying the transformation of random variables [A-1, p. 143] in (A.19) and (A.20) in (A.34) gives

$$f(\Lambda, \psi|\Theta) = \frac{\Lambda}{2\pi p_{11}} \exp\left[-\frac{1}{2p_{11}}\left((\Lambda\cos\psi - \bar{s}_I)^2 + (\Lambda\sin\psi - \bar{s}_Q)^2\right)\right]$$

$$= \frac{\Lambda}{2\pi p_{11}} \exp\left[-\frac{1}{2p_{11}}\left(\Lambda^2 + \bar{s}_I^2 + \bar{s}_Q^2\right) + \frac{\Lambda}{p_{11}}\left(\bar{s}_I\cos\psi + \bar{s}_Q\sin\psi\right)\right] \tag{A.35}$$

Using [A-2, No. 3.937.2] for integration of (A.35) with respect to ψ from $-\pi$ to π gives the PDF of Λ as

$$f(\Lambda|\Theta) = \int_{-\pi}^{\pi} f(\Lambda, \psi|\Theta)\, d\psi$$

$$= \frac{\Lambda}{p_{11}} I_0\left(\frac{\Lambda}{p_{11}}\sqrt{\bar{s}_I^2 + \bar{s}_Q^2}\right) \exp\left[-\frac{1}{2p_{11}}(\Lambda^2 + \bar{s}_I^2 + \bar{s}_Q^2)\right] \tag{A.36}$$

Using the transformation of the random variable [A-1, p. 95] of (A.26) in (A.36) and expressing p_{11} in terms of $\Re_R$ gives (A.31). Then (A.32) is given by

$$
\begin{aligned}
E[\Re_o | \Theta] &= \int_0^\infty \Re_o \ f(\Re_o | \Theta) \ d\Re_o \\
&= \frac{1}{\Re_R + 1} \exp\left[-\frac{1}{2\sigma_S^2}(\bar{s}_I^2 + \bar{s}_Q^2) \right] \\
&\quad \times \int_0^\infty \Re_o I_0\left(\frac{2\sqrt{\Re_o}}{\Re_R + 1} \sqrt{\frac{\bar{s}_I^2}{2\sigma_S^2} + \frac{\bar{s}_Q^2}{2\sigma_S^2}} \right) \exp\left[-\frac{\Re_o}{\Re_R + 1} \right] d\Re_o \\
&= \frac{1}{2\sigma_S^2}(\bar{s}_I^2 + \bar{s}_Q^2) + \Re_R + 1
\end{aligned}
\tag{A.37}
$$

where [A-2, No. 6.643.2] provides the definite integral. Also, (A.33) is given by

$$
\begin{aligned}
E[\Re_o^2 | \Theta] &= \int_0^\infty \Re_o^2 f(\Re_o | \Theta) \ d\Re_o \\
&= \frac{1}{\Re_R + 1} \exp\left[-\frac{1}{2\sigma_S^2}(\bar{s}_I^2 + \bar{s}_Q^2) \right] \\
&\quad \times \int_0^\infty \Re_o^2 I_0\left(\frac{\sqrt{2\Re_o}}{\Re_R + 1} \sqrt{\frac{\bar{s}_I^2}{2\sigma_S^2} + \frac{\bar{s}_Q^2}{2\sigma_S^2}} \right) \exp\left[-\frac{\Re_o}{\Re_R + 1} \right] d\Re_o \\
&= 2\left(\frac{1}{2\sigma_S^2}(\bar{s}_I^2 + \bar{s}_Q^2) + \Re_R + 1 \right)^2 - \left(\frac{1}{2\sigma_S^2}(\bar{s}_I^2 + \bar{s}_Q^2) \right)^2
\end{aligned}
\tag{A.38}
$$

where [A-2, No. 6.643.2] provides the definite integral. Using

$$
\text{VAR}[\Re_o | \Theta] = E[\Re_o^2 | \Theta] - (E[\Re_o | \Theta])^2
\tag{A.39}
$$

with (A.37) and (A.38) gives (A.33).   **Q.E.D.**

The PDF and statistics of the complex monopulse ratio are developed next. Denoting $s = s_I + js_Q$ and $d = d_I + jd_Q$, the in-phase and quadrature parts of the monopulse ratio are given by

$$
y_I = \text{Re}\left(\frac{d}{s} \right) = \frac{d_I s_I + s_Q d_Q}{s_I^2 + s_Q^2}
\tag{A.40}
$$

$$
y_Q = \text{Im}\left(\frac{d}{s} \right) = \frac{d_Q s_I - d_I s_Q}{s_I^2 + s_Q^2}
\tag{A.41}
$$

The joint PDF of y_I and y_Q is obtained by applying the one-to-one transformation of random variables of (A.19), (A.20), (A.40), and (A.41) in the PDF $f(s_I, s_Q, d_I, d_Q | \Theta)$, integrating the result with respect to ψ, and conditioning the density on Λ. The following theorem gives the result in a general form.

Theorem A.2 Let the in-phase and quadrature parts of the sum and difference signals be Gaussian signals with

$$\bar{s}_I = E[s_I|\Theta] \tag{A.42}$$

$$\bar{s}_Q = E[s_Q|\Theta] \tag{A.43}$$

$$\bar{d}_I = E[d_I|\Theta] \tag{A.44}$$

$$\bar{d}_Q = E[d_Q|\Theta] \tag{A.45}$$

$$p_{11} = E[(s_I - \bar{s}_I)^2|\Theta] = E[(s_Q - \bar{s}_Q)^2|\Theta] \tag{A.46}$$

$$p_{22} = E[(d_I - \bar{d}_I)^2|\Theta] = E[(d_Q - \bar{d}_Q)^2|\Theta] \tag{A.47}$$

$$p_{12} = E[(s_I - \bar{s}_I)(d_I - \bar{d}_I)|\Theta] = E[(s_Q - \bar{s}_Q)(d_Q - \bar{d}_Q)|\Theta] \tag{A.48}$$

and $E[(s_I - \bar{s}_I)(s_Q - \bar{s}_Q)|\Theta] = E[(d_I - \bar{d}_I)(d_Q - \bar{d}_Q)|\Theta] = 0$, where Θ denotes the set of given parameters. Then the PDF of y_I and y_Q conditioned on the measured amplitude of the sum signal is given by

$$
\begin{aligned}
f(y_I, y_Q|\Lambda, \Theta) =& \frac{\Lambda^2 p_{11}}{2\pi(p_{11}p_{22} - p_{12}^2)I_0\Big(\frac{\Lambda}{p_{11}}\sqrt{\bar{s}_I^2 + \bar{s}_Q^2}\Big)} \\
&\times I_0\Big(\frac{\Lambda p_{11}}{p_{11}p_{22} - p_{12}^2}\sqrt{A_1 + A_2 + A_3 + A_4}\Big) \\
&\times \exp\Big[-\frac{p_{11}}{2(p_{11}p_{22} - p_{12}^2)}\Big[\Big(\bar{d}_I - \bar{s}_I\frac{p_{12}}{p_{11}}\Big)^2 + \Big(\bar{d}_Q - \bar{s}_Q\frac{p_{12}}{p_{11}}\Big)^2\Big]\Big] \\
&\times \exp\Big[-\frac{\Lambda^2 p_{11}}{2(p_{11}p_{22} - p_{12}^2)}\Big[\Big(y_I - \frac{p_{12}}{p_{11}}\Big)^2 + y_Q^2\Big]\Big]
\end{aligned} \tag{A.49}
$$

where

$$A_1 = \Big[\Big(\frac{p_{22}}{p_{11}} - \frac{p_{12}^2}{p_{11}^2} + \frac{p_{12}}{p_{11}}(1 - y_I)\Big)^2 + \frac{p_{12}^2}{p_{11}^2}y_Q^2\Big]\Big(\bar{s}_I^2 + \bar{s}_Q^2\Big) \tag{A.50}$$

$$A_2 = \Big[\Big(y_I - \frac{p_{12}}{p_{11}}\Big)^2 + y_Q^2\Big]\Big(\bar{d}_I^2 + \bar{d}_Q^2\Big) \tag{A.51}$$

$$A_3 = 2\Big[\Big(\frac{p_{12}^2}{p_{11}^2} - \frac{p_{22}}{p_{11}} - \frac{p_{12}}{p_{11}}(1 - y_I)\Big)\Big(\frac{p_{12}}{p_{11}} - y_I\Big) - \frac{p_{12}}{p_{11}}y_Q^2\Big]\Big(\bar{s}_I\bar{d}_I + \bar{s}_Q\bar{d}_Q\Big) \tag{A.52}$$

$$A_4 = 2\Big[\frac{p_{22}}{p_{11}} - \frac{p_{12}^2}{p_{11}^2}(1 + y_Q) + \frac{p_{12}}{p_{11}}y_Q\Big]\Big(\bar{s}_I\bar{d}_Q - \bar{s}_Q\bar{d}_I\Big) \tag{A.53}$$

The first- and second-order moments of y_I and y_Q are given by

$$E[y_I|\Lambda, \Theta] = \frac{p_{12}}{p_{11}} + I_{1|0}\Big(\frac{\Lambda}{p_{11}}\sqrt{\bar{s}_I^2 + \bar{s}_Q^2}\Big)\Big[\frac{\bar{s}_I\bar{d}_I + \bar{s}_Q\bar{d}_Q}{\Lambda\sqrt{\bar{s}_I^2 + \bar{s}_Q^2}} - \frac{p_{12}}{p_{11}\Lambda}\sqrt{\bar{s}_I^2 + \bar{s}_Q^2}\Big] \tag{A.54}$$

$$E[y_Q|\Lambda,\Theta] = I_{1|0}\Big(\frac{\Lambda}{p_{11}}\sqrt{\bar{s}_I^2 + \bar{s}_Q^2}\Big)\Big[\frac{\bar{s}_I\bar{d}_Q - \bar{s}_Q\bar{d}_I}{\Lambda\sqrt{\bar{s}_I^2 + \bar{s}_Q^2}}\Big] \qquad (A.55)$$

$$\mathrm{COV}[y_I, y_Q|\Lambda,\Theta] = \Big[\frac{\bar{d}_I\bar{d}_Q(\bar{s}_I^2 - \bar{s}_Q^2) - \bar{s}_I\bar{s}_Q(\bar{d}_I^2 - \bar{d}_Q^2)}{\Lambda^2(\bar{s}_I^2 + \bar{s}_Q^2)} - \frac{p_{12}}{\Lambda^2 p_{11}}[\bar{s}_I\bar{d}_Q - \bar{s}_Q\bar{d}_I]\Big]$$

$$\times I_{1|0}^*\Big(\frac{\Lambda}{p_{11}}\sqrt{\bar{s}_I^2 + \bar{s}_Q^2}\Big) \qquad (A.56)$$

$$\mathrm{VAR}[y_I|\Lambda,\Theta] = \frac{p_{11}p_{22} - p_{12}^2}{\Lambda^2 p_{11}}$$

$$+ \frac{[\bar{s}_I\bar{d}_I + \bar{s}_Q\bar{d}_Q - p_{12}p_{11}^{-1}(\bar{s}_I^2 + \bar{s}_Q^2)]^2}{\Lambda^2(\bar{s}_I^2 + \bar{s}_Q^2)}I_{1|0}^*\Big(\frac{\Lambda}{p_{11}}\sqrt{\bar{s}_I^2 + \bar{s}_Q^2}\Big)$$

$$+ \Big[\Big(\bar{d}_I - \bar{s}_I\frac{p_{12}}{p_{11}}\Big)^2 + \Big(\bar{d}_Q - \bar{s}_Q\frac{p_{12}}{p_{11}}\Big)^2\Big]\frac{p_{11}}{\Lambda^3\sqrt{\bar{s}_I^2 + \bar{s}_Q^2}}$$

$$\times I_{1|0}\Big(\frac{\Lambda}{p_{11}}\sqrt{\bar{s}_I^2 + \bar{s}_Q^2}\Big) \qquad (A.57)$$

$$\mathrm{VAR}[y_Q|\Lambda,\Theta] = \frac{p_{11}p_{22} - p_{12}^2}{\Lambda^2 p_{11}} + I_{1|0}^*\Big(\frac{\Lambda}{p_{11}}\sqrt{\bar{s}_I^2 + \bar{s}_Q^2}\Big)\frac{[\bar{s}_I\bar{d}_Q - \bar{s}_Q\bar{d}_I]^2}{\Lambda^2(\bar{s}_I^2 + \bar{s}_Q^2)}$$

$$+ \Big[\Big(\bar{d}_I - \bar{s}_I\frac{p_{12}}{p_{11}}\Big)^2 + \Big(\bar{d}_Q - \bar{s}_Q\frac{p_{12}}{p_{11}}\Big)^2\Big]\frac{p_{11}}{\Lambda^3\sqrt{\bar{s}_I^2 + \bar{s}_Q^2}}$$

$$\times I_{1|0}\Big(\frac{\Lambda}{p_{11}}\sqrt{\bar{s}_I^2 + \bar{s}_Q^2}\Big) \qquad (A.58)$$

where

$$I_{1|0}(x) = \frac{I_1(x)}{I_0(x)} \qquad (A.59)$$

$$I_{1|0}^*(x) = 1 - \frac{2}{x}I_{1|0}(x) - I_{1|0}^2(x) \qquad (A.60)$$

and $I_1(\cdot)$ is the first-order modified Bessel function of the first kind.

Proof:

Let

$$X = \begin{bmatrix} s_I & d_I & s_Q & d_Q \end{bmatrix}^T \qquad (A.61)$$

Since the sum and difference signals are Gaussian distributed given the parameter set Θ, the joint PDF of the signals is defined by the mean $\overline{X} = E[X|\Theta]$ and covariance

A-7

$P = E[(X - \overline{X})(X - \overline{X})^T | \Theta]$. Then

$$\overline{X} = \begin{bmatrix} \bar{s}_I \\ \bar{d}_I \\ \bar{s}_Q \\ \bar{d}_Q \end{bmatrix} \tag{A.62}$$

$$P = \begin{bmatrix} p_{11} & p_{12} & 0 & 0 \\ p_{12} & p_{22} & 0 & 0 \\ 0 & 0 & p_{11} & p_{12} \\ 0 & 0 & p_{12} & p_{22} \end{bmatrix} \tag{A.63}$$

The inverse and determinant of P are given by

$$P^{-1} = \frac{1}{(p_{11}p_{22} - p_{12}^2)} \begin{bmatrix} p_{22} & -p_{12} & 0 & 0 \\ -p_{12} & p_{11} & 0 & 0 \\ 0 & 0 & p_{22} & -p_{12} \\ 0 & 0 & -p_{12} & p_{11} \end{bmatrix} \tag{A.64}$$

$$|P| = (p_{11}p_{22} - p_{12}^2)^2 \tag{A.65}$$

Then

$$f(X|\Theta) = \frac{1}{4\pi^2(p_{11}p_{22} - p_{12}^2)} \exp\left\{ -\frac{p_{11}}{2(p_{11}p_{22} - p_{12}^2)} \left[\frac{p_{22}}{p_{11}} \left((s_I - \bar{s}_I)^2 + (s_Q - \bar{s}_Q)^2 \right) \right. \right.$$
$$+ \left((d_I - \bar{d}_I)^2 + (d_Q - \bar{d}_Q)^2 \right) - \frac{2p_{12}}{p_{11}} \left((s_I - \bar{s}_I)(d_I - \bar{d}_I) \right.$$
$$\left. \left. + (s_Q - \bar{s}_Q)(d_Q - \bar{d}_Q) \right) \right] \right\} \tag{A.66}$$

Using (A.19), (A.20), (A.40), and (A.41) gives

$$d_I = s_I y_I - s_Q y_Q = y_I \Lambda \cos\psi - y_Q \Lambda \sin\psi \tag{A.67}$$
$$d_Q = s_I y_Q + s_Q y_I = y_Q \Lambda \cos\psi + y_I \Lambda \sin\psi \tag{A.68}$$

Let

$$Y = \begin{bmatrix} \Lambda \\ \psi \\ y_I \\ y_Q \end{bmatrix} \tag{A.69}$$

Then

$$X = h(Y) \tag{A.70}$$

where $h(\cdot)$ is a one-to-one transformation of random variables defined by (A.19), (A.20), (A.67), and (A.68). Then

$$\left| \frac{\partial h(Y)}{\partial X} \right| = \Lambda^3 \tag{A.71}$$

A-8

Using the transformation of random variables [A-1, p. 173] of (A.70) in (A.66) gives

$$
f(Y|\Theta) = \frac{\Lambda^3}{4\pi^2(p_{11}p_{22} - p_{12}^2)} \exp\left\{ - \frac{p_{11}}{2(p_{11}p_{22} - p_{12}^2)} \right.
$$

$$
\times \left[\frac{p_{22}}{p_{11}}\left(\Lambda^2 + \bar{s}_I^2 + \bar{s}_Q^2 - 2\Lambda(\bar{s}_I \cos\psi + \bar{s}_Q \sin\psi) \right) \right.
$$

$$
+ \left(\Lambda^2(y_I^2 + y_Q^2) - 2y_I\Lambda(\bar{d}_I \cos\psi + \bar{d}_Q \sin\psi) \right.
$$

$$
- 2y_Q\Lambda(\bar{d}_Q \cos\psi - \bar{d}_I \sin\psi) + \bar{d}_I^2 + \bar{d}_Q^2 \Big)
$$

$$
- 2\frac{p_{21}}{p_{11}}\left(\Lambda^2 y_I - \Lambda y_I(\bar{s}_I \cos\psi + \bar{s}_Q \sin\psi) - \Lambda y_Q(\bar{s}_Q \cos\psi - \bar{s}_I \sin\psi) \right.
$$

$$
\left. \left. - \Lambda(\bar{d}_I \cos\psi + \bar{d}_Q \sin\psi) + \bar{s}_I\bar{d}_I + \bar{s}_Q\bar{d}_Q \right) \right] \right\} \tag{A.72}
$$

where $\Lambda \geq 0$, $-\infty < y_I < +\infty$, $-\infty < y_Q < +\infty$, and $-\pi < \psi \leq \pi$. Completing the squares with respect to y_I and y_Q in (A.72) gives

$$
f(Y|\Theta) = \frac{\Lambda^3}{4\pi^2(p_{11}p_{22} - p_{12}^2)} \exp\left\{ - \frac{1}{p_{11}}\left(\Lambda + \bar{s}_I^2 + \bar{s}_Q^2 - 2\Lambda(\bar{s}_I \cos\psi + \bar{s}_Q \sin\psi) \right) \right\}
$$

$$
\times \exp\left\{ - \frac{\Lambda^2 p_{11}}{2(p_{11}p_{22} - p_{12}^2)} \right.
$$

$$
\times \left[\left(y_I^2 - 2y_I\left(\frac{\bar{d}_I}{\Lambda}\cos\psi + \frac{\bar{d}_Q}{\Lambda}\sin\psi \right) - 2y_I\frac{p_{12}}{p_{11}}\left(1 - \frac{\bar{s}_I}{\Lambda}\cos\psi - \frac{\bar{s}_Q}{\Lambda}\sin\psi \right) \right) \right.
$$

$$
+ \left(y_Q^2 - 2y_Q\left(\frac{\bar{d}_Q}{\Lambda}\cos\psi - \frac{\bar{d}_I}{\Lambda}\sin\psi \right) + 2y_Q\frac{p_{12}}{p_{11}}\left(\frac{\bar{s}_Q}{\Lambda}\cos\psi - \frac{\bar{s}_I}{\Lambda}\sin\psi \right) \right)
$$

$$
+ \left(\frac{\bar{d}_I^2}{\Lambda^2} + \frac{\bar{d}_Q^2}{\Lambda^2} - 2\frac{p_{12}}{p_{11}}\left(\frac{\bar{s}_I\bar{d}_I}{\Lambda^2} + \frac{\bar{s}_Q\bar{d}_Q}{\Lambda^2} - \frac{\bar{d}_I}{\Lambda}\cos\psi - \frac{\bar{d}_Q}{\Lambda}\sin\psi \right) \right.
$$

$$
\left. \left. + \frac{p_{12}}{p_{11}}\left(1 + \frac{\bar{s}_I^2}{\Lambda^2} + \frac{\bar{s}_Q^2}{\Lambda^2} - 2\frac{\bar{s}_I}{\Lambda}\cos\psi - 2\frac{\bar{s}_Q}{\Lambda}\sin\psi \right) \right) \right] \right\}
$$

$$
= \frac{\Lambda^3}{4\pi^2(p_{11}p_{22} - p_{12}^2)}\exp\left\{ - \frac{1}{2p_{11}}\left(\Lambda^2 + \bar{s}_I + \bar{s}_Q - 2\Lambda(\bar{s}_I \cos\psi + \bar{s}_Q \sin\psi) \right) \right\}
$$

$$
\times \exp\left\{ - \frac{\Lambda^2 p_{11}}{2(p_{11}p_{22} - p_{12}^2)} \right.
$$

$$
\times \left[\left(y_I - \left(\frac{\bar{d}_I}{\Lambda}\cos\psi + \frac{\bar{d}_Q}{\Lambda}\sin\psi + \frac{p_{12}}{p_{11}}\left(1 - \frac{\bar{s}_I}{\Lambda}\cos\psi - \frac{\bar{s}_Q}{\Lambda}\sin\psi \right) \right) \right)^2 \right.
$$

$$
\left. \left. + \left(y_Q + \left(\frac{\bar{d}_I}{\Lambda}\sin\psi + \frac{\bar{d}_Q}{\Lambda}\cos\psi - \frac{p_{12}}{p_{11}}\left(\frac{\bar{s}_I}{\Lambda}\sin\psi - \frac{\bar{s}_Q}{\Lambda}\cos\psi \right) \right) \right)^2 \right] \right\} \tag{A.73}
$$

Using (A.30) to condition the PDF of (A.73) on Λ gives

$$f(\psi, y_I, y_Q | \Lambda, \Theta) = \frac{\Lambda^2 p_{11}}{4\pi^2 (p_{11}p_{22} - p_{12}^2) I_0\left(\frac{\Lambda}{p_{11}}\sqrt{\bar{s}^2 + \bar{s}_Q^2}\right)} \exp\left\{ -\frac{\Lambda^2 p_{11}}{2(p_{11}p_{22} - p_{12}^2)} \right.$$
$$\times \left[\left(y_I - \left(\frac{\bar{d}_I}{\Lambda}\cos\psi + \frac{\bar{d}_Q}{\Lambda}\sin\psi + \frac{p_{12}}{p_{11}}\left(1 - \frac{\bar{s}_I}{\Lambda}\cos\psi - \frac{\bar{s}_Q}{\Lambda}\sin\psi\right)\right)\right)^2 \right.$$
$$\left. \left. + \left(y_Q + \left(\frac{\bar{d}_I}{\Lambda}\sin\psi - \frac{\bar{d}_Q}{\Lambda}\cos\psi - \frac{p_{12}}{p_{11}}\left(\frac{\bar{s}_I}{\Lambda}\sin\psi - \frac{\bar{s}_Q}{\Lambda}\cos\psi\right)\right)\right)^2 \right] \right\}$$
$$\times \exp\left\{ \frac{\Lambda}{p_{11}}\left(\bar{s}_I \cos\psi + \bar{s}_Q \sin\psi\right) \right\} \tag{A.74}$$

The amplitude-conditioned, joint PDF of y_I and y_Q is given by

$$f(y_I, y_Q | \Lambda, \Theta) = \frac{\Lambda^2 p_{11}}{4\pi^2 (p_{11}p_{22} - p_{12}^2) I_0\left(\frac{\Lambda}{p_{11}}\sqrt{\bar{s}_I^2 + \bar{s}_Q^2}\right)} \exp\left\{ -\frac{\Lambda^2 p_{11}}{2(p_{11}p_{22} - p_{12}^2)} \right.$$
$$\times \left. \left(\left(y_I - \frac{p_{12}}{p_{11}}\right)^2 + y_Q^2 + \left(\frac{\bar{d}_I}{\Lambda} - \frac{\bar{s}_I}{\Lambda}\frac{p_{12}}{p_{11}}\right)^2 + \left(\frac{\bar{d}_Q}{\Lambda} - \frac{\bar{s}_Q}{\Lambda}\frac{p_{12}}{p_{11}}\right)^2 \right) \right\}$$
$$\times \int_{-pi}^{+\pi} d\psi \exp\left\{ -\frac{\Lambda^2 p_{11}}{(p_{11}p_{22} - p_{12}^2)} \left[\left(\frac{p_{11}p_{22} - p_{12}^2}{\Lambda p_{11}^2}\bar{s}_I + y_I\left(\frac{\bar{s}_I p_{12}}{\Lambda p_{11}} - \frac{\bar{d}_I}{\Lambda}\right) \right.\right.\right.$$
$$\left. - \frac{p_{12}}{p_{11}}\left(\frac{\bar{s}_I}{\Lambda} - \frac{\bar{d}_I}{\Lambda}\right) + y_Q\left(\frac{\bar{s}_Q p_{12}}{\Lambda p_{11}} - \frac{\bar{d}_Q}{\Lambda}\right) \right)\cos\psi + \left(\frac{p_{11}p_{22} - p_{12}^2}{\Lambda p_{11}^2}\bar{s}_Q \right.$$
$$\left. \left. \left. + y_I\left(\frac{\bar{s}_Q p_{12}}{\Lambda p_{11}} - \frac{\bar{d}_Q}{\Lambda}\right) - \frac{p_{12}}{p_{11}}\left(\frac{\bar{s}_Q}{\Lambda} - \frac{\bar{d}_Q}{\Lambda}\right) - y_Q\left(\frac{\bar{s}_I p_{12}}{\Lambda p_{11}} - \frac{\bar{d}_I}{\Lambda}\right) \right)\sin\psi \right] \right\}$$

$$\tag{A.75}$$

Evaluating the integral with [A-2, No. 3.937.2] gives the amplitude-conditioned, joint PDF of y_I and y_Q in (A.49).

If $\bar{s}_I = \bar{s}_Q = \bar{d}_I = \bar{d}_Q = 0$ in (A.75),

$$f(y_I, y_Q | \Lambda, \Theta, \|\overline{X}\| = 0) = \frac{\Lambda^2 p_{11}}{2\pi (p_{11}p_{22} - p_{12}^2)} \exp\left\{ -\frac{\Lambda^2 p_{11}[y_Q^2 + (y_I - p_{12}p_{11}^{-1})^2]}{2(p_{11}p_{22} - p_{12}^2)} \right\}$$
$$= f(y_I | \Lambda, \Theta, \|\overline{X}\| = 0) f(y_Q | \Lambda, \Theta \|\overline{X}\| = 0) \tag{A.76}$$

where

$$f(y_I | \Lambda, \Theta, \|\overline{X}\| = 0) = N\left(\frac{p_{12}}{p_{11}}, \frac{p_{11}p_{22} - p_{12}^2}{\Lambda^2 p_{11}}\right) \tag{A.77}$$

$$f(y_Q | \Lambda, \Theta, \|\overline{X}\| = 0) = N\left(0, \frac{p_{11}p_{22} - p_{12}^2}{\Lambda^2 p_{11}}\right) \tag{A.78}$$

Thus, if $\bar{s}_I = \bar{s}_Q = \bar{d}_I = \bar{d}_Q = 0$, as in the case of a Rayleigh target, y_I and y_Q are conditionally independent, Gaussian random variables with variance inversely proportional to Λ^2 and the observed SNR $\Re_o$ of (A.26).

Since $f(y_I, y_Q | \Lambda, \Theta)$ has a difficult form for computing the moments directly, the joint characteristic function [A-1, p. 158] of y_I and y_Q is used and given by

$$
\Phi(\omega_1, \omega_2) = \int_{-\infty}^{\infty} \int_{-\infty}^{\infty} \int_{-\pi}^{\pi} \exp[j\omega_1 y_I + j\omega_2 y_Q] f(\psi, y_I, y_Q | \Lambda, \Theta) \, d\psi \, dy_I \, y_Q
$$

$$
= \frac{\Lambda^2 p_{11}}{4\pi^2 (p_{11} p_{22} - p_{12}^2) I_0 \left(\frac{\Lambda}{p_{11}} \sqrt{\bar{s}^2 + \bar{s}_Q^2} \right)}
$$

$$
\times \int_{-\pi}^{\pi} d\psi \, \exp\left\{ \frac{\Lambda}{p_{11}} \left(\bar{s}_I \cos \psi + \bar{s}_Q \sin \psi \right) \right\}
$$

$$
\times \int_{-\infty}^{+\infty} \int_{-\infty}^{+\infty} dy_I \, dy_Q \, \exp[j\omega_1 y_I + j\omega_2 y_Q] \exp\left\{ -\frac{\Lambda^2 p_{11}}{2(p_{11} p_{22} - p_{12}^2)} \right.
$$

$$
\times \left[\left(y_I - \left(\frac{\bar{d}_I}{\Lambda} \cos \psi + \frac{\bar{d}_Q}{\Lambda} \sin \psi + \frac{p_{12}}{p_{11}} \left(1 - \frac{\bar{s}_I}{\Lambda} \cos \psi - \frac{\bar{s}_Q}{\Lambda} \sin \psi \right) \right) \right)^2 \right.
$$

$$
\left. \left. + \left(y_Q + \left(\frac{\bar{d}_I}{\Lambda} \sin \psi - \frac{\bar{d}_Q}{\Lambda} \cos \psi - \frac{p_{12}}{p_{11}} \left(\frac{\bar{s}_I}{\Lambda} \sin \psi - \frac{\bar{s}_Q}{\Lambda} \cos \psi \right) \right) \right)^2 \right] \right\}
$$

$$
= \frac{1}{2\pi I_0 \left(\frac{\Lambda}{p_{11}} \sqrt{\bar{s}_I^2 + \bar{s}_Q^2} \right)} \exp\left\{ -\frac{(p_{11} p_{22} - p_{12}^2)}{2 p_{11} \Lambda^2} (\omega_1^2 + \omega_2^2) + j \frac{p_{12}}{p_{11}} \omega_1 \right\}
$$

$$
\times \int_{-\pi}^{\pi} d\psi \, \exp\left[\left(\frac{\Lambda}{p_{11}} \bar{s}_I + j\omega_1 \left(\frac{\bar{d}_I}{\Lambda} - \frac{p_{12} \bar{s}_I}{p_{11} \Lambda} \right) + j\omega_2 \left(\frac{\bar{d}_Q}{\Lambda} - \frac{p_{12} \bar{s}_Q}{p_{11} \Lambda} \right) \right) \cos \psi \right]
$$

$$
\times \exp\left[\left(\frac{\Lambda}{p_{11}} \bar{s}_Q + j\omega_1 \left(\frac{\bar{d}_Q}{\Lambda} - \frac{p_{12} \bar{s}_Q}{p_{11} \Lambda} \right) - j\omega_2 \left(\frac{\bar{d}_I}{\Lambda} - \frac{p_{12} \bar{s}_I}{p_{11} \Lambda} \right) \right) \sin \psi \right] \quad (A.79)
$$

Thus, the joint characteristic function is given by

$$
\Phi(\omega_1, \omega_2) = \frac{1}{I_0 \left(\frac{\Lambda}{p_{11}} \sqrt{\bar{s}_I^2 + \bar{s}_Q^2} \right)} \exp\left\{ -\frac{(p_{11} p_{22} - p_{12}^2)}{2 p_{11} \Lambda^2} (\omega_1^2 + \omega_2^2) + j \frac{p_{12}}{p_{11}} \omega_1 \right\}
$$

$$
\times I_0 \left(\sqrt{\frac{\Lambda^2}{p_{11}^2} (\bar{s}_I^2 + \bar{s}_Q^2) - (\omega_1^2 + \omega_2^2) C_1 + 2 j \omega_1 C_2 + 2 j \omega_2 C_3} \right) \quad (A.80)
$$

where

$$
C_1 = \frac{1}{\Lambda^2} \left[\left(\bar{d}_I - \bar{s}_I \frac{p_{12}}{p_{11}} \right)^2 + \left(\bar{d}_Q - \bar{s}_Q \frac{p_{12}}{p_{11}} \right)^2 \right] \quad (A.81)
$$

$$
C_2 = \frac{1}{p_{11}} \left[\bar{s}_I \bar{d}_I + \bar{s}_Q \bar{d}_Q - \frac{p_{12}}{p_{11}} (\bar{s}_I^2 + \bar{s}_Q^2) \right] \quad (A.82)
$$

$$
C_3 = \frac{1}{p_{11}} \left[\bar{s}_I \bar{d}_Q - \bar{s}_Q \bar{d}_I \right] \quad (A.83)
$$

The marginal characteristic functions of y_I and y_Q are then given by

$$\Phi_{y_I}(\omega_1) = \Phi(\omega_1, 0) = \frac{1}{I_0\left(\frac{\Lambda}{p_{11}}\sqrt{\bar{s}_I^2 + \bar{s}_Q^2}\right)} \exp\left\{-\frac{(p_{11}p_{22} - p_{12}^2)}{2p_{11}\Lambda^2}\omega_1^2 + j\frac{p_{12}}{p_{11}}\omega_1\right\}$$

$$\times I_0\left(\sqrt{\frac{\Lambda^2}{p_{11}^2}(\bar{s}_I^2 + \bar{s}_Q^2) - C_1\omega_1^2 + 2C_2 j\omega_1}\right) \qquad (A.84)$$

$$\Phi_{y_Q}(\omega_2) = \Phi(0, \omega_2) = \frac{1}{I_0\left(\frac{\Lambda^2}{p_{11}^2}\sqrt{\bar{s}_I^2 + \bar{s}_Q^2}\right)} \exp\left\{-\frac{(p_{11}p_{22} - p_{12}^2)}{2p_{11}\Lambda^2}\omega_2^2\right\}$$

$$\times I_0\left(\sqrt{\frac{\Lambda^2}{p_{11}^2}(\bar{s}_I^2 + \bar{s}_Q^2) - C_1\omega_2^2 + 2C_3 j\omega_2}\right) \qquad (A.85)$$

Thus, (A.84) and (A.85) show that neither y_I nor y_Q are not in general Gaussian random variables. Also, since for $\|\overline{X}\| \neq 0$

$$\Phi(\omega_1, \omega_2) \neq \Phi_{y_I}(\omega_1)\Phi_{y_Q}(\omega_2) \qquad (A.86)$$

y_I and y_Q are not in general independent random variables. Setting $s_1 = j\omega_1$ and $s_2 = j\omega_2$ in (A.80) gives the joint moment-generating function as

$$M(s_1, s_2) = \frac{1}{I_0\left(\frac{\Lambda}{p_{11}}\sqrt{\bar{s}_I^2 + \bar{s}_Q^2}\right)} \exp\left\{\frac{(p_{11}p_{22} - p_{12}^2)}{2p_{11}\Lambda^2}(s_1^2 + s_2^2) + \frac{p_{12}}{p_{11}}s_1\right\}$$

$$\times I_0\left(\sqrt{\frac{\Lambda^2}{p_{11}^2}(\bar{s}_I^2 + \bar{s}_Q^2) + C_1(s_1^2 + s_2^2) + 2C_2 s_1 + 2C_3 s_2}\right) \qquad (A.87)$$

The form of (A.87) suggests the use of joint cumulants for the computation of moments of y_I and y_Q. The joint cumulants [A-1, p. 158] are given by

$$\lambda_{kr} = \frac{\partial^k \partial^r}{\partial s_1^k \partial s_2^r}\Psi(s_1, s_2)\bigg|_{s_1=0, s_2=0} \qquad (A.88)$$

where

$$\Psi(s_1, s_2) = \ln\left[M(s_1, s_2)\right]$$

$$= -\ln\left[I_0\left(\frac{\Lambda}{p_{11}}\sqrt{\bar{s}_I^2 + \bar{s}_Q^2}\right)\right] + \frac{(p_{11}p_{22} - p_{12}^2)}{2\Lambda^2 p_{11}}(s_1^2 + s_2^2) + \frac{p_{12}}{p_{11}}s_1$$

$$+ \ln\left[I_0\left(\sqrt{\frac{\Lambda^2}{p_{11}^2}(\bar{s}_I^2 + \bar{s}_Q^2) + C_1(s_1^2 + s_2^2) + 2C_2 s_1 + 2C_3 s_2}\right)\right] \quad (A.89)$$

Taking the first partial derivatives of $\Psi(s_1, s_2)$ gives

$$
\frac{\partial \Psi(s_1, s_2)}{\partial s_1} = \frac{(p_{11}p_{22} - p_{12}^2)}{\Lambda^2 p_{11}} s_1 + \frac{p_{12}}{p_{11}}
$$

$$
+ I_{1|0}\left(\sqrt{\frac{\Lambda^2}{p_{11}^2}(\bar{s}_I^2 + \bar{s}_Q^2) + C_1(s_1^2 + s_2^2) + 2C_2 s_1 + 2C_3 s_2}\right)
$$

$$
\times \frac{C_1 s_1 + C_2}{\sqrt{\frac{\Lambda^2}{p_{11}^2}(\bar{s}_I^2 + \bar{s}_Q^2) + C_1(s_1^2 + s_2^2) + 2C_2 s_1 + 2C_3 s_2}} \tag{A.90}
$$

$$
\frac{\partial \Psi(s_1, s_2)}{\partial s_2} = \frac{(p_{11}p_{22} - p_{12}^2)}{\Lambda^2 p_{11}} s_2
$$

$$
+ I_{1|0}\left(\sqrt{\frac{\Lambda^2}{p_{11}^2}(\bar{s}_I^2 + \bar{s}_Q^2) + C_1(s_1^2 + s_2^2) + 2C_2 s_1 + 2C_3 s_2}\right)
$$

$$
\times \frac{C_1 s_1 + C_3}{\sqrt{\frac{\Lambda^2}{p_{11}^2}(\bar{s}_I^2 + \bar{s}_Q^2) + C_1(s_1^2 + s_2^2) + 2C_2 s_1 + 2C_3 s_2}} \tag{A.91}
$$

where

$$
I_{1|0}(x) = \frac{I_1(x)}{I_0(x)} \tag{A.92}
$$

with $I_1(\cdot)$ denoting the first-order modified Bessel function of the first kind. Then (A.90) and (A.91) give first-order moments or expected values of y_I and y_Q [A-1, p. 158] as

$$
E[y_I | \Lambda, \Theta] = \lambda_{10} = \frac{p_{12}}{p_{11}} + I_{1|0}\left(\frac{\Lambda}{p_{11}}\sqrt{\bar{s}_I^2 + \bar{s}_Q^2}\right)\frac{C_2 p_{11}}{\Lambda\sqrt{\bar{s}_I^2 + \bar{s}_Q^2}} \tag{A.93}
$$

$$
E[y_Q | \Lambda, \Theta] = \lambda_{01} = I_{1|0}\left(\frac{\Lambda}{p_{11}}\sqrt{\bar{s}_I^2 + \bar{s}_Q^2}\right)\frac{C_3 p_{11}}{\Lambda\sqrt{\bar{s}_I^2 + \bar{s}_Q^2}} \tag{A.94}
$$

Inserting C_2 and C_3 of (A.82) and (A.83) in (A.93) and (A.94) gives (A.54) and (A.55), respectively.

Taking the first partial derivative of (A.90) with respect to s_2 gives

$$
\frac{\partial^2 \Psi(s_1, s_2)}{\partial s_1 \partial s_2} = I'_{1|0}\left(\sqrt{\frac{\Lambda^2}{p_{11}^2}(\bar{s}_I^2 + \bar{s}_Q^2) + C_1(s_1^2 + s_2^2) + 2s_1 C_2 + 2s_2 C_3}\right)
$$

$$
\times \frac{(C_1 s_1 + C_2)^2(C_1 s_2 + C_3)}{\left[\frac{\Lambda^2}{p_{11}^2}(\bar{s}_I^2 + \bar{s}_Q^2) + C_1(s_1^2 + s_2^2) + 2s_1 C_2 + 2s_2 C_3\right]}
$$

$$+ I_{1|0}\left(\sqrt{\frac{\Lambda^2}{p_{11}^2}(\bar{s}_I^2 + \bar{s}_Q^2) + C_1(s_1^2 + s_2^2) + 2C_2 s_1 + 2C_3 s_2}\right)$$

$$\times \frac{(C_1 s_1 + C_2)^2 (C_1 s_2 + C_3)}{\left[\frac{\Lambda^2}{p_{11}^2}(\bar{s}_I^2 + \bar{s}_Q^2) + C_1(s_1^2 + s_2^2) + 2C_2 s_1 + 2C_3 s_2\right]^{\frac{3}{2}}} \qquad (A.95)$$

where

$$I'_{1|0}(x) = \frac{d}{dx} I_{1|0}(x) = 1 - \frac{1}{x} I_{1|0}(x) - I_{1|0}^2(x) \qquad (A.96)$$

Thus, (A.95) gives the covariance of y_I and y_Q as

$$\mathrm{COV}[y_I, y_Q | \Lambda, \Theta] = \lambda_{11} = \frac{C_2 C_3 p_{11}^2}{\Lambda^2 (\bar{s}_I^2 + \bar{s}_Q^2)} I_{1|0}^*\left(\frac{\Lambda}{p_{11}}\sqrt{\bar{s}_I^2 + \bar{s}_Q^2}\right) \qquad (A.97)$$

where

$$I_{1|0}^*(x) = 1 - \frac{2}{x} I_{1|0}(x) - I_{1|0}^2(x) \qquad (A.98)$$

Inserting C_2 and C_3 in (A.97) gives the covariance of (A.56).

Taking the second partial derivatives of (A.90) and (A.91) with respect to s_1 and s_2, respectively, gives

$$\frac{\partial^2 \Psi(s_1, s_2)}{\partial s_1^2} = \frac{(p_{11} p_{22} - p_{12}^2)}{\Lambda^2 p_{11}} + I_{1|0}^*\left(\sqrt{\frac{\Lambda^2}{p_{11}^2}(\bar{s}_I^2 + \bar{s}_Q^2) + C_1(s_1^2 + s_2^2) + 2C_2 s_1 + 2C_3 s_2}\right)$$

$$\times \frac{(C_1 s_1 + C_2)^2}{\left[\frac{\Lambda^2}{p_{11}^2}(\bar{s}_I^2 + \bar{s}_Q^2) + C_1(s_1^2 + s_2^2) + 2C_2 s_1 + 2C_3 s_2\right]}$$

$$+ I_{1|0}\left(\sqrt{\frac{\Lambda^2}{p_{11}^2}(\bar{s}_I^2 + \bar{s}_Q^2) + C_1(s_1^2 + s_2^2) + 2C_2 s_1 + 2C_3 s_2}\right)$$

$$\times \frac{C_1}{\sqrt{\frac{\Lambda^2}{p_{11}^2}(\bar{s}_I^2 + \bar{s}_Q^2) + C_1(s_1^2 + s_2^2) + 2C_2 s_1 + 2C_3 s_2}} \qquad (A.99)$$

$$\frac{\partial^2 \Psi(s_1, s_2)}{\partial s_2^2} = \frac{(p_{11} p_{22} - p_{12}^2)}{\Lambda^2 p_{11}} + I_{1|0}^*\left(\sqrt{\frac{\Lambda^2}{p_{11}^2}(\bar{s}_I^2 + \bar{s}_Q^2) + C_1(s_1^2 + s_2^2) + 2C_2 s_1 + 2C_3 s_2}\right)$$

$$\times \frac{(C_1 s_1 + C_3)^2}{\left[\frac{\Lambda^2}{p_{11}^2}(\bar{s}_I^2 + \bar{s}_Q^2) + C_1(s_1^2 + s_2^2) + 2C_2 s_1 + 2C_3 s_2\right]}$$

$$+ I_{1|0}\left(\sqrt{\frac{\Lambda^2}{p_{11}^2}(\bar{s}_I^2 + \bar{s}_Q^2) + C_1(s_1^2 + s_2^2) + 2C_2 s_1 + 2C_3 s_2}\right)$$

$$\times \frac{C_1}{\sqrt{\frac{\Lambda^2}{p_{11}^2}(\bar{s}_I^2 + \bar{s}_Q^2) + C_1(s_1^2 + s_2^2) + 2C_2s_1 + 2C_3s_2}} \qquad (A.100)$$

Then (A.99) and (A.100) give the variances of y_I and y_Q as

$$\text{VAR}[y_I | \Lambda, \Theta] = \lambda_{20} = \frac{(p_{11}p_{22} - p_{12}^2)}{\Lambda^2 p_{11}} + \frac{C_2^2 p_{11}^2}{\Lambda^2 \left(\bar{s}_I^2 + \bar{s}_Q^2 \right)} I_{1|0}^* \left(\frac{\Lambda}{p_{11}} \sqrt{\bar{s}_I^2 + \bar{s}_Q^2} \right)$$
$$+ \frac{C_1 p_{11}}{\Lambda \sqrt{\bar{s}_I^2 + \bar{s}_Q^2}} I_{1|0} \left(\frac{\Lambda}{p_{11}} \sqrt{\bar{s}_I^2 + \bar{s}_Q^2} \right) \qquad (A.101)$$

$$\text{VAR}[y_Q | \Lambda, \Theta] = \lambda_{02} = \frac{(p_{11}p_{22} - p_{12}^2)}{\Lambda^2 p_{11}} + \frac{C_3^2 p_{11}^2}{\Lambda^2 \left(\bar{s}_I^2 + \bar{s}_Q^2 \right)} I_{1|0}^* \left(\frac{\Lambda}{p_{11}} \sqrt{\bar{s}_I^2 + \bar{s}_Q^2} \right)$$
$$+ \frac{C_1 p_{11}}{\Lambda \sqrt{\bar{s}_I^2 + \bar{s}_Q^2}} I_{1|0} \left(\frac{\Lambda}{p_{11}} \sqrt{\bar{s}_I^2 + \bar{s}_Q^2} \right) \qquad (A.102)$$

Inserting C_1, C_2, and C_3 of (A.81) through (A.83) in (A.101) and (A.102) gives (A.57) and (A.58), respectively.

Q.E.D.

REFERENCES

A-1. A. Papoulis, *Probability, Random Variables, and Stochastic Processes, 2rd Ed.*, McGraw-Hill, Inc., New York, NY, 1991.

A-2. I. S. Gradshteyn and I. M. Ryzhik, *Table of Integrals, Series, and Products, Fifth Edition*, A. Jeffrey, Ed., Academic Press, Inc., San Diego, CA, 1990.

Appendix B

DERIVATION OF THE UNCONDITIONAL PDF AND STATISTICS OF THE COMPLEX MONOPULSE RATIO FOR A RAYLEIGH TARGET

The unconditional PDFs of the monopulse ratios and the unconditional CRLBs are developed in this appendix. The unconditional PDFs of the monopulse ratios for a single Rayleigh target are given by

$$
\begin{aligned}
f(y_I, y_Q | \Psi_R) &= \int_0^\infty f(y_I, y_Q, \Re_o | \Psi_R) \, d\Re_o \\
&= \int_0^\infty f(y_I, y_Q | \Re_o, \Psi_R) f(\Re_o | \Psi_R) \, d\Re_o \\
&= \frac{p}{\pi(\Re_{R1} + 1)\left[(y_I - \bar{y}_I)^2 + y_Q^2 + \dfrac{p}{\Re_{R1} + 1}\right]^2}
\end{aligned} \tag{B.1}
$$

$$
\begin{aligned}
f(y_I | \Psi_R) &= \int_{-\infty}^\infty \int_0^\infty f(y_I, y_Q, \Re_o | \Psi_R) \, d\Re_o \, dy_Q \\
&= \int_{-\infty}^\infty \int_0^\infty f(y_I, y_Q | \Re_o, \Psi_R) f(\Re_o | \Psi_R) \, d\Re_o \, dy_Q \\
&= \frac{p}{\pi(\Re_{R1} + 1)\left[(y_I - \bar{y}_I)^2 + \dfrac{p}{\Re_{R1} + 1}\right]^{\frac{3}{2}}}
\end{aligned} \tag{B.2}
$$

$$
\begin{aligned}
f(y_Q | \Psi_R) &= \int_{-\infty}^\infty \int_0^\infty f(y_I, y_Q, \Re_o | \Psi_R) \, d\Re_o \, dy_I \\
&= \int_{-\infty}^\infty \int_0^\infty f(y_I, y_Q | \Re_o, \Psi_R) f(\Re_o | \Psi_R) \, d\Re_o \, dy_I \\
&= \frac{p}{\pi(\Re_{R1} + 1)\left[y_Q^2 + \dfrac{p}{\Re_{R1} + 1}\right]^{\frac{3}{2}}}
\end{aligned} \tag{B.3}
$$

where

$$
\bar{y}_I = \frac{\Re_{R1}\eta + \rho\sigma_d\sigma_S^{-1}}{\Re_{R1} + 1} \tag{B.4}
$$

$$p = \left[\frac{\sigma_d^2}{\sigma_S^2} + \frac{\Re_{R1}\eta(\eta - 2\rho\sigma_d\sigma_S^{-1}) - \rho^2\sigma_d^2\sigma_S^{-2}}{\Re_{R1} + 1}\right] \qquad (B.5)$$

$$\Psi_R = \{\alpha_o, \eta, \sigma_d, \sigma_S, \rho\} \qquad (B.6)$$

Note that the definitions of $\bar{y}_I$, p, and Ψ_R are consistent with their definitions in the main body of this paper. Also, (B.1) through (B.3) show that y_I and y_Q are not independent. However, y_I and y_Q are uncorrelated. The unconditional mean of y_I is $\bar{y}_I$, the unconditional mean of y_Q is zero, and the variance of y_I and y_Q are infinite. The joint PDF of (B.1) can be shown to agree with (26) of [B-1].

The unconditional CRLB associated with $\hat{\eta}$, based on N observations of y_I and y_Q, is given by

$$J_{y_I, y_Q}(\hat{\eta}|N, \Psi_R) = \left[-\sum_{i=1}^{N} E\left[\frac{\partial^2 \ln f(y_{Ii}, y_{Qi}|\Psi_R)}{\partial \eta^2}\bigg|\Psi_R\right]\right]^{-1} \qquad (B.7)$$

where y_{Ii} and y_{Qi} are the in-phase and quadrature monopulse ratios for pulse i, respectively, and $f(y_{Ii}, y_{Qi}|\Psi_R)$ is the joint PDF of y_{Ii} and y_{Qi}. Using (B.1) in (B.5) gives

$$J_{y_I, y_Q}(\hat{\eta}|N, \Psi_R) = \frac{3p}{4N\Re_{R1}}\left[1 + \frac{1}{\Re_{R1}}\right]^2 \left[1 + \frac{1}{\Re_{R1}} + \frac{(\eta - \rho\sigma_d\sigma_S^{-1})^2}{\Re_{R1}\,p}\right]^{-1} \qquad (B.8)$$

Using (B.2) gives the unconditional CRLB associated with $\hat{\eta}$ based on N observations of y_I only as

$$J_{y_I}(\hat{\eta}|N, \Psi_R) = \frac{5p}{6N\Re_{R1}}\left[1 + \frac{1}{\Re_{R1}}\right]^2 \left[1 + \frac{1}{\Re_{R1}} + \frac{2(\eta - \rho\sigma_d\sigma_S^{-1})^2}{3\Re_{R1}\,p}\right]^{-1} \qquad (B.9)$$

Using (B.3) gives the unconditional CRLB associated with $\hat{\eta}$ based on N observations of y_Q only as

$$J_{y_Q}(\hat{\eta}|N, \Psi_R) = \frac{5p^2}{4N(\eta - \rho\sigma_d\sigma_S^{-1})^2}\left[1 + \frac{1}{\Re_{R1}}\right]^2 \qquad (B.10)$$

Comparing (B.10) with (5.4) shows that the conditional CRLB associated with η and based on N observations of y_Q is less than the corresponding unconditional CRLB. For an average observation represented by $Y_N = E[Y_N] = \Re_{R1} + 1$, the conditional CRLB based on N observations of y_I and y_Q in (5.2) is less than the corresponding unconditional CRLB for $\Re_{R1} > 2$. Also, for an average observation represented by $Y_N = E[Y_N] = \Re_{R1} + 1$, the conditional CRLB based on N observations of y_I in (5.3) is less than the corresponding unconditional CRLB for $\Re_{R1} > 2$. Since the conditional CRLBs are less than the unconditional CRLBs for $\Re_{R1} > 3$ dB, DOA estimators utilizing monopulse processing should be developed from the conditional PDF or the conditional statistics.

REFERENCES

B-1. G. W. Groves, W. D. Blair, and W. C. Chow, "Probability Distribution of the Complex Monopulse Ratio with Arbitrary Correlation Between the Channels," *IEEE Trans. Aero. Elect. Sys.*, Oct 1997.

DISTRIBUTION

	Copies		Copies

DOD ACTIVITIES (CONUS)

	Copies
ATTN DR RABINDER MADAN	2
JAMES BUSS	1
JAMES K HALL	1
WILLIAM J MICELI	1

CODE 313
OFFICE OF NAVAL RESEARCH
800 N QUINCY ST
ARLINGTON VA 22217-5660

ATTN DR JULIA ABRAHAMS	1

CODE 311
OFFICE OF NAVAL RESEARCH
800 N QUINCY ST
ARLINGTON VA 22217-5660

ATTN JEFF LAYNE	2
AL WOODS	1
DEVERT WICKER	1

WRIGHT LABORATORY
AVIONICS DIRECTORATE
WL/AACF BLDG 620
2241 AVIONICS CIRCLE
WPAFB OH 45433-7318

ATTN ROY L STREIT	1

CODE 2002 BLDG 1171
NAVAL UNDERSEA WARFARE CTR
1176 HOWELL ST
NEWPORT RI 02841

ATTN DR ROGER OXLEY	1

CODE 5720
NRL
WASHINGTON DC 20375

ATTN DR GERRY TRUNK	1

CODE 5317
RADAR DIVISION
NRL
WASHINGTON DC 20375

ATTN JOSEPH WILLIAMS	1

PMS400B33
NAVAL SEA SYSTEMS COMMAND
2531 JEFFERSON DAVIS HIGHWAY
ARLINGTON VA 22242-5160   1

ATTN DICK ZIEGLER	1

PMS400B33
NAVAL SEA SYSTEMS COMMAND
2531 JEFFERSON DAVIS HIGHWAY
ARLINGTON VA 22242-5160

ATTN RICHARD BRITTON	1

PMS400BX
NAVAL SEA SYSTEMS COMMAND
2531 JEFFERSON DAVIS HIGHWAY
ARLINGTON VA 22242-5160

ATTN DOUG MARKER	1

PEO-TAD-SET
THEATER AIR DEFENSE
2531 JEFFERSON DAVIS HIGHWAY
ARLINGTON VA 22242-5170

ATTN PASHANG ESFANDIARI	1

PEO-TAD-B
THEATER AIR DEFENSE
2531 JEFFERSON DAVIS HIGHWAY
ARLINGTON VA 22242-5170

ATTN CODE A76	
(TECHNICAL LIBRARY)	1

COMMANDING OFFICER
CSSDD NSWC
6703 W HIGHWAY 98
PANAMA CITY FL 32407-7001

DEFENSE TECH INFORMATION CTR
8725 JOHN J KINGMAN RD
SUITE 0944

FORT BELVOIR VA 22060-6218	2

DISTRIBUTION (Continued)

Copies   Copies

NON-DOD ACTIVITIES (CONUS)

ATTN DR YAAKOV BAR-SHALOM	2
ESE DEPT U-157	
260 GLENBROOK RD	
STORRS CT 06269-3157	

ATTN DR MAITE BRANDT-PEARCE   4
DEPT OF ELECTRICAL ENGINEERING
UNIVERSITY OF VIRGINIA
CHARLOTTESVILLE VA 22903-2442

ATTN DR RAMAN K MEHRA   1
       DR CONSTANTINO RAGO   1
SCIENTIFIC SYSTEMS
500 W CUMMINGS PK SUITE 3950
WOBURN MA 01801

ATTN PHILIP O WEST   1
       BENJAMIN J SLOCUMB   1
GEORGIA TECH RESEARCH INSTITUTE
ELECTRONIC SYSTEMS LABORATORY
CONCEPTS ANALYSIS DIVISION
ATLANTA GA 30332-0800

ATTN WILLIAM D BLAIR   50
       MELVIN BELCHER JR   1
       JEFF HOLDER   1
       ROBERT N TREBITS   1
       JAMES SANGSTON   1
GEORGIA TECH RESEARCH INSTITUTE
SENSORS AND ELECTROMAGNETIC
LABORATORY
RADAR SYSTEMS DIVISION
ATLANTA GA 30332-0800

ATTN DR EDWARD KAMEN   1
SCHOOL OF ELECTRICAL AND
       COMPUTER ENGINEERING
GEORGIA INSTITUTE OF TECHNOLOGY
ATLANTA GA 30332

ATTN DR PAUL SINGER   1
       SAM BLACKMAN   1
       ROBERT DEMPSTER   1
       DOREEN SASAKI   1
HUGHES AIRCRAFT
EO E1 MAIL STOP B102
PO BOX 902
EL SEGUNDO CA 90245

ATTN JOSEPH S PRIMERANO   1
       CHRISTOPHER KNOWLTON   1
PLANNING CONSULTANT INC
PO BOX 1676
DAHLGREN VA 22448

ATTN DR EDWARD PRICE   1
UNITED DEFENSE
1 DANUBE DR
KING GEORGE VA 22485

ATTN DR KUO CHU CHANG   1
DEPT OF SYSTEMS ENGINEERING
SCHOOL OF INFORMATION
       TECHNOLOGY AND ENGINEERING
GEORGE MASON UNIVERSITY
FAIRFAX VA 22030-4444

ATTN DR XIA-RONG LI   2
EE DEPT
UNIVERSITY OF NEW ORLEANS
NEW ORLEANS LA 70148

ATTN DR A T ALOUANI   1
DEPT OF ELECTRICAL AND
       COMPUTER ENGINEERING
TTU BOX 05004
COOKEVILLE TN 38505

ATTN DR PAUL KALATA   1
ECE DEPT
DREXEL UNIVERSITY
PHILADELPHIA PA 19104

ATTN GLENN WOODARD   1
       GARY L HILD   1
       ANDREW MITTURA   1
LOGICON/SYSCON CORPORATION
PO BOX 1480
DAHLGREN VA 22448-1480

ATTN FRANK REFLIER   1
LOCKHEED MARTIN
GOVERNMENT ELECTRONIC SYSTEMS
MISSILE SYSTEM DESIGN
199 BORTON LANDING RD
MOORESTOWN NJ 08057-3075

DISTRIBUTION (Continued)

	Copies		Copies

ATTN BOB OTTINGER — 1
        INGAR BLOSFELDS — 1
LOCKHEED MARTIN GES
NAVAL ADVANCED SYSTEMS
BUILDING 127-207
BORTON LANDING RD
MOORESTOWN NJ 08057

ATTN BORIS L ROZOVSKY — 1
CENTER FOR APPLIED
        MATHEMATICAL SCIENCES
UNIVERSITY OF SOUTHER
        CALIFORNIA
1042 W 36TH PLACE DRB 306
LOS ANGELES CA 90089-1113

ATTN DR OLIVER E DRUMMOND — 1
10705 CRANKS RD
CULVER CITY CA 90230

ATTN RON HELMICK — 1
TECHNOLOGY SERVICE CORP
962 WAYNE AVENUE
SUITE 800
SILVER SPRING MD 20910

ATTN DR DAVID CASTANON — 1
DEPT OF ELECTRICAL COMPUTER
        AND SYSTEMS ENGINEERING
BOSTON UNIVERSITY
44 CUMMINGTON ST
BOSTON MA 02215

ATTN FREDERICK E DAUM — 1
RAYTHEON COMPANY
1001 BOSTON POST ROAD
MARLBOROUGH MA 01752

ATTN WILLIAM M STONESTREET — 1
        ALAN WILLSKY — 1
ALPHATECH INC
EXECUTIVE PLACE III
50 MALL RD
BURLINGTON MA 01803

ATTN ROBERT FITZGERALD — 1
MS S4S-H1
RAYTHEON COMPANY
BEDFORD MA 01730

ATTN CHARLES GLOVER — 1
        AL PERRELLA — 1
POET
1745 JEFFERSON DAVIS HWY
SUITE 1100
ARLINGTON VA 22202

ATTN DONALD T LERRO — 1
INFORMATION SCIENCES DEPT
ENGINEERING TECHNOLOGY CTR
ANALYSIS AND TECHNOLOGY INC
240 ORAL SCHOOL ROAD
MYSTIC CT 06355-1208

THE CNA CORPORATION
P O BOX 16268

ATTN KEITH KASTELLA — 1
LOCKHEED-MARTIN TACTICAL
        DEFENSE SYSTEMS
BOX 64525-MS U1 T21
ST PAUL MN 55164-0525

ALEXANDRIA VA 22302-0268 — 1

NON-DOD ACTIVITIES (EX-CONUS)

ATTN RONALD P MAHLER — 1
LOCKHEED-MARTIN
3333 PILOT KNOB ROAD
ENGAN MN 55121

ATTN DR NEIL GORDON — 1
CIS SECTION
DRA MALVERN
ST ANDREWS ROAD
MALVERN WORCS
WR14 3PS UK

ATTN RON ROTHROCK — 1
BDM FEDERAL INC
CONSOLIDATED SUPPORT
        FACILITY (CSF)
1901 NORTH MOORE STREET
        SUITE 750
ARLINGTON VA 22209

ATTN DR ALFONSO FARINA — 1
SYSTEMS ANALYSIS GROUP ALENIA
VIA TIBURTINA KM 12.400,00131
ROME ITALY

DISTRIBUTION (Continued)

	Copies
INTERNAL	
B05 STATON	1
B20 CHU	1
B30	1
B32	1
B32 ANTHONY	1
B32 BLAIR	5
B32 CONTE	1
B32 GENTRY	1
B32 GROVES	1
B32 MCCABE	1
B32 RICE	1
B32 WATSON	2
B32 PAULA R WERME	1
B35 BAILEY	1
B35 FENNEMORE	1
B35 HARRISON	1
B60	3
B60 HENNESSEY	1
B60 IRWIN	1
B60 NGUYEN	1
B60 SCHEID	1
B60 WAITS	1
B60 WILEY	1
G23 BIBEL	1
G23 GRAFF	1
G23 OHLMEYER	1
G72	1
N05	1
N05 HALES	1
N10	1
N14	1
N14 ADDAIR	1
N14 BOYER	1
N14 MURRAY	1
N25 VENABLE	1
N92 GRAY	1
N92 LAMBERTSON	1
N92 FOSTER	1
T	1
T04	1
T05	1
T05 MARKER	1
T10 KNICELY	1
T20	1
T20 BEUGLASS	1
T23 AFRICA	1
T40	1
T40 STAPLETON	1
T406	1

	Copies
T41 FONTANA	1
T41 MARTIN	1
T41 MIMS	1
T41 PAWLAK	1
T41 STUMP	1
T42 CALDWELL	1
T42 CARPENTER	1
T42 KLOCHAK	1
T42 LEONG	1
T50 LUCAS	1